FE-2757-3
Distribution Category UC-90c

HOT, LOW-BTU PRODUCER GAS DESULFURIZATION IN FIXED BED OF IRON OXIDE-FLY ASH

1. ECONOMIC SENSITIVITY ANALYSIS.
2. DIRECT FORMATION OF ELEMENTAL SULFUR DURING REGENERATION.
3. APPLICATION OF APCI SIMULATION MODEL.

FINAL REPORT

PERIOD JULY 1977 TO MARCH 1978

DILIP JOSHI
JON H. OLSON
MALCOLM L. HAYES
VASTUPAL SHAH

AIR PRODUCTS AND CHEMICALS, INC.
P. O. BOX 427
MARCUS HOOK, PENNSYLVANIA 19061

DATE PUBLISHED 1 JUNE 1979

PREPARED FOR THE UNITED STATES DEPARTMENT OF ENERGY

UNDER CONTRACT NO. EF-77-C-01-2757

TABLE OF CONTENTS

TABLE OF CONTENTS

TABLE OF CONTENTS

TABLE OF CONTENTS

LIST OF FIGURES

LIST OF FIGURES

LIST OF TABLES

LIST OF TABLES

DOE CONTRACT EF-77-C-01-2757

AIR PRODUCTS AND CHEMICALS, INC.
MARCUS HOOK, PENNSYLVANIA 19061

FINAL REPORT

1.0 ABSTRACT

This work was undertaken to aid DOE in the development of a fixed-bed cyclic process for desulfurizing hot, low-BTU (100-140 BTU/SCF) producer gas with iron oxide sorbents. The work described in this report is an extension of previous DOE supported APCI efforts in this area (NTIS Publication No. FE-2033-19 (1977)). In this process low-BTU producer gas contaminated with hydrogen sulfide passes through a freshly regenerated fixed bed of supported iron oxide at 1200°F and 150 psig. Hydrogen sulfide reacts with iron oxide to yield iron sulfide and steam. Absorption from the producer gas continues until the hydrogen sulfide concentration in the exit stream rises to ten percent of the inlet concentration. Most of the iron oxide in the bed is converted to iron sulfide at this breakthrough point. The bed then is regenerated with a mixture of air and diluent gas. The regeneration reactions are highly exothermic, and the diluent gas limits the maximum temperature rise in the bed. During regeneration iron sulfide is converted to iron oxide, and sulfur dioxide is formed.

Specific objectives of this work are listed below.

a) To prepare a preliminary cost estimate and cost sensitivity analysis to identify technological areas for further research and development work.

b) To investigate conditions under which substantial elemental sulfur is formed along with sulfur dioxide during regeneration of sulfided sorbents.

c) To apply the APCI simulation model to unpublished data from MERC regeneration experiments, and to investigate conditions under which the sorbent is damaged by excessive temperature.

The economics of hot stage desulfurization of low-BTU producer gas in a cyclic fixed bed were evaluated over a wide range of process variables including linear velocity of the producer gas, operating pressure, onstream cycle length, iron oxide content of the sorbent, pellet diameter, sorbent life and sorbent cost. Capital investment for a regenerative fixed-bed desulfurization unit designed to process producer gas for a 500 megawatt generating plant is 22.4 to 26.2 million dollars for typical operating conditions. Nearly 75 percent of the cost is for regeneration

facilities, and the compressors account for nearly 50 percent of the major equipment cost. The total processing cost for desulfurizing low-BTU producer gas ranges from 16.5 cents per MM BTU to 28.1 cents per MM BTU for typical operating conditions. Major contributions to the total processing cost are from sorbent cost, finance charges and depreciation.

The highest possible iron oxide content of the sorbent should be used to reduce plant investment and total processing cost. The shortest feasible onstream cycle length should be used since plant investment and total processing cost decrease sharply with a decrease in onstream cycle length. The sorbent life and price have a significant impact on the total processing cost. Plant investment and the total processing cost have a shallow minimum with respect to operating pressure at approximately 150 psi. Pellet size and superficial velocity have a small influence on the desulfurization economics.

The economic analysis identified several areas for further research and development work. The useful lifetime of the sorbent needs to be determined, and the operating parameters which affect lifetime should be identified. Development of sorbents which are physically strong, operate at high temperature, and have a high content of iron oxide is recommended.

An exploratory experimental program was carried out in a bench-scale unit to investigate conditions under which a substantial quantity of elemental sulfur is produced directly during regeneration of the sulfided sorbent. The process variables investigated included water, air and sulfur dioxide content of the regeneration feed gas, type of sorbent support, purity of iron oxide, iron oxide content and GHSV. Selectivity for the formation of elemental sulfur was defined as the fraction of the total sulfur in regeneration effluent gases occurring as elemental sulfur.

The amount of elemental sulfur produced during the regeneration of sulfided sorbents was as high as 45 mol percent of the total sulfur in the product. The concentration of elemental sulfur depended on the feed gas composition, sorbent characteristics and operating variables. Use of regeneration feed gas with high water content (greater than 90 mol percent), low oxygen content, and low sulfur dioxide content produces high selectivity to elemental sulfur. Silica supported sorbents showed a greater selectivity for the formation of elemental sulfur than fly ash supported sorbent. Sorbents made with chemically pure iron oxide had a greater selectivity for sulfur formation compared to sorbents made with commercial iron oxide. An increase in GHSV resulted in an increase in the selectivity for elemental sulfur.

The APCI simulation model was used to represent the regeneration experiments at MERC. The MERC experiments were troubled by excessive temperatures during regeneration; the maximum temperature was as high as 1840°F. The APCI model predicts these high temperatures for the method of operation used by MERC. MERC operators shut off the reactor heaters at the beginning of the regeneration process and consequently the reactor inlet temperature decreased from 1030°F to 100°F over a ten-hour period. The APCI model shows that decreasing the inlet temperature has the effect of increasing the rate at which the reaction zone moves through the reactor in

comparison to the rate predicted for a constant inlet temperature. The increase in the velocity of the reaction zone has two effects; the regeneration is not complete, and the temperature in the reaction zone increases.

If the inlet temperature of the regenerator were held constant, the APCI model predicts that the maximum bed temperature is only slightly greater than the adiabatic temperature rise. These simulations suggest that fixing the inlet temperature and oxygen content will yield stable operation of the regenerator.

Based on the work done in this contract, this process is a viable method of desulfurizing hot, low-BTU producer gas.

2.0 SUMMARY

2.1 General

This work was undertaken to contribute to the development of a process for desulfurizing hot, low-BTU (100-140 BTU/SCF) producer gas with iron oxide sorbents. Specific tasks of this work are listed below.

a) To prepare a preliminary cost estimate and cost sensitivity analysis to identify technological areas for further research and development work.

b) To investigate conditions under which substantial elemental sulfur is formed along with sulfur dioxide during regeneration of sulfided sorbents.

c) To apply the APCI simulation model to unpublished data from MERC regeneration experiments, and to investigate conditions under which the sorbent is damaged by excessive temperature.

This work is an extension of previous DOE supported efforts by APCI to develop a fixed-bed regenerative desulfurization system (NTIS publication No. FE-2033-19 (1977)). The previous work included development of suitable sorbents and criteria for process design.

2.2 Process Description

Low-BTU producer gas contaminated with hydrogen sulfide is desulfurized by passing through a freshly regenerated fixed bed of supported iron oxide at 1200°F and 150 psig. The hydrogen sulfide reacts with iron oxide to yield iron sulfide and steam. After most of the iron oxide in the bed is converted to iron sulfide and the hydrogen sulfide content in the effluent producer gas increases to ten percent of the inlet hydrogen sulfide concentration, the bed is regenerated with gas containing air and a diluent. The regeneration reaction is highly exothermic, and the diluent limits the maximum temperature in the bed to 1500°F. During regeneration, solid iron sulfide is converted to iron oxide solid and gaseous sulfur dioxide. The sulfur dioxide product is converted further to elemental sulfur in a Claus or Resox unit.

2.3 Economic Sensitivity Analysis

The economics of hot stage desulfurization of low-BTU producer gas for a 500 megawatt generating plant were evaluated over a wide range of operating variables and pellet characteristics. The process design used recycle gas containing nitrogen and sulfur dioxide as a diluent to limit the adiabatic temperature rise across the bed to 500°F. The final product of regeneration was assumed to be sulfur dioxide-containing gas, and the additional cost of a sulfur recovery unit was not included in the analysis. All the costs are in late 1977 dollars.

The operating variables investigated were linear velocity of the producer gas in the reactor, operating pressure, and onstream cycle length. The pellet characteristics evaluated were iron oxide content of the sorbent, pellet diameter, sorbent life and sorbent cost. An economic model was developed to understand the complex relationships of the operating variables and pellet properties with the various cost components. Results of the analysis are summarized below.

The capital investment for a regenerative fixed-bed desulfurization unit with capacity to process producer gas for a 500 megawatt generating plant is 22.4 to 26.2 million dollars for typical operating conditions. Nearly 75 percent of the cost is for regeneration facilities. Compressors to recycle the large volume of effluents and air compressors to supply air for regeneration account for nearly 50 percent of the major equipment cost.

The total processing cost for desulfurizing low-BTU producer gas ranges from 16.5 cents per MM BTU to 28.1 cents per MM BTU for typical operating conditions. Major contributions to the total processing cost are given below for the base case.

Cost Component		Cost, Cents/MM BTU
Direct Processing Cost		8.51
Sorbent ($1.00/Lb, 1 Year Life)	5.06	
Labor	0.51	
Maintenance	2.12	
Net Utilities	0.82	
Indirect Processing Cost		0.55
Plant Overhead	0.55	
Fixed Processing Cost		5.15
Depreciation (20 Year Linear)	3.53	
Insurance & Property Tax (2.3% of Investment)	1.62	
General Expenses		6.99
Administration	0.43	
Finance (9.0% Interest)	6.36	
TOTAL PROCESSING COST		21.0

The highest possible iron oxide content of the sorbent should be used. Plant investment and total processing cost decrease monotonically with increasing iron oxide content in the sorbent. The shortest feasible onstream cycle length should be used since plant investment and total processing cost decrease sharply with a decrease in onstream cycle length. Sorbent life and sorbent price have an important effect on the total processing cost due to the significant contribution of the sorbent cost to the total processing cost.

Plant investment and the total processing cost have a shallow minimum with respect to pressure at approximately 150 psi. However, the operating pressure of the desulfurizing unit is set externally by the pressure of the producer gas plant. Pellet size and superficial velocity of the producer gas have a small influence on the desulfurization economics.

The following conditions are recommended as optimum based on the analysis in this work.

Onstream Cycle Length	-	2 Hours or Shortest Possible
Producer Gas Velocity	-	5.0 Ft/Sec
Operating Pressure	-	150 psi
Iron Oxide Content	-	80 Wt. Percent or Maximum
Pellet Diameter	-	1/4 Inch

The total processing cost for this case is estimated to be 12.05 cents per MM BTU.

2.4 Direct Elemental Sulfur Formation During Regeneration

The objective of this exploratory experimental program was to investigate conditions under which elemental sulfur is produced directly on regeneration of the sulfided sorbent. A bench-scale pilot unit was constructed for this work.

The process variables investigated included feed gas compositions, sorbent characteristics and operating conditions. Specifically the effects of water, air and sulfur dioxide content were evaluated. The sorbent characteristics investigated included type of support, purity of iron oxide, and iron oxide content. The effect of GHSV also was studied.

Sulfur material balances on most runs were within 20 percent. Material balances were expected to be within 15 percent due to the crude method of estimating the amount of sulfur deposited on the sorbent during absorption. Selectivity for the formation of elemental sulfur was defined as the fraction of the total sulfur in regeneration effluent gases occurring as elemental sulfur.

$$\text{Selectivity for Elemental Sulfur Formation, \%} = \frac{W_S}{W_S + \frac{32}{64} W_{SO_2} + \frac{32}{80} W_{SO_3} + \frac{32}{64} W_{H_2S}} \times 100$$

where W_S = Grams of elemental sulfur in regeneration effluents,

W_{SO_2} = Grams of sulfur dioxide in regeneration effluents,

W_{SO_3} = Grams of sulfur trioxide in regeneration effluents,

W_{H_2S} = Grams of hydrogen sulfide in regeneration effluents.

The amount of elemental sulfur produced during the regeneration of sulfided sorbents was as high as 45 mol percent of the total sulfur in product. The concentration of elemental sulfur depended on the feed gas composition, sorbent characteristics and operating variables.

Regeneration feed gas with high water content (greater than 90 mol percent) should be used to increase the selectivity for elemental sulfur. Water content is a major process variable. Elemental sulfur formation was favored with oxygen-starved regeneration gas. When sulfur dioxide was used as a diluent in the regeneration gas mixture of air, steam and sulfur dioxide, the regeneration reactions produced a negligible amount of sulfur, a small amount of sulfur trioxide and sulfur dioxide. Thus sulfur formation is suppressed in SO_2-rich systems.

Silica supported sorbents showed a greater selectivity for the formation of elemental sulfur than fly ash supported sorbent. Sorbents made with chemically pure iron oxide had a greater selectivity for elemental sulfur formation than sorbents made with commercial iron oxide. An increase in GHSV resulted in an increase in the selectivity for elemental sulfur.

A thermodynamic chemical equilibrium analysis was done to provide guidance on the choice of feed composition. The analysis predicted an increase in the selectivity for elemental sulfur formation with an increase in water content and decrease in air content of the regeneration feed gas. It did not predict the large magnitude of selectivity for elemental sulfur formation observed by APCI and others, and thus the production of sulfur is controlled by kinetic processes.

2.5 APCI Simulation of MERC Data

The Morgantown Energy Research Center began a pilot-plant scale experimental program on hot, low-BTU producer gas desulfurization in 1976. The bed temperature during regeneration was observed to be much higher than the adiabatic temperature increase for the gas phase in some of these runs. Under this contract the APCI simulation model (described in NTIS Publication No. FE-2033-19 (1977)) was modified to approach more closely the operating methods used by MERC and then used to predict the temperature profiles in the reactor during regeneration. The purpose of this comparison is to test the APCI model critically. From this investigation APCI is to present methods which avoid excessive bed temperatures during regeneration.

The APCI model shows that bed temperatures well in excess of the adiabatic temperature rise are predicted for the operating method used by MERC. MERC attempted to control the excess temperature peak during regeneration by turning off the reactor heaters. The inlet temperature to the reactor then fell from 1030°F to 100°F over a ten-hour period. Although common sense suggests that decreasing the reactor inlet temperature should help reduce the peak temperature in the reactor, the analysis suggests the contrary. The maximum temperature during regeneration depends critically upon the ratio of the rate the regeneration reaction zone passes through the reactor to the rate at which a thermal disturbance moves through the bed. If the MERC reactor were operated with a fixed inlet temperature and composition, a thermal disturbance would move through the unit much more rapidly than the chemical reaction zone. Existing analysis for this situation shows that increasing the effective chemical velocity will increase the maximum temperature in the reactor. Thus when the inlet gas is cooled, the regeneration zone is incompletely reacted, and the velocity of the reaction zone increases. APCI simulation shows under these conditions that the maximum temperature in the bed then becomes much larger than the adiabatic temperature rise.

The APCI simulation model predicts that the maximum bed temperature will be only slightly greater than the adiabatic temperature when the inlet gas temperature is held at the initial uniform temperature of the bed and the oxygen content is held constant. Constant inlet conditions are easy to implement.

2.6 Recommendations for Future Work

The iron oxide based fixed-bed regenerative process for desulfurization of hot, low-BTU producer gas has been demonstrated successfully in bench-scale units and process design criteria have been established. Areas of further work to improve process economics and accelerate commercialization are given below.

1. The low-BTU producer gas contains impurities besides hydrogen sulfide such as COS, NH_3, HCN and tar. Applicability of the iron oxide sorbent in the presence of these compounds should be investigated.

2. Economic comparisons between alternative producer gas clean-up systems are needed. These comparisons should be made on the same financial basis and with the same starting and end points on the process flow diagram.

3. The useful lifetime of the sorbent needs to be determined and the operating parameters which affect lifetime should be identified.

4. Short cycle lengths favor process economics. The shortest feasible cycle length needs to be investigated.

5. Fluid bed operation with continuous absorption and regeneration has several potential benefits of technical and economic nature. This concept should be evaluated.

6. Regeneration at high temperatures ($\sim$1800°F) will reduce process costs. Development of sorbents which operate at high temperatures is recommended.

7. Development of strong sorbents with high iron oxide content will improve the process economics. Sorbent development along these lines is urged.

3.0 INTRODUCTION

This work was undertaken to support DOE in the development of a process for desulfurizing hot, low-BTU producer gas with iron oxide sorbents. In this process hot, low-BTU producer gas contaminated with hydrogen sulfide passes through a freshly regenerated fixed bed of supported iron oxide at 1200°F and 150 psig. Hydrogen sulfide reacts with iron oxide to yield iron sulfide and steam. After most of the iron oxide in the bed is converted to iron sulfide, and the sulfur content in the effluent producer gas increases to ten percent of the feed value, the bed is regenerated with a gas containing a small amount of air and a diluent. The regeneration reaction is highly exothermic, and the diluent limits the maximum temperature in the bed to 1500°F. During regeneration, solid iron sulfide is converted to iron oxide solid and gaseous sulfur dioxide. The sulfur dioxide product is converted further to elemental sulfur in a Claus or Resox unit.

The work described in this report is an extension of previous DOE supported APCI efforts in this area.[1] The previous work included development of suitable sorbents and definition of the scale-up criteria.

Specific tasks of the work described in this report are listed below.

a) To prepare a preliminary cost estimate and cost sensitivity analysis to identify technological areas for further research and development work.

b) To investigate conditions under which substantial elemental sulfur is formed along with sulfur dioxide during regeneration of sulfided sorbents.

c) To apply the APCI simulation model to unpublished data from MERC regeneration experiments, and to investigate conditions under which the sorbent is damaged by excessive temperature.

3.1 Economic Analysis

Preliminary process designs were made in the previous work done by APCI.[1] Section 4 of this report describes an economic analysis made to optimize the design of a workable process for hot gas desulfurization. The preliminary design identified a large number of important process variables which are evaluated quantitatively in this work. Specifically, the process variables evaluated include iron oxide content of the sorbent, pellet diameter, sorbent life, operating pressure, linear gas velocity and onstream cycle length.

3.2 Production of Elemental Sulfur

In the previous work by APCI[1] performed under DOE support, a significant amount of elemental sulfur was formed during regeneration of sulfided iron oxide sorbents. In the conventional regeneration method, sulfur dioxide is formed. The sulfur dioxide product is further converted to elemental sulfur in a Claus or Resox unit. If elemental sulfur were produced directly during regeneration, the sulfur recovery unit could be of reduced size or even eliminated. This process modification might reduce the total processing cost substantially.

The goal of this experimental program was to identify regeneration conditions which result in the production of elemental sulfur and then to determine the controlling process variables. The process variables included several regeneration feed gas compositions, sorbent compositions and operating conditions. This work is described in Section 5 of this report.

3.3 Simulation of Regeneration

The regeneration of the iron oxide sorbent converts iron sulfide to Fe_2O_3 or FeO by oxidation with air. The regeneration reaction is highly exothermic, and the support can be sintered by excessive bed temperatures during regeneration. The bed temperature cannot rise above 1800°F during regeneration of iron oxide supported on silica, and the maximum bed temperature for fly ash probably should be limited to 1600°F if the sorbent is to have a useful lifetime.

Experiments at MERC show bed temperatures substantially above the adiabatic temperature rise for the reaction and also large enough to degrade the support markedly. Section 6 presents a comparison of the results from the APCI simulation of regeneration with MERC data. The analysis is used to develop a simple way to operate the reactor with a controlled exotherm.

4.0 ECONOMIC ANALYSIS

4.1 INTRODUCTION

Low-BTU producer gas has many potential industrial applications, such as steel production or combined cycle power generation. In all these applications the removal of hydrogen sulfide from the producer gas now is necessary for pollution control and equipment protection. The hot desulfurization process removes hydrogen sulfide from the producer gas without cooling the gas, thus preserving the sensible heat of the gas and improving the thermal efficiency of the process. Air Products and Chemicals, Inc. previously has participated with DOE in efforts to develop a regenerative cyclic fixed-bed process for hot producer-gas desulfurization using pellets of supported iron oxide.[1]

A schematic diagram of the process is given in Figure 4.1. The basic chemistry of the desulfurization step is given in Table 4.1. The gasifier generates low-BTU producer gas containing hydrogen sulfide at about 1200°F and 150 psig. After removal of particulates in a cyclone, the hot-producer gas passes through a fixed bed of supported iron oxide to remove hydrogen sulfide. Hydrogen sulfide reacts with iron oxide to yield iron sulfide and steam. After most of the iron oxide in the bed is converted to iron sulfide, the bed is regenerated with gas containing air and a diluent. The regeneration reaction is highly exothermic, and the diluent limits the temperature rise in the reactor. During regeneration solid iron sulfide is converted to iron oxide (solid) and gaseous sulfur dioxide. The sulfur dioxide product is converted further to elemental sulfur in a Claus or Resox unit.

In previous work done by Air Products and Chemicals, Inc. an iron oxide sorbent was developed, the absorption and regeneration characteristics of the sorbent were described by a quantitative model, and preliminary process designs were made.[1] This section describes new efforts made to optimize the design of a process for hot gas desulfurization.

The preliminary design identified a large number of important process variables which are evaluated quantitatively in this effort. Specifically, the effects of these process variables upon process economics are determined. Section 4.2 explains the approach adopted for this analysis. Details of the process, specifics of the process variables investigated, and the design trade-offs considered are given in this section. Section 4.3 describes the process design basis and constraints. This section gives the assumptions made and explains the choice of design cases used to achieve the objectives of this task. Section 4.4 summarizes the results and lists the conclusions and recommendations of this economic analysis.

FIGURE 4.1

TYPICAL PROCESS FLOW SCHEME

FOR A HOT PURIFICATION COMBINED CYCLE POWER SYSTEM*

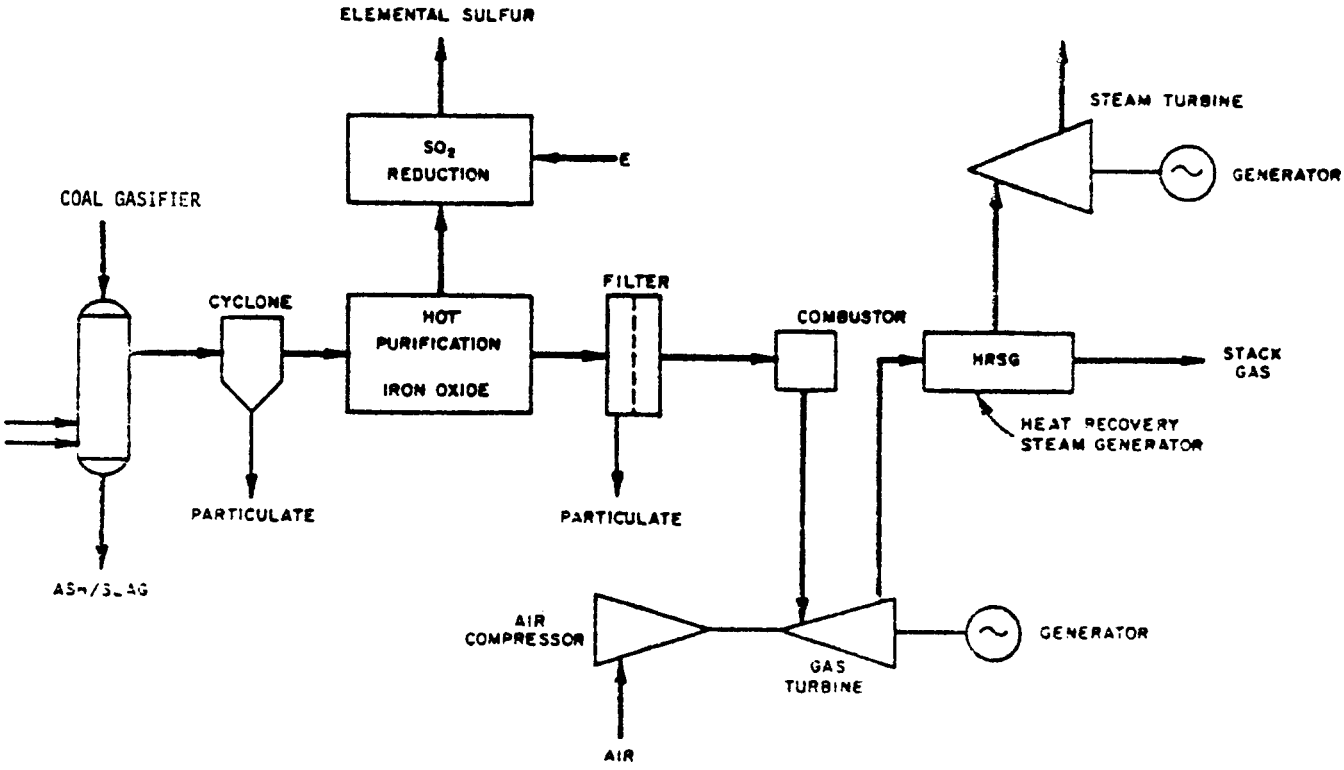

* See Reference No. 2.

TABLE 4.1

HOT FUEL GAS DESULFURIZATION WITH IRON OXIDE

TYPICAL REACTION SCHEME*

SULFUR ABSORPTION PROCESSES

$$Fe_2O_3 + 2H_2S + CO = 2FeS + 2H_2O + CO_2$$

$$Fe_2O_3 + 2H_2S + H_2 = 2FeS + 3H_2O$$

$$FeS + H_2S = FeS_2 + H_2$$

Average Process Representation

$$Fe_2O_3 + 3H_2S = 2FeS_{1.5} + 3H_2O$$

Average Process Representation

$$Fe_2O_3 + 3H_2S + CO = 2FeS_{1.5} + 2H_2O + CO_2 + H_2$$

ABSORBENT REGENERATION PROCESSES

$$2FeS + 3O_2 = 2FeO + 2SO_2$$

$$2FeS_2 + 5O_2 = 2FeO + 4SO_2$$

Average Regeneration Representation - FeO Production

$$2FeS_{1.5} + 4O_2 = 2FeO + 3SO_2$$

Average Regeneration Representation - Fe_2O_3 Production

$$4FeS_{1.5} + 9O_2 = 2Fe_2O_3 + 6SO_2$$

Ferrous Oxide Oxidation

$$4FeO + O_2 = 2Fe_2O_3$$

Direct Elemental Sulfur Production

$$2FeS_{1.5} + SO_2 = 2FeO + 4S$$

COKE BURNING

$$C + O_2 = CO_2$$

---

*This table is a modified version of Table 2-2 published by Jones, C. H., and Donohue, J. M., "Comparative Evaluation of High and Low Temperature Gas Cleaning for Coal Gasification-Combined Cycle Power Systems", EPRI Publication No. EPRI-AF-416 (1977).

4.2 Approach

4.2.1 Scope of Work

The economic analysis presented in this section is for the fixed-bed regenerative process for hydrogen sulfide removal from hot, low-BTU producer gas. Figure 4.1 shows the location of this process step in the flow diagram for low-BTU producer gas clean-up and utilization. This analysis assumes that all sulfur from the sulfided sorbent is liberated as sulfur dioxide during regeneration. The economics of the additional facilities needed to convert sulfur dioxide produced in regeneration to elemental sulfur are independent of the desulfurization process when the outlet conditions of the regeneration gas are fixed. Therefore, the economic analysis of the SO_2 reduction process is not considered in this development.

The desulfurization plant capacity is determined by the size of the facility using the producer gas. A 500 megawatt generating plant powered by low BTU producer gas was selected as the design basis for this study. The analysis requires determining the plant investment and the processing costs.

4.2.2 Process Concept

A flow sheet for the desulfurization and regeneration process is given in Figure 4.2. The following paragraphs describe the process.

The proposed hot stage desulfurization process consists of several fixed-bed reactors loaded with iron oxide sorbents. At a given time, some of these reactors are undergoing hydrogen sulfide absorption while others are undergoing regeneration to restore the sorbent activity. During the absorption cycle, the desulfurization reactor is operated at conditions determined by the gasifier (typically 1200°F and 150 psig). Absorption is a mildly exothermic reaction with the heat of reaction 22 kcal/g-mol Fe_2O_3. The hydrogen sulfide content of the cleaned producer gas is monitored. When hydrogen sulfide content of the cleaned producer gas exceeds a predetermined acceptable value (0.06% for this analysis), the producer gas feed is switched to a freshly regenerated reactor. The saturated bed is regenerated using a mixture of air and diluent gas to produce sulfur dioxide and iron oxide. Regeneration of iron sulfide is a highly exothermic reaction. The heat of reaction at 1200°F is 85 kcal/g-mol oxygen for the reaction

$$FeS + \frac{7}{4} O_2 \longrightarrow \frac{1}{2} Fe_2O_3 + SO_2$$

The oxygen concentration in the regeneration feed gas has to be kept sufficiently low to avoid excessive temperature rise and sorbent damage.

FIGURE 4.2

SCHEMATIC FLOW DIAGRAM FOR DESULFURIZATION AND REGENERATION

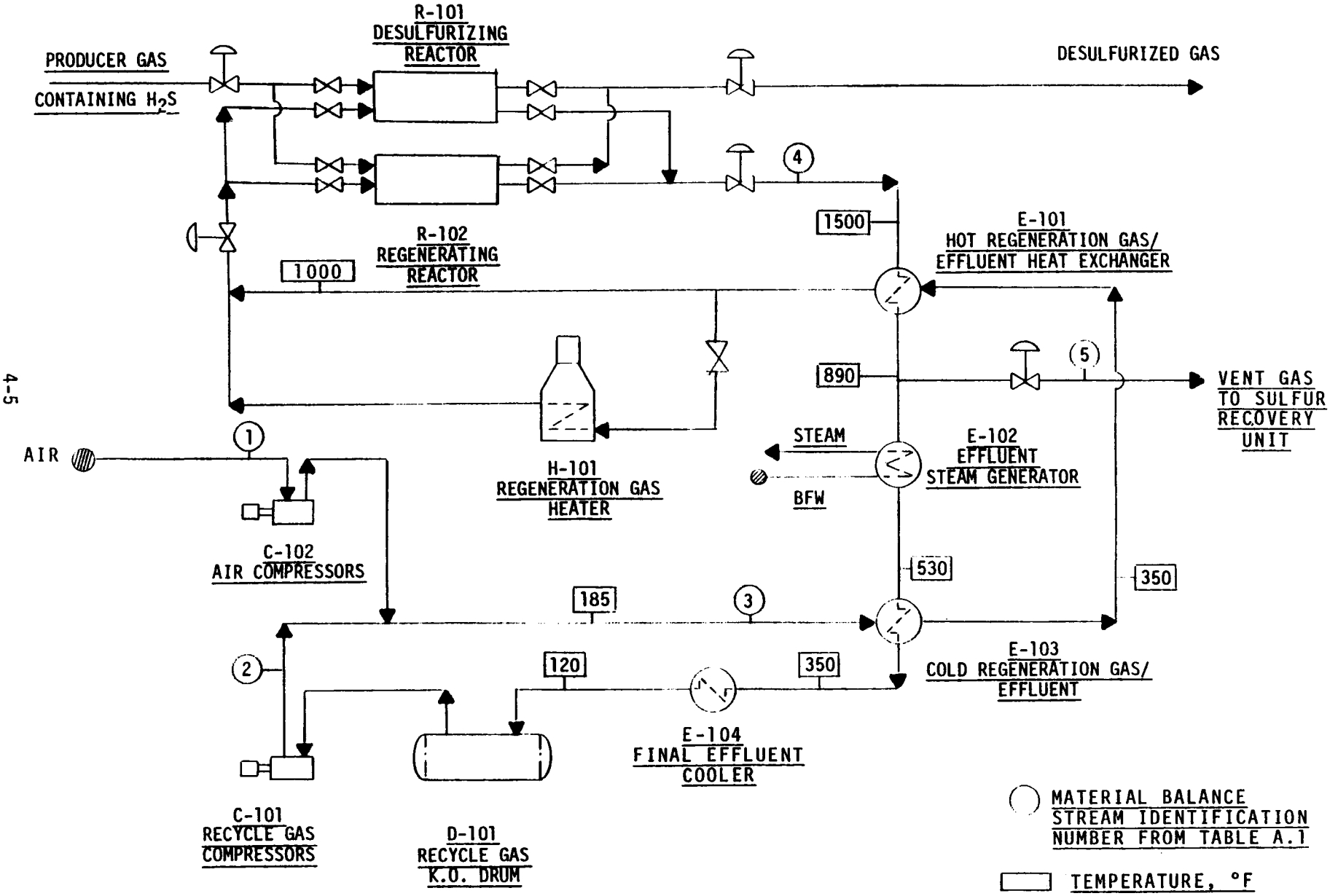

The recirculation system used in this analysis is designed to recover energy from the regeneration reactions in a valuable form. The process equipment can be identified by reference to Figure 4.2. The major items in the process are the reactors (R-101 and R-102), the hot regeneration gas/effluent heat exchanger (E-101), the effluent steam generator (E-102), the cold regeneration gas/effluent heat exchanger (E-103), the effluent cooler (E-104), the recycle gas compressors (C-101), the air compressors (C-102), and the regeneration gas heater (H-101).

At any given time some reactors are operating in the absorption mode while others are being regenerated. Hydrogen sulfide is removed from the hot producer gas during the absorption cycle by reaction with iron oxide held on the support. When the hydrogen sulfide concentration in the exiting producer gas is too high, the producer gas flow is switched to another reactor. The saturated reactor is purged and then regenerated with a mixture of air and recycle gas. The ratio of fresh air to recycle gas is chosen to limit the adiabatic temperature rise of the gas to 500°F. Regeneration feed gas enters the reactor (R-102) at 1000°F, and regeneration effluents containing 24% sulfur dioxide leave the reactor at 1500°F. The sensible heat of the regeneration effluents is utilized in a hot regeneration feed gas/effluent heat exchanger (E-101) to preheat the regeneration feed gas to 1000°F. About 10% of the total regeneration effluents are discharged to a sulfur recovery unit where sulfur dioxide in the effluents is converted to elemental sulfur. The sensible heat of the cooled regeneration effluents (890°F) is further utilized in an effluent steam generator (E-102) which produces 250 psig steam. The regeneration effluents leave the steam generator at 530°F, and the remaining sensible heat is recovered in the cold regeneration feed gas/effluent heat exchanger (E-103). The regeneration effluents leave this heat exchanger at 350°F and are cooled to 120°F in a final effluent cooler (E-104). The cold effluents pass through a recycle gas compressor (C-101) where the effluents are compressed to make up for the pressure loss in the reactors and heat exchangers.

Fresh air is brought to operating pressure in the air compressors and then is added to the compressed recycle gas to form the cold regeneration feed gas. The cold regeneration feed gas is preheated to 1000°F by heat exchange with the hot effluents, first in the cold regeneration gas/effluents heat exchanger (E-103), and then in the hot regeneration gas/effluents heat exchanger (E-101). A regeneration gas heater (H-101) is provided to preheat the regeneration gas during start-up of the desulfurization unit.

The process design method is described in Section 4.3. The several process variables studied for influence on process economics are described next in Section 4.2.3.

4.2.3 Qualitative Effect of Process Variables

The process variables evaluated for investment and processing cost sensitivity in this work include linear gas velocity, reactor pressure, duration of the cycle, iron oxide content of the sorbent, pellet diameter, sorbent life and sorbent price.

The qualitative impact of each variable is described below.

- Linear Gas Velocity During Sorption

  The linear gas velocity in the reactor is used as an independent design parameter in this study because the remainder of the design can be calculated in a straightforward manner after the linear velocity during the sorption cycle is specified. The gas velocity in the regeneration cycle is set by stoichiometric constraints.

  The mass flow rate of gas through reactors is independent of the design configuration. The volume of a reactor also is nearly independent of gas velocity. At constant reactor volume the diameter and shell thickness of the reactor decrease with increasing gas velocity while the length increases. Thus the investment cost is a weak function of linear gas velocity.

  The pressure drop across the reactor increases with gas velocity. Thus the utility cost increases with gas velocity.

- Operating Pressure

  The operating pressure of the system is set by the specific use of the producer gas. However, the cost of operating the desulfurization plant depends upon operating pressure. Thus pressure is a parameter in the economic analysis set by external factors. The operating pressure for regeneration is assumed to be the same as the operating pressure for absorption. This is an arbitrary choice made to minimize mechanical problems.

  The investment cost in reactors is a complex function of pressure. For a fixed reactor volume and a selected linear velocity, the diameter of the reactor decreases and the reactor length increases with increasing pressure. In addition the reactor wall thickness increases with pressure. The mass of the reactor and hence the investment depends upon shell thickness, reactor diameter, and reactor length. The interaction of these parameters with pressure does not have a simple qualitative description. However, the investment cost of accessory equipment such as heat exchangers, drums, compressors, etc., all increase with operating pressure.

The utility cost for the regeneration air increases with increasing operating pressure. The utility cost for a recycle gas compression decreases with increasing operating pressure because the ratio of input/output pressure decreases with increasing pressure. Thus the total utility costs can be minimized with respect to operating pressure.

The above discussion shows that the cost of the reactors and total cost of compressors does not have a simple qualitative description as the operating pressure and linear gas velocity change. Appendix A contains a development of algebraic expressions relating the investment and processing costs to the operating variables. These derivations are given to facilitate the understanding of the complex relationships of the operating variables with various cost components. However, these algebraic expressions were not used in the calculations of the cases used in the design analysis. Calculations for the cases were made using existing design computer programs. These design packages consider details of the equipment such as reactor nozzles, insulation, and dome structure, and hence the results are a more realistic initial analysis. These data are then used to establish parameters in the optimized design.

- Cycle Length

As the onstream cycle length decreases, the sorbent requirement and the reactor size decrease. Thus the investments in reactors and sorbent decrease with shorter cycle length.

At a given linear gas velocity, the decrease in reactor volume reduces the bed length. The smaller bed depth results in a lower pressure drop and lower utility cost.

- Iron Oxide Content of the Sorbent

An increase in the iron oxide content of the sorbent results in an increase in the capacity of the sorbent. Therefore, the investment in reactors decreases with iron oxide content. The investment in sorbent also can decrease with increasing iron oxide content if the additional cost for iron oxide is offset by the decrease in the sorbent needed.

At a fixed gas velocity the decrease in the reactor volume with higher iron oxide content of the sorbent decreases the bed depth. The utility costs decrease with increasing iron oxide content of the sorbent because the pressure drop decreases.

- Pellet Diameter

  The plant investment is nearly independent of pellet diameter since the reactor volume does not depend on pellet diameter. A more careful consideration suggests that the reactor investment increases slightly with pellet diameter because the efficiency is lower. On the other hand, the pressure drop across the reactor increases with a decrease in pellet size, and therefore the utility costs and compressor investment increase. Thus there is a weak minimum for total process costs.

- Sorbent Life

  An increase in sorbent life reduces the sorbent replacement cost and total processing cost.

- Sorbent Price

  An increase in sorbent price increases the sorbent cost and total processing cost. It may be possible to develop new sorbents with greater absorption capacity and longer life. These new sorbents are expected to be more expensive. Some quantitative analysis is necessary to determine whether the benefits of such new sorbents are greater than the penalty in sorbent price increase.

4.3 Process Design Method

This section lists the technical and economic assumptions made in the process design. A description of the method of process design and the cases studied follows.

4.3.1 Process Conditions

The technical assumptions made for the process design are given below.

1) The desulfurization unit is designed for processing producer gas for a 500 megawatt generating plant.

2) Efficiency of converting heating value of producer gas to electricity is 47 percent.

3) Composition of the producer gas is:

	Mol Percent
Nitrogen	48.6
Carbon Monoxide	20.5
Hydrogen	14.9
Carbon Dioxide	6.5
Methane	1.9
Hydrogen Sulfide	0.6
Steam	7.0

4) This gas has a heating value of 130 BTU/SCF. The oxygen concentrated in the regeneration gas is chosen to limit the adiabatic gas temperature rise across the reactor to 500°F.

5) All sulfur absorbed by the sorbent during absorption is released as sulfur dioxide during regeneration. No sulfur trioxide and elemental sulfur are formed.

6) The estimated bed sorption efficiency for absorption of hydrogen sulfide is approximately 80 percent for most cases. This means ten percent breakthrough for hydrogen sulfide occurs when the bed is saturated 80 percent. Specifically, an expression based on model development and experimental data[1] was used to estimate sorption efficiency for each case.

4.3.2 Economic Assumptions

The assumptions made for economic analysis are given below.

1. All costs are for late 1977. This corresponds to the Chemical Engineering Erection Cost Index of 177.2.

2. The ratio of plant investment to major equipment material and erection cost is 3.06. This figure is based upon Air Products and Chemicals design experience. A breakdown of the cost components included in the factor of 3.06 is given in Table A.9 of Appendix A.

3. Depreciation time for the plant is 20 years. This lifetime is traditional for utilities.

4. Land costs are not included.

5. Interest charges are 9 percent of the total plant investment. Profit on invested capital is not included in this analysis.

6. Maintenance costs are 3 percent of the plant investment.

7. Labor requirements for the desulfurization plant are 2 men/shift at $9.55 per hour.

8. Plant overhead charges are 110 percent of labor charges.

9. Administrative charges are 3 percent of the processing cost.

10. Insurance and property tax is 2.3 percent of plant investment.

11. Costs and credit of the utilities are:

Electric Power	-	2.4 Cents/KWH
Cooling Water	-	2.5 Cents/1000 Gallons
Steam	-	3.5 Dollars/1000 Pounds
Boiler Feed Water	-	2.0 Dollars/1000 Gallons

4.3.3 Details of Design Method

4.3.3.1 Material Balance

Flow rate of the producer gas to be desulfurized is calculated based on the capacity of the power generating plant (500 megawatts) and efficiency of converting the heating value of the producer gas into electricity (47 percent). For a known onstream cycle length, the total amount of sulfur absorbed by the sorbent is calculated. This sulfur on the sorbent is removed during regeneration.

Inspection of Figure 4.2 shows that during regeneration the only gas input is air and the only gas output is a fraction of the total regeneration effluents. The effluent is processed further in a sulfur recovery unit where sulfur dioxide from the regeneration effluents is converted to elemental sulfur.

The regeneration air rate is 5 percent excess over the quantity necessary to supply the stoichiometric oxygen requirement. The recycle gas rate is based on limiting adiabatic gas temperature rise across the reactor to less than 500°F. A design material balance for the regeneration system is presented in Table A.1 of Appendix A.

4.3.3.2 Reactor Size

The reactor bed volume was determined based on the total amount of sulfur to be removed, ultimate sorption capacity of the sorbent, and the absorption efficiency. Computation of the bed volume involved a trial-and-error calculation. Details of this method are given in Section A.2.2.1 of Appendix A.

In all cases, the number of reactors provided for regeneration is equal to the number of reactors onstream. Since one reactor is undergoing valve changes and reactor purging operations, the actual number of reactor beds being regenerated at any given time is one less than the number of reactors onstream. In addition, one spare vessel is provided for sorbent charge and operating flexibility. The optimum number of reactors was determined for the base case by minimizing the reactor investment.

The producer gas flow rate through each reactor is determined by the number of reactors in operation. The diameter of the reactor then is calculated to match the flow rate with the specified gas velocity, pressure and temperature. The reactor length then is calculated to yield the bed volume required to give the specified cycle time and calculated sorption efficiency.

The desulfurization reactor vessel consists of a carbon steel shell lined with eight inches of refractory. The iron oxide sorbent bed is supported on a firebrick dome structure. A sketch of a typical desulfurization reactor and reactor specifications for the cases studied are given on Figure A.1 of Appendix A.

4.3.3.3 Other Equipment

Pressure drop through the fixed bed was estimated using Happel's correlation.[3] The reactor pressure drop was calculated knowing the reactor length, the sorbent size and the pressure, temperature and linear velocity of the gas. The pressure drop across the bed was calculated both for absorption and regeneration cycle. The pressure drop across the rest of the regeneration circuit was estimated to be 35 psi for all cases since the operation of this portion of the plant is not a function of the design variables.

The large volume of recirculating gas requires fairly large recycle gas compressors. Regeneration was carried out at the same pressure as the onstream operating pressure.

Air compressors were sized based on the air requirements and regeneration pressure. Specifications for the recycle gas compressors and air compressors are given in Table A.2 of Appendix A.

Fifty percent excess capacity was provided for both recycle gas compressors and air compressors to provide uninterrupted service of the desulfurization unit and to handle occasional excess flows.

The heat exchange duty for each heat exchanger was calculated based on the material balance and temperatures shown on Figure 4.2. The hot regeneration gas/effluent heat exchanger is made of Alonized 18-8 chrome-nickel steel. The steam generator is made with a carbon-steel shell and aluminum tubes. The cold regeneration gas/effluent heat exchanger is made of aluminum. Details of the heat exchangers such as heat duty and surface area are given in Table A.4 of Appendix A.

4.3.3.4 Plant Investment

The total plant investment was estimated by multiplying the total cost of major equipment (material and erection) by a factor of 3.06. This number is similar to a Lang[4] factor and accounts for the cost of accessories and installation.

The accessories include piping, structural steel, instrumentation, valves, timer, insulation, electrical work, painting, site development, buildings, foundations and temporary structures. The total installation cost was obtained by adding the cost of field labor, field charges, home office expenses and overhead. Cost of the land and costs associated with plant start-up are not included in this analysis. Detailed breakdown of all these cost components for a typical case is given in Table A.9 of Appendix A.

Table A.7 in Appendix A provides estimated plant investments for the cases studied. A major portion of the total investment is associated with the sorbent regeneration facilites. Compressors represent approximately two-thirds of the total investment for regeneration equipment. If the spare compressors were eliminated, plant investment would be reduced by about 4 million dollars - a saving of close to 17 percent.

4.3.3.5 Processing Cost

The total annual processing cost presented in Table A.7 consists of four major items described below:

a) Direct Processing Cost

This consists of sorbent cost, labor cost, maintenance cost and utilities cost. The basis for estimating the labor cost and maintenance cost is stated in Section 4.3.2.

The utility cost was calculated as stated before.

The cost of pressure loss during regeneration consists of the cost of compressing the recycle gas and compressing fresh air. The cost of on-stream pressure loss was assumed to be equal to the increased power cost required to supply air at the incrementally higher pressure to the gasifier to overcome the pressure drop in the desulfurization unit. Credit for steam produced in the plant partially offsets the high utility cost. In computing the actual steam credit, steam required for purging reactors and sealing the reactor valves was deducted from the total steam produced.

b) Indirect Processing Cost

The indirect processing cost consists of the plant overhead. It is assumed to be 110 percent of the labor cost.

c) Fixed Processing Cost

The fixed processing cost consists of depreciation and insurance and property taxes. Depreciation is assumed to be linear and calculated for a plant life of 20 years. Insurance and property taxes are assumed to be 2.3 percent of the investment.

d) General Expenses

The processing cost is calculated by adding direct processing cost, indirect processing cost and fixed processing cost. General expenses consist of administration and finance charges. Administration expenses are assumed to be 3 percent of the processing cost. Finance charges are assumed to be 9 percent of investment.

The total annual processing cost is calculated by adding direct processing cost, indirect processing cost, fixed processing cost and general expenses.

Details of estimating each cost component are given in Appendix A. The total annual processing cost can be reduced to a simple formula:

$$T = 1.03(A + U_T) + 2.163C_L + 0.1961C_T$$

where T = total annual processing cost

A = annual sorbent cost

U_T = net utility cost

C_L = labor cost

C_T = total plant investment

Under the assumptions made the labor costs are independent of the plant design, the net utility costs are very small, and the total costs are a strong function of sorbent cost and plant investment.

4.3.4 Plan of Cases for Economic Study

The process variables examined for economic sensitivity and the values at which the analysis was done are given below.

Operating Variables

Producer Gas Velocity, ft/sec	2.2,	3.2,	4.5,	5.5,
Operating Pressure, psig	100,	150,	400,	
Onstream Cycle Length, hours	4,	8,	16,	

Pellet Properties

Iron Oxide Content of Sorbent, wt. %	21,	42,	63,	80,
Pellet Diameter, inches	1/8,	1/4,	1/2,	
Sorbent Life, Years	1/2,	1,	2,	
Nominal Sorbent Cost, Dollars/Lb	1,	2,		

Table 4.2 is a summary of the cases studied in the economic analysis. Most of the design variables were studied by holding all variables but one at base values. Some cases considered the possible interaction of two variables; these studies were made for the most important variables. The plan for the cases is presented below.

Iron Oxide Content

The effect of iron oxide content of the sorbent was studied at the constant conditions of 8 hours onstream period, 3.2 ft/sec producer gas linear velocity, 150 psig pressure, one year sorbent life, and 1/4 inch pellet diameter. The sorbent cost was assumed to increase slightly with iron oxide content. The following cases demonstrate the effect of iron oxide content.

Iron Oxide Content, Wt. %	Sorbent Price, Dollar/Lb	Case No.
21	0.95	8
42	1.00	1 (Base)
63	1.05	9
80	1.20	12

TABLE 4.2

ECONOMIC CASES STUDIED

[ ] DENOTES VARIABLE ALTERED FROM BASE VALUE

Case No	Onstream Time, Hr	Producer Gas Velocity, Ft/Sec	Pressure, psig(1)	Sorbent Life, Years	Iron Oxide, Wt. % in Sorbent	Pellet Diameter, Inches	Sorbent Cost, $/Lb
1	8	3.2	150	1.0	42	0.25	1.00 base
2	8	3.2	150	1.0	42	[0.125]	1.00
3	8	3.2	150	1.0	42	[0.50]	1.00
4	8	3.2	150	[0.5]	42	0.25	1.00
5	8	3.2	150	[2.0]	42	0.25	1.00
6	8	3.2	150	1.0	42	0.25	[2.00]
7	8	3.2	150	[2.0]	42	0.25	[2.00]
8	8	3.2	150	1.0	[21]	0.25	0.95
9	8	3.2	150	1.0	[63]	0.25	1.05
10	8	3.2	150	1.0	[63]	[0.125]	1.05
11	8	3.2	150	1.0	[63]	[0.50]	1.05
12	8	3.2	150	1.0	[80]	0.25	1.20
13	8	3.2	150	1.0	[80]	0.25	[2.00]
14	8	3.2	150	[2.0]	[80]	0.25	1.20
15	[4]	3.2	150	1.0	42	0.25	1.00
16	[16]	3.2	150	1.0	42	0.25	1.00
17	8	[2.2]	150	1.0	42	0.25	1.00
18	8	[4.5]	150	1.0	42	0.25	1.00
19	8	[5.5]	150	1.0	42	0.25	1.00
20	8	3.2	[400]	1.0	42	0.25	1.00
21	8	3.2	[400]	1.0	42	[0.125]	1.00
22	8	3.2	[400]	1.0	42	[0.5]	1.00
23	8	3.2	[100]	1.0	42	0.25	1.00
24	8	3.2	[100]	1.0	42	[0.125]	1.00
25	8	3.2	[100]	1.0	42	[0.5]	1.00

(1) Refers to operating pressure during sorption and regeneration

Linear Gas Velocity

Effect of producer gas linear velocity was studied at the constant conditions of 8 hour onstream time, 150 psig pressure, one year sorbent life, 42 percent iron oxide content of the sorbent, 1/4 inch pellet diameter, and one dollar/lb sorbent cost. The following cases demonstrate the effect of producer gas linear velocity.

Producer Gas Linear Velocity, ft/sec	Case No.
2.2	17
3.2	1
4.5	18
5.5	19

Pressure/Pellet Diameter

Effect of reactor pressure and pellet diameter was studied at three values of pressure and three values of pellet diameter. Constant conditions for this study were: 8 hour onstream time, 3.2 ft/sec linear gas velocity, 42 percent iron oxide in the sorbent, one year sorbent life and one dollar/lb sorbent cost. The following table lists the cases demonstrating the effect of pressure/pellet diameter. The circled numbers refer to case numbers in Table 4.2.

		Reactor Pressure, psig		
		100	150	400
Pellet Diameter, inches	0.125	(24)	(2)	(21)
	0.25	(23)	(1) base	(20)
	0.50	(25)	(3)	(22)

Onstream Cycle Length

Effect of onstream cycle length was studied at the constant conditions of 3.2 ft/sec linear gas velocity, 150 psig pressure, one year sorbent life, 42 percent iron oxide content, 1/4 inch pellet diameter, and one dollar/lb sorbent cost. The following cases demonstrate the effect of onstream length.

Cycle Length, hours	Case No.
4	15
8	1
16	16

Pellet Diameter/Iron Oxide Content

The effect of pellet diameter and iron oxide content of the sorbent was studied at three values of pellet diameter and two values of iron oxide content. Constant conditions were: 8 hour onstream time, 3.2 ft/sec producer gas linear velocity, 150 psig pressure and one year sorbent life. The following table lists the cases demonstrating the effect of pellet diameter/iron oxide content.

		Pellet Diameter, inch		
		0.125	0.25	0.5
Iron Oxide Content, wt. %	42	(2)	(1) base	(3)
	63	(10)	(9)	(11)

Sorbent Life/Iron Oxide Content

The effect of sorbent life was studied at two values of iron oxide content. Constant conditions were: 8 hour onstream time, 3.2 ft/sec producer gas velocity, 150 psig pressure, and 1/4 inch pellet diameter. The following cases demonstrate the effect of sorbent life at two levels of iron oxide content.

Iron Oxide Content of Sorbent, wt. %	Sorbent Life, Years 0.5	1	2
42	(4)	(1) base	(5)
80	-	(12)	(14)

Sorbent Cost/Iron Oxide Content

The effect of sorbent cost was studied at two values of iron oxide content. Constant conditions were: 8 hour onstream time, 150 psig operating pressure, 3.2 ft/sec producer gas linear velocity, one year sorbent life, and 1/4 inch pellet diameter. The effect was investigated at 42 and 80 percent iron oxide levels. The nominal sorbent costs were $1.0 dollar/lb and $2.0 dollars/lb. The following cases describe the effect of sorbent cost and iron oxide content.

Iron Oxide Content of Sorbent, wt. %	Nominal Sorbent Price, Dollars/Lb 1	2
42	(1) base	(6)
80	(12)	(13)

Results of the analysis described in this section are summarized in Section 4.4.

4.4 Results

This section contains an analysis of the results. A qualitative treatment is presented in Sections A.1 through A.6 of Appendix A for a better understanding of the trends and trade-offs observed in evaluating the impact of process variables. Section 4.4.1 contains the results of the economic analysis for cases described in Table 4.2. Conclusions and recommendations of this analysis are given in a separate section.

4.4.1 Quantitative Analysis

This section contains results of the cases described in Table 4.2. Details associated with process design are given in Appendix A. In this section, effects of process variables on the plant investment, sorbent cost, utility cost and total processing cost are illustrated in a graphical form. Observed trends and trade-offs are considered, and an attempt is made to optimize the variables.

Details of the reactor are given in Figure A.1 and Table A.2 of Appendix A. For the cases studied, the reactor volume varies from 1090 ft^3 to 7235 ft^3.

Specifications for air compressors and the recycle gas compressor are given in Table A.2 of Appendix A. For a typical case, nine air compressors of 1070 BHP each and three recycle gas compressors of 2500 BHP each are provided.

The heat duty, required surface area and material of construction for the heat exchangers are given in Table A.4 of Appendix A. Hot regeneration gas/effluent is the most expensive heat exchanger. Specifications for miscellaneous items are given in Tables A.3 and A.5 of Appendix A.

Table A.6 in Appendix A summarizes the estimated annual sorbent and utility costs for all cases. It lists the sorbent requirements, pressure drop across the reactor during onstream and regeneration period and cost of the pressure drop. Net utility cost was calculated by deducting the net credit for steam generation from the total power cost. The net credit for steam generation was found to be quite significant compared to the total power cost. Hence in several cases the net utility costs are nearly zero.

Table A.7 in Appendix A lists a breakdown of the plant investment cost and processing cost for each case.

Table 4.3 extracts the pertinent information from Table A.7. A detailed analysis of the results is given below.

TABLE 4.3

SUMMARY OF RESULTS FOR THE ECONOMIC CASES STUDIED[1]

Case No.	Plant Investment, MM $	Sorbent Cost, Cents/MM BTU	Utility Cost,[2] Cents/MM BTU	Total Processing, Cost, Cents/MM BTU
1	23.300	5.07	0.82	21.0
2	23.895	4.78	2.27	22.6
3	23.570	5.91	0.26	21.5
4	23.300	10.15	0.82	26.3
5	23.300	2.54	0.82	18.4
6	23.300	10.15	0.82	26.3
7	23.300	5.07	0.82	21.0
8	25.460	9.13	2.14	27.9
9	22.650	3.83	0.34	18.9
10	22.550	3.43	1.11	19.2
11	22.900	4.91	0.04	19.8
12	22.410	3.69	0.16	18.4
13	22.410	6.15	0.16	20.9
14	22.410	1.84	0.16	16.5
15	22.610	2.80	0.30	17.8
16	25.460	9.60	1.89	28.1
17	25.230	5.15	0.11	21.5
18	22.970	4.99	2.66	22.7
19	23.320	4.96	4.73	25.0
20	25.590	4.85	2.37	23.8
21	26.200	4.67	5.82	27.5
22	25.550	5.38	0.85	22.7
23	24.120	5.19	1.18	22.0
24	24.630	4.83	2.27	23.1
25	24.400	6.18	0.75	22.8

(1) Process variables for these cases are given in Table 4.2

(2) Utility cost of 1 cent/MM BTU corresponds to utility requirement of 1422 BTU/MM BTU.

Effect of Iron Oxide Content of the Sorbent

Increasing the iron oxide content of the absorbent decreases the reactor size and the pressure drop. Figure 4.3 shows that the plant investment drops to $22.4 million and the utility costs decrease to 0.16 cents/million BTU by increasing the iron oxide content to 80 percent. Although the total absorbent cost per pound increases with iron oxide content, the absorbent cost in the process decreases with iron oxide content. Figure 4.3 shows that the total processing costs decrease monotonically with increasing iron oxide content.

Plant investment, total processing cost, sorbent and utility costs are all nearly insensitive to iron oxide contents between 40 and 80 percent. Development of 80+ percent sorbents is not warranted based on these studies.

FIGURE 4.3

EFFECT OF IRON OXIDE CONTENT OF THE SORBENT ON PROCESS ECONOMICS

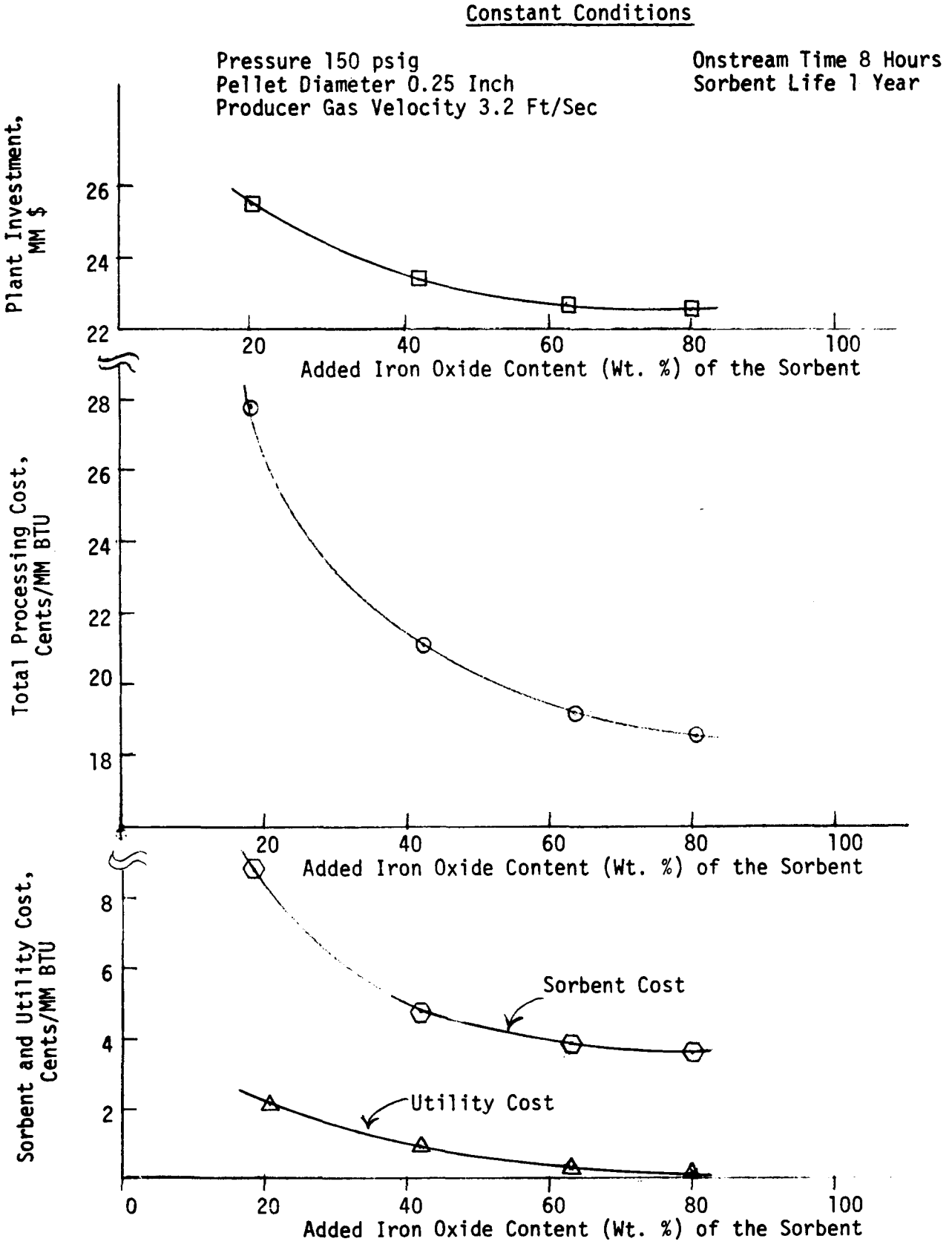

Effect of Superficial Velocity of the Producer Gas

Figure 4.4 shows the changes in plant investment, sorbent cost and total processing cost as the superficial velocity of the producer gas is changed from 2.2 ft/sec to 5.5 ft/sec.

The sorption efficiency of the sorbent increases only slightly as the superficial velocity of the producer gas increases. Hence the sorbent bed volume remains nearly constant as the superficial gas velocity changes. An increase in superficial gas velocity results in a decrease in reactor diameter at a fixed producer gas rate. Since the total bed volume is constant, a decrease in bed diameter is accompanied by an increase in reactor length. The cost of the reactor decreased with an increase in superficial gas velocity over the range studied.

Pressure drop across the reactor is proportional to length of the bed and square of gas velocity. Hence pressure drop increases at higher velocity. The compressor investment also increases somewhat with gas velocity.

Combined result of the changes in reactor cost and compressor cost is reflected in the plant investment cost. Figure 4.4 shows that beyond a velocity of 3 ft/sec, the plant investment is rather insensitive to the changes in velocity. The details of the investment costs appear in Table A.7.

The sorbent requirement, and hence sorbent cost, remains nearly unchanged with an increase in gas velocity. The increase in pressure drop at a higher gas velocity increases the power requirements for compressors and total utility cost.

Total processing cost, which includes contributions from both plant investment and utility cost, shows a shallow minimum around linear gas velocity of 3.2 ft/sec. Sorption gas velocities between 2.0 and 5.0 ft/sec are acceptable.

FIGURE 4.4

EFFECT OF SUPERFICIAL VELOCITY OF

THE PRODUCER GAS ON PROCESS ECONOMICS

Constant Conditions

Operating Pressure 150 psig
Sorbent Life 1 Year
Onstream Time 8 Hours

Iron Oxide Content in Sorbent Wt. %
Pellet Diameter 0.25 Inch
Sorbent Cost $1.00/Lb

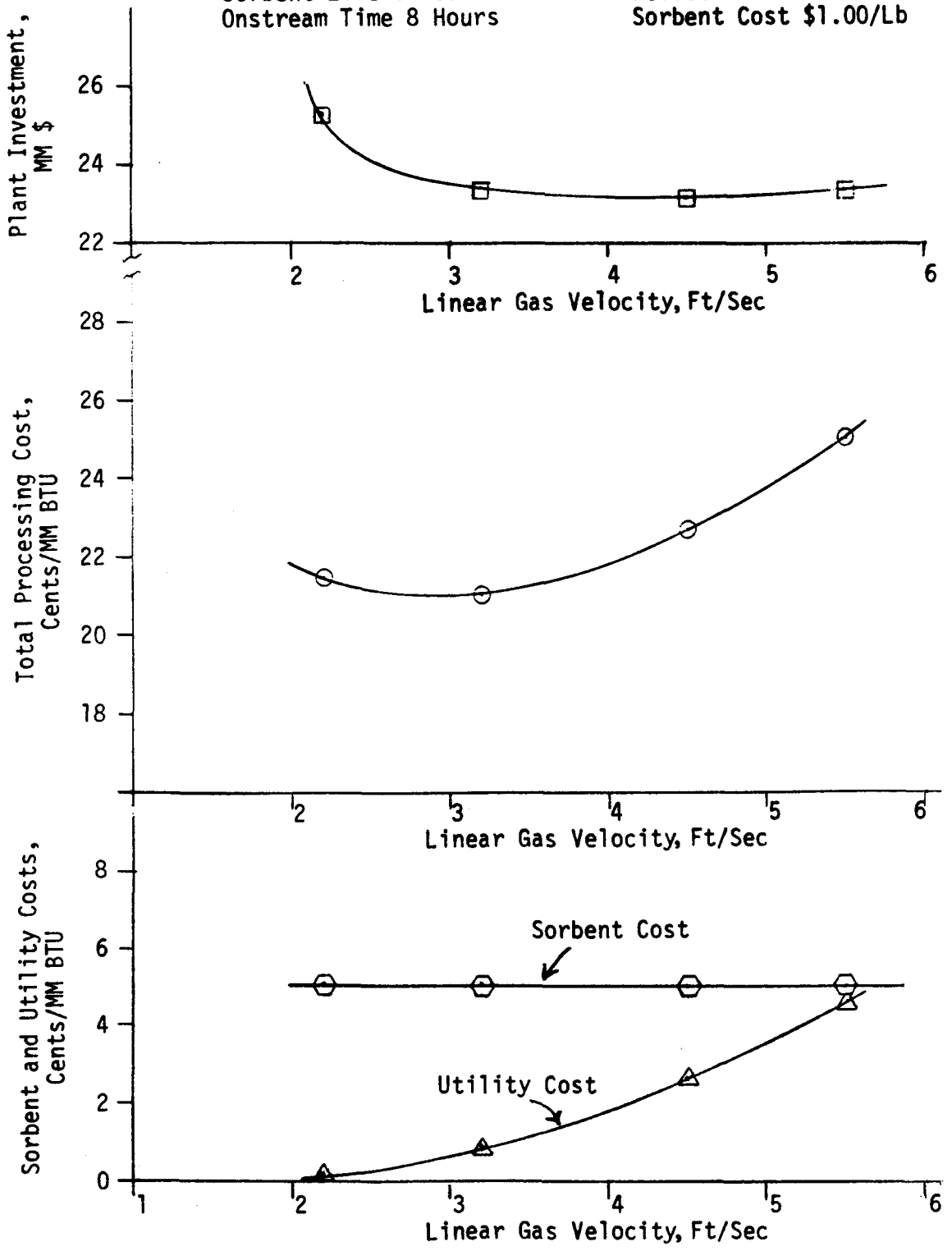

Effect of Pressure

Figures 4.5, 4.6 and 4.7 show the changes in plant investment, sorbent cost, utility cost and total processing cost as the reactor operating pressure changes from 100 to 400 psi for three different pellet sizes.

The volumetric flow rate of the producer gas decreases with increasing pressure. At constant linear gas velocity the diameter of the reactor decreases and the length increases with increasing pressure. The shell thickness increases with pressure at a given diameter. For the cases studied the decrease in reactor cost due to a decrease in the diameter was found to be greater than the increase in reactor cost due to an increase in the shell thickness and length. Hence the reactor cost was found to decrease with an increase in pressure.

The cost of the make-up air compressors increases and investment for recycle gas compressor decreases with an increase in the operating pressure level. Section A.2.3.1-3 in Appendix A explains why such trends are observed. Cost of other equipment such as heat exchangers and heater increases somewhat with an increase in the operating pressure.

The combined effect of all equipment costs is that the plant investment cost goes through a shallow minima with an increase in pressure.

The sorption efficiency estimated by the expression in Section A.2.2.1 of Appendix A increases slightly with an increase in pressure. Hence the sorbent requirement and sorbent cost decrease slightly with an increase in pressure.

As operating pressure increases at fixed linear velocity, the pressure drop across the bed increases due to the increase in bed depth. This results in an increased cost of onstream pressure loss. The cost of compressed air for regeneration also increases with an increase in the operating pressure. The cost of compressing the recycle gas decreases with increasing operating pressure; the compression ratio (P_{out}/P_{in}) decreases. As a result, the utility cost is lowest at 150 psig.

The combined effect on processing cost is that it shows a minimum around 150 psig.

The pressure effect was investigated at three different particle sizes: 1/8, 1/4 and 1/2 inch. Qualitatively, the same trends are observed. The utility costs of 400 psi for 1/8 inch pellets are very high due to the large onstream pressure loss.

The total processing costs for the three pellet sizes are shown in Figures 4.5, 4.6 and 4.7. These figures show that the 1/4 inch pellets give lower cost for operation below 220 psig and 1/2 inch pellets above 220 psig. The variation in costs is very small.

Based on these studies, the optimum pressure for the total operation (gasification, desulfurization and power generation) should be determined from gasification and power generation economics.

FIGURE 4.5

EFFECT OF PRESSURE LEVEL FOR 1/8 INCH PELLETS ON PROCESS ECONOMICS

Constant Conditions

Pellet Diameter 1/8 Inch
Onstream Time 8 Hours
Producer Gas Velocity 3.2 Ft/Sec
Iron Oxide Content 42 Wt. %
Sorbent Life 1 Year
Sorbent Cost $1.00/Lb

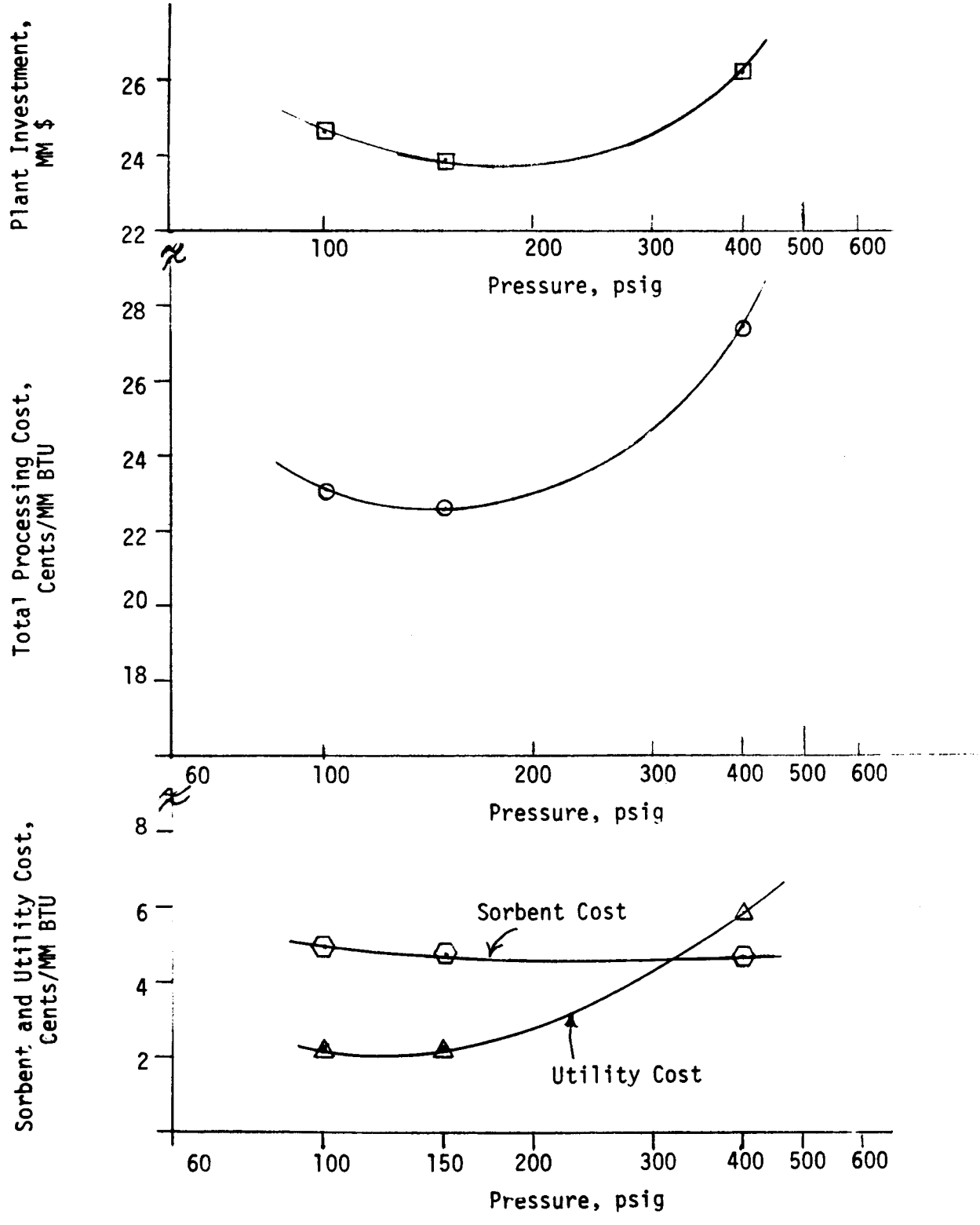

FIGURE 4.6

EFFECT OF PRESSURE LEVEL FOR 1/4 INCH PELLETS ON PROCESS ECONOMICS

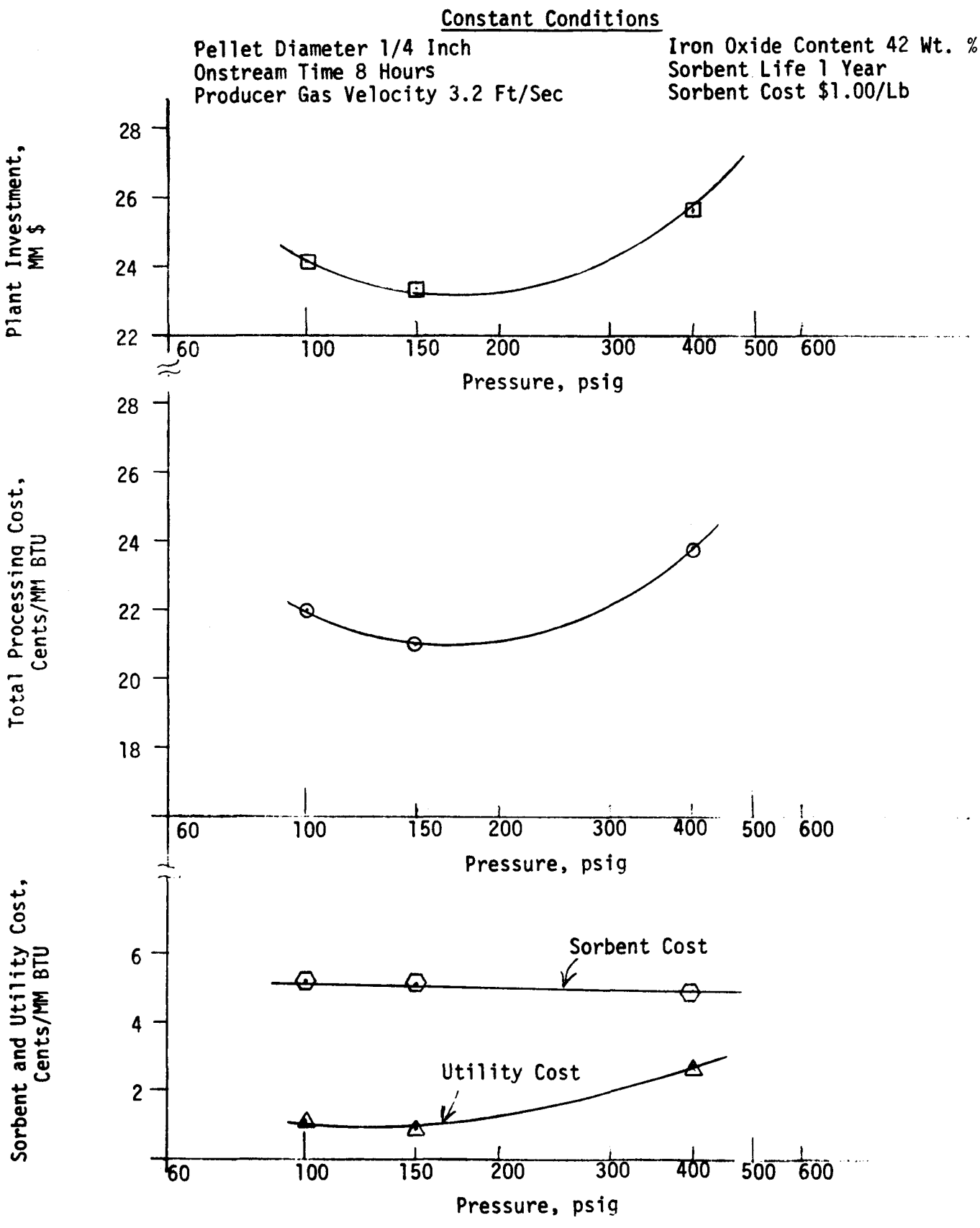

FIGURE 4.7

EFFECT OF PRESSURE LEVEL FOR 1/2 INCH PELLETS ON PROCESS ECONOMICS

Constant Conditons

Pellet Diameter 1/2 Inch
Onstream Time 8 Hours
Producer Gas Velocity 3.2 Ft/Sec

Iron Oxide Content 42 Wt. %
Sorbent Life 1 Year
Sorbent Cost $1.00/LB

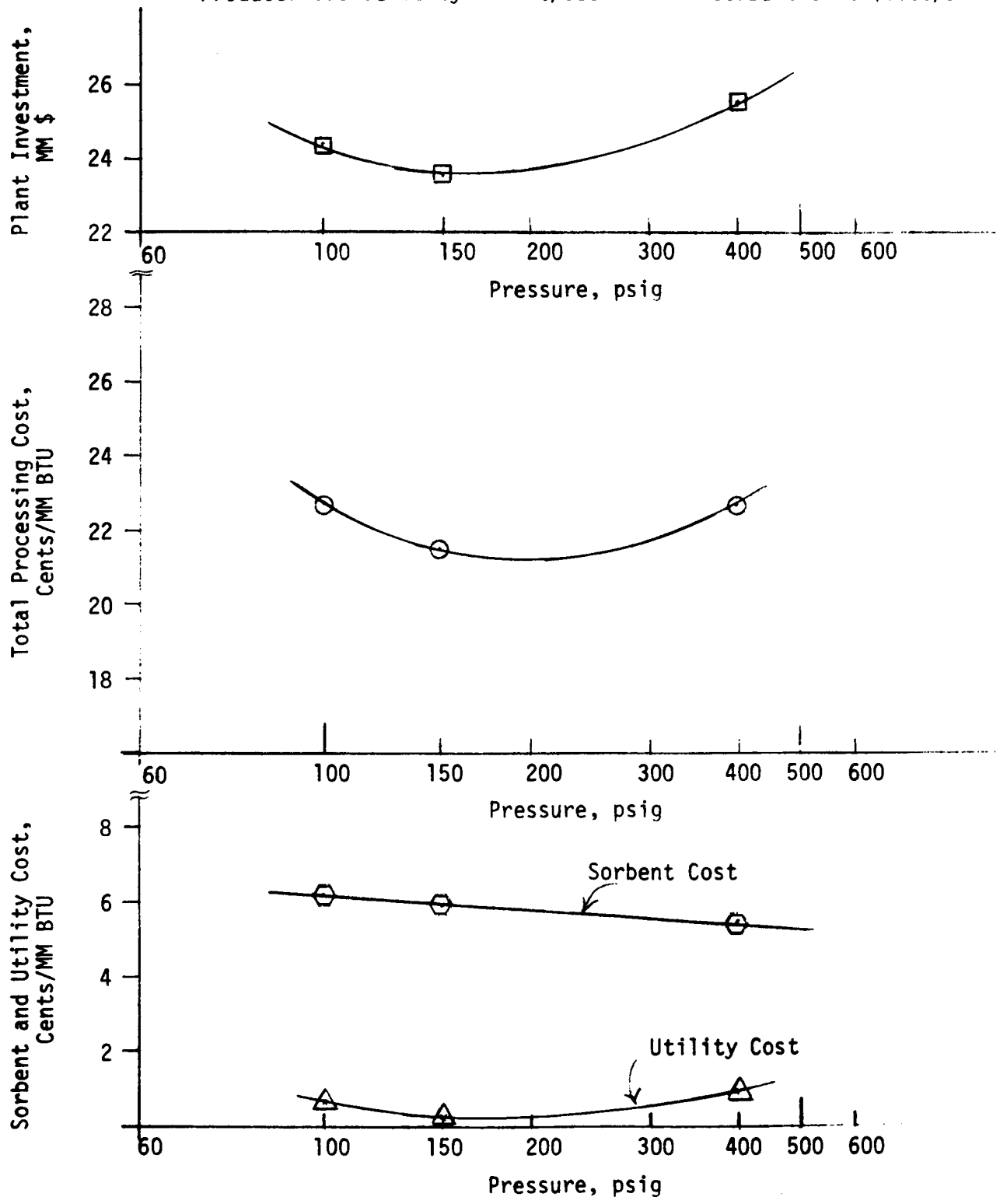

Effect of Pellet Size

Figures 4.8 and 4.9 show the effect of pellet size on the investment and processing cost at two levels of iron oxide content.

The sorption efficiency of the sorbent decreases slightly as the pellet diameter increases. Hence the reactor volume and reactor cost increase slightly as the pellet size increases. The sorbent requirement and sorbent cost also increase as the pellet size increases.

The pressure drop across the bed decreases as the pellet size increases. Hence the utility cost and investment for compressors decrease with an increase in pellet size.

At 63 percent iron oxide content, the total plant investment is relatively insensitive to the pellet size due to the opposing effects on reactor costs and compressor costs. At 42 percent iron oxide, a shallow minima in plant investment is seen.

The total processing cost shows a shallow minima between 3/8 and 1/4 inch pellet diameter for both 42 percent and 63 percent iron oxide content. The shallow minima in plant investment and processing cost indicate that changes in the pellet size do not have much impact on the processing cost.

All the costs are lower with 63 percent iron oxide content compared to 42 percent iron oxide content in the sorbent. This relation is explained later in "Effect of Iron Oxide Content of the Sorbent".

FIGURE 4.8

EFFECT OF PELLET SIZE FOR
42 WEIGHT PERCENT IRON OXIDE SORBENT ON PROCESS ECONOMICS

Constant Conditions

Operating Pressure 150 psig
Sorbent Life 1 Year
Onstream Time 8 Hours
Iron Oxide Content in Sorbent 42 Wt. %
Sorbent Cost $1.00/Lb
Producer Gas Velocity 3.2 Ft/Sec

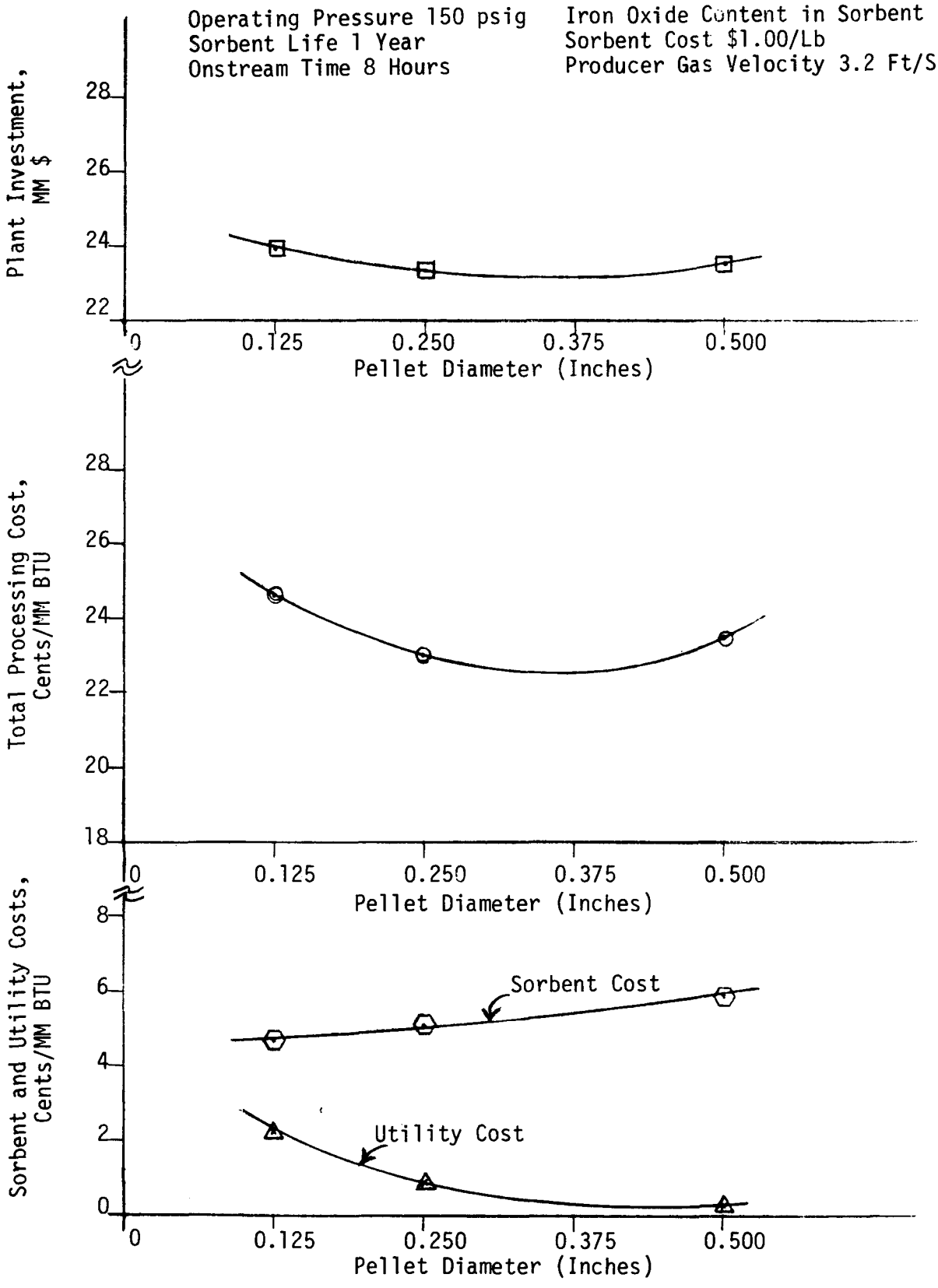

FIGURE 4.9

EFFECT OF PELLET SIZE FOR

63 WEIGHT PERCENT IRON OXIDE SORBENT ON PROCESS ECONOMICS

Constant Conditions

Operating Pressure 150 psig
Sorbent Life 1 Year
Onstream Time 8 Hours
Iron Oxide Content in Sorbent 63 Wt.%
Sorbent Cost $1.00/Lb
Producer Gas Velocity 3.2 Ft/Sec

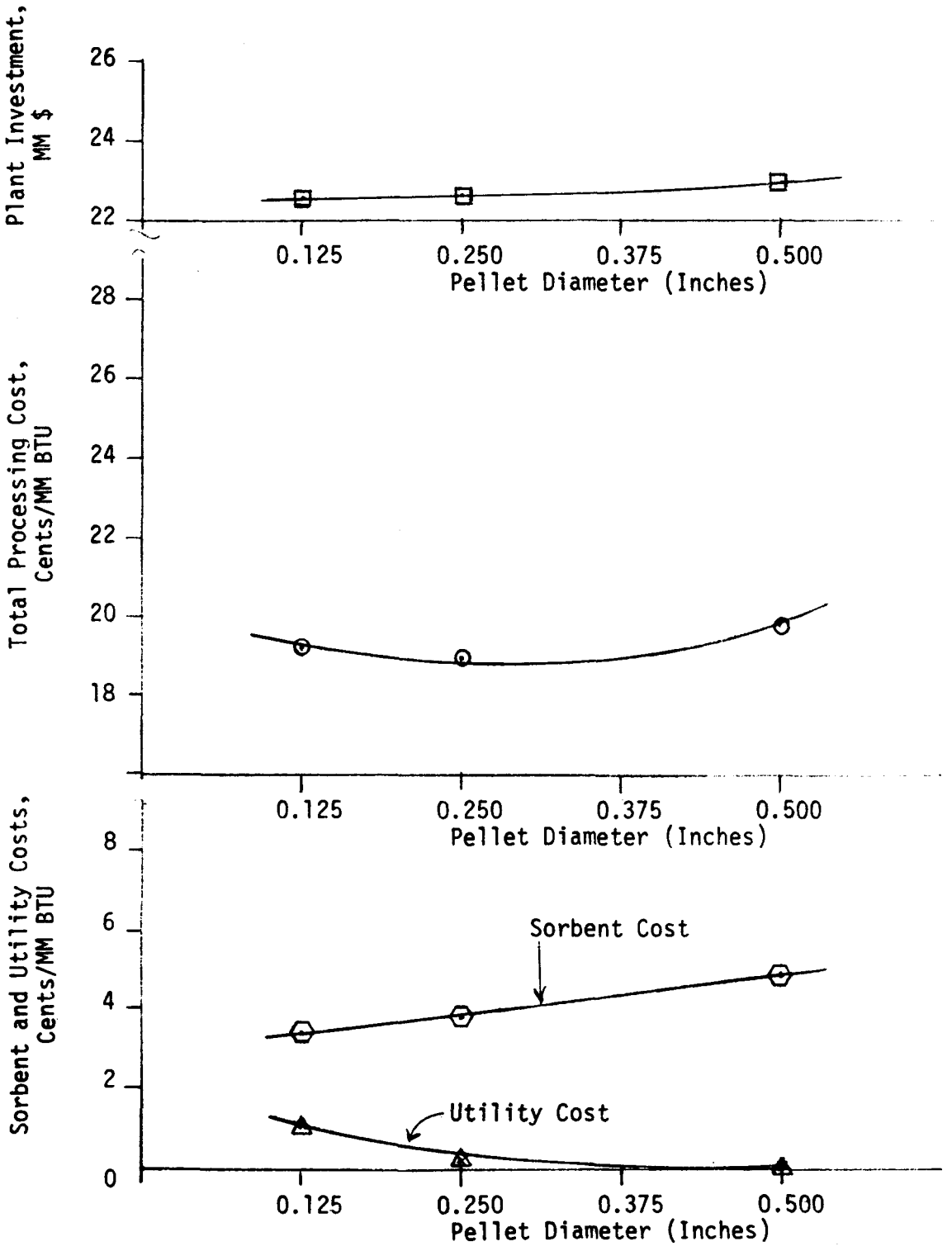

Effect of Onstream Cycle Length

Figure 4.10 illustrates the effect of onstream cycle length on the investment and processing cost.

As the onstream cycle length decreases, the required sulfur absorption capacity and the sorbent requirement decrease. This results in a decrease in reactor volume, reactor cost and total plant investment.

At a fixed linear gas velocity, the decrease in reactor volume is achieved by a decrease in the bed depth. Lower bed depth results in a lower pressure drop and lower utility cost. Hence the utility cost decreases as the onstream cycle length decreases.

Since all major cost components decrease with a decrease in the cycle length, the total processing cost decreases significantly with a decrease in onstream cycle length.

FIGURE 4.10

EFFECT OF ONSTREAM CYCLE LENGTH ON PROCESS ECONOMICS

Constant Conditions

Sorbent Cost $1.00/Lb
Producer Gas Velocity 3.2 Ft/Sec
Operating Pressure 150 psig
Sorbent Life 1 Year
Iron Oxide Content of Sorbent 42 Wt.%
Pellet Diameter 0.25 Inch

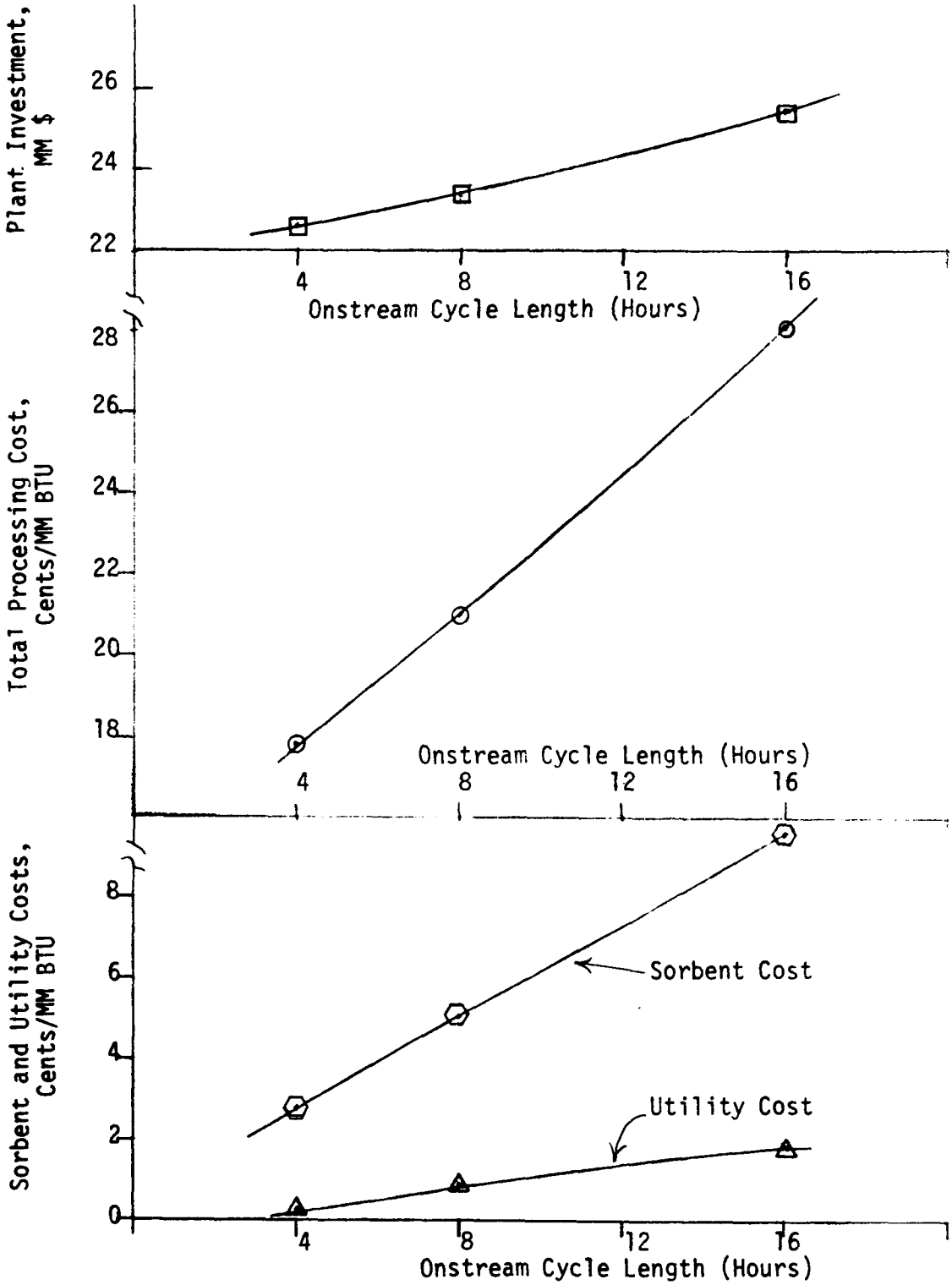

Effect of Sorbent Life

Figure 4.11 illustrates the effect of sorbent life on the total sorbent cost and processing cost at different sorbent prices. Figure 4.12 illustrates the effect of sorbent life on the total sorbent cost and processing cost at different iron oxide levels.

The annual sorbent cost decreases as the sorbent life increases. The cost of sorbent was found to be the most important component of sorbent replacement cost. Labor requirement for sorbent changeover is negligible compared to the cost of sorbent. Since one spare desulfurization reactor is provided, there is no loss of production during sorbent changeover.

The plant investment and utility cost are independent of sorbent life. The total processing cost decreases significantly with an increase in sorbent life due to a decrease in sorbent cost.

Since the cost of labor required for sorbent change is a negligible fraction of the total sorbent cost, the effect of doubling sorbent life is the same as reducing the sorbent price by half. Figure 4.11 shows that for sorbent containing 42 percent iron oxide, the processing cost change when doubling the sorbent life from one year to two years at $2.0/lb sorbent price is the same as reducing the price from $2.0/lb to $1.0/lb at one year sorbent life.

Similar trends are observed for sorbents containing 42 percent iron oxide and 80 percent iron oxide.

FIGURE 4.11

EFFECT OF SORBENT LIFE AT

DIFFERENT SORBENT PRICES ON PROCESS ECONOMICS

Constant Conditions

Operating Pressure 150 psig
Producer Gas Velocity 3.2 Ft/Sec
Onstream Time 8 Hours

Pellet Diameter 0.25 Inch
Iron Oxide Content 42 Wt. %

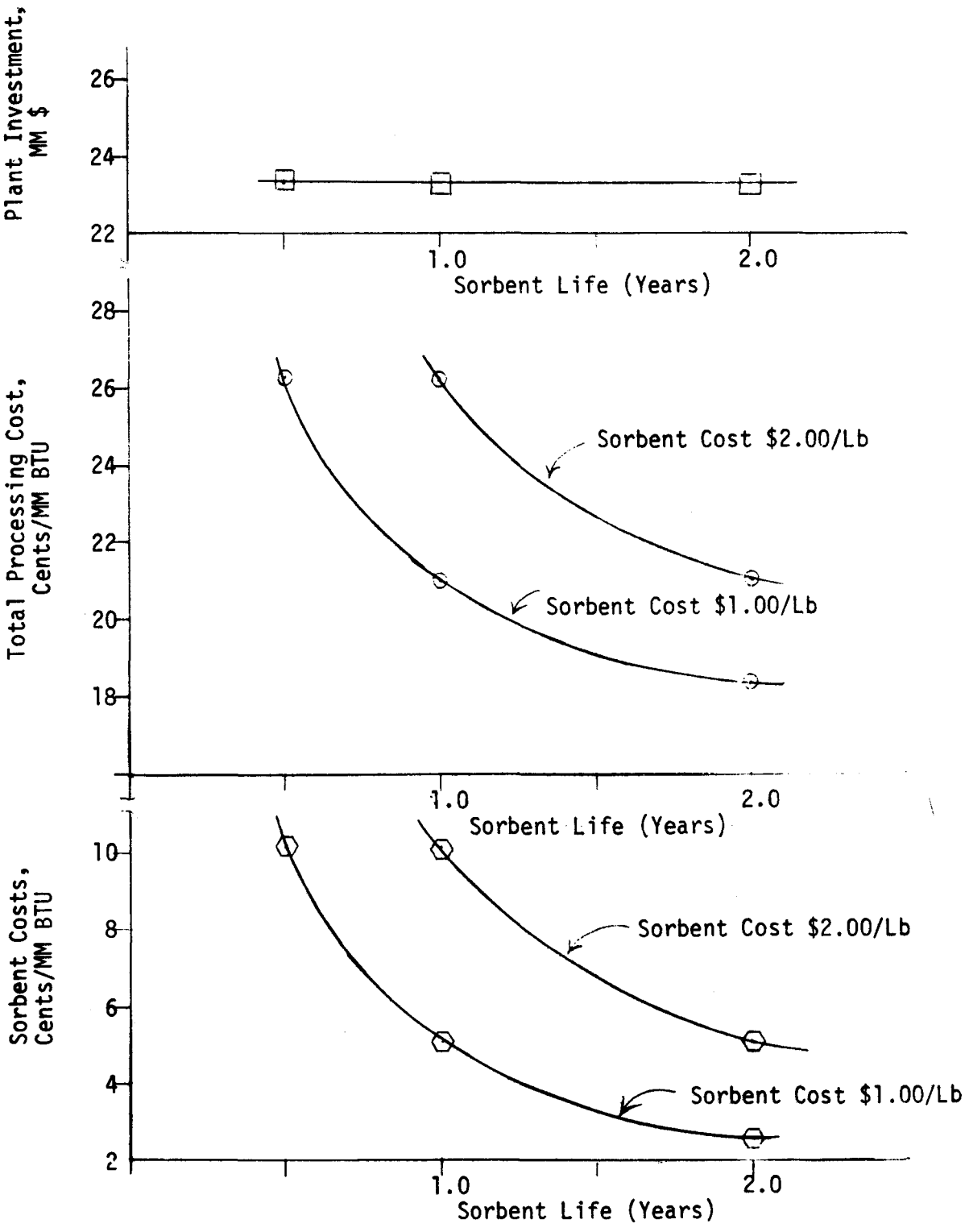

FIGURE 4.12

EFFECT OF SORBENT LIFE AT

DIFFERENT IRON OXIDE CONTENT ON PROCESS ECONOMICS

Constant Conditions

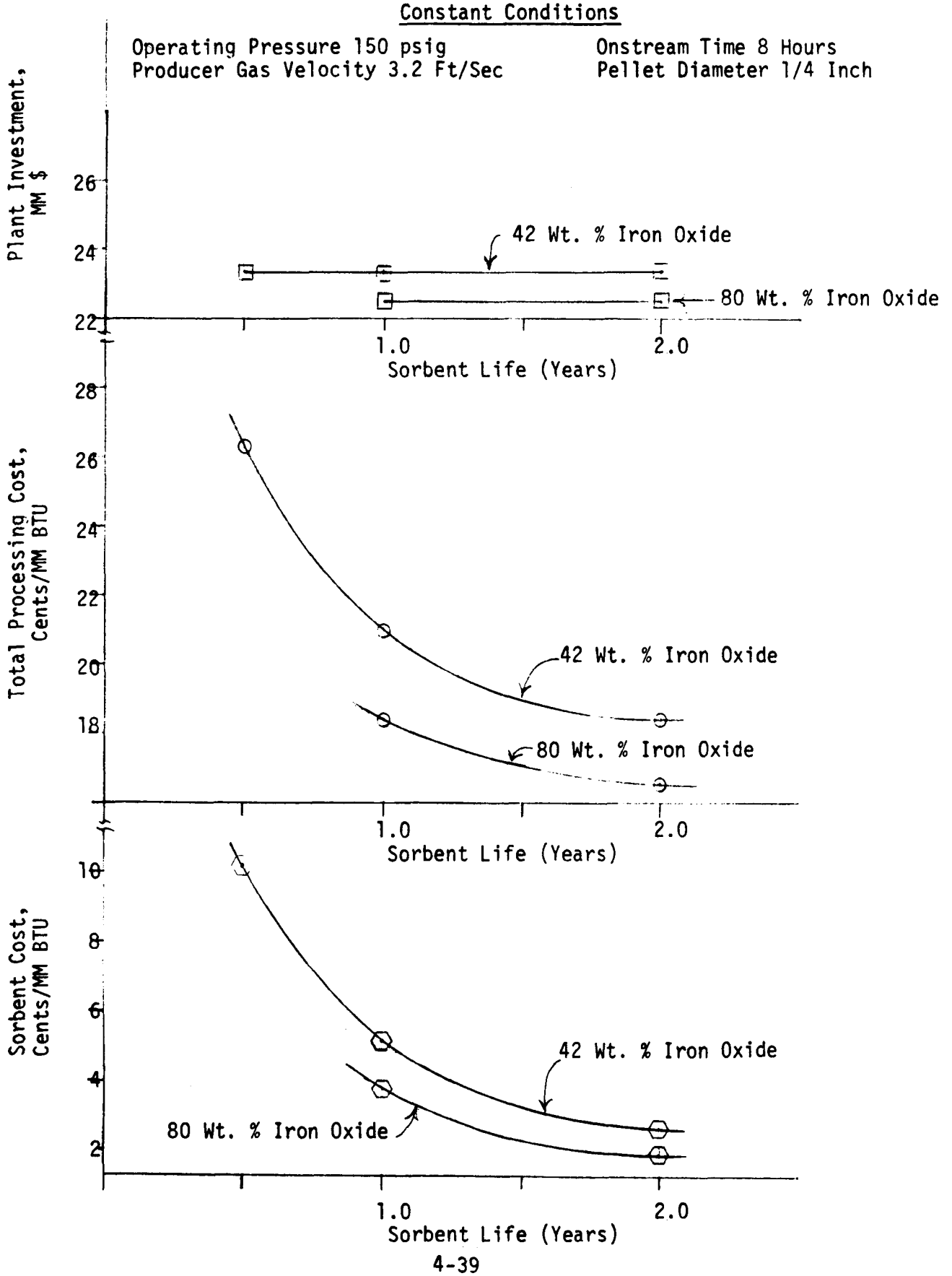

Effect of Sorbent Price

Figure 4.13 illustrates the effect of sorbent price on the sorbent cost and total processing cost.

As the sorbent price increases, the sorbent cost increases at fixed sorbent requirement. Plant investment and utility cost remain unchanged. Sorbent cost is a significant fraction of the total processing cost. Hence total processing cost increases as sorbent price increases.

The processing cost is more sensitive to the sorbent price at 42 percent iron oxide content than at 63 percent iron oxide content. This observation is not surprising. At a lower iron oxide content, the sorbent requirement is high and the sorbent cost is a greater fraction of the processing cost.

Summary

Figures 4.3 through 4.12 present a complex array of data which should be simplified.

Table 4.4 presents a summary of the results from the 25 design cases as a list of design factors with the most advantageous values of these factors.

FIGURE 4.13

EFFECT OF SORBENT PRICE ON PROCESS ECONOMICS

Constant Conditions

Operating Pressure 150 psig
Producer Gas Velocity 3.2 Ft/Sec
Sorbent Life 1 Year
Pellet Diameter 0.25 Inch

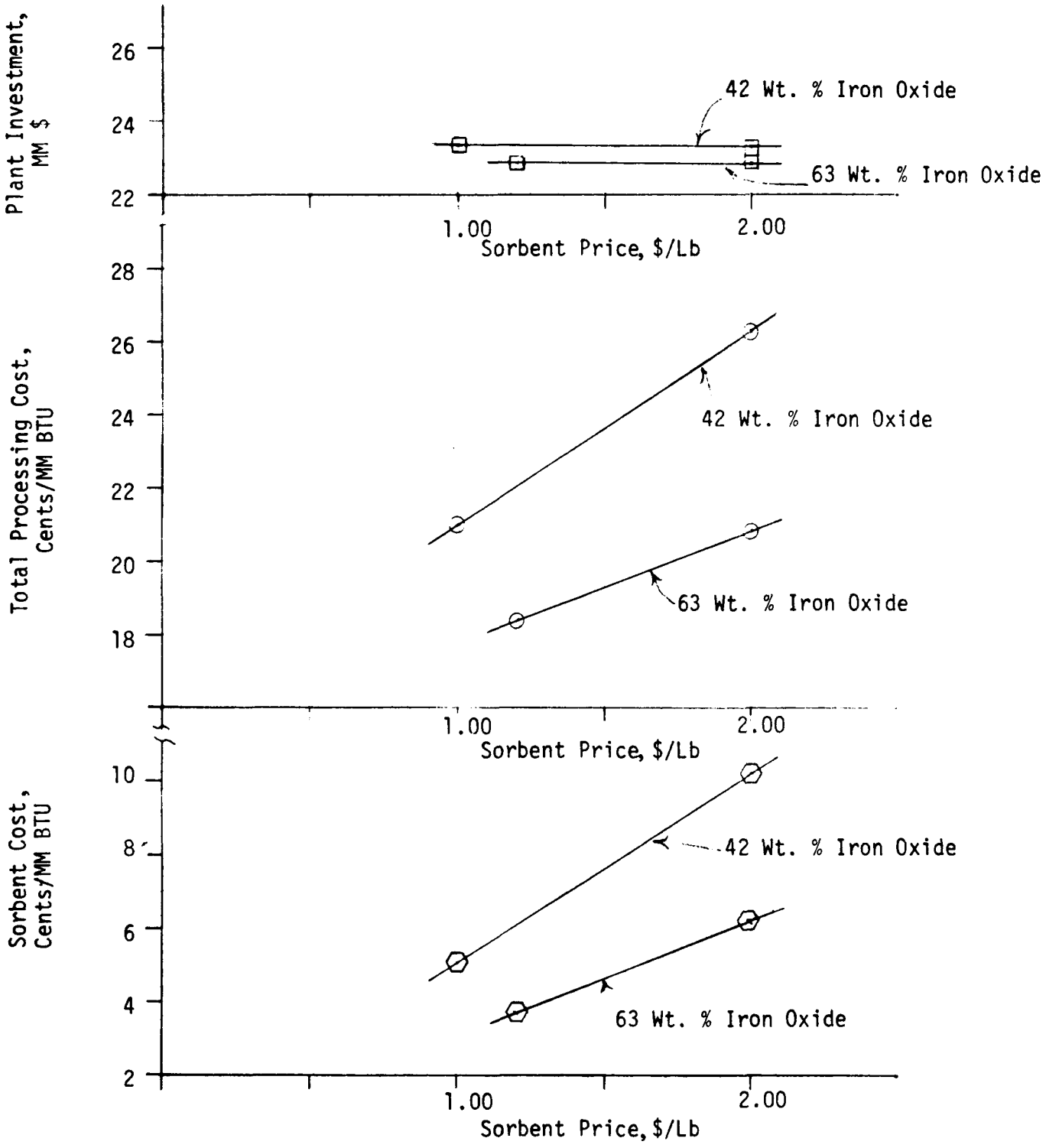

TABLE 4.4

SUMMARY OF THE RESULTS

Factor	Result
a) Iron oxide content of sorbent	• Use maximum possible. Recommend 80 percent by weight.
b) Linear gas velocity	• Processing cost has a shallow minimum at 3.2 fps.
c) Pressure - pellet size	• Processing cost has a shallow minimum around 3/8 inch pellet diameter. • Above 220 psi use 0.5 inch pellets. • Below 220 psi use 0.25 inch pellets.
d) Pellet size - iron oxide content	• Processing cost has a shallow minimum between 3/8 inch and 1/4 inch pellet diameter for sorbents containing 42 and 63 percent iron oxide.
e) Cycle length	• Use minimum possible. Recommend 2 hours.
f) Sorbent life	• Use maximum possible.
g) Sorbent price	• Use minimum possible.

4.4.2 Illustration of the Economic Model

Appendix A describes an economic model relating the investment and total process processing cost to the operating variables and sorbent properties. This model was derived from the cases described in this section. Calculations for the case studies were done using existing design computer programs which considered several details of the equipment such as reactor nozzles, insulation, and dome structure and hence provide a more realistic analysis. The case studies were used to obtain constants for the algebraic expressions described in the model.

The economic model described in Appendix A facilitates the understanding of the complex relationships of the operating variables with various cost components. The expressions developed in this section may be used to optimize the design with respect to all the variables.

The example given below illustrates the use of the expressions developed in Appendix A to extrapolate at different conditions. It also examines the effect of the choice of the velocity of producer gas for design at a set of conditions different from the base conditions described in Section 4.3. The fixed pellet characteristics and operating variables are:

Iron Oxide Content	-	80 Weight Percent
Pellet Diameter	-	1/4 Inch
Sorbent Life	-	1 Year
Cycle Length	-	2 Hours
Operating Pressure	-	150 psig

Sorption efficiency is calculated by the iteration method described in Section A.2.2.1. It is set at 0.8 in this illustration to simplify the calculations. The number of onstream reactors (N) is 4. Thus the total number of reactors provided is 9. The linear gas velocity is chosen. The reactor dimensions, reactor cost, pressure drop, utility requirement, compressor size and cost are determined using the equations given in Sections A.2.3.1-3. The cost or credit components that do not depend on velocity are: absorbent cost, labor cost, cost of air compressors, cost of heat exchangers, and utility costs for cooling water, regeneration air compression and credit for steam generation. The cost components that depend on velocity are the cost of onstream pressure loss, power requirement for the recycle gas compressor, investment cost for the reactors and recycle gas compressors.

All these cost components and total costs are evaluated for different values of linear gas velocity. Table 4.5 and Figure 4.14 summarize the results. Total processing cost has a shallow minimum around linear gas velocity of 5 ft/sec. However, the minimum is so shallow that the total processing cost does not change much between linear gas velocity of 3 ft/sec and 7 ft/sec.

TABLE 4.5

EFFECT OF VELOCITY ON THE INVESTMENT AND TOTAL PROCESSING COST

(Constant Conditions: Iron Oxide Content 80 Percent, Pellet Diameter 1/4 Inch, Sorbent Life 1 Year, Cycle Length 2 Hours, Operating Pressure 150 psi)

Velocity, Ft/Sec	Absorbent Cost, MM Dollars/Yr	Labor Cost, MM Dollars/Yr	Net Utility Cost, MM Dollars/Yr	Plant Investment, MM Dollars	Total Processing Cost, MM Dollars/Yr	Total Processing Cost, Cents/MM BTU
2	1.07715	0.1673	-0.4290	19.07	4.7690	14.21
3	1.07715	0.1673	-0.4014	16.35	4.2641	12.71
4	1.07715	0.1673	-0.3575	15.22	4.0877	12.18
5	1.07715	0.1673	-0.2947	14.67	4.0445	12.05
6	1.07715	0.1673	-0.2101	14.40	4.0787	12.15
7	1.77015	0.1673	-0.1007	14.05	4.1228	12.28

FIGURE 4.14

EFFECT OF SUPERFICIAL VELOCITY

OF THE PRODUCER GAS ON PROCESS ECONOMICS

Constant Conditions

Operating Pressure 150 psig
Sorbent Life 1 Year
Onstream Time 2 Hours
Iron Oxide Content 80 Wt. %
Pellet Diameter 0.25 Inch

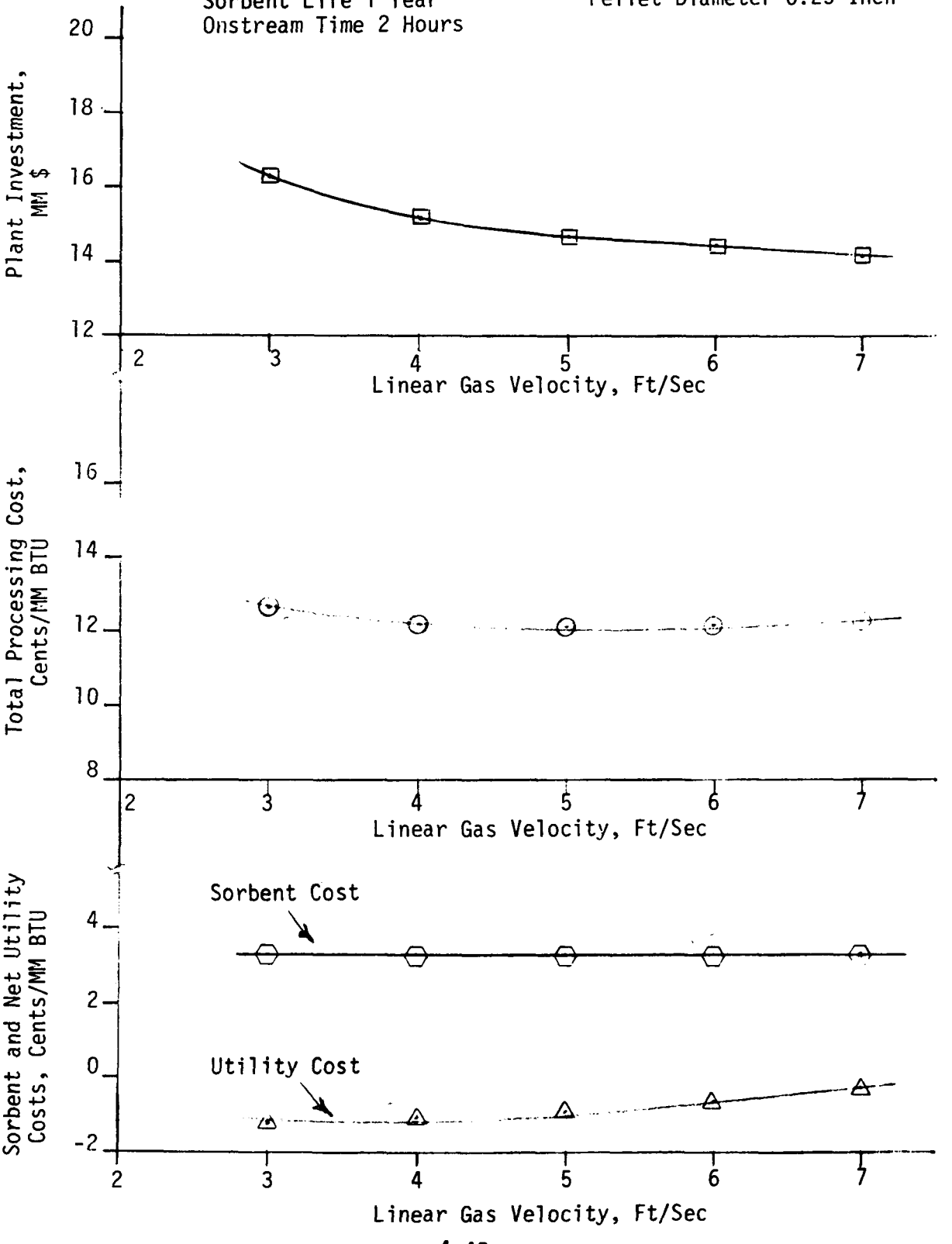

4.5 Conclusions

The following conclusions are drawn from the economic analysis.

1. The capital investment for a regenerative fixed-bed desulfurization unit based on iron oxide to process producer gas for a 500 megawatt generating plant is 22.4 to 26.2 million dollars for typical operating conditions. Compressors to recycle the large volume of effluents and air compressors to supply air for regeneration account for nearly 50 percent of the major equipment cost. Major contributions to the plant investment are given below for the base case.

	MM Dollars
Reactors	1.810
Heat Exchangers	1.678
Compressors	4.013
Drums	0.084
Heater	0.181
Other Items	15.534
Total Investment	23.300

2. The total processing cost for desulfurizing low-BTU producer gas ranges from 16.5 cents/MM BTU to 28.1 cents/MM BTU for typical operating conditions. Major contributions to the total processing cost are given below for the base case.

Component		Cost, Cents/MM BTU
Direct Processing Cost		8.51
Sorbent (42% Iron Oxide, One Year Lifetime)	5.06	
Labor	0.51	
Maintenance	2.12	
Net Utilities	0.82	
Indirect Processing Cost		0.55
Plant Overhead	0.55	
Fixed Processing Cost		5.15
Depreciation (20-Year Linear)	3.53	
Insurance & Property Tax (2.3% of Plant Investment)	1.62	
General Expenses		6.79
Administration	0.43	
Finance (9% Interest)	6.36	
Total Processing Cost		21.0

3. The highest possible iron oxide content of the sorbent should be used. Plant investment and total processing cost decrease monotonically with increasing iron oxide content of the sorbent.

4. Superficial velocity of the producer gas has a small effect on desulfurization economics. The total processing cost has a shallow minimum with respect to the superficial velocity of the producer gas.

5. Plant investment and the total processing cost have a shallow minimum with respect to the pressure at approximately 150 psig. The operating pressure of the desulfurizing unit is set externally by the pressure of the producer gas plant and power generating facility.

6. Pellet size has a small influence on th desulfurization economics. The total processing cost has a shallow minimum between 3/8 inch and 1/4 inch pellet diameter.

7. The shortest practically feasible onstream cycle length should be used since plant investment and total processing cost decrease sharply with a decrease in onstream cycle length.

8. Sorbent life and sorbent price have an important effect on the total processing cost due to the significant contribution of the sorbent cost to the total processing cost.

9. The following conditions are recommended as optimum based on the design cases presented in this section:

Iron Oxide Content of Sorbent	-	80 Weight Percent or Maximum Possible
Producer Gas Velocity	-	3.2 ft/sec
Operating Pressure	-	150 psi
Pellet Diameter	-	1/4 Inch
Onstream Cycle Length	-	4 Hours or Shortest Possible

This case was not in the list of cases planned for economic evaluation. However, the total processing cost for this case can be obtained by a limited extrapolation of the results from calculated cases. The total processing cost is estimated to be 16.5 cents/MM BTU. The estimated breakdown of different cost components for this case is given below.

Cost Component	Cost, Cents/MM BTU
Sorbent ($1.0/Lb, 1 Year Life)	2.03
Labor	0.51
Maintenance	2.03
Net Utilities	0.06
Plant Overhead	0.56
Depreciation (20-Year Linear)	3.37
Insurance & Property Tax (2.3% of Investment)	1.55
Administration	0.30
Finance (9% Interest)	6.07
Estimated Total Processing Cost	16.48

10. A calculation based on the economic optimization model given in Appendix A shows that the estimated total processing cost is further reduced to 12.05 cents/MM BTU if the onstream cycle length is reduced to 2 hours, the linear gas velocity is increased to 5 ft/sec, and all other conditions are the same as above.

11. The net utility requirement for desulfurizing hot, low-BTU producer gas is less than 0.5 percent of the heating value of the low-BTU producer gas.

5.0 EXPERIMENTAL WORK: FORMATION OF ELEMENTAL SULFUR DURING REGENERATION

5.1 Introduction

In the previous Air Products project[1] a significant amount of elemental sulfur was formed during regeneration of sulfided iron oxide sorbents. The elemental sulfur caused plugging in the valves, condenser coils and piping; the sulfur was not expected. Consequently an analytical procedure was developed for quantitative measurement of the amount of elemental sulfur in the regeneration effluents, and some instantaneous measurements were made. These measurements showed that the instantaneous elemental sulfur formed was as high as 20-30 percent of the total sulfur in the effluents under some conditions. Detailed investigation of this phenomenon was outside the scope of the previous work.

In the conventional regeneration method the iron sulfide is contacted with a gas dilute in oxygen. Solid iron sulfide is converted to iron oxide (solid) and gaseous sulfur dioxide. The sulfur dioxide product is further converted to elemental sulfur in a Claus or Resox unit. If elemental sulfur were produced directly during regeneration, the sulfur recovery unit could be reduced in size or even eliminated. This process modification would reduce the total processing cost substantially. Hence in the current work the conditions that produce elemental sulfur during regeneration were investigated experimentally.

The goal of this experimental program was to identify regeneration conditions which result in the production of elemental sulfur and then to determine the controlling process variables. The process variables investigated included several regeneration feed gas compositions, sorbent compositions, and operating conditions. The regeneration feed gas contained four components: water, oxygen, nitrogen and sulfur dioxide. The experimental program was exploratory, and only a limited number of experiments could be done to map the entire feed gas composition range.

A thermodynamic chemical equilibrium analysis was carried out to determine conditions favorable for sulfur formation during regeneration. This thermodynamic chemical equilibrium analysis provided some guidance in choosing the different feed gas compositions for the experimental work. The experimental work was done in a flow reactor for which a simple thermodynamic representation does not exist. However, the thermodynamic analysis described in this section does relate to the conditions before significant oxygen breakthrough.

The thermodynamic calculations and conclusions are presented in Section 5.2. All the experimental work is described in Section 5.3. This section includes the details of experimental plan, equipment and procedure, comments on material balance, experimental results and conclusions.

5.2 Thermodynamic Chemical Equilibrium

There is no simple thermodynamic representation of a flow reactor in which one of the reactants is supplied from the solid phase. The solid and gas concentrations vary with time and depth in the bed. However, thermodynamic analysis of two batch systems approximately describes portions of the operation of the flow reactor. A batch system with a large amount of solid and a limited amount of gas approximates conditions at the exit of the reactor at the beginning of regeneration. At the beginning of regeneration, a differential amount of gas reacts with the solid at the inlet, and will be in contact with the unreacted solid of a constant composition for the remainder of its residence time. Thus conditions at the exit of the reactor and at the beginning of reaction are approximately given by the equilibrium composition for a batch system with a large amount of solid of initial composition and a small amount of gas. On the other hand, a batch system with a small amount of solid and a large amount of gas approximately describes conditions at the end of regeneration. At the end of the reaction, a large amount of gas (the total throughput) of constant composition is in contact with a small amount of solid. Thus conditions at the end of regeneration are approximately given by the equilibrium composition for a batch system with a large amount of gas and small amount of solid.

The approach for the thermodynamic analysis was as follows. Equilibrium compositions were calculated for two different feed gas compositions assuming first excess gas and then excess solid. The results showed that elemental sulfur formation is likely to occur with a large amount of solid iron sulfide and a limited amount of feed gas; i.e., conditions at the beginning of the process. Then a number of cases with different feed gas compositions in the presence of excess solid were evaluated to determine the relationship between elemental sulfur formation and feed gas composition.

The thermodynamic chemical equilibrium analysis was done by free energy minimization technique. Given a reacting system this technique adjusts the mol fractions of all species so as to minimize the free energy of the system. Thermodynamic correlations were based on JANAF tables. All gases are assumed to be ideal, regardless of their pressure and temperature. Details of the formulation of the free energy minimization problem and the methods of solution are fully described in the literature.[5]

Comparison of Results For An Excess of Solid With An Excess of Gas

Four cases were examined to determine whether elemental sulfur formation is favored in the presence of excess gas or excess solid.

The initial and final compositions for the four cases are described in Table 5.1. The results indicate that calculations made with 15 mols of FeS and 1000 mols of feed gas did not produce any elemental sulfur or hydrogen sulfide. These runs had an excess of oxygen and produced SO_2 and SO_3 as the product of regeneration. Runs with 1000 mols of FeS and 15 mols of feed gas had some hydrogen sulfide and elemental sulfur in the product. Thus elemental sulfur and hydrogen sulfide can be produced in oxygen-starved conditions. These conditions are obtained by assuming a large excess of solid FeS and can be approximately related to conditions at the beginning of the regeneration process at the bed exit.

TABLE 5.1

COMPARISON OF EQUILIBRIUM FOR AN EXCESS OF SOLID FeS WITH EQUILIBRIUM FOR AN EXCESS OF REGENERATION FEED GAS

PRESSURE = 1.0 ATM

Case No.	Feed Composition, Mols					Temperature, °F	Product Distribution at Equilibrium, Mols							
	FeS	SO_2	H_2O	O_2	N_2		FeS	SO_2	H_2O	O_2	N_2	H_2S	S_2	SO_3
1	15	0	850	30	120	1200	-	12.10	850	2.30	120	-	-	2.90
						1600	-	14.63	850	3.566	120	--	--	0.3688
2	15	620	150	48.3	181.7	1200	-	591.3	150	0.214	181.7	-	-	43.67
						1600	-	609.8	150	9.457	181.7	-	-	25:91
3	1000	0	12.75	0.45	1.80	1200	999.6	0.2411	12.64	-	1.80	0.1064	-	-
						1600	999.6	0.2941	12.62	-	1.80	0.1327	0.0121	-
4	1000	9.3	2.25	0.725	2.726	1200	999.5	9.636	2.218	-	2.726	0.0316	0.0846	-
						1600	999.4	9.594	2.225	-	2.726	0.02506	0.1349	-

Effect of Feed Composition With Excess Solid

Results described in the previous section showed that the amount of elemental sulfur formed is large with excess solid. Hence several feed gas compositions were examined with excess solid iron sulfide. The feed compositions investigated are given in Table 5.2. Equilibrium product gas compositions at 1200°F and 1600°F are given in Table 5.3.

Figure 5.1 is a plot of the selectivity for elemental sulfur against the initial steam content of the feed. The selectivity for elemental sulfur (S_e) is defined as the fraction of the total amount of sulfur in product gas occurring as elemental sulfur.

$$S_e = \frac{2 \times M_{S_2}}{2 \times M_{S_2} + M_{SO_2} + M_{H_2S}}$$

where M_{S_2} = mols of S_2 in product,

M_{SO_2} = mols of SO_2 in product,

M_{H_2S} = mols of H_2S in product.

TABLE 5.2

FEED COMPOSITIONS EVALUATED FOR EFFECT ON EQUILIBRIUM SULFUR FORMATION

Constant Conditions: Excess of Solid, 15 psi Pressure

Case No.	FeS, Mols	Water, Mols	Sulfur Dioxide, Mols	Oxygen, Mols	Relative Water Content, $X \equiv \frac{H_2O^\circ}{H_2O^\circ + SO_2^\circ + nO_2^\circ}$ Value for Formation of FeO	Value for Formation of Fe_2O_3
1	1000	1.5	7.5	1.75	0.1482	0.1500
2	1000	3.5	5.5	1.75	0.3460	0.3500
3	1000	5.5	3.5	1.75	0.5437	0.5500
4	1000	7.5	1.5	1.75	0.7414	0.7500
5	1000	9.0	0	1.75	0.8897	0.9000
6	100	98.571	0	2.5	0.9834	0.9857
7	100	99.429	0	1.0	0.9939	0.9943
8	100	99.714	0	0.5	0.9967	0.9971
9	1000	9.486	0	1.0	0.9343	0.9432

TABLE 5.3

EFFECT OF FEED COMPOSITION ON THE EQUILIBRIUM SULFUR FORMATION

Case No.	Product Gas Composition at 1200°F					Product Gas Composition at 1600°F				
	Water, Mols	Hydrogen Sulfide, Mols	Sulfur Dioxide, Mols	S_2, Mols	S_e	Water, Mols	Hydrogen Sulfide, Mols	Sulfur Dioxide, Mols	S_2, Mols	S_e
1	1.479	0.02066	8.439	0.06625	0.0154	1.483	0.0167	8.404	0.1086	0.0251
2	3.454	0.04642	6.448	0.05259	0.0159	3.462	0.03751	6.420	0.0862	0.0260
3	5.431	0.06925	4.457	0.03832	0.01665	5.443	0.05724	4.622	0.06695	0.0278
4	7.413	0.08688	2.468	0.02308	0.01775	7.422	0.07806	2.636	0.04603	0.0328
5	8.908	0.09151	0.9801	0.01046	0.01915	8.906	0.09367	1.151	0.02649	0.04083
6	97.82	0.7535	1.307	0.01861	0.01774	97.55	1.026	1.621	0.07135	0.0512
7	98.77	0.6580	0.4729	0.007784	0.01358	98.39	1.035	0.6432	0.0385	0.0439
8	99.13	0.5845	0.2012	0.003742	0.00994	98.68	1.038	0.3194	0.02414	0.03435
9	9.397	0.08893	0.5554	0.006435	0.01958	9.387	0.09873	0.6567	0.01821	0.04599

The relative water content of the feed (X) is defined as fraction of initial mols of water (M°_{H2O}) to the initial total mols of water and sulfur dioxide ($M^{\circ}_{H2O} + MT_{SO2}$). The initial total mols of sulfur dioxide (MT_{SO2}) are calculated as the sum of initial sulfur dioxide mols (M°_{SO2}) in the feed and the additional mols of sulfur dioxide (ΔSO_2) formed by reaction of oxygen with iron sulfide given below.

$$FeS + \frac{3}{2} O_2 \longrightarrow FeO + SO_2$$

$$FeS + \frac{7}{4} O_2 \longrightarrow \frac{1}{2} Fe_2O_3 + SO_2$$

Thus $\Delta SO_2 = n \cdot M^{\circ}_{O_2}$

where $M^{\circ}_{O_2}$ = initial number of mols of oxygen in feed,

$n = \frac{2}{3}$ if final product is FeO,

$n = \frac{4}{7}$ if final product is Fe_2O_3.

The relative water content of feed (X) is calculated as

$$X = \frac{M^{\circ}_{H_2O}}{M^{\circ}_{H_2O} + M^{\circ}_{SO_2} + nM^{\circ}_{O_2}}$$

The values of X for the eight cases are given in Table 5.2 for both formation of FeO and Fe_2O_3.

Figure 5.1 describes the effect of changing feed composition on the selectivity for elemental sulfur. The results indicate that the selectivity for elemental sulfur increases with X. Thus feed composition with high water content, low oxygen content and low sulfur dioxide content favors elemental sulfur formation.

Although the data are not presented in Figure 5.1, the equilibrium composition depends uniquely upon X and not upon the feed mixture used to obtain X. Thus the relative water content, X, simplifies the description of the equilibrium calculations.

An increase in temperature results in an increase in the selectivity for elemental sulfur. The thermodynamic results in Figure 5.1 show that the selectivity for sulfur goes to zero rapidly as the feed composition approaches 100 percent water. Thus some presence of sulfur dioxide in the feed (either in the initial feed or formed by oxidation of FeS) is required for sulfur formation at equilibrium.

The maximum selectivity for elemental sulfur at 1600°F, predicted by these calculations, is 5.2 percent at 1600°F. This number is much lower than the experimentally observed value of 20 to 30 percent by APCI in previous work.[1] The experiments in the current work also report such high selectivities. It is interesting to note that another independent investigator has also observed elemental sulfur selectivities of the order of 10-30 percent during regeneration of sulfided coal ash sorbents.[6] These high selectivities for elemental sulfur are not explained by this thermodynamic chemical equilibrium analysis.

Morgantown Energy Research Center[7] has studied the chemical equilibrium for the reactions:

$$2FeS + 1.056SO_2 \longrightarrow 2.112Fe_{0.947}O + 1.528S_2$$

$$3FeS + 2SO_2 \longrightarrow Fe_3O_4 + \frac{5}{2}S_2$$

$$3FeS + 2O_2 \longrightarrow Fe_3O_4 + \frac{3}{2}S_2$$

FIGURE 5.1

EFFECT OF INITIAL WATER CONTENT ON SULFUR FORMATION WITH AN EXCESS OF IRON SULFIDE

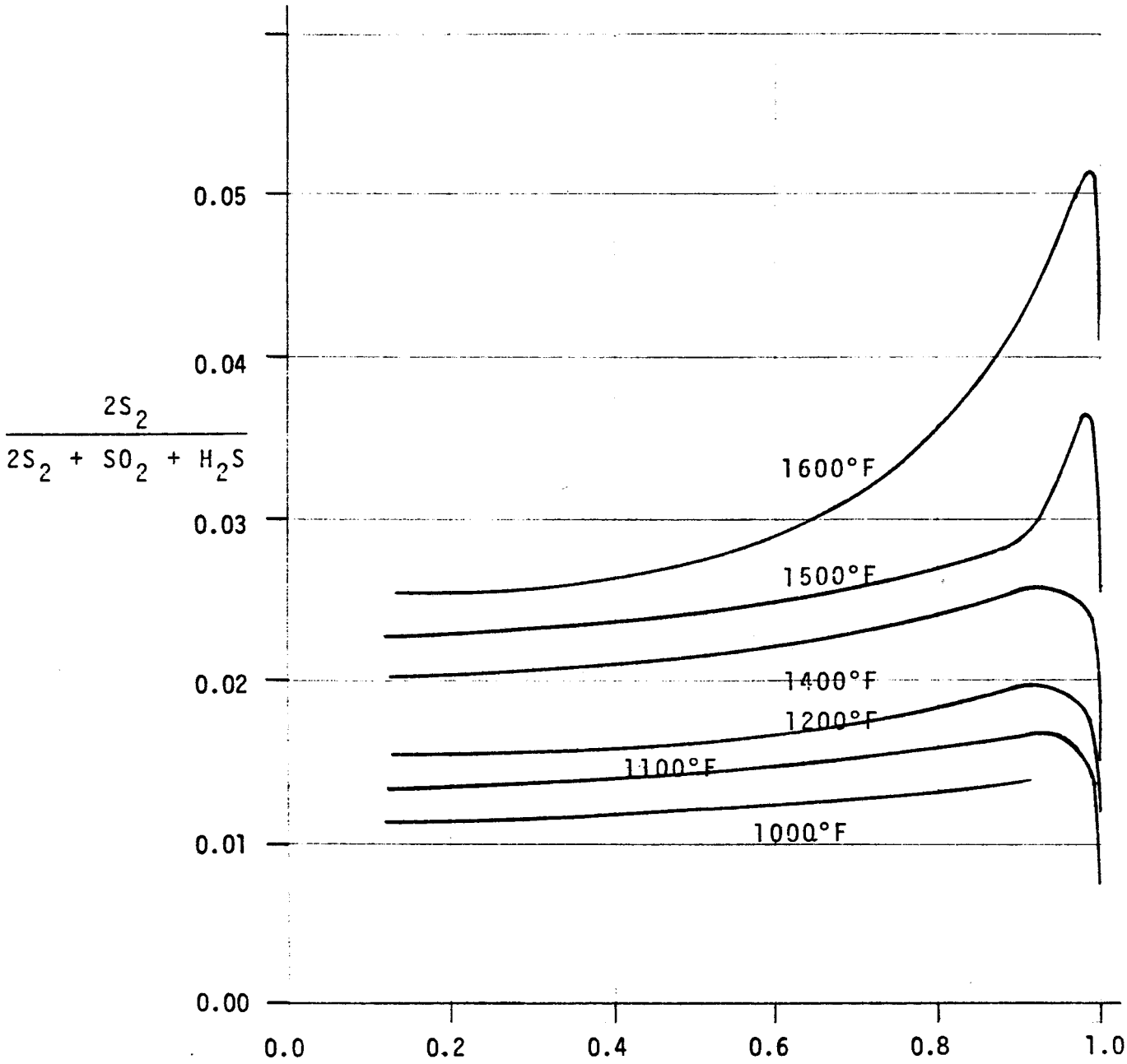

Their analysis also shows that the maximum possible yield of elemental sulfur at 1300°F is 4.7 percent. They have also proposed a SO_2 recycle regeneration scheme to convert FeS to S_2. The reaction scheme considered by MERC is different from the reaction scheme considered by APCI. Both scnemes yield low selectivity for elemental sulfur. MERC suggests that the experimentally observed high selectivity for elemental sulfur could be due to a built in Trail or Resox reaction.

MERC has also investigated other metal sulfides for regeneration with SO_2 to produce elemental sulfur. They have concluded that iron appears to be the only sorbent system which offers reasonable recovery of elemental sulfur without excess interference from side reactions such as sulfate formation.

5.3 Experimental Plan and Procedures

In this section the process variables investigated and experimental program are described. Details of the equipment, experimental procedure and analytical techniques are given.

5.3.1 Experimental Program

The objective of this exploratory experimental program was to identify the process variables that influence elemental sulfur formation during regeneration of sulfided sorbents. Development of a complete process was beyond the scope of this work.

The regeneration process variables evaluated in this study were regeneration feed gas compositions, sorbent characteristics and regeneration operating conditions. The regeneration feed gas compositions evaluated included several levels of water, sulfur dioxide and oxygen compositions. Thermodynamic chemical equilibrium analysis described in Section 5.2 provided guidance to select the feed gas compositions. The sorbent characteristics evaluated included iron oxide content, type of support, purity of iron oxide, and effect of cycling. Since this was an exploratory program, the experimental program considered changes in one or two factors at a time. Although thermodynamics suggests that the sulfur yield increases with temperature, this study was conducted at 1000°F. This value was selected to be equal to the planned value for the producer gas. The nominal operating temperature for a gasifier subsequently was raised to 1200°F.

A summary of all the experimental conditions is given in Table 5.4.

TABLE 5.4

OPERATING CONDITIONS FOR REGENERATION EXPERIMENTS

Run No.	2102	2106	2107	2109	2113	2114	2115	2116	2117	2118	2119	2120	2125	2126	2128	2129
H_2S Absorption:																
Means[1]	In Situ	In Situ	In Situ	In Situ	In Situ	In Situ	In Situ	In Situ	In Situ	In Situ	Pre sulfided[2]	In Situ	In Situ	Pre-sulfided[3]	Pre-sulfided[3]	Pre-sulfided[3]
Duration, Hr	5	5	5	5	5	5	5	5	5	5	-	5	5	-	-	-
Regeneration:																
Gas, Volume %																
H_2O	85	85	10	85	85	10	16	10	15	95	85	95	95	95	92	95
Air	15	15	15	15	5	5	8	15	23	5	15	5	5	5	0	0
SO_2	0	0	0	0	0	0	76	0	62	0	0	0	0	0	8	0
N_2	0	0	75	0	10	85	0	75	0	0	0	0	0	0	0	5
	100	100	100	100	100	100	100	100	100	100	100	100	100	100	100	100
Duration, Hr	14	14	14	14	42	42	42	14	14	42	14	21	10	10	10	10
Sorbent Volume, cc	40	40	40	40	40	40	40		40	40	40	40	40	40	40	40
GHSV	600	600	600	600	600	600	600	600	600	600	600	1200	1200	1200	1200	1200
Reactor Block Temperature, °F	1000	1000	1000	1000	1000	1000	1000	1000	1000	1000	1000	1000	1000	1000	1000	1000
Sorbent:																
Fe_2O_3																
Source[4]	U.S. Steel	U.S. Steel	U.S. Steel	U.S. Steel	U.S. Steel	U.S. Steel	U.S. Steel	U.S. Steel	U.S. Steel	U.S. Steel	U.S. Steel	Chem. Pure	U.S. Steel	U.S. Steel	U.S. Steel	U.S. Steel
Wt. %[5]	40	40	40	40	40	40	40	60	40	40	40	40	40	40	40	40
Support	Silica	Fly Ash	Fly Ash	Fly Ash	Fly Ash	Fly Ash	Fly Ash	Fly Ash	Fly Ash	Silica	Fly Ash	Silica	Silica	Silica	Silica	Silica

Notes:

(1) In Situ sulfiding done with 1175°F producer gas containing 1.0 volume % H_2S. Weight percent S in the sulfided sorbent was approximately 7.
(2) High level of sulfur on absorbent. Presulfiding done at 1200°F with 45% H_2S, 55% N_2. Weight percent S in the sulfided sorbent was 20.9.
(3) Low level of sulfur on absorbent. Presulfiding done at 400°F with 5% H_2S, 95% N_2. Weight percent S in the sulfided sorbent was 1.5.
(4) U.S. Steel source was 79.8 wt. % Fe_2O_3.
(5) Added Fe_2O_3. Iron oxide in fly ash not included.

The planned experimental program is described below.

a) Effect of Water and Air Content in the Regeneration Feed

The effect of water and air concentration in the regeneration gas was investigated at two different levels for the fly ash supported sorbents. The following table illustrates the cases.

		Water Content of Feed, Mol Percent	
		85	10
Air Content of Feed, Mol Percent	15	Run 2106	Run 2107
	5	Run 2113	Run 2114

The remainder of the regeneration gas was nitrogen. In addition, the effect of air and water concentration was investigated for silica supported sorbents. The following table illustrates the cases.

Run No.	Air Content, Mol Percent	Water Content, Mol Percent
2102	15	85
2118	5	95

b) Effect of Sulfur Dioxide Content in the Regeneration Feed

Effect of sulfur dioxide concentration was studied at two different levels relative to air concentration. The following table illustrates the cases.

Run No.	Water, Mol Percent	Air, Mol Percent	Sulfur Dioxide, Mol Percent
2115	16	8	76
2117	15	23	62

In addition, one more experiment of exploratory nature was carried out. The objective of this experiment (Run 2128) was to determine if elemental sulfur is formed from a feed containing a low concentration of sulfur and a high concentration of water.

Mol Percent	Run 2128
Water	92
Air	0
Sulfur Dioxide	8

c) Effect of the Sorbent Support

The effect of fly ash and silica supports was investigated at two levels of air content. The cases are given in the following table.

Sorbent Support	Air, Mol Percent in Feed 15	5
Fly Ash	2106	2113
Silica	2102	2118

d) Effect of Iron Oxide Content of the Sorbent

Effect of iron oxide content in the sorbent was studied for commercial iron oxide and fly ash support. The following table illustrates the cases.

Iron Oxide Content, Weight Percent	Run No.
42	2107
63	2116

e) Purity of Iron Oxide

Effect of the source of iron oxide in the sorbent was evaluated using chemically pure iron oxide and commercial (U.S. Steel) iron oxide. The following table illustrates the case.

Source of Iron Oxide	Run No.
Commercial (U.S. Steel)	2125
Chemically Pure	2120

f) Gas Hourly Space Velocity (GHSV)

Effect of GHSV was studied by keeping the same sorbent volume and changing regeneration feed gas rate. The following table illustrates the cases.

GHSV	Run No.
600	2106
300	2109

g) Method of Sulfiding

A comparison was made of the effect of sulfiding in situ versus using presulfided sorbent. Some regeneration experiments in previous work[1] that had reported high elemental sulfur formation were made with presulfided sorbent. Hence these runs were made to determine the effect of the method of sulfiding. In situ sulfiding was done in the reactor just before regeneration using simulated producer gas. Presulfiding was done in a separate reactor and the sorbent was cooled and stored before charging for regeneration. The following table illustrates the cases.

Method of Sulfiding	Run No.
In Situ	2106
Presulfided	2119

5.3.2 Experimental Method

Each experiment consisted of two parts -- absorption and regeneration. The reactor was charged with 40 cc of fresh iron oxide sorbent. The sorbent was sulfided in an absorption cycle. Absorption was carried out at 1175°F with simulated low-BTU producer gas containing hydrogen sulfide. Composition of the simulated producer gas was:

Component	Mol Percent
N_2	48.2
CO	20.5
H_2	14.9
CO_2	6.5
CH_4	1.9
H_2S	1.0
H_2O	7.0
	100.0

Absorption runs were carried out at 5000 GHSV at STP. Length of each absorption run was 5 hours. Ideal stoichiometric sorption time under these conditions was 2.8 hours for sorbents containing 42 weight percent iron oxide. At the end of the absorption run, the reactor was purged with nitrogen and the reactor block was cooled to 1000°F in preparation for regeneration. The amount of hydrogen sulfide fed to the reactor was calculated by knowing the hydrogen sulfide flow rate and duration of the absorption run. The amount of hydrogen sulfide in the effluents was measured by the analytical method described in this section. Total amount of sulfur on the sorbent was calculated by difference. In some experiments, presulfided sorbent was used.

The regeneration experiments were carried out after purging the hot sulfided sorbent. Regeneration conditions for the runs are given in Table 5.4. The duration of regeneration experiments was sufficiently long to regenerate the sorbent completely. The total amount of elemental sulfur, sulfur dioxide and sulfur trioxide in the regeneration product was measured by the analytical method described in Section 5.3.3. Residual sulfur on the regenerated sorbent was determined by x-ray fluorescence technique. Material balance and yield structure were established for each run.

Section 5.3.3 describes the details of equipment and operating procedures. Results are given in Section 5.4.

5.3.3 Equipment and Analytical Methods

The major items in the pilot unit consist of the reactors, feed manifold and analytical train. Figure 5.2 is a schematic flow diagram of the unit. The reactor assembly consists of two heater blocks of Inconel 601, each 3.5 inches in diameter and 18 inches long. Each heater block has two separate preheater assemblies. Five thermowells monitor temperatures in each block. Heater blocks and transfer lines are wound by electrical heating circuits controlled by a temperature controller.

Each heater block has a separate feed manifold. The feed manifold consists of nine rotameters to introduce metered quantities of different gases such as air, nitrogen, sulfur dioxide, hydrogen sulfide, carbon monoxide, carbon dioxide, methane and hydrogen. Water is introduced in the feed by pumping water with syringe pumps and evaporating the water by electrical heating circuits.

Effluents from each reactor pass through a separate analytical train. The analytical train consists of three glass bubblers in series. The analytical method determines the total amount of hydrogen sulfide, elemental sulfur, sulfur dioxide and sulfur trioxide produced during the entire run. Breakthrough curves were not determined.

When the reactors were in absorption mode of operation, the glass bubblers contained an aqueous solution of $CdCl_2$. Hydrogen sulfide in the reactor effluents was absorbed in the $CdCl_2$ solution forming CdS. The total amount of hydrogen sulfide was determined by oxidation of the $CdCl_2$-CdS solution with potassium dichromate and then titration with thiosulfate using starch indicator.

For reactors in regeneration mode of operation, the first bubbler contained 4:1 solution of isopropanol-water maintained at 0°C with an ice bath. Sulfur trioxide was trapped in the isopropanol solution, and elemental sulfur also precipitated in this solution. The remaining gas containing sulfur dioxide was passed through two bubblers in series containing a solution of sodium hydroxide and hydrogen peroxide. The last bubbler in the train also contained methyl red solution as an indicator to signal SO_2 breakthrough by color change. Amount of elemental sulfur was determined by extraction with carbon disulfide and then evaporation to dryness. The concentration of sulfur trioxide was determined by titration of the isopropanol solution with barium perchlorate using Thorin indicator. The quantity of sulfur dioxide absorbed in the sodium hydroxide-hydrogen peroxide solution was determined by boiling off excess hydrogen peroxide and then titrating with sulfuric acid using methyl red indicator.

FIGURE 5.2

SCHEMATIC FLOW DIAGRAM OF THE PILOT UNIT

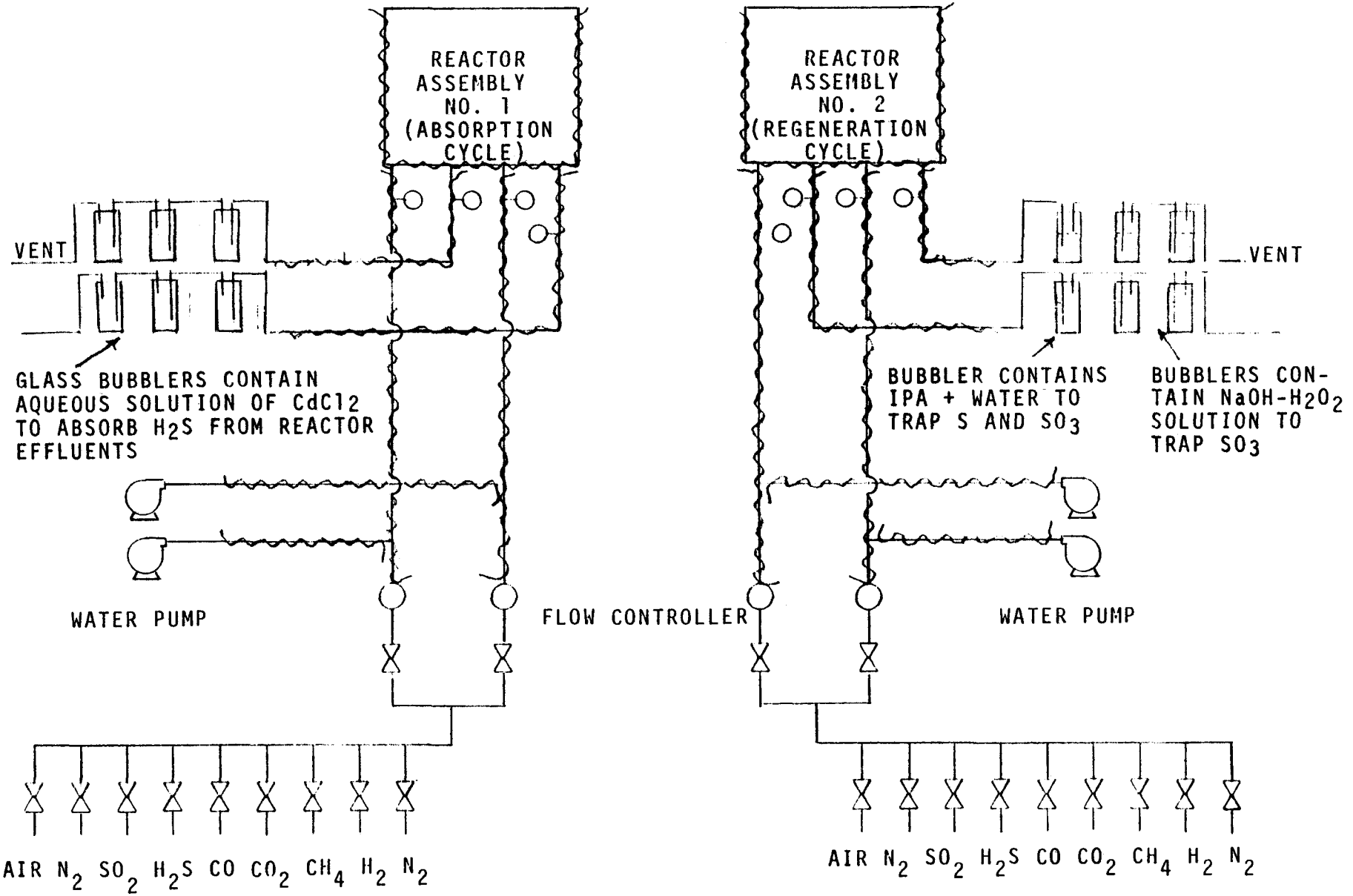

5.4 Results

In this section details for calculating material balances and selectivities are given, and experimentally observed effects of the process variables are described.

5.4.1 Calculation Methods

The analysis of the experimental results required calculations of selectivities and material balance for each run. These calculation methods are described below.

The amount of sulfur deposited on the sorbent during absorption (S_O) was not directly measured, but calculated as the difference between the amount of sulfur entering the reactor as hydrogen sulfide in producer gas and the amount of unreacted sulfur in the reactor effluents. A direct measure of the amount of sulfur deposited on the sorbent by x-ray fluorescence would have been more accurate. However, it would have required cooling the reactor and discharging part of the sorbent. The commercial operation would regenerate the hot sulfided sorbent without an intermediate cooling period. Cooling down after absorption, exposing the cold sulfided sorbent to air, and heating up before regeneration could change the sorbent properties. Hence the indirect method of calculating the amount of sulfur deposited on the sorbent by difference was adopted.

The total amount of sulfur entering the reactor during the absorption run was calculated from the hydrogen sulfide flow rate and duration of the absorption run. The total amount of unreacted sulfur on the reactor effluents was measured for the entire absorption run by the analytical method described in section 5.3.

$$S_O = S_{In} - S_{Out}$$

S_O	S_{In}	S_{Out}
Sulfur Deposited on the Sorbent	Total Sulfur Entering the Reactor	Total Unreacted Sulfur in Reactor Effluents

The method of estimating the amount of sulfur deposited on the sorbent may introduce an error in material balance. The total sulfur entering the reactor (S_{In}) is calculated from rotameter flow rates and the relative error in flow rate is at least 5 percent. There is a relative error in the analysis of the amount of unreacted sulfur in reactor effluents due to incomplete absorption in the $CdCl_2$ solution and relative errors in titration. Thus relative error in the amount of sulfur deposited on the sorbent depends both on the relative error in S_{In} and S_{Out}.

The regeneration product distribution in reactor effluents was measured by the analytical methods described in Section 5.3. The effluents for the entire regeneration run were analyzed for total elemental sulfur (W_S, grams), total sulfur dioxide (W_{SO_2}, grams), total sulfur trioxide (W_{SO_3}, grams). The total amount of residual sulfur on regenerated sorbent (S_R, grams) was determined by x-ray fluorescence. The overall material balance for the entire run was determined based on the total recovery of sulfur.

$$\text{Material Balance, \%} = \frac{\begin{array}{l}\text{(Elemental S Formed + S Occurring as } SO_2 \\ \text{+ S Occurring as } SO_3 \text{ + Residual S on} \\ \text{Regenerated Sorbent + S Occurring as } H_2S \\ \text{During Regeneration)}\end{array}}{\text{S Deposited on Sorbent During Absorption}} \times 100$$

$$= \frac{W_S + \frac{32}{64} W_{SO_2} + \frac{32}{80} W_{SO_3} + S_R + \frac{32}{34} W_{H_2S}}{S_o} \times 100$$

The selectivity for elemental sulfur formation was defined as the fraction of the total sulfur in regeneration effluent gases occurring as elemental sulfur.

$$\text{Selectivity for Elemental Sulfur Formation, \%} = \frac{W_S}{W_S + \frac{32}{64} W_{SO_2} + \frac{32}{80} W_{SO_3} + \frac{32}{34} W_{H_2S}} \times 100$$

The selectivities for sulfur dioxide and sulfur trioxide formation were defined similarly.

$$\text{Selectivity for Sulfur Dioxide Formation, \%} = \frac{\frac{32}{64} W_{SO_2}}{W_S + \frac{32}{64} W_{SO_2} + \frac{32}{80} W_{SO_3} + \frac{32}{34} W_{H_2S}} \times 100$$

$$\text{Selectivity for Sulfur Trioxide Formation, \%} = \frac{\frac{32}{80} W_{SO_3}}{W_S + \frac{32}{64} W_{SO_2} + \frac{32}{80} W_{SO_3} + \frac{32}{34} W_{H_2S}} \times 100$$

In three experimental runs (2115, 2117, 2128) the regeneration feed gas contained significant amount of sulfur dioxide. Due to the large amount of sulfur dioxide in the feed, it was not possible to get an accurate estimate of the small amount of incremental sulfur dioxide formed during regeneration using available analytical techniques. Since the total sulfur in regeneration effluents could not be measured, the selectivities were based on the amount of sulfur deposited on the sorbent during absorption as given below. These definitions of selectivity assume that material balance for sorption is correct and elemental sulfur or sulfur trioxide formed is due to regeneration of iron sulfide and not due to side reactions of the diluent sulfur dioxide gas in feed.

$$\text{Selectivity for Elemental Sulfur Formation, \%} = \frac{W_S}{S_o - S_R} \times 100$$

$$\text{Selectivity for Sulfur Trioxide Formation, \%} = \frac{\frac{32}{80} W_{SO_3}}{S_o - S_R} \times 100$$

5.4.2 Comments on Material Balance

The analytical results and calculated material balances for all experiments are summarized in Table 5.5. These results indicate that from a total of eighteen runs, eight runs had material balance closed within fifteen percent, two runs had material balance closed within twenty-five percent and four runs had material balance within forty-five percent. Material balance could not be calculated for four runs in which the regeneration feed gas contained sulfur dioxide. Since the amount of sulfur absorbed is estimated from the difference of the flow input and the quantity of sulfur found on the analytical train, material balance errors of greater than twenty-five percent are expected in half of the runs.

There are four potential reasons for errors in the material balance. They are as follows:

a) Hold-up of elemental sulfur at cold spots in the reactor or system piping.

b) Hold-up or reaction of H_2S with the Inconel 601 reactor or Carpenter 20 steel piping.

c) Leaks.

d) Error in the measurement of the sulfur input in absorption.

The sulfur hold-up at cold spots was eliminated by careful tracing of the reactor piping. Although it is now known that H_2S reacts with the materials of construction, the total absorption of H_2S is expected to be less than 0.1 milligram and therefore unimportant in the computation. The equipment was palpably free of leaks. Thus the material balance error is believed to stem primarily from the crude method used to determine sulfur laydown. The selectivity estimates have a relative accuracy of ± 5 percent.

TABLE 5.5

RESULTS FOR REGENERATION EXPERIMENTS

Run No.	2102	2106	2107	2109	2113	2114	2115	2116	2117	2118	2119	2120	2125	2126	2128	2129
Sulfur in Sulfided Sorbent, grams	5.322	3.162	5.281	4.250	3.589	4.925	5.292	4.161	4.919	3.078	11.16	3.219	3.543	0.745	0.745	0.745
Sulfur in Regenerated Sorbent, grams	0.740	0.326	0.394	0.479	0.178	0.240	1.113	1.548	1.487	0.209	4.398	0.036	0.936	0.106	0.076	0.061
Elemental Sulfur in Product as Grams Sulfur	0.946	0.394	0.056	0.178	2.001	0.026	0.024	0.086	-	3.185	0.916	1.376	1.148	0.180	0.295	0.235
SO_2 in Product as Grams Sulfur	3.130	2.260	4.500	2.507	2.238	3.953	*	2.560	*	0.994	1.225	1.482	2.910	0.340	*	-
SO_3 in Product as Grams Sulfur	0.220	0.088	0.030	0.026	0.107	0.014	0.035	0.109	0.204	0.058	0.057	0.121	0.027	0.022	0.413	0.019
Total Recovered Sulfur, Grams Sulfur	5.036	3.068	4.980	3.190	4.524	4.233	*	4.303	*	4.448	6.595	3.015	5.021	0.648	*	0.479 (0.164 gm S was recovered as H_2S
% Material Balance	95	97	94	75	126	86	*	103	*	145	59	94	142	87	*	64
% Sulfur Selectivity as																
Elemental Sulfur	22.0	14.4	1.2	6.6	46.0	0.7	0.6	3.1	0	75.1	41.7	46.2	28.1	33.2	44.1	56.3
SO_2	72.9	82.4	98.1	92.4	51.5	98.9	-	92.9	-	23.5	55.7	49.7	71.2	62.7	-	0
SO_3	5.1	3.2	0.7	1.0	2.5	0.4	0.8	4.0	5.94	1.4	2.6	4.1	0.7	4.1	61.7	$39.2^{4,5}$ for H_2S

*These runs were carried out with regeneration feed gas containing high quantities of SO_2. The small amount of SO_2 generated during regeneration could not be accurately determined for these runs due to limited sensitivity of the analytical technique. Hence the amount of SO_2 generated and material balance are not listed for regeneration runs 2115, 2117 and 2128. The method of calculating the selectivities for these runs is described in Section 5.4.1.

5.4.3 Observed Effects of Process Variables

In this section the observed effects of the variables are described. A summary of all experimental results is given in Table 5.5. Effect of each variable studied is described below.

a) Effect of Water Content

Table 5.6 illustrates the effect of water content in regeneration feed. A comparison of Runs 2106 and 2107 shows that an increase in water concentration with 15 percent air in feed results in a marked increase in the selectivity for elemental sulfur formation. The same trend is observed with 5 percent air in feed (Runs 2113 and 2114).

One regeneration run (2129) was carried out with 95 mol percent water, 5 mol percent nitrogen and no air. The results are summarized in Table 5.6. This run resulted in a high selectivity for elemental sulfur and hydrogen sulfide. Some hydrogen sulfide formation in this run was expected due to oxidation of iron sulfide by water. The large quantity of elemental sulfur formed is surprising. This result is encouraging and requires further confirmation.

The large changes in the selectivity for formation of elemental sulfur with changes in water content indicate that water content of the regeneration feed gas is a major process variable. This result is consistent with the thermodynamic analysis.

TABLE 5.6

EFFECT OF WATER CONTENT ON REGENERATION PRODUCT DISTRIBUTION

	High Air Content		Low Air Content		Zero Air Content
Run No.	2106	2107	2113	2114	2129
Regeneration Feed Gas, Mol Percent					
Water	85	10	85	10	95
Air	15	15	5	5	0
Sulfur Dioxide	0	0	0	0	0
Nitrogen	0	75	10	85	5
Sorbent	42 Percent Added Commerical Iron Oxide on Fly Ash	42 Percent Added Commercial Iron Oxide on Fly Ash	42 Percent Added Commercial Iron Oxide on Fly Ash	42 Percent Added Commercial Iron Oxide on Fly Ash	42 Percent Added Commercial Iron Oxide on Silica
Sorbent Volume, cc	40	40	40	40	40
GHSV	600	600	600	600	1200
Regeneration Duration, Hours	14	14	42	42	10
Reactor Block Temperature, °F	1000	1000	1000	1000	1000
Material Balance, Percent	97	94	126	86	64
Selectivity for Elemental Sulfur, Percent	14.4	1.2	46	0.7	56.3
Selectivity for Sulfur Dioxide, Percent	82.4	98.1	51.5	98.9	-
Selectivity for Sulfur Trioxide, Percent	3.2	0.7	2.5	0.4	4.5
Selectivity for Hydrogen Sulfide, Percent	-	-	-	-	39.2

b) Effect of Air Content

Table 5.7 illustrates the effect of air content of the regeneration feed gas. The results indicate that the selectivity for elemental sulfur formation decreases with an increase in the air content of the regeneration feed gas. The same trend is observed for three sets of experiments: fly ash supported sorbent at high level of water content (Run 2106 versus Run 2113), fly ash supported sorbent at low level of water content (Run 2107 versus Run 2114) and silica supported sorbent at high level of water content (Run 2102 versus Run 2118).

The observed large changes in the selectivity for elemental sulfur formation with changes in air content show that air content of the regeneration feed gas is a very important variable for elemental sulfur formation. Excess oxygen converts S_2 to SO_2 and SO_3.

TABLE 5.7

EFFECT OF AIR CONTENT ON REGENERATION PRODUCT DISTRIBUTION

	Fly Ash Support-High Water Content		Silica Support-High Water Content		Fly Ash Support-Low Water Content	
Run No.	2106	2113	2102	2118	2107	2114
Regeneration Feed Gas, Mol Percent						
Water	85	85	85	95	10	10
Air	15	5	15	5	15	5
Sulfur Dioxide	0	0	0	0	0	0
Nitrogen	0	10	0	0	75	85
Sorbent	42 Percent Added Commercial Iron Oxide on Fly Ash	42 Percent Added Commercial Iron Oxide on Fly Ash	42 Percent Added Commercial Iron Oxide on Silica	42 Percent Added Commercial Iron Oxide on Silica	42 Percent Added Commercial Iron Oxide on Fly Ash	42 Percent Added Commercial Iron Oxide on Fly Ash
Sorbent Volume, cc	40	40	40	40	40	40
GHSV	600	600	600	600	600	600
Regeneration Duration, Hours	14	42	14	42	14	42
Reactor Block Temperature, °F	1000	1000	1000	1000	1000	1000
Material Balance, Percent	97	126	95	145	94	86
Selectivity for Elemental Sulfur, Percent	14.4	46.0	22.0	75.1	1.2	0.7
Selectivity for Sulfur Dioxide, Percent	82.4	51.5	72.9	23.5	98.1	98.9
Selectivity for Sulfur Trioxide, Percent	3.2	2.5	5.1	1.4	0.7	0.4

c) Effect of Sulfur Dioxide Content

Table 5.8 illustrates the effect of sulfur dioxide content of the regeneration feed gas. The effect of sulfur dioxide content of the regeneration feed gas depends on its water content.

A comparison of Runs 2115 and 2117 shows that at low steam content (15 mol percent) and high sulfur dioxide content (nominally 70 mol percent), the selectivity for elemental sulfur formation is very low and does not depend on the air content of the feed.

Run 2128 shows that regeneration feed gas with high steam content (92 mol percent) and low sulfur dioxide content (8 mol percent) results in the formation of significant amount of elemental sulfur.

TABLE 5.8

EFFECT OF SULFUR DIOXIDE CONTENT ON REGENERATION PRODUCT DISTRIBUTION

Run No.	2115	2117	2128
Regeneration Feed Gas, Mol Percent			
Water	16	15	92
Air	8	23	0
Sulfur Dioxide	76	62	8
Nitrogen	0	0	0
Sorbent	42 Percent Added Commercial Iron Oxide on Fly Ash	42 Percent Added Commercial Iron Oxide on Fly Ash	Presulfided 42 Percent Added Commercial Iron Oxide on Silica
Sorbent Volume, cc	40	40	40
GHSV	600	600	600
Regeneration Duration, Hours	42	14	10
Reactor Block Temperature, °F	1000	1000	1000
Selectivity for Elemental Sulfur,(1) Percent	0.6	0.0	44.1
Selectivity for Sulfur Trioxide,(1) Percent	0.8	5.94	61.7

(1) Selectivity is given as yield percent of sulfur removed from the sorbent during regeneration. Material balance could not be determined due to the high SO_2 content of feed.

d) Effect of Sorbent Support

Table 5.9 shows the comparison of the results with fly ash and silica sorbent supports at two levels of air content of feed gas. Significant quantities of elemental sulfur were formed with both sorbents. In both cases sorbents with silica as the support show greater selectivity for elemental sulfur formation than sorbents with fly ash as the support.

The exact reason for the changes observed with change in sorbent support is not known. Fly ash contains several compounds including iron oxide, alumina and silica. Previous DOE supported work done by APCI[1] has demonstrated that iron oxide in fly ash makes a small contribution to the sulfur absorption capacity of the sorbent (2.5 weight percent sulfur for a 100 percent fly ash sorbent). Thus the iron content of fly ash is not the reason for the observed changes in selectivity.

TABLE 5.9

EFFECT OF SORBENT SUPPORT ON REGENERATION PRODUCT DISTRIBUTION

	High Air Content		Low Air Content	
Run No.	2106	2102	2113	2118
Regeneration Feed Gas, Mol Percent				
Water	85	85	85	95
Air	15	15	5	5
Sulfur Dioxide	0	0	0	0
Nitrogen	0	0	10	0
Sorbent	42 Percent Added Commercial Iron Oxide on Fly Ash	42 Percent Added Commercial Iron Oxide on Silica	42 Percent Added Commercial Iron Oxide on Fly Ash	42 Percent Added Commercial Iron Oxide on Silica
Sorbent Volume, cc	40	40	40	40
GHSV	600	600	600	600
Regeneration Duration, Hours	14.4	22	42	42
Reactor Block Temperature, °F	1000	1000	1000	1000
Material Balance, Percent	97	95	126	145
Selectivity for Elemental Sulfur, Percent	14.4	22	46.0	75.1
Selectivity for Sulfur Dioxide, Percent	82.4	72.9	51.5	23.5
Selectivity for Sulfur Trioxide, Percent	3.2	5.1	2.5	1.4

e) Effect of Iron Oxide Content of the Sorbent

Table 5.10 is a comparison of Runs 2107 and 2116 illustrating the effect of iron oxide content of the sorbent. With regeneration feed gas containing low moisture, the selectivity for elemental sulfur formation increased slightly with an increase in iron oxide content of the sorbent. These comparisons are made at low sulfur selectivity levels, and the observed changes in selectivity are within experimental error. The effect of iron oxide content at conditions favorable to a high selectivity for elemental sulfur is not known.

TABLE 5.10

EFFECT OF IRON OXIDE CONTENT OF THE SORBENT ON REGENERATION PRODUCT DISTRIBUTION

Run No.	2107	2116
Regeneration Feed Gas, Mol Percent		
Water	10	10
Air	15	15
Sulfur Dioxide	0	0
Nitrogen	75	75
Sorbent	42 Percent Commercial Iron Oxide on Fly Ash	63 Percent Commercial Iron Oxide on Fly Ash
Sorbent Volume, cc	40	40
GHSV	600	600
Regeneration Duration, Hours	14	14
Reactor Block Temperature, °F	1000	1000
Material Balance, Percent	94	103
Selectivity for Elemental Sulfur, Percent	1.2	3.1
Selectivity for Sulfur Dioxide, Percent	98.1	92.9
Selectivity for Sulfur Trioxide, Percent	0.7	4.0

f) Effect of Purity of Iron Oxide

Table 5.11 shows the effect of the purity of iron oxide. Sorbent made with chemically pure iron oxide had greater selectivity for elemental sulfur formation than sorbent made with commercial (U.S. Steel) iron oxide.

TABLE 5.11

EFFECT OF PURITY OF IRON OXIDE ON REGENERATION PRODUCT DISTRIBUTION

Run No.	2125	2120
Regeneration Feed Gas, Mol Percent		
Water	95	95
Air	5	5
Sulfur Dioxide	0	0
Nitrogen	0	0
Sorbent	42 Percent Commercial Iron Oxide on Silica	42 Percent Chemically Pure Iron Oxide on Silica
Sorbent Volume, cc	40	40
GHSV	1200	1200
Regeneration Duration, Hours	10	21
Reactor Block Temperature, °F	1000	1000
Material Balance, Percent	142	94
Selectivity for Elemental Sulfur, Percent	28.1	46.2
Selectivity for Sulfur Dioxide, Percent	71.2	49.7
Selectivity for Sulfur Trioxide, Percent	0.7	4.1

g) Effect of GHSV

Table 5.12 shows the effect of GHSV on regeneration product distribution for sorbents with fly ash support. Selectivity for elemental sulfur formation increased from 6.6 to 14.4 percent with an increase in GHSV from 300 to 600.

TABLE 5.12

EFFECT OF GHSV ON REGENERATION PRODUCT DISTRIBUTION

	Fly Ash Support	
Run No.	2109	2106
Regeneration Feed Gas, Mol Percent		
Water	85	85
Air	15	15
Sulfur Dioxide	0	0
Nitrogen	0	0
Sorbent	42 Percent Commercial Iron Oxide on Fly Ash	42 Percent Commercial Iron Oxide on Fly Ash
Sorbent Volume, cc	40	40
GHSV	300	600
Regeneration Duration, Hours	14	14
Reactor Block Temperature, °F	1000	1000
Material Balance, Percent	75	97
Selectivity for Elemental Sulfur, Percent	6.6	14.4
Selectivity for Sulfur Dioxide, Percent	92.4	82.4
Selectivity for Sulfur Trioxide,, Percent	1.0	3.2

h) Method of Sulfiding Sorbent

Table 5.13 compares the effect of in situ method of sulfiding sorbent with the effect of using presulfided sorbent. Selectivity for elemental sulfur is higher for the presulfided sorbent.

The sulfur content of the presulfided sorbent was much higher than in situ sulfided sorbent. This may have resulted in the presence of higher iron sulfides in the presulfided sorbent. Thus the elemental sulfur forming mechanisms may be different for the presulfided and in situ sulfided sorbents. Secondly, the presulfided sorbent was exposed to air at room temperature. Usually sulfided material is oxidized easily when exposed to air.

TABLE 5.13

EFFECT OF THE METHOD OF SULFIDING SORBENT ON REGENERATION PRODUCT DISTRIBUTION

Run No.	2106	2119
Regeneration Feed Gas, Mol Percent		
Water	85	85
Air	15	15
Sulfur Dioxide	0	0
Nitrogen	0	0
Sorbent	42 Percent Commercial Iron Oxide on Fly Ash	42 Percent Commercial Iron Oxide on Fly Ash
Sorbent Volume, cc	40	40
Method of Sulfiding	In Situ	Presulfided to High Level of Sulfur Content(1)
GHSV	600	600
Regeneration Duration, Hours	14	14
Reactor Block Temperature, °F	1000	1000
Material Balance, Percent	97	59
Selectivity for Elemental Sulfur, Percent	14.4	41.7
Selectivity for Sulfur Dioxide, Percent	82.4	55.7
Selectivity for Sulfur Trioxide, Percent	3.2	2.6

(1) Presulfiding was done at 1200°F using a feed containing 45% H_2S and 55% N_2.

5.5 Conclusions

Conclusions of this experimental work are listed below.

1. The amount of elemental sulfur produced during the regeneration of sulfided sorbents can be as high as 45 mol percent of the total sulfur product. The concentration of elemental sulfur depends on the feed gas composition, sorbent characteristics and operating conditions.

2. Regeneration feed gas with high water content greater than 90 mol percent should be used to increase the selectivity for elemental sulfur. Water content is a critical process variable.

3. Elemental sulfur formation is favored in a reducing atmosphere or oxygen starved regeneration gas. The elemental sulfur is further oxidized to SO_2 in an oxidizing atmosphere.

4. The formation of elemental sulfur is inhibited when sulfur dioxide is a major constituent of the regeneration gas.

5. Silica supported sorbents have a greater selectivity for the formation of elemental sulfur than fly ash supported sorbent.

6. Sorbents made with chemically pure iron oxide have a greater selectivity for elemental sulfur formation than sorbents made with commercial iron oxide.

7. An increase in GHSV results in an increase in the elemental sulfur selectivity for the fly ash sorbents.

8. Thermodynamic chemical equilibrium analysis predicted the experimentally observed increase in the selectivity for elemental sulfur formation with an increase in water content and decrease in air content. It did not predict the large magnitude of selectivity for elemental sulfur formation observed by APCI and by Schrodt.[6]

6.0 APPLICATION OF THE APCI SIMULATION MODEL

6.1 Background

In the previous APCI work under DOE Contract EX-76-C-01-2033 a process simulation model was developed for the absorption of H_2S into iron oxide held on an inert support and the subsequent regeneration of the bed with dilute oxygen. The simulation model gives guidance for experimental work and is a powerful tool in process design and optimization.

This contract (DOE EF-77-C-01-2757) was drafted when MERC was engaged in a limited experimental program at the pilot scale on the hot desulfurization of producer gas. The contract was based upon the assumption that MERC would make three runs which would follow closely the cycles of plant-scale operation; namely, the inlet temperature and composition would be held constant during absorption and regeneration.

The actual regeneration operation deviated from this plan in several ways. First, only two runs were made. Second, the inlet conditions were not held constant in these runs. In the first regeneration run the inlet oxygen concentration and total gas flow rate were adjusted in trying to keep the maximum bed temperature below 1500°F. In addition the inlet temperature was decreased intentionally during the run from 1035°F to 115°F. This decrease was obtained by turning off the electric heaters to the reactor. In the second run the inlet oxygen concentration and total gas flow rates were held constant; the maximum temperature in the bed increased to 1845°F. The inlet temperature was decreased intentionally from 1130°F to 110°F. The inlet and exit oxygen concentrations were not measured, and there is an apparent calibration error in the reported SO_2 exit concentration. Thus the experimental data are confounded by factors which go beyond the scope of the APCI simulation model.

MERC observed bed temperatures substantially larger than the adiabatic temperature rise for complete reaction in the gas phase. These very large increases can damage the sorbent support, endanger the reactor, or simply deactivate the sorbent. Thus it is useful to find a simple explanation for the excessive temperatures in the regeneration process and then to develop ways to control the bed temperature during regeneration.

This chapter is divided into five parts. The objectives and important conclusions are presented in Sections 6.2 and 6.3. Section 6.4 presents the comparison of the APCI simulation to the MERC data. Section 6.5 develops a method for control of the maximum bed temperature.

6.2 Objectives

The objectives of this portion of the project are as follows:

a) To demonstrate the utility of the APCI simulation model for representing the excessive temperature levels observed in the MERC studies,

b) To compare, where possible, the MERC data during regeneration to the APCI model,

c) To develop methods for controlling the maximum temperature in the reactor during regeneration.

6.3 Summary

The excessive temperature levels observed in the MERC experiments are predicted by the APCI model for regeneration. These extreme temperature levels occur because the rate at which a narrow regeneration zone moves through the reactor approaches more closely the rate at which thermal energy is convected through the unit. Under these conditions the reaction rate snowballs in the narrow reaction zone and the bed temperature exceeds the gas-phase adiabatic temperature rise.

The easiest way to control the maximum bed temperature is to hold the inlet temperature and oxygen concentration constant. When this mode of operation is used, the maximum bed temperature will be less than about 125 percent of the gas phase temperature increase. The oxygen concentration can be used to control the maximum bed temperature effectively.

6.4 Application of the APCI Simulation Model to MERC Data

6.4.1 Selection of Data

A simulation package for the transient fixed-bed absorption and regeneration of the hot desulfurization process was developed previously by APCI.[1] In this contract the APCI analysis is applied to some data for regeneration gathered at MERC. The purpose of this comparison is to test the APCI model severely. The simulation then is to provide insight into the causes of the very high peak bed temperatures observed in the MERC regeneration cycle.

MERC provided APCI with data on two absorption-regeneration cycles. The complete report of these data are given in Appendix B. In the first run the flow rate and gas composition were altered in an attempt to keep the maximum bed temperature below 1500. The oxygen content was reduced by increasing the flow of diluent gas or decreasing the flow of air. In the second run the inlet composition and flow rate were held constant. In both of these runs the regeneration gas was supplied to the reactor at ambient temperature and passed through a set of ceramic supports which acted as a gas preheater. The bed temperature at the inception of regeneration was nearly uniform in both runs. The electric heaters were turned off at the start of the run, and consequently the gas temperature at the entrance of the bed decayed from 1000°F to 100°F over a ten-hour period.

The bed temperature was measured at one-foot intervals along the centerline of the unit and at six-inch intervals located four inches radially from the centerline. The data from the off-center probes are confounded by a small radial temperature loss and consequently show about a 40°F lower peak temperature. The temperature data for the centerline thermocouples are shown on Figure 6.1. These curves are the major information for the run. The corresponding data for the off-center data are shown on Figure 6.2. The centerline data show that the peak bed temperature is about 1845°F and increases only slightly as the peak moves down the reactor. The sharpness (maximum slope) of the leading edge of the wave is greater than the trailing edge for the data taken at the one-foot position in the bed. Just the opposite behavior is observed for the peak recorded at the four-foot position in the bed. The width of the temperature wave at 1400°F is nearly constant. Thus the wave appears to have constant-pattern behavior superficially but not in detail. If the bed exhibited constant pattern behavior, then a simplified, steady-state analysis could be made. The MERC data cannot be represented by the constant-pattern model.

The data for the four-inch radial position shown in Figure 6.2 do not show the uniformity observed at the centerline. These data also show substantial variation in the wave shape and are confounded by radial heat conduction. Therefore, these data were not used in the analysis in a quantitative way.

FIGURE 6.1

MERC CENTERLINE TEMPERATURE PROFILES

MERC RUN 11, CYCLE NO. 2

SEE TABLE 6-2, APPENDIX B

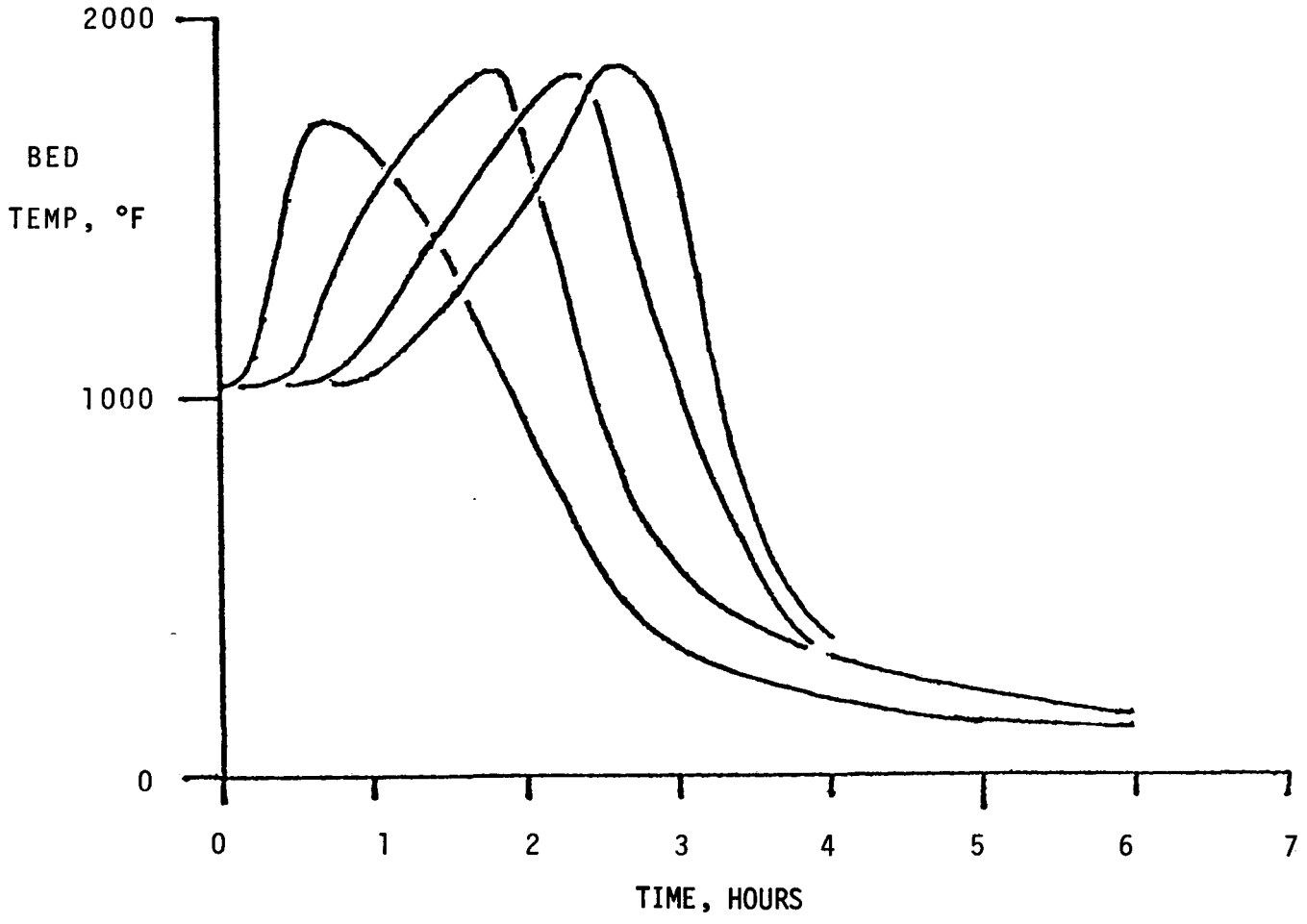

FIGURE 6.2

MERC NEAR WALL TEMPERATURE DATA

MERC RUN 11, CYCLE NO. 2

SEE TABLE 6-2, APPENDIX B

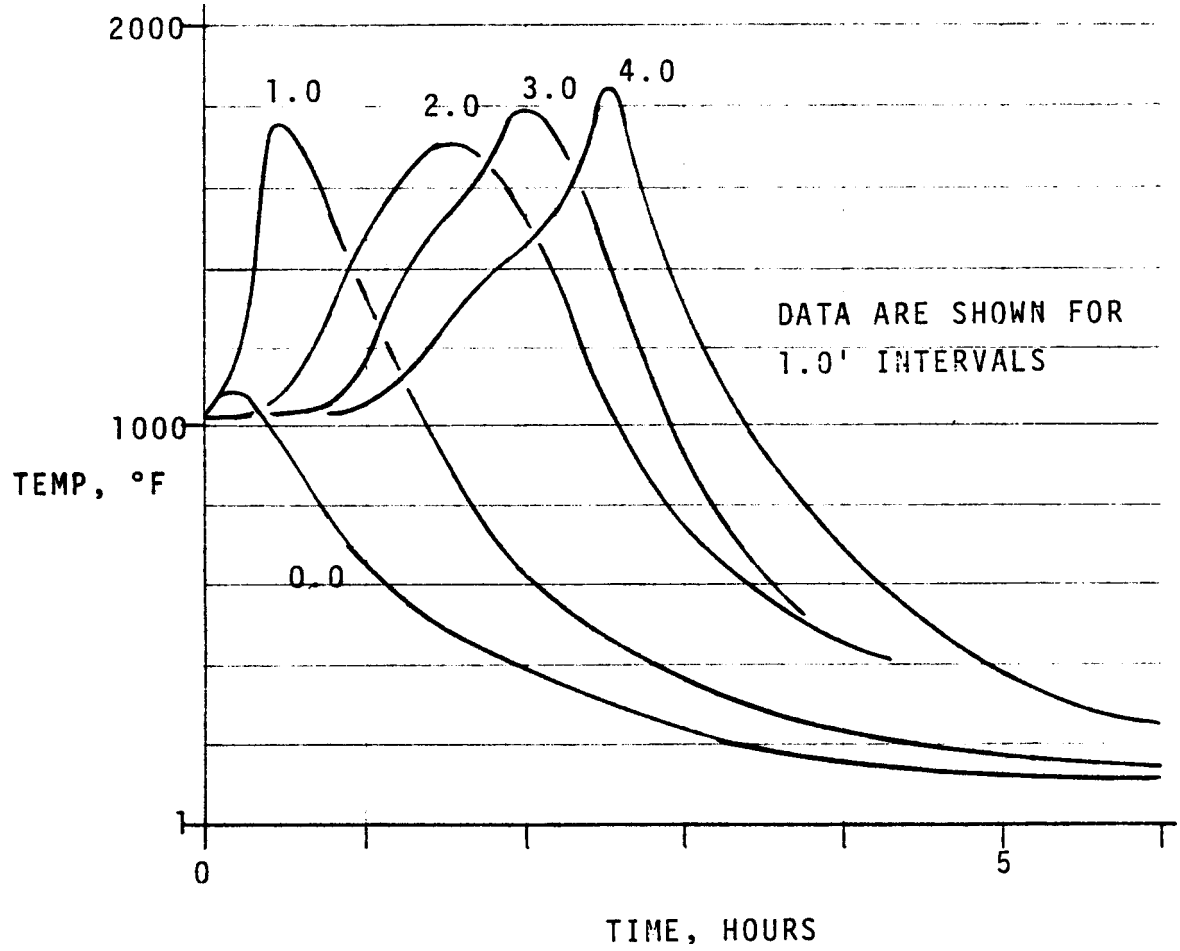

The second absorption cycle required considerably less time than the first; this observation suggests that the bed was not completely regenerated during the first cycle. This conjecture will be examined in greater detail later.

MERC did not record the oxygen breakthrough during regeneration. The negative SO_2 concentration reported for the first run appears to be an instrument offset error. Positive SO_2 concentrations were recorded during the second regeneration run. In the absence of any oxygen breakthrough data or measurement of residual sulfur on the regenerated sorbent, the major data available are the centerline temperature profiles shown on Figure 6.1.

6.4.2 Application of the APCI Model

The derivation of the simulation model for this process is discussed at length in the last report to DOE,[1] and portions of this development are given in Appendix C. The former development was modified to allow the gas and solid temperature to have different values. The previous APCI work developed three models for sorption and regeneration; the film model, the shrinking core model, and the film-kinetic model. The kinetic-film model appeared to fit the data best. Therefore only the kinetic-film model was used in this effort. The partial differential equations which were used to model the MERC data are given in Table 6.1. The definition of the parameters is given in Table 6.2 and in greater detail in Appendix C. The group N_H is the new parameter in the APCI model. This group is proportional to the resistance for heat transfer between the sorbent and the gas. When N_H is zero, the gas and solid are forced to have identical temperatures. In addition the APCI model was altered to use the measured temperature at the entrance of the bed as input data.

The partial differential equations were solved as characteristic equations in a program which has high stability and accuracy for low values of the transport numbers, N^F and N_H. There are seven parameters in the total model, and hence efficiency demands that only a few of these be treated as adjustable parameters. Appendix D shows the calculation of these parameters in detail. These calculations are summarized in Table 6.3; this table also lists the expected range of these parameters.

The most direct test of the APCI model is to compare the simulation based on the parameters listed in Table 6.3 with the MERC data for the second cycle. The second cycle was chosen because the flow rate and composition were held constant, and therefore the programming for the parameters in the simulation model was simplified. Figure 6.3 is a plot of the calculated temperatures at the centerline of the reactor at the four locations of thermocouples. These curves can be compared to the MERC data by comparing Figure 6.3, the simulation, with Figure 6.1, a smooth-curve version of the data. In addition Figure 6.3 displays the MERC data for the thermocouple 4.0 feet from the entrance as a series of dots.

The simulation predicts a maximum temperature of 1960°F, 100 degrees greater than observed, and locates this peak about 30 minutes later than the data. Thus the ex nihilo calculation is qualitatively correct in many features but hardly an optimized representation of the system. The estimated saturation time, T_{SAT}, cannot be estimated accurately from the data available; this problem is explored more completely in Appendix D. In particular the estimated value of T_{SAT} must be reduced if the bed is incompletely converted to sulfide.. The parameter N^F has the next greatest uncertainty. Figure 6.4 shows the simulated temperature profiles with the value of T_{SAT} reduced and N^F increased. The simulation fits the data somewhat better; the location of the temperature maxima corresponds to the data.

TABLE 6.1

MODEL FOR TRANSIENT REGENERATION

INCLUDING PARTICLE-FLUID HEAT TRANSFER

DIMENSIONLESS OXYGEN CONCENTRATION IN THE GAS PHASE

$$\frac{\partial F}{\partial X} = -R_X$$

$F(\tau, 0)$ = specified function of dimensionless time

$$R_X = \frac{FW}{N^F + N^K W}$$

DIMENSIONLESS SULFIDE CONCENTRATION IN THE SOLID PHASE

$$\frac{\partial W}{\partial \tau} = -R_X$$

$W(0, X) = 1$ when the bed is saturated with FeS at the beginning of the regeneration cycle.

GAS TEMPERATURE

$$\frac{\partial T_G}{\partial X} = \frac{(T_S - T_G)}{N_H}$$

$T_G(\tau, 0)$ is a specified function of time; this function was measured.

SOLID TEMPERATURE

$$\frac{\partial T_S}{\partial \tau} = \frac{1}{N_{CP}} \left(\frac{(T_G - T_S)}{N_H} \right) + \Delta T_{Ab} \cdot R_X$$

$T_S(0, Z) = T_{SO}$ when the temperature distribution in the bed is uniform at the beginning of the operation.

TABLE 6.2

NOTATION FOR SECTION SIX

DEPENDENT VARIABLES

F	Fraction of bulk oxygen remaining
W	Fraction of solid reactant remaining
T_G	Gas temperature in the bed, °F
T_S	Solid temperature in the bed, °F

INDEPENDENT VARIABLES

X	Dimensionless position, x/ℓ
τ	Dimensionless time, $v_o t/\ell$

DIMENSIONLESS PARAMETERS

N_{CP}	Heat capacity parameter, v_C/v_T
N^F	Film sorption parameter, $(\beta Co \cdot a_B \ell)^{-1}$
N_H	Heat transfer parameter, $(St \cdot a_B \ell)^{-1}$
N^K	Kinetic sorption number, $V/(k_1$
R_X	Dimensionless reaction rate, $-\frac{W}{N + N^K W}$
γ	Activation energy group, $(-\Delta E/(R_G T_{ref}))$

TABLE 6.2 (continued)

NOTATION FOR SECTION SIX

DIMENSIONAL PARAMETERS

T_{SAT} Saturation time, ℓ/v_G

T_{Ab} Gas phase adiabatic temperature rise

DEFINING TERMS

a_B External area per unit volume of bed, ft^{-1}

Co Colburn number, $\frac{k_F}{V}$

Cp_s Heat capacity of solid, BTU/lb/°F

Cp_G Heat capacity of gas, BTU/lb-mol/°F

ΔE Reaction activation energy, BTU/lb-mol/°F

G Mass flux of gas, $lb/ft^2/hr$

$\underline{G}$ Mol flux of gas, $lb\text{-}mols/ft^2/hr$

h Heat transfer coefficient, $BTU/hr/ft^2/°F$

k_F Film transfer coefficient, ft/hr

ak^K Reaction rate in solid phase, cu ft/lb-mol iron oxide/hr

k_1 First order rate, $ak^K(1 - \varepsilon)M_o$, hr^{-1}

ℓ Bed length

TABLE 6.2 (continued)

NOTATION FOR SECTION SIX

DEFINING TERMS (continued)

M_o	Iron oxide concentration in solid, lb-mols/ft^3
R_G	Gas constant, BTU/lb-mol/°R
St	Stanton number, (h/(GCp)
T_{ref}	Reference temperature, °R
V	Superficial gas velocity
V_c	Chemical velocity, $\alpha M_o(1 - \varepsilon)\ell/(GY_o)$
V_t	Thermal velocity, $(\rho Cp)_s(1 - \varepsilon)\ell/(GCp)$
Y_o	Mol fraction of oxygen at inlet
β	Empirical parameter in film parameter
ε	Void fraction in bed

TABLE 6.3

ESTIMATED PARAMETERS FOR MERC EXPERIMENT

PARAMETER	NOMINAL VALUE	RANGE
DIMENSIONAL PARAMETERS		
T_{SAT} Ideal saturation time	11.1 hr	7.7-13.3 hr
T_{Ab} Gas-phase adiabatic temperature rise	426°F	300-500°F
DIMENSIONLESS PARAMETERS		
N^F Film sorption parameter	0.0167	0.01-0.07
N^H Heat transfer number	0.005	0.004-0.008
N^K Kinetic sorption number	0.262	0.05-0.3
N_{CP} Heat capacity number	0.135	0.06-0.20
γ Activation energy parameter	10.92	6-15

FIGURE 6.3

SIMULATED TEMPERATURE WAVES

BASE CASE

DOTS (•) ARE MERC DATA

SEE TABLE 6-2, APPENDIX B

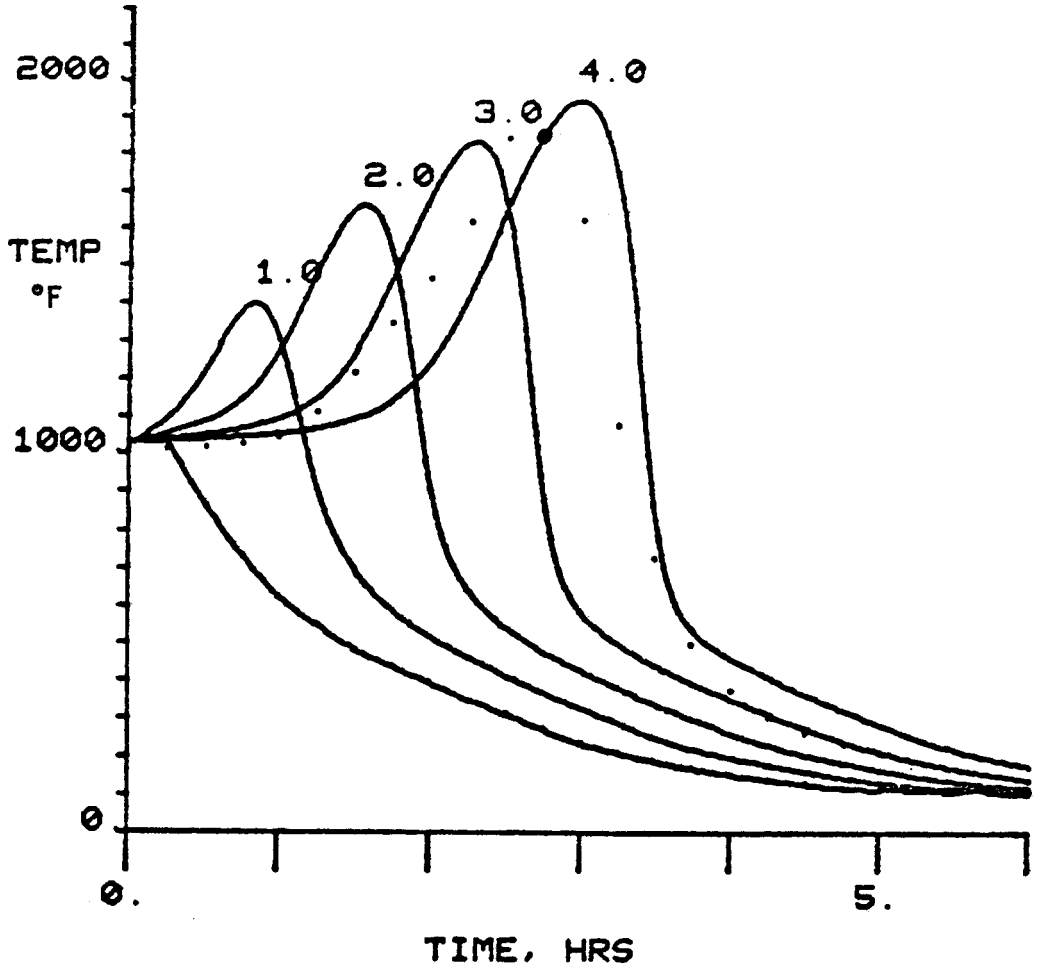

T_{SAT}	=	13.3 HOURS	N_{Ab}^{K}	=	0.262
T_{Ab}	=	426°F	N_{CP}	=	0.135
N^{F}	=	0.050	γ	=	10.92
N_{H}	=	0.005			

Table 6.4 presents a set of parameters which show some of the flexibility of the model to fit the regeneration data with other choices of these parameters. These cases are reported on Figures 6.4-6.7. These figures show that the simulation represents the data adequately, but no unique set of parameters can be identified from the simulation. The range suitable parameter choices spans the error limits of the parameter estimates. Table 6.5 presents a quantitative summary of the effect of changes in the parameters on the temperature waves.

These simulation studies provide other insights into the MERC experiment. Figure 6.8 shows the regeneration profile at the end of the run; the model suggests that the bed was incompletely regenerated. Figure 6.9 shows the temperature difference between the gas and the solid sorbent as a function of time. The difference is not large enough to affect the regeneration process greatly. Similar results were observed for all other cases. Therefore, the rate of heat transfer between the gas and the solid is not a critical parameter; however, the temperature difference between the gas and the solid depends directly upon the value of the heat transfer coefficient. Finally the predicted breakthrough curve for regeneration is very sharp. Figure 6.10 shows the calculated breakthrough curve for oxygen and the MERC data on the SO_2 concentration in the exit gas. The high temperature in the reactor makes the reaction zone very thin, and the resulting breakthrough occurs very quickly.

Figure 6.11 shows the predicted temperature waves for the MERC reactor for constant inlet temperature and oxygen composition. The maximum temperature in the unit is about 1540°F, substantially less than observed by MERC. These results appear to be a paradox; the maximum temperature in the bed is less when the inlet conditions are held constant than when the inlet temperature falls. The paradox is explained below.

The behavior of the temperature peak can be explained by examining the reaction zone in the reactor. If the kinetic resistance measured by N^K is large, then the reaction occurs throughout the entire bed and there always is some oxygen in the efflux from the reactor. If the kinetic resistance is low, however, the reaction occurs in a narrow zone. There is little consumption of oxygen on the entrance side of the reaction zone and very little oxygen remaining on the exit side of the zone. The regeneration reaction rate is large enough that regeneration occurs in a reaction zone.

TABLE 6.4

MODEL PARAMETERS FOR CASES

	CASE				
	BASE	1	2	3	4
T_{SAT}, hr	13.3	11.1	11.1	10.8	4.4
T_{Ab}, °F	426	-	-	-	-
N^F	0.050	0.017	0.010	0.067	0.033
N_H	5.0-0.3	-	-	-	-
N^K	0.262	-	-	0.111	0.0625
N_{CP}	0.1354	-	-	-	0.50
γ	10.92	-	-	-	-
T_{MAX},°F	1960	1860	1790	1840	1880

TABLE 6.5

EFFECT OF PARAMETERS ON THE MAXIMUM TEMPERATURE

$N_{CP} < 1$

[The thermal velocity is greater than chemical velocity.]

Parameter	Effect of Increasing Parameter
T_{SAT}	Time for maximum temperature increases
T_{Ab}	Increases maximum temperature
N^F	Increases peak temperature Decreases the slope of the trailing edge of the temperature wave
N_H	Small increase in peak maximum
N^K	Increases maximum temperature in parameter range studied
N_{CP}	Increases maximum temperature
γ	Increases maximum temperature Maximum temperature moves toward bed entrance

FIGURE 6.4

SIMULATED TEMPERATURE WAVES

CASE 2

DOTS (•) ARE MERC DATA

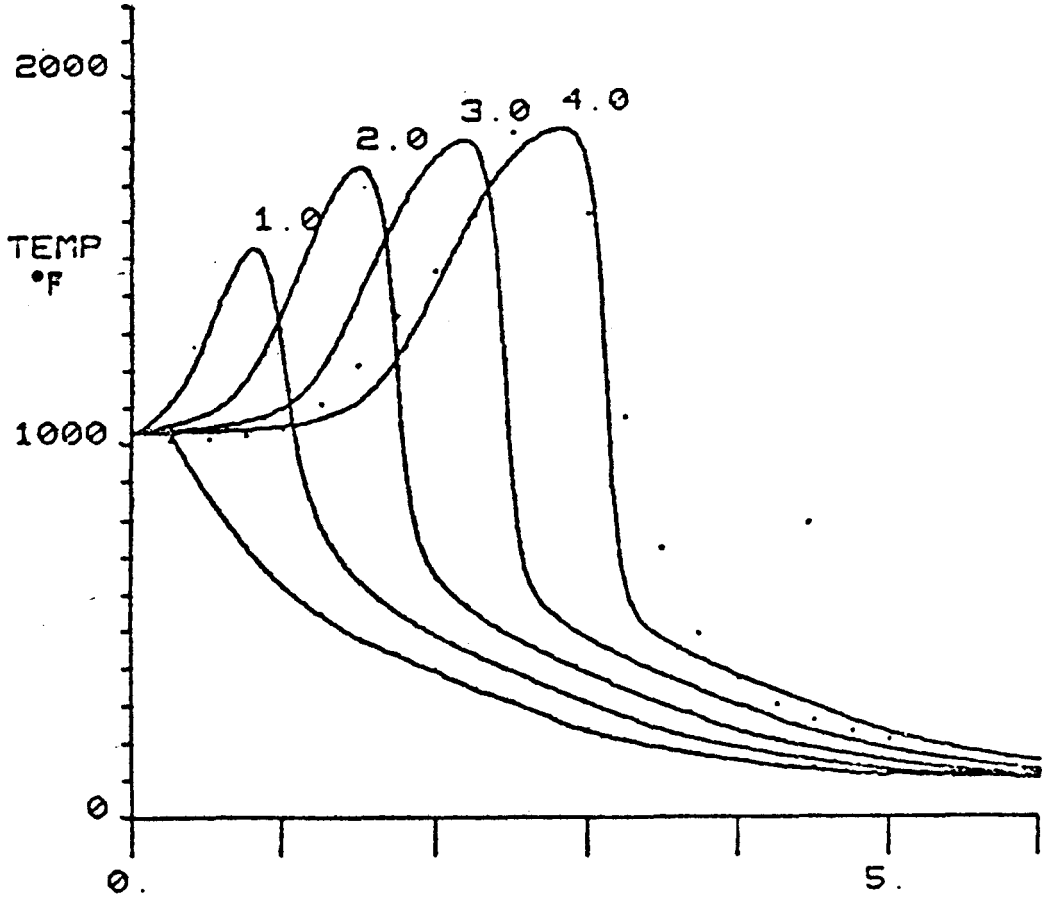

T_{SAT} = 11.1 HOURS		N_{Ab}^{K} = 0.262	
T_{Ab} = 426°F		N_{CP} = 0.135	
N^{F} = 0.017		γ = 10.92	
N_{H} = 0.005			

FIGURE 6.5
SIMULATED TEMPERATURE WAVES
CASE 3

DOTS (•) ARE MERC DATA

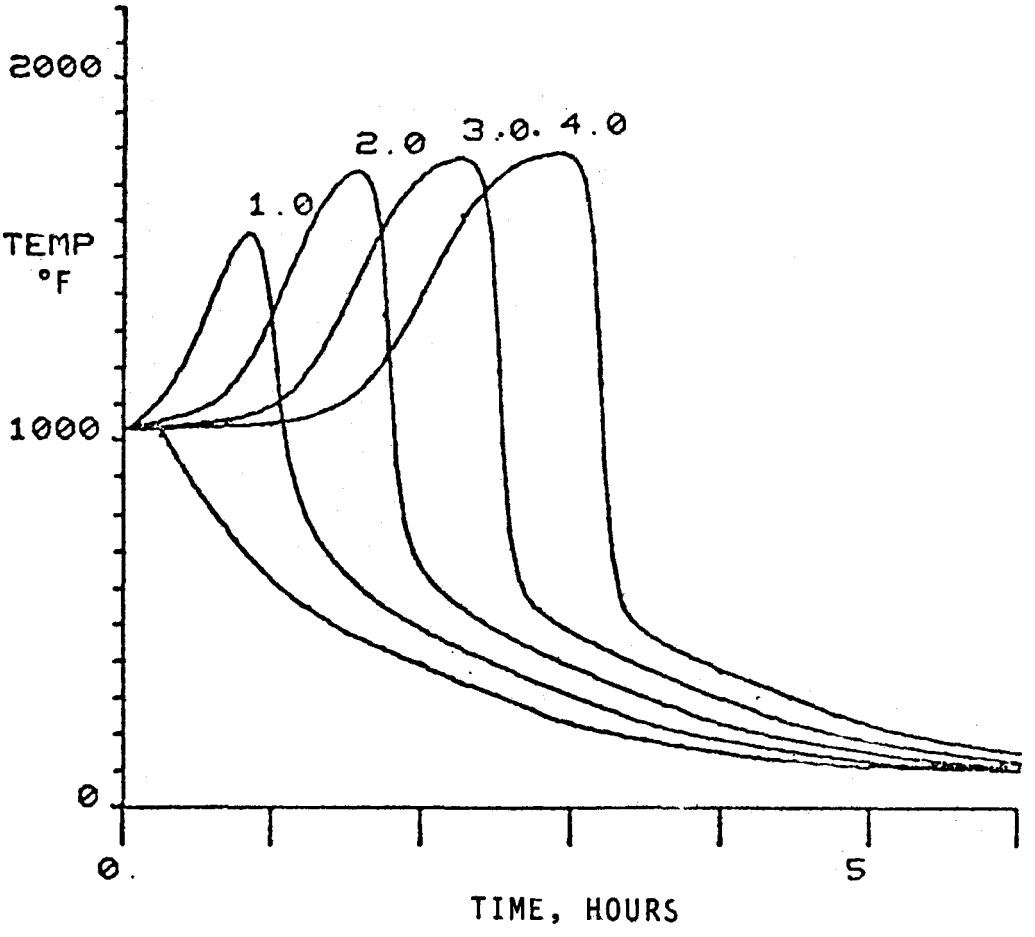

T_{SAT}	=	11.1 HOURS	$N_{Ab}{}^{K}$	=	0.262
T_{Ab}	=	426°F	N_{CP}	=	0.135
N^{F}	=	0.010	γ	=	10.92
N_{H}	=	0.005			

FIGURE 6.6

SIMULATED TEMPERATURE WAVES

CASE 4

DOTS (•) ARE MERC DATA

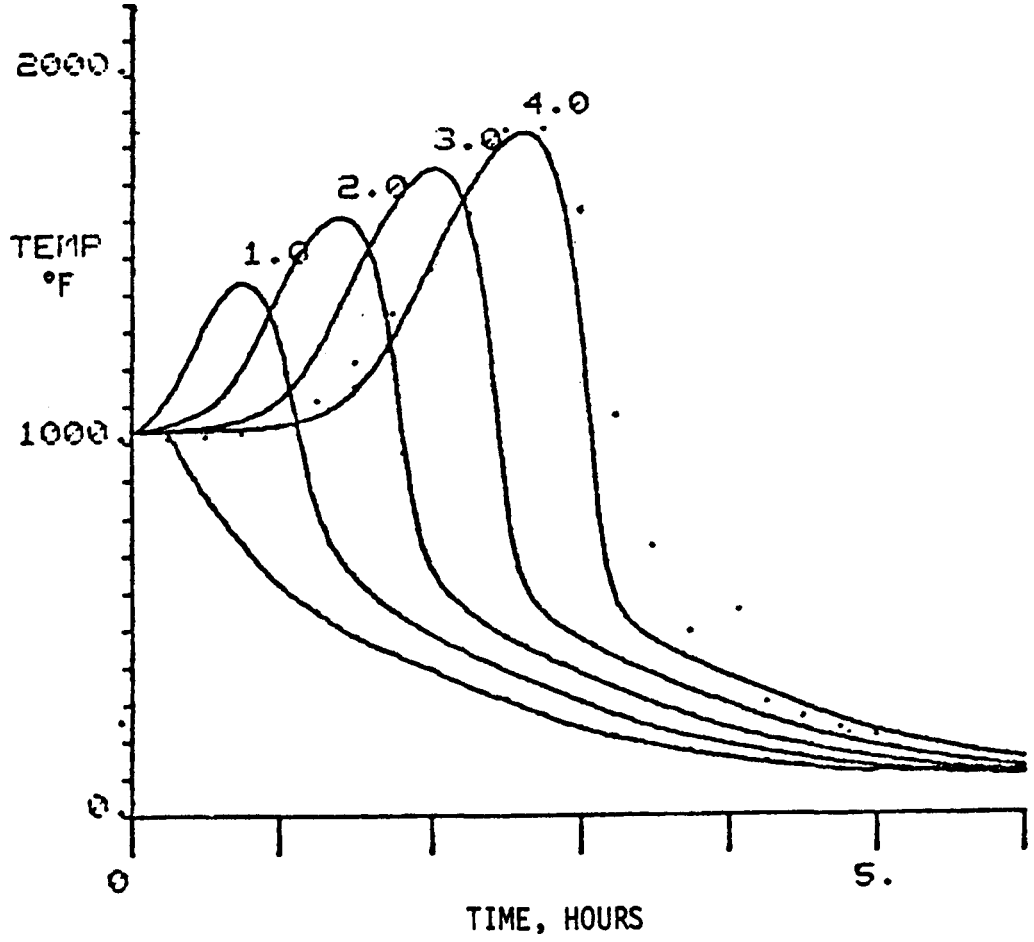

T_{SAT}	=	10.8 HOURS	N_{Ab}^{K}	=	0.111
T_{Ab}	=	426°F	N_{CP}	=	0.135
N^{F}	=	0.067	γ	=	10.9
N_{H}	=	0.005			

FIGURE 6.7
SIMULATED TEMPERATURE WAVES
CASE 5

DOTS (•) ARE MERC DATA

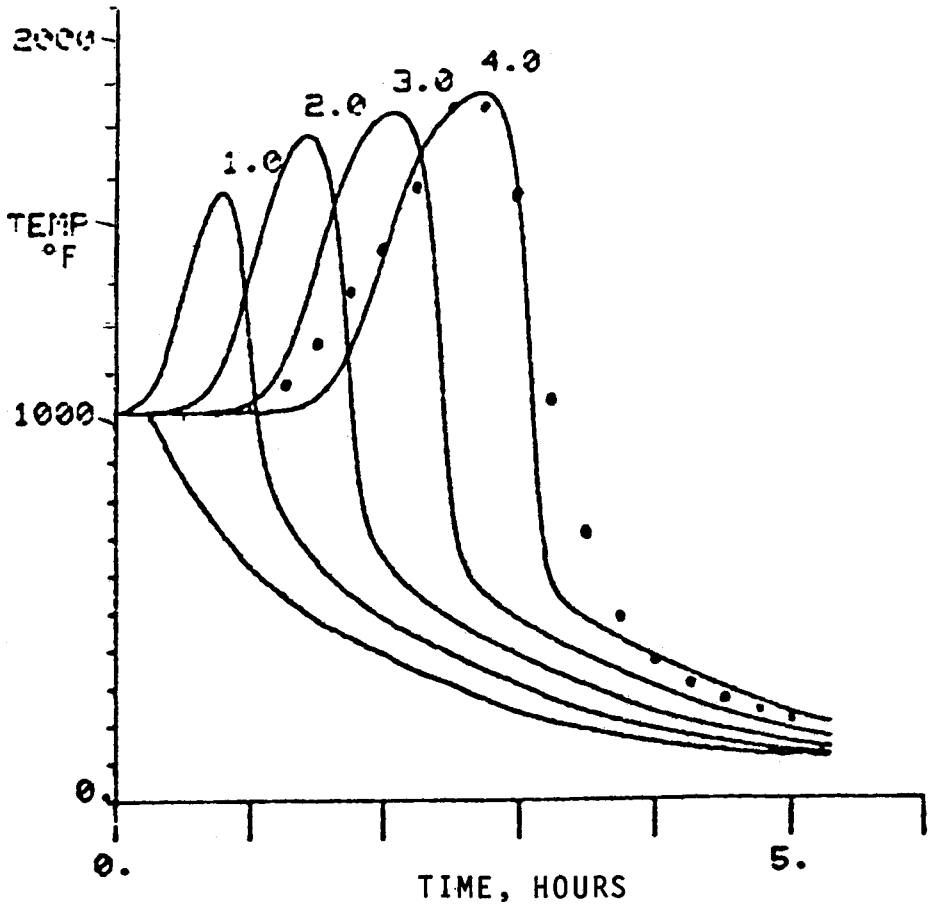

T_{SAT}	=	4.4 HOURS	$N_{Ab}{}^{K}$	=	0.0625
T_{Ab}	=	426°F	N_{CP}	=	0.500
N^{F}	=	0.033	γ	=	10.9
N_{H}	=	0.005			

FIGURE 6.8

REGENERATION PROFILE AT END OF RUN

CASE 2

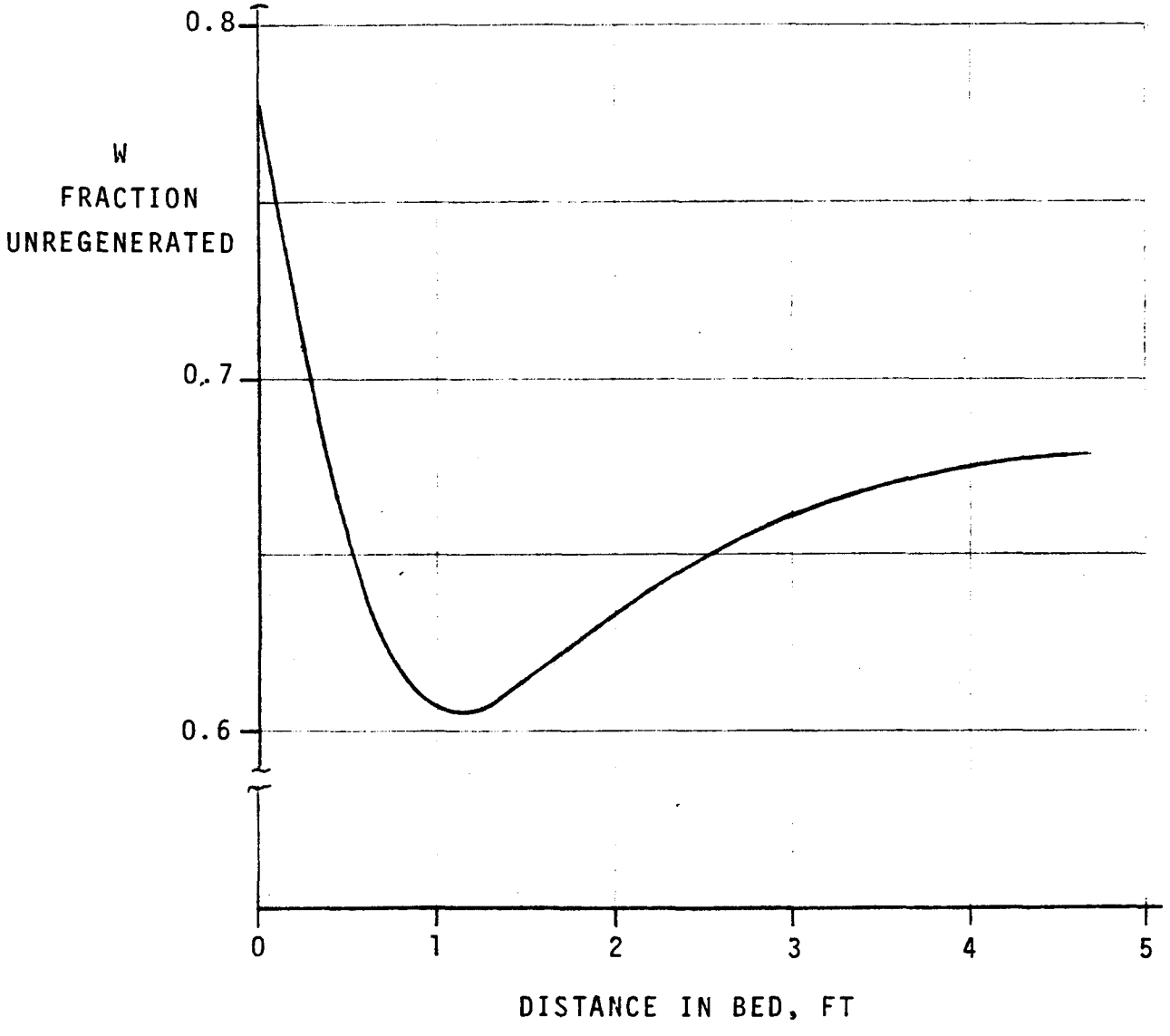

FIGURE 6.9

CALCULATED SOLID-GAS TEMPERATURE DIFFERENCE

CASE 2

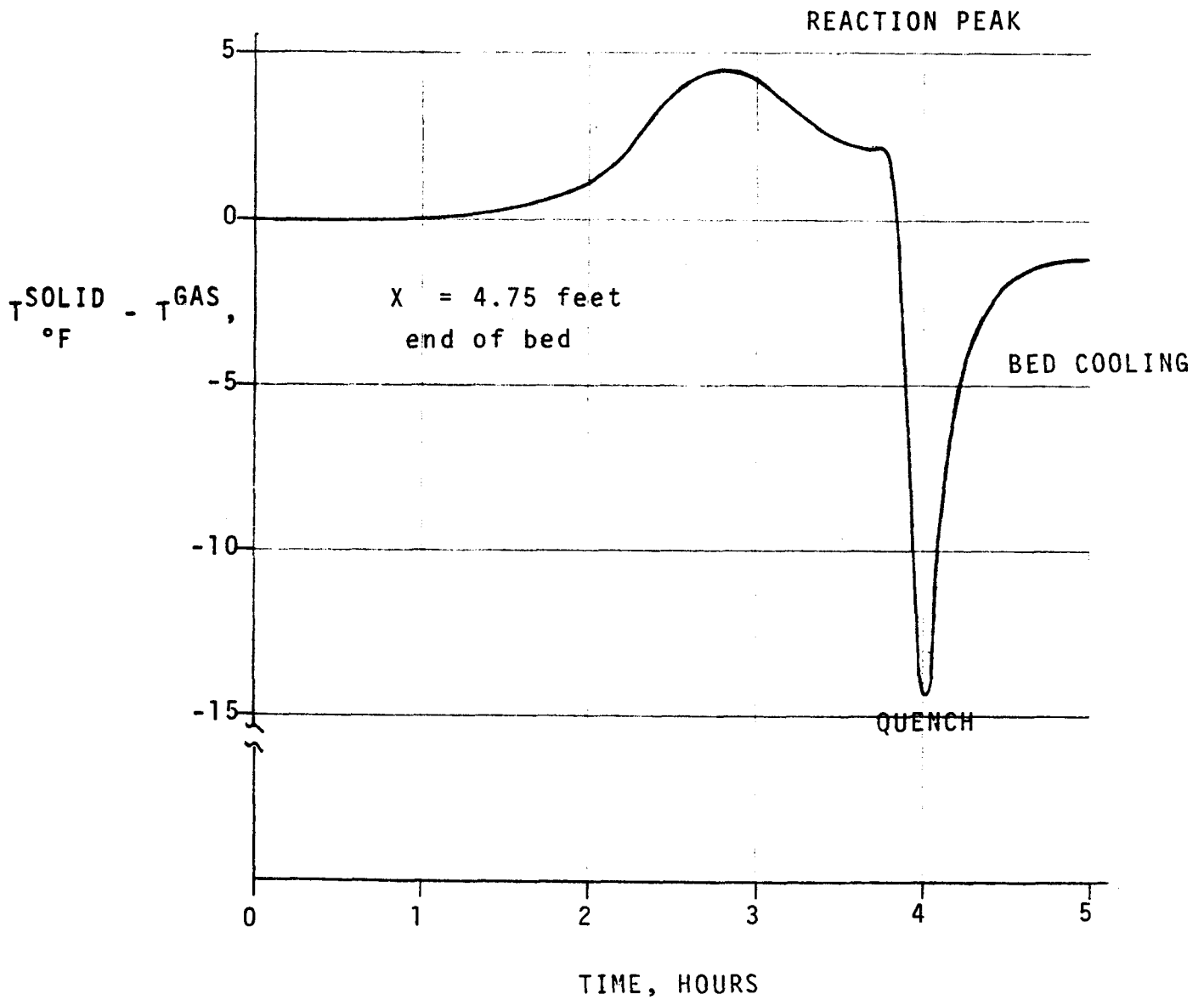

FIGURE 6.10
CALCULATED BREAKTHROUGH CURVE
CASE 2

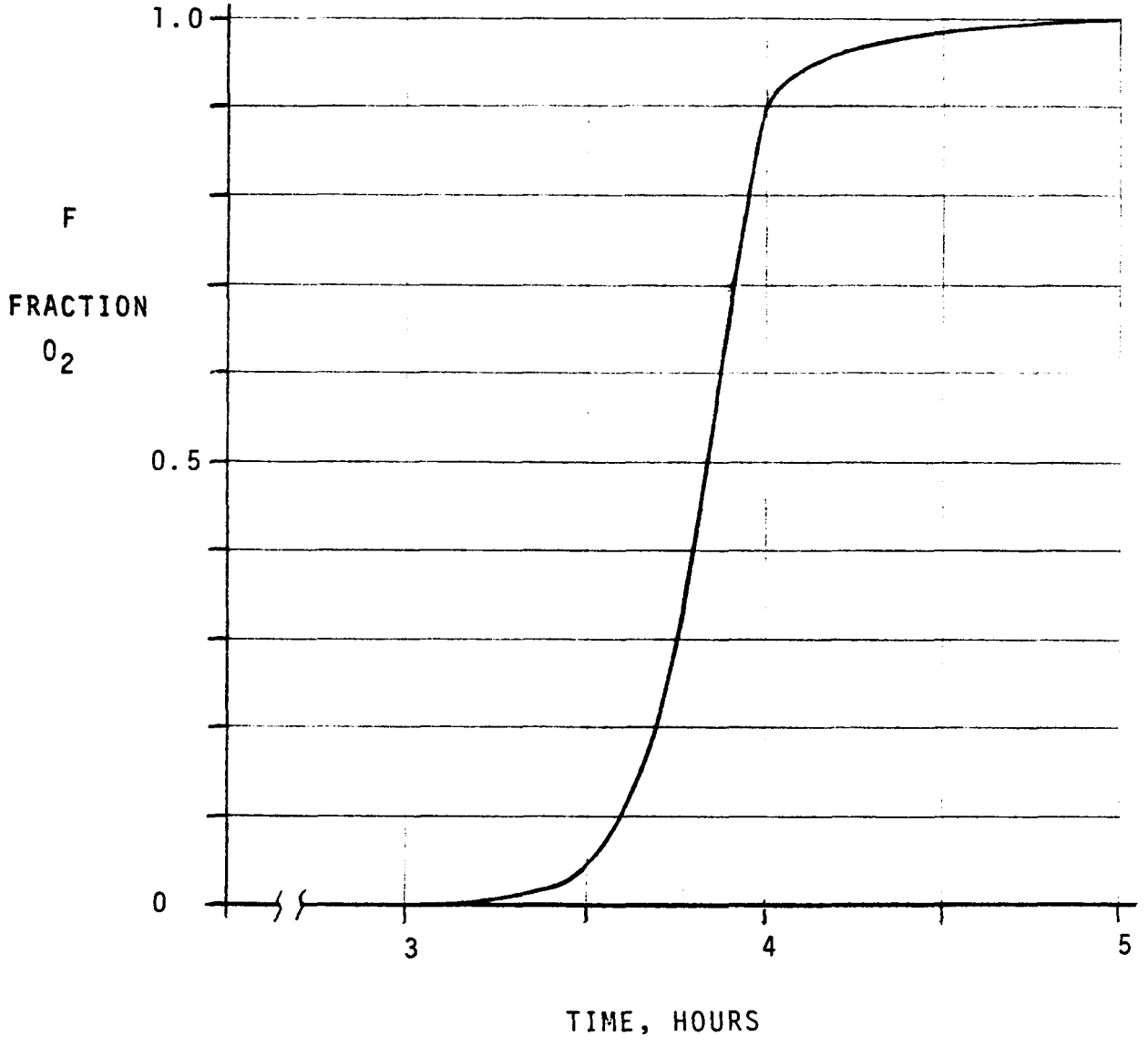

FIGURE 6.11

TEMPERATURE WAVES

FIXED INLET TEMPERATURE

CASE 4

DOTS (•) ARE MERC DATA

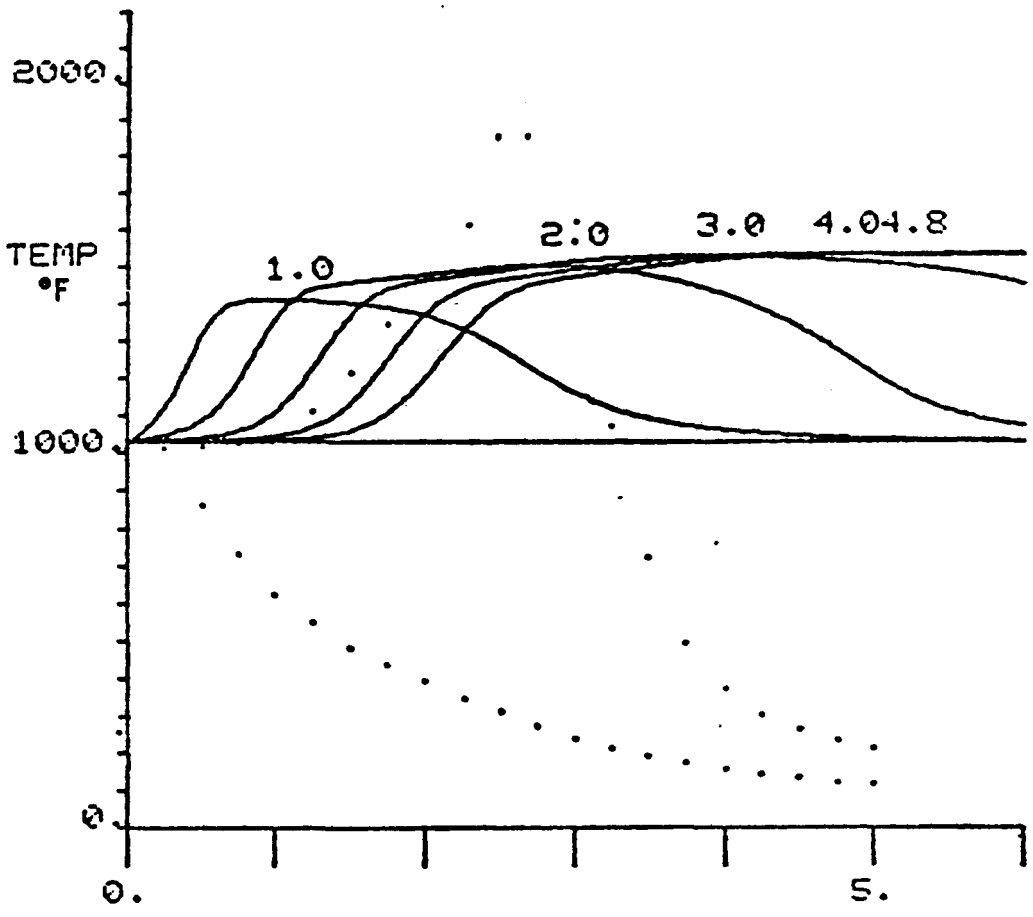

T_{SAT}	=	10.8 HOURS	N_{Ab}^{K}	=	0.262
T_{Ab}	=	426°F	N_{CP}	=	0.135
N^{F}	=	0.067	γ	=	10.92
N_{H}	=	0.005			

The shape of a temperature spike on the regenerator can be explained as an interaction of chemical and thermal wave fronts. The thermal wave velocity is the rate at which an ideal step change in temperature can move through an adiabatic reactor. This velocity can be found from a simple heat balance as:

$$V_T = \frac{(GCp)_G}{(\rho Cp)_S(1 - \varepsilon)} \qquad (6.1)$$

where v_T is the thermal velocity, ft/hr

G_G is the mass flow rate of gas, lb/hr/ft^2

Cp_G is the heat capacity of the gas, BTU/lb/°F

ρ_S is the density of the solid, lb/ft^3

Cp_S is the heat capacity of the solid, BTU/lb/°F

$(1 - \varepsilon)$ is the volume fraction solid in the bed

The chemical velocity describes the speed at which a very narrow regeneration wave would move through the bed. This velocity can be calculated from a mass balance:

$$v_c = \frac{\underline{G} y_o}{M_o \alpha (1 - \varepsilon)} \qquad (6.2)$$

where v_c is the chemical velocity, ft/sec

y_o is the inlet mol fraction oxygen

$\underline{G}$ is the molar flow of gas, lb-mols/ft^2/hr

M_o is the molar density of iron oxide in the sorbent, lb-mols/ft^3

α is the stoichiometric requirement of oxygen in regeneration, mols of oxygen/mol of Fe_2O_3

For constant inlet conditions the thermal velocity is much faster than the chemical velocity; the parameter N_{CP} shows that the thermal velocity is 7.36 faster than the chemical velocity. However, when the inlet temperature drops enough to stop the reaction rate in the reaction zone, then the effective chemical velocity is much higher and the regeneration is incomplete. Figure 6.12 shows a plot of the position of the thermal and chemical contribution of the temperature peak. The plot indicates that the thermal velocity is about 1.8 ft/hr for both thermocouple positions. The chemical velocity is much less constant but appears to be of the same order as the thermal velocity. If the reaction were complete, the chemical velocity is much less than the thermal velocity. Thus these data indicate that the regeneration reaction is incomplete since an incomplete reaction is equivalent to reducing M_o in the definition for the chemical velocity.

FIGURE 6.12

APPARENT THERMAL AND CHEMICAL WAVE POSITIONS FOR MERC REGENERATION

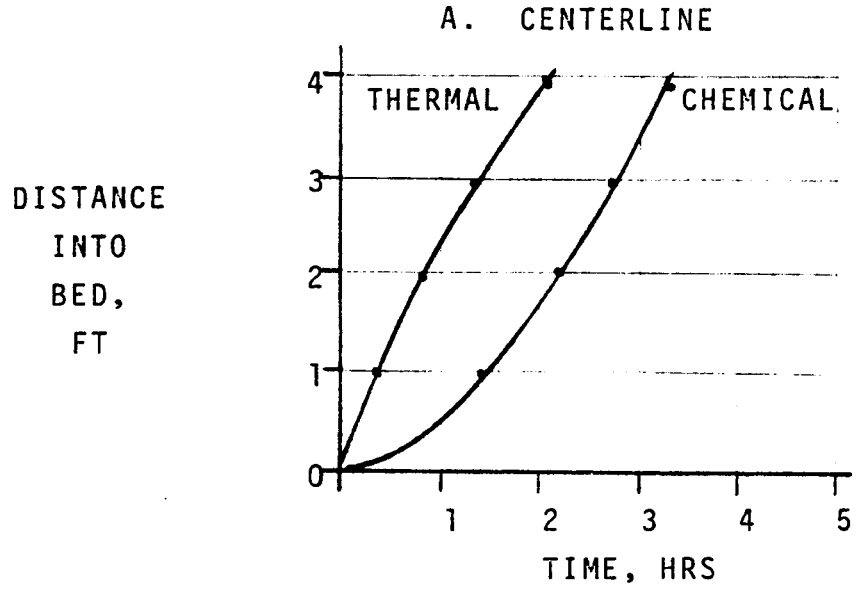

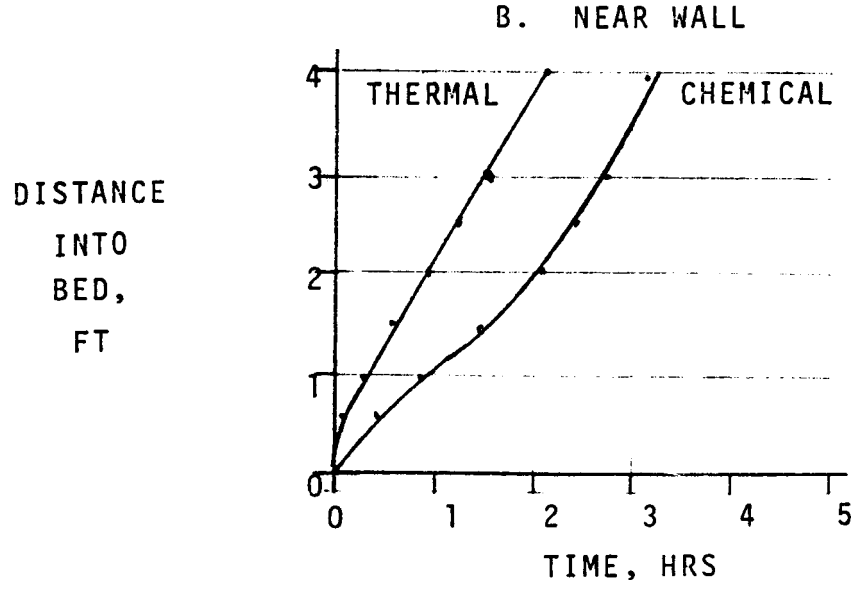

When the chemical and thermal velocities are nearly the same, the temperature in the reaction zone snowballs upward because the thermal energy of the reaction is carried away from the peak at rate proportional to the difference between the thermal velocity and chemical velocity. As this difference becomes small, the temperature in the reaction zone must increase. The maximum temperature paradox occurs because the effective chemical velocity is increased to approach the thermal velocity when the inlet gas temperature drops during regeneration. The regeneration reaction is less complete but occurs under conditions which raise the peak temperature far above the gas phase adiabatic temperature rise.

The comparison of the MERC data with the estimations from the APCI simulation model show that the model fits the data qualitatively using no adjustable parameters. With minor adjustment the model represents the data adequately. This simulation shows that the bed is not regenerated completely when the inlet temperature falls during regeneration. The effect of incomplete regeneration is to increase the effective chemical velocity in the bed. Although less material is reacted, the reaction occurs under conditions which reduce the rate of energy transport away from the reacting zone. Consequently the temperature in the reaction zone is paradoxically high.

6.4.3 Limitations of the APCI Model

All simulation models are defective to some degree. This section reviews potential weaknesses of the simulation model.

Appendix E contains a set of calculations developed by Carberry[8] which indicate the important transport processes for a fixed-bed catalytic reactor. This analysis indicates that axial dispersion, internal heat-transfer and external mass-transfer are not important. These transport processes are ignored in the APCI model.

The Carberry method suggests that heat transfer between the sorbent and the external gas may be significant since the maximum possible temperature difference has an upper bound of 40°F. The APCI model was modified to consider external heat transfer, and the calculations show that external heat transfer does not make a significant contribution to the overall simulation.

The critical assumptions in the model are outlined below:

1. Adiabatic Operation

   The assumption of adiabatic operation gives uniform radial temperature profiles in the simulation. The MERC reactor had a small radial temperature profile which was ignored. Thus the model applies best to the centerline data.

2. Film-Kinetic Rate Model

   The film-kinetic model was identified as the most effective model for simulation in the previous DOE supported work. The model contains three parameters: N^F, N^K and γ; and hence is flexible enough to represent data over a wide range. However, the model has not been compared to rate data above 1200°F.

3. System Chemistry

   The regeneration reaction is assumed to be

   $$2FeS + \frac{7}{4} O_2 \longrightarrow Fe_2O_3 + 2SO_2$$

   The reaction is nearly irreversible and highly exothermic. However, the state of the sulfide after sorption has not been determined, and consequently the regeneration cycle may produce other species. Therefore the adiabatic temperature rise may not be correct. This possibility does not change the conclusions of the analysis.

The APCI simulation has been compared to MERC temperature profile data. The simulation was not compared to breakthrough data or unaccomplished regeneration, both critical tests, because the experimental data needed were not available.

6.5 Control of the Maximum Temperature in the Regenerator

6.5.1 Introduction

The regeneration reaction for conversion of FeS_x to Fe_2O_3 is highly exothermic, and under some run conditions MERC has observed transient temperatures which are substantially greater than the gas phase adiabatic temperature rise. The maximum temperature in the reactor must be controlled to maintain the activity of the sorbent.

This section applies a mathematical model for transient fixed-bed reactors to the regeneration reaction for the desulfurization process. The objectives of this effort are twofold:

> To show that transient temperatures greater than the adiabatic temperature can be explained analytically.
>
> To develop simple operating method for limiting the maximum temperature during normal regeneration.

6.5.2 Development of the Model

When a component in the gas phase reacts with a component held in the solid phase of a fixed-bed reactor, the reactor cannot be operated at steady-state since the reactant in the solid phase is consumed with time. The analysis of these reactors has an extensive literature which has been reviewed by Butt.[9] This development extends the work of Johnson, et al.[10] Van Deemter[11] presented an often referenced preliminary version, and Bischoff[12] extended the mathematics to more general form.

The assumptions of the model developed by Froment[10] are in harmony with the regeneration process. These assumptions are:

1. Adiabatic operation of the reactor in which the radial temperature profile is uniform. This assumption is certainly true for large (>5-ft diameter) reactors and nearly valid for well-insulated pilot-plant reactors.

2. The fluid and solid have identical temperatures. The digital simulation of the MERC process showed that temperature differences are less than 5°F when the reaction is occurring.

3. Heat transfer in the axial direction occurs only by convection. The extremely large temperature gradients near the transient peak also transfer heat by radiation and conduction. Neglecting these modes of heat transfer is conservative.

4. The gas velocity is constant across the tube at all points in the reactor. This assumption flows from the assumption of adiabatic operation.

5. The rate equation can be written as:

$$r = K^K Y W$$

where K^K = sorption kinetic group

Y = fraction of oxygen remaining in the gas

W = fraction of original iron sulfide on the solid remaining unreacted

This rate expression is equivalent to assuming K^F is zero.

6. The reaction rate is independent of temperature. This assumption requires the reaction to be diffusion limited at high temperatures. The MERC data were represented by the film-kinetic model which limits substantially the increase in reaction rate with temperature. Therefore, although this assumption is not satisfied completely for regeneration, the approximation remains useful. The approximation is reviewed in greater detail later in this section.

7. The bed is assumed to be at a constant initial temperature to which the entering gases are preheated and to which temperature rises are referred. This assumption is valid for regeneration because the sorption process is nearly athermal.

Using the notation of Appendix C with minor modifications, the model equations are as follows.

Fluid Phase

$$K^K \frac{\partial Y}{\partial X} = -YW \qquad (6.3)$$

$Y(0, \tau) = 1$ The inlet concentration is held constant.

Solid Phase

$$K^K \frac{\partial W}{\partial X} = -YW \qquad (6.4)$$

$W(\tau, 0) = 1$ The bed is completely saturated initially.

Energy Equation

$$K^K \frac{\partial \theta}{\partial X} + K^K K_{CP} \frac{\partial \theta}{\partial \tau} = +YW \qquad (6.5)$$

where $\theta = \dfrac{T_G - T_G^\circ}{T_{Ab}}$, the dimensionless ratio of the actual temperature increase in the reactor divided by the adiabatic temperature rise

T_G is the gas or solid temperature, °F

T_G° is the uniform inlet temperature, °F

T_{Ab} is the gas phase adiabatic temperature rise, °F

$\theta(0, \tau) = 0$ The inlet temperature is held constant.

$\theta(X, 0) = 0$ The initial temperature is uniform.

This formulation neglects the accumulation of oxygen in the gas phase and the sensible heat of the gas phase relative to the solid phase. Both simplifications represent a very small error.

The solution to these partial differential equations is given in Butt[9] or Johnson.[10] The solution has a very simple form.

$$\frac{T_G - T_G^\circ}{T_{Ab}} = \frac{1}{2(1 - N_{CP})} \left[\tanh \frac{X - \tau}{2N^K} - \tanh \frac{N_{CP}X + \tau}{2N^K} \right] \quad (6.6)$$

The maximum temperature is found by differentiating the solution with respect to X. Butt[9] gives a solution equivalent to the following:

$$\frac{T_G - T_G^\circ}{T_{Ab}} = \frac{1}{(1 - N_{CP})} \tanh \left(\frac{(1 - N_{CP})X}{4N^K} \right) \quad (6.7)$$

The maximum temperature is found at the end of the bed where X is unity.

6.5.3 Application of the Froment Model

Equation 6.7 predicts that the maximum bed temperature is infinite if N_{CP} were unity and N^K were zero. The maximum temperature for any positive value of N^K occurs when N_{CP} is unity. When N_{CP} is unity, the minimum regeneration time is equal to the minimum time required to heat the bed from a step change in the inlet gas temperature. This time is called the ideal heating time even though the bed isn't required to be heated. The length of the reactor divided by the ideal saturation time is called the chemical velocity in the bed, and the length of the reactor divided by the ideal heating time is called the thermal velocity. These velocities are quite low, for the MERC system the chemical velocity is about 0.5 ft/hr for a fully saturated bed and the thermal velocity is about 3.6 ft/hr. The heat balance number, N_{CP}, is the chemical velocity divided by the thermal velocity. In most fixed-bed operations this term is less than unity.

The parameter N^K is inversely proportional to the reaction rate parameter, and thus N^K approaches zero as the bed temperature increases. A low value of N^K yields a very narrow reaction zone in the reactor which moves through the reactor at the chemical velocity. If the chemical velocity and the thermal velocity were the same, then an observer moving along with the reaction zone would find that thermal energy would not be carried away from the reaction zone. Consequently the temperature in the reaction zone would increase. The maximum temperature in the reaction zone decreases as the value of the N_{CP} parameter decreases from unity because the rate of energy transfer from the reaction zone increases. These qualitative observations can be developed quantitatively by examining the behavior of equation 6.7.

Figure 6.13 shows a plot of the maximum temperature predicted by the Froment analysis as a function of the heat balance number, N_{CP}. The dependent variable on this plot is the temperature in the reactor based on the assumptions that the adiabatic temperature rise is 500°F and the inlet temperature is 1000°F; both of these values are typical for regeneration. The plot shows that very large temperature spikes will occur when N_{CP} is near unity and the kinetic parameter N_{Ab}^K is low.

Some useful qualitative guidelines can be established by inspection of Figure 6.13. First, the maximum temperature increases with increasing value of the heat capacity parameter. These curves have a mirror image about the N_{CP} value of unity. Second, the absolute maximum temperature is very large for values of N^K below 0.1 at N_{CP} equal to unity. Therefore operation of the reactor at unity N_{CP} should be avoided. By following along one of the curves for N^K from left to right, the curves join on a common upper locus. Thus if the temperature rise of this locus can be tolerated, there is no need to examine the specific value of N^K.

FIGURE 6.13

TEMPERATURE MAXIMUM DURING REGENERATION

(FROMENT ANALYSIS)

T_{INLET} = 1000°F

ΔT_{Ab} = 500°F

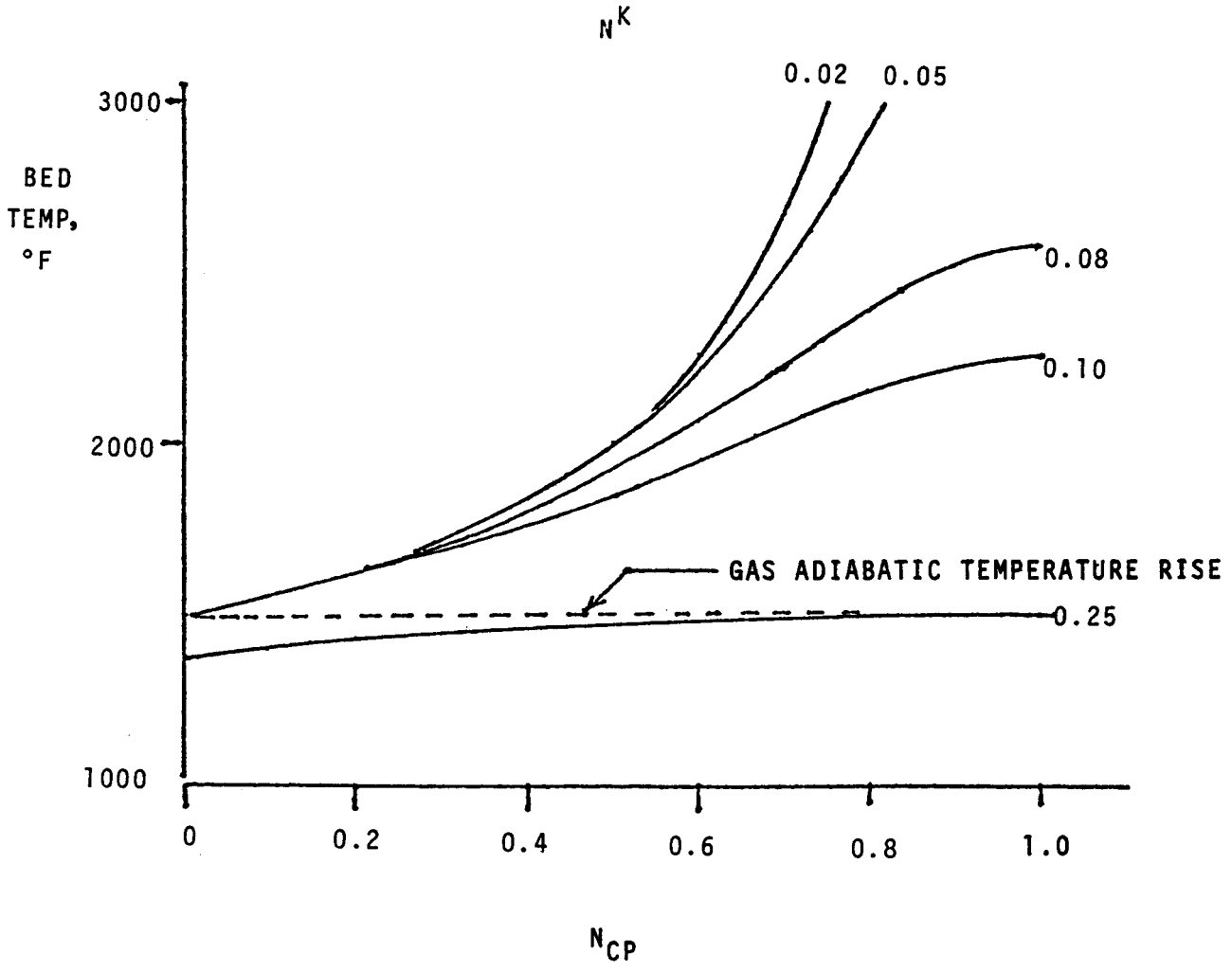

Figure 6.14 shows a small portion of Figure 6.13 for the N_{CP} parameter range 0.1 to 0.2. This range represents the operation of the MERC unit. It is clear that N^K greater than 0.25 will hold the bed temperature rise below the adiabatic maximum. Further the absolute maximum temperature is 1627°F (1.25 ΔT_{Ab}) for regeneration of the most active sorbents in this range of the heat capacity parameter.

It also is useful to appreciate the importance of finding a limit for the maximum temperature rise with increasing reaction rate for regeneration. Using the activation energy group, γ = 10.92, the reaction rate increases by a factor of 16.2 when the temperature increases from 1000 to 1500°F. The value of the parameter N^K then decreases by sixteenfold in response to the change in temperature; specifically the value of N^K = 0.25 decreases to 0.016 with this change. However, a useful approximation for the behavior of the reactor is obtained by using the results for the lowest value of $N_{Ab}{}^K$. Under these circumstances the maximum bed temperature for a reactor with constant inlet temperature is about 1625°F.

A comparison of the numerical simulation for the MERC unit shown on Figure 6.11 with the prediction of the simplified model is instructive. The N_{CP} value for the simulation is 0.136. The maximum temperature for this value of N_{CP} on Figure 6.14 is 1572°F. This temperature can be transformed to yield an estimate of the maximum bed temperature as follows:

$$\left(\frac{1572 - 1000}{500}\right)(426) + 1030 = \underline{1517°F}$$

The numerical solution yields a maximum temperature of 1538°F. Therefore the two models are close agreement, and the Froment analysis can be used to guide operation of the unit.

FIGURE 6.14

TEMPERATURE MAXIMUM DURING REGENERATION

T_{INLET} = 1000°F

ΔT_{Ab} = 500°F

(LIMITED RANGE)

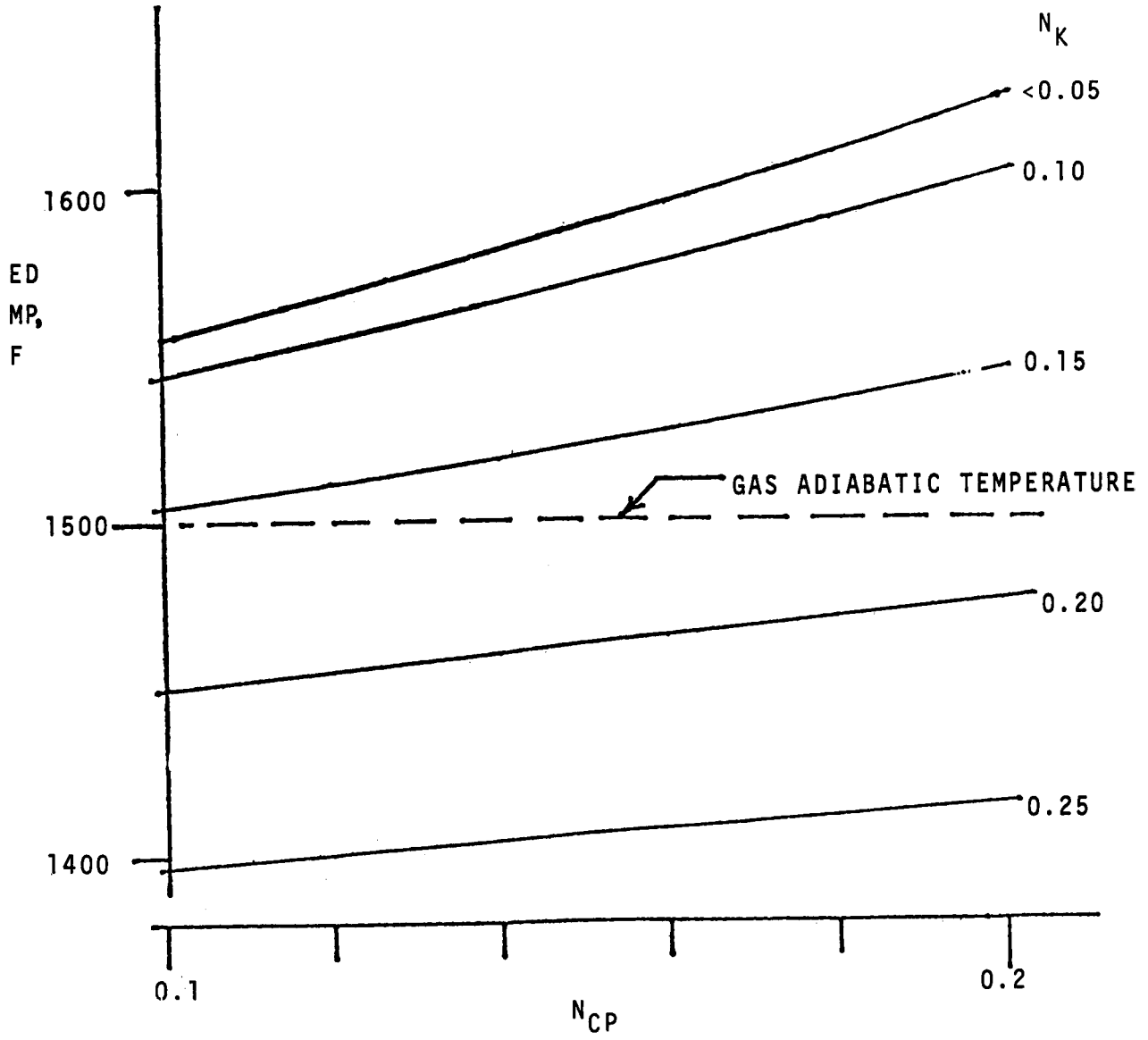

6.5.4 Selection of Operating Parameters to Control the Maximum Temperature During Regeneration

The inlet temperature and composition usually is held constant in the cyclic operation of fixed-bed reactors. The fluid is supplied to several reactors simultaneously from one source, and operation is easiest when the input process variables are held constant. This section describes the use of the Froment model for guiding the operation of a plant.

The Froment model assumes the parameter N^K is not a function of temperature. If this assumption were true for regeneration, then it is possible to calculate the combination of N^K and N_{CP} which will give a fixed value of the maximum temperature in the reactor by modification of equation 6.7. Figure 6.15 displays the resulting contour plot. This figure is drawn for a 1000°F inlet temperature and a 500°F adiabatic temperature rise. The contours of constant temperature appear as semicircles about the point $N_{Ab}{}^K = 0$ and $N_{CP} = 0$. This figure is a global version of the data on Figures 6.13 and 6.14. For example Figure 6.14 shows that N^K is 0.18 at $N_{CP} = 0.2$ and 1500°F bed temperature; this point also is found as a point on the 1500°F contour. Figure 6.15 also shows that the maximum bed temperature is independent of N^K for low values of this group. The constant temperature contours are perpendicular to the N_{CP} axis, and hence the maximum temperaure in the bed is not a function of the particular value of the N^K parameter. This independence is useful in the operation of the reactor.

After the unit is constructed the operator has only a few variables with which to control the maximum temperature during regeneration. These variables are the flow rate, temperature, and oxygen concentration. As observed previously, decreasing the inlet temperature can increase the maximum bed temperature substantially above the value observed for uniform inlet temperature. Although the inlet temperature can be used for control, the complex response of the system to these variations makes temperature difficult to use as a control variable.

The flow rate or GHSV to the reactor also is a potential control variable. In the face of excess temperature, decreasing the flow rate decreases N^F and N_H with the half power and N^K with the first power. Heat transfer between the gas and pellet is not a major variable, and decreasing the reaction rate parameters eventually will drive the bed temperature higher. If the gas flow rate is increased when the bed temperature is too high, the reaction group will increase linearly; a factor of two variation can be achieved. However, the effect of temperature on reaction rate is much stronger, perhaps a factor of 25, and therefore GHSV alone can be used to trim the operation of the unit.

FIGURE 6.15

SAFE OPERATING REGION IN TERMS OF DIMENSIONLESS GROUPS

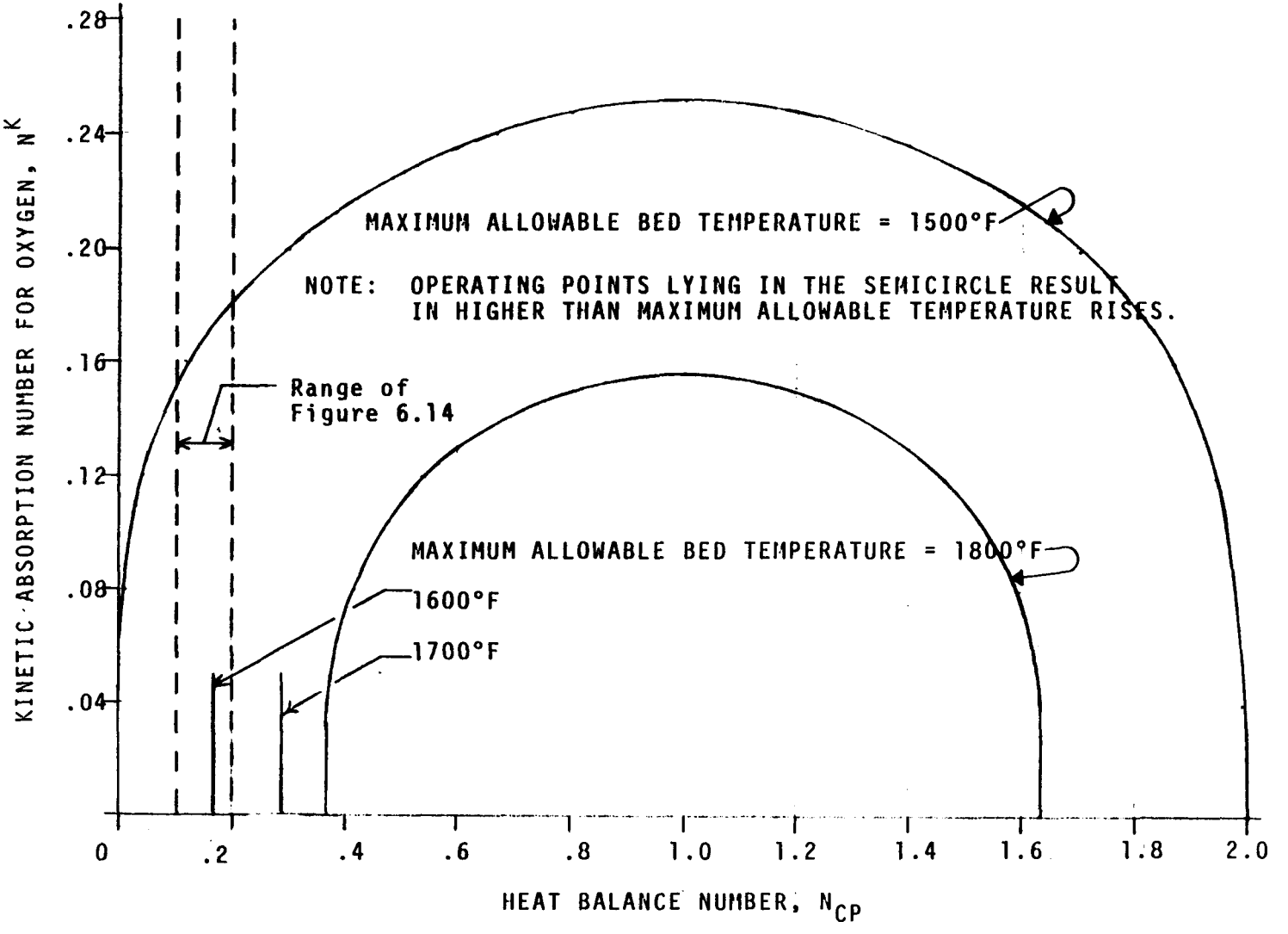

However, oxygen concentration in the influx gas to the regenerator is the major control variable for these units. The following analysis gives a direct way to set the maximum bed temperature.

Figures 6.13-6.15 show that the maximum bed temperature depends only on the adiabatic temperature rise and the N_{CP} parameter when N^K is small. The group N^K diminishes dramatically with increasing temperature. The maximum temperature in the bed is described by the obvious relation

$$T_{MAX} = T_{BASE} + rT_{Ab} \qquad (6.8)$$

where T_{BASE} is the constant inlet temperature

T_{MAX} is the maximum temperature in the bed

T_{Ab} is the adiabatic temperature rise

r is the ratio of the actual temperature rise in the reactor to the adiabatic temperature rise

The gas phase adiabatic temperature rise is a linear function of the mol fraction of oxygen. To illustrate this approach, the adiabatic temperature rise for the work described in the previous report[1] is expressed as:

$$T_{Ab} = 17200\ Y_o$$

where Y_o is the inlet mol fraction of oxygen (about 0.029)

T_{Ab} is the temperature rise, °F

The other parameter is N_{CP}, the heat capacity parameter. This parameter also is proportional to oxygen concentration.

$$N_{CP} = \frac{Y_o(Cp\rho(1 - \varepsilon))_s}{(1 - \varepsilon)M_B \underline{Cp}}$$

where N_{CP} = heat capacity parameter

$(Cp\rho(1 - \varepsilon))_s$ = volumetric heat capacity of the bed

$(1 - \varepsilon)M_B$ = oxygen demand (mols/cu ft) of the sulfided sorbent

$\underline{Cp}$ = molar specific heat of the gas

For the experimental work in the previous report[1]

$$N_{CP} = 1.41Y_o$$

The value of the coefficient is directly proportional to the content of active iron. This sorbent contained 21.9 weight percent iron oxide.

The parameter r depends upon N_{CP} alone. This group is plotted as a function of N_{CP} on Figure 6.16. The relation is calculated from the Froment analysis for low values of $N_{Ab}K$.

An example illustrates the computation. Assume T_{BASE} is 1030°F and the maximum temperature allowed is 1600°F. Find the maximum mol fraction oxygen.

In the range $0 < N_{CP} < 0.2$, the curve shown on Figure 6.16 is represented as

$$r = 1 + 0.99\, N_{CP} + 1.30\, N_{CP}^2$$

$$1600 - 1030 = r\, T_{Ab}$$

$$570 = (1 + 1.3959\, Y_o + 2.5845\, Y_o^2)(17200 Y_o)$$

Solving first for Y_o and then for the related parameters T_{Ab}, N_{CP} and r gives

$$Y_o = 0.0316$$

$$T_{Ab} = 545°F$$

$$N_{CP} = 0.0446$$

$$r = 1.047$$

This example shows that thermal velocity is so much greater than the chemical velocity that the reaction zone achieves a temperature only slightly greater than the adiabatic temperature rise. Again it should be stressed that the inlet temperature must be held constant.

The adiabatic temperature rise is not likely to be more than 800°F for the regeneration reaction; a maximum bed-temperature of 1800°F will degrade most sorbent supports. Thus the oxygen concentration will be less than 0.05 mol fraction. The iron oxide concentration of a successful sorbent will be in the area of 80 percent, about twice the content of the example above. However, to give an upper bound on the value of N_{CP}, the iron oxide content should be lowered to the minimum practical value. The minimum iron oxide level certainly will be greater than 20 percent, or half the value of the example. Thus the maximum value of N_{CP} is about 0.15, and the maximum value of r is then 1.18. Consequently the oxygen concentration for regeneration can be selected easily as that value which will satisfy the approximation

$$T_{Ab} = \frac{T_{MAX} - T_{BASE}}{1.25}$$

FIGURE 6.16

MAXIMUM TEMPERATURE RATIO

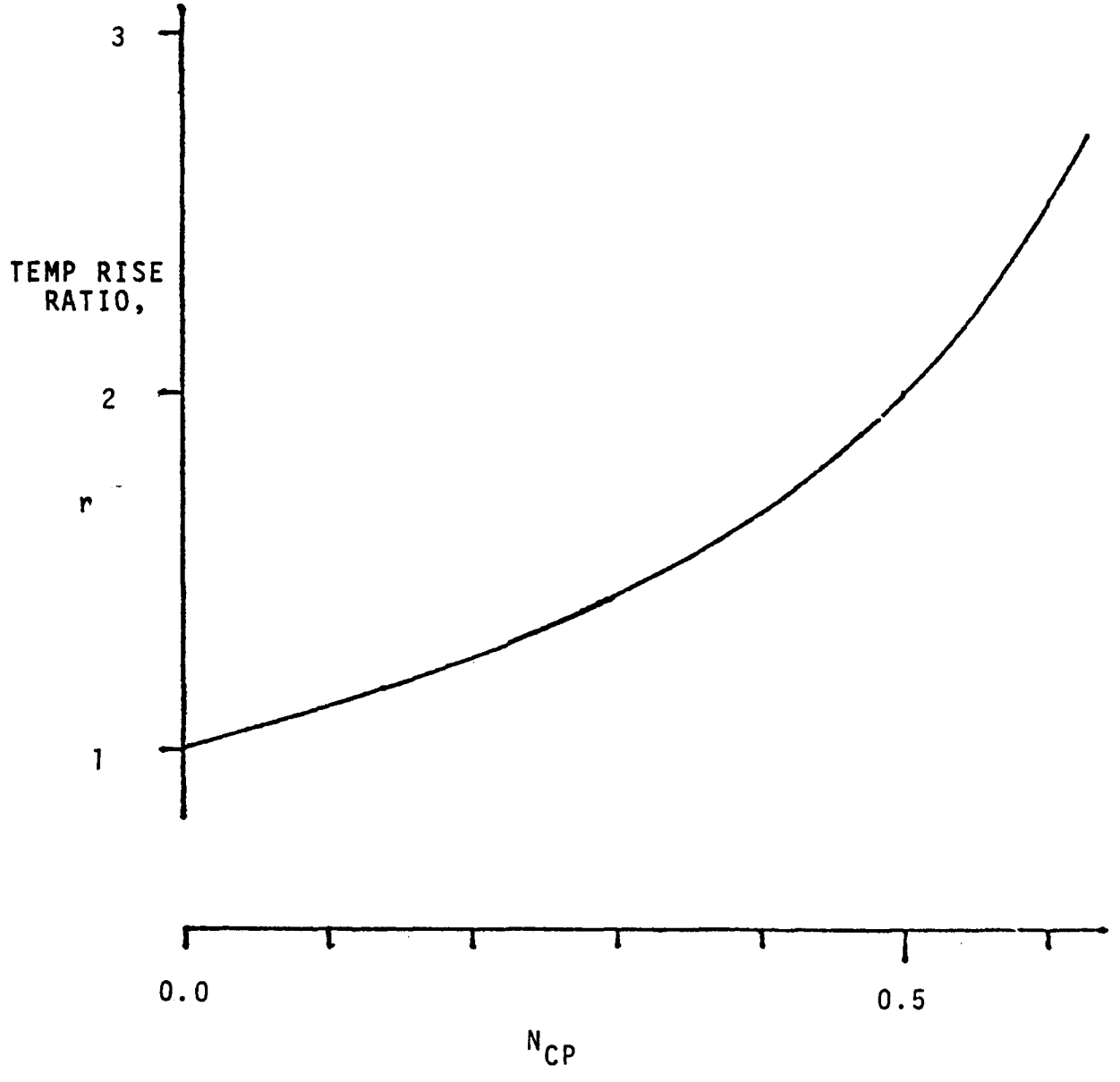

This section has demonstrated tnat the Froment analysis for the maximum temperature in transient operation of a fixed-bed reactor can be applied to the regeneration of fixed-bed desulfurization units. Further, the analysis shows that the difference between the inlet temperature and the maximum temperature in the bed is less than 120 percent of the adiabatic temperature increase for the gas phase. The regeneration process can be operated easily by holding the gas inlet temperature and the oxygen concentration constant.

6.5.5 Effect of Parameter Choices Upon Operation

This section shows how the operating parameters in the simulation model depend upon design and operating variables. This review shows that most of the system variables are set by constraints.

Table 6.6 gives the power dependence of the seven parameters of the simulation model upon the external variables: velocity, particle diameter, bed length, iron oxide concentration, and oxygen mol fraction. The table is constructed easily from the notation; however, it is helpful to show how the table can be used.

Operation with 0.03 mol fraction oxygen on a support loaded with 42 percent iron oxide gives a maximum bed temperature in regeneration of about 1550 when the sorption cycle operates at 1000°F. Further, the regeneration time is set to be about two-thirds of the sorption time because the six active beds are operated in cycle of three on sorption, two in regeneration and one on the purge cycle.

Problem: The operation during the absorption cycle can be improved by increasing the operating temperature to 1200°F. Further the plant investment can be reduced by increasing the iron oxide content from 42 to 84 percent and decreasing the cycle time from 2.0 to 1.0 hours. Find the new oxygen concentration in the regeneration gas, the gas flowrate during regeneration and the bed depth.

Answer: The adiabatic temperature rise is the first critical parameter of the analysis. Since the adiabatic temperature rise is proportional to the oxygen concentration, the new inlet oxygen concentration will be 350/550 = 0.64 of the base value.

$$Y_N = 0.64 Y_O$$

$$Y_N = 0.0192$$

where Y is the mol fraction of oxygen in the regenerating gas and the subscripts N and O denote "new" and "old".

Next the depth of the absorbent bed is calculated from a material balance. Thus forming the ratio of the new and old conditions, the bed depth is found from the relation

$$\frac{(V_s T_{SAT})_N}{(V_s T_{SAT})_O} = \frac{(M_o L)_N}{(M_o L)_O}$$

where V_s is the superficial velocity in the bed during absorption. The remainder of the symbols are defined in Table 6.6.

TABLE 6.6

DEPENDENCE OF THE MODEL PARAMETERS

The numbers in this table give the exponential dependence of the parameter upon the design variable.

	VARIABLES				
	V	a	L	M_o	Y_o
	velocity	particle diameter	bed length	iron oxide concentration	oxygen mol fraction
Parameters					
Dimensional					
T_{SAT} minimum time for regeneration	-1	0	+1	+1	-1
T_{Ab} adiabatic temperature rise in the gas phase	0	0	0	0	1
Dimensionless					
N^F film sorption number	0.575	1.575	-1	0	0
N_H heat transfer number	0.51	1.51	-1	0	0
N^K kinetic sorption number	1	0	-1	-1	0
N_{CP} heat capacity parameter	0	0	0	-1	+1
γ activation energy parameter	0	0	0	0	0

The economic analysis showed that the process cost is only a weak function of the producer gas velocity, and therefore this variable is unchanged to keep the design near optimum. Thus

$$\frac{L_N}{L_0} = \frac{(T_{SAT})_N}{(T_{SAT})_0} \cdot \frac{(M_o)_0}{(M_o)_N} = \frac{1}{2} \cdot \frac{1}{2} = \frac{1}{4}$$

The saturation time for regeneration remains fixed as two-thirds of the saturation time for sorption. By reference to Table 6.6 the saturation ratio is

$$\frac{(T_{SAT})_N}{(T_{SAT})_0} = \frac{(LM_o)_N}{(LM_o)_0} \cdot \frac{(VY_o)_0}{(VY_o)_N}$$

Thus substituting the known ratios an equation for the regeneration gas velocity, V, is found as

$$\left(\frac{1}{2}\right) = \left(\frac{1}{4}\right) \cdot 2 \cdot \frac{V_0}{V_N} \cdot \frac{1}{0.64}$$

The required flow ratio in regeneration, therefore, is

$$\left(\frac{V_N}{V_0}\right) = \frac{1}{0.64} = 1.56$$

which is simply the inverse ratio of the change on mol fraction oxygen.

Again, by reference to Table 6.6, the ratio of the transport parameters then is

$$\frac{(N^F)_N}{(N^F)_0} = \left(\frac{V^N}{V^0}\right)^{0.58}\left(\frac{L^0}{L^N}\right) = 5.16$$

Similarly

$$\frac{(N_H)_N}{(N_H)_0} = \left(\frac{V^N}{V_0}\right)^{0.51}\left(\frac{L^0}{L^N}\right) = 5.01$$

and the kinetic parameter ratio is found as

$$\frac{(N^K)_N}{(N^K)_0} = \left(\frac{V^N}{V^0}\right)\left(\frac{L^0}{L_N}\right)\left(\frac{M^0}{M_N}\right) = 3.12$$

A fivefold increase in the heat transport parameter and the kinetic film parameter is a major change in the contribution of these variables to the overall process. These changes would require a slight ($\sim$10 percent) increase in the regeneration gas velocity to compensate for the loss in regeneration efficiency. The threefold increase in N^K is less important because the effective kinetic resistance is reduced substantially by the exponential dependence of rate constant on temperature.

The heat capacity parameter ratio will change as

$$\frac{(N_{CP})_N}{(N_{CP})_0} = \left(\frac{M_0}{M_N}\right)\left(\frac{Y_N}{Y_0}\right) = \left(\frac{1}{2}\right)(0.64) = 1.28$$

The 28 percent increase in this parameter would increase the maximum bed temperature slightly.

Thus the answer to the original problem is:

Y_N	=	0.0192	mol fraction oxygen
V_N/V_0	=	1.56	ratio of regeneration gas velocities
L_N/L_0	=	0.25	ratio of the length of sorbent

This representation of the operating trade-offs is simple because most of the parameters, e.g., N^F, N_H, N^K and N_{CP}, are specified by the selection of the maximum bed temperature and the saturation time. Thus Table 6.6 provides useful, if simple, information.

APPENDIX A

OPTIMIZATION OF THE ECONOMIC ANALYSIS

FIGURE A.1
SKETCH OF TYPICAL DESULFURIZATION REACTOR

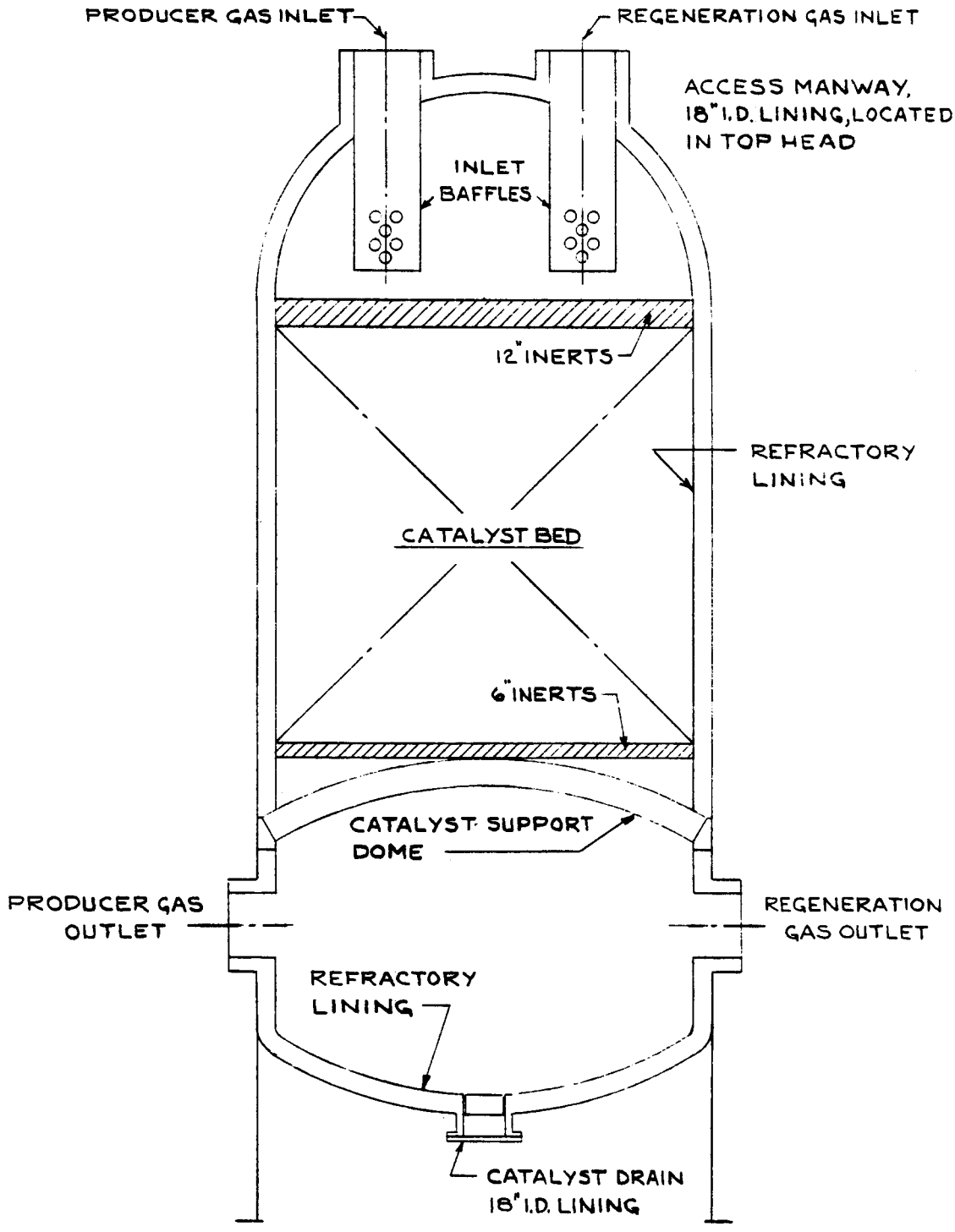

NOTE - GAS INLET & OUTLET NOZZLES ARE 28" I.D. REFRACTORY LINING

TABLE A.1

REGENERATION SYSTEM MATERIAL BALANCE, LBS/HR[1]

Stream No.[2]	1	2	3	4	5
Stream	Regeneration Air	Recycle Gas	Total Regeneration Gas Feed	Total Regeneration Effluent	Regeneration Vent Gas to Sulfur Recovery Unit
Component					
N_2	83,500	778,677	862,177	862,177	83,500
O_2	25,367	11,265	36,632	12,473	1,208
SO_2	--	246,006	246,006	272,386	26,380
Total, Lbs/Hr	108,867	1,035,948	1,144,815	1,147,036	111,088

(1) For a plant processing 28.9 MM SCFH of producer gas containing 0.6 mol percent hydrogen sulfide.

(2) Material balance stream identification numbers are shown in Figure 4.2.

TABLE A.2

REACTOR AND COMPRESSOR SPECIFICATIONS

Case Number	No. of Reactors	Reactor Bed Dimensions Vol. (Cu Ft)	Dia. (Ft)	Depth (Ft)	Inlet & Outlet Pipe Size (In)	Producer Gas Valve Size (In)	Regeneration Valve Size (In)	Reactor Op. Press. Maximum PSIG	No. of Air Compr. (1)	No. of R.G. Compr. (2)	Air Compr. BHP/ Machine	R.G. Compr. BHP/ Machine
1,4-7	9	2,575	15.0	14.6	24	12	10	160	9	3	1,070	2,435
2	9	2,425	15.0	13.7	24	12	10	160	9	3	1,070	2,679
3	9	3,000	15.0	17.0	24	12	10	160	9	3	1,070	2,334
8	7	7,235	17.4	30.4	30	14	12	160	9	3	1,070	2,739
9	9	1,485	15.0	8.4	24	12	10	160	9	3	1,070	2,353
10	9	1,330	15.0	7.5	24	12	10	160	9	3	1,070	2,481
11	9	1,905	15.0	10.8	24	12	10	160	9	3	1,070	2,298
12-14	9	1,090	15.0	6.2	24	12	10	160	9	3	1,070	2,322
15	9	1,420	15.0	8.0	24	12	10	160	9	3	1,070	2,339
16	7	6,500	17.4	27.3	30	14	12	160	9	3	1,070	2,688
17	7	3,485	21.0	10.1	30	14	12	160	9	3	1,070	2,324
18	7	3,375	14.7	19.9	30	14	12	160	9	3	1,070	2,833
19	7	3,354	13.2	24.3	30	14	12	160	9	3	1,070	3,266
20	7	3,285	11.0	34.6	24	8	8	415	12	3	1,095	1,295
21	7	3,160	11.0	33.3	24	8	8	415	12	3	1,112	1,824
22	7	3,640	11.0	38.3	24	8	8	415	12	3	1,086	1,046
23	7	3,510	20.8	10.3	30	16	14	110	9	3	915	3,530
24	7	3,270	20.8	9.6	30	16	14	110	9	3	915	3,770
25	7	4,185	20.8	12.3	30	16	14	110	9	3	915	3,435

(1) Except for Cases 20-22, 3 stages of compression employed. For Cases 20-22, 4 stages. For each stage, three 50% machines are provided.

(2) For recycle gas compressor service, three 50% machines are provided.

TABLE A.3

COMPRESSOR K.O. DRUM & INT. STAGE COOLER SPECIFICATIONS[1]

Case Numbers	1-19	20-22	23-25
R.G. K.O. Drum (D-101)			
Dimension, I.D. x TTL	11'0" x 33'0"	8'0" x 24'0"	12'0" x 36'0"
Op. Conditions (Max)			
Temp., °F	150	150	150
Press., PSIG	140	390	90
Second Stage Air Comp. Suction K.O. Drum (D-102)			
Dimension, I.D. x TTL	7'0" x 16'0"	7'0" x 16'0"	7'0" x 16'0"
Op. Conditions (Max)			
Temp., °F	150	150	150
Press., PSIG	30	35	30
Third Stage Air Comp. Suction K.O. Drum (D-103)			
Dimension, I.D. x TTL	5'6" x 14'0"	5'6" x 14'0"	5'6" x 14'0"
Op. Conditions (Max)			
Temp., °F	150	150	150
Press., PSIG	75	80	60
Fourth Stage Air Comp. Suction K.O. Drum (D-104)			
Dimension, I.D. x TTL	Not Required	4'6" x 12'0"	Not Required
Op. Conditions (Max)			
Temp., °F		150	
Press., PSIG		185	
Interstage Cooler (E-105)			
Shell Side Press., PSIG	20	25	20
Tube Side Press., PSIG	50	50	50
Est. Surface Area, Ft^2	2,725	2,600	2,500
Interstage Cooler (E-106)			
Shell Side Press., PSIG	63	70	50
Tube Side Press., PSIG	50	50	50
Est. Surface Area, Ft^2	2,725	2,600	2,500
Interstage Cooler (E-107)			
Shell Side Press., PSIG	Not Required	170	Not Required
Tube Side Press., PSIG		50	
Est. Surface Area, Ft^2		2,600	

(1) Materials of construction - carbon steel.

TABLE A.4

HEAT EXCHANGER SPECIFICATIONS[1]

Item No.	Service			Temperature, °F	Operating Pressure, PSIG	Material of Construction	Duty, MMBTU/HR	Surface, Sq. Ft.	Remarks
E-101	Hot Regeneration Gas/Effluent	Shell	In	350	165	Alonized 18-8 Cr-Ni	179.5	17,000	Total area for two shells in series.
			Out	1,000					
		Tube	In	1,500	150	Alonized 18-8 Cr-Ni			
			Out	890					
E-102	Steam Generator	Shell	In	405	250	Carbon Steel	90.0	6,300	250 PSIG saturated steam is produced.
			Out	405					
		Tube	In	890	145	Aluminum			
			Out	530					
E-103	Cold Regeneration Gas/ Effluent	Shell	In	185	170	Aluminum	43.0	15,600	
			Out	350					
		Tube	In	530	140	Aluminum			
			Out	350					
E-104	Final Effluent Cooler	Shell	In	85					Bare tube area for air cooled exchanger.
			Out						
		Tube	In	350	135	Aluminum	53.7	28,500	
			Out	120					

(1) Corresponds to Cases 1-19 which are based on reactor outlet pressure level of 150 PSIG during sorbent regeneration. Except for operating pressure level, specifications applicable to the remaining cases as well. By fixing regeneration pressure at 400 PSIG and 100 PSIG, respectively, exchanger operating pressure level for Cases 20-22 and Cases 23-25 can be estimated.

TABLE A.5

MISCELLANEOUS ITEMS SPECIFICATIONS

Regeneration Gas Heater, H-101

Material Handled		Air and Regeneration Gas
Temperature, °F,	Inlet	350
	Outlet	1200 (Maximum)
Absorbed Duty, MM BTU/Hr		20
Tube Material		18-8 Cr-Ni
Note		Required During the Plant Start-up Only

Vibrating Screens

Required for Sorbent-Inert Separation

TABLE A.6

ESTIMATED ANNUAL SORBENT AND UTILITY COSTS

Case No.	Total Initial Sorbent Loading, 1000 Lbs	Annual Sorbent Cost, $1000	Reactor Pressure Drop, PSI		Major Annual Power Cost,(1) $1000				Total Power Cost(2), $1000	Net Credit for Steam Production,(3) $1000	Cooling Water Cost(4), $1000	Net Utility Cost, $1000
			On-Stream	Regeneration	On-Stream Pressure Loss	Recycle Gas Compressor	Air Compressor	Total				
1	1668.6	1668.6	5.9	3.4	311.6	803.7	1059.4	2174.7	2206.2	1956.2	19.9	269.9
2	1571.4	1571.4	13.6	7.6	706.8	884.3	1059.4	2650.5	2682.0	1956.2	19.9	745.7
3	1944.0	1944.0	3.0	1.7	159.6	770.3	1059.4	1989.3	2020.8	1956.2	19.9	84.5
4	1668.6	3337.2	5.9	3.4	311.6	803.7	1059.4	2174.7	2206.2	1956.2	19.9	269.9
5	1668.6	834.3	5.9	3.4	311.6	803.7	1059.4	2174.7	2206.2	1956.2	19.9	269.9
6	1668.6	3337.2	5.9	3.4	311.6	803.7	1059.4	2174.7	2206.2	1956.2	19.9	269.9
7	1668.6	1668.6	5.9	3.4	311.6	803.7	1059.4	2174.7	2206.2	1956.2	19.9	269.9
8	3160.2	3002.2	12.3	8.6	646.1	904.0	1059.4	2609.5	2641.0	1956.2	19.9	704.7
9	1200.0	1260.0	3.4	2.0	180.6	776.4	1059.4	2016.4	2047.9	1956.2	19.9	111.6
10	1074.6	1128.4	7.5	4.2	392.1	818.9	1059.4	2270.4	2301.9	1956.2	19.9	365.6
11	1539.2	1616.2	1.9	1.0	101.1	758.6	1059.4	1919.1	1950.6	1956.2	19.9	14.3
12	1011.5	1213.8	2.5	1.5	133.1	766.3	1059.4	1958.8	1990.3	1956.2	19.9	54.0
13	1011.5	2023.0	2.5	1.5	133.1	766.3	1059.4	1958.8	1990.3	1956.2	19.9	54.0
14	1011.5	606.9	2.5	1.5	133.1	766.3	1059.4	1958.8	1990.3	1956.2	19.9	54.0
15	920.2	920.2	3.3	1.9	172.1	772.2	1059.4	2003.7	2035.2	1956.2	19.9	98.9
16	3159.0	3159.0	11.1	7.8	579.8	887.2	1059.4	2526.4	2557.9	1956.2	19.9	621.6
17	1693.7	1693.7	2.2	1.5	115.4	767.0	1059.4	1941.8	1973.3	1956.2	19.9	37.0
18	1640.2	1640.2	15.2	10.3	786.5	934.9	1059.4	2780.8	2812.3	1956.2	19.9	876.0
19	1630.0	1630.0	26.2	18.1	1323.7	1077.9	1059.4	3461.0	3492.5	1956.2	19.9	1556.2
20	1596.5	1596.5	29.0	19.6	801.0	427.5	1445.2	2673.7	2705.2	1956.2	29.0	778.0
21	1535.8	1535.8	64.8	44.4	1740.0	602.0	1468.1	3810.1	3841.6	1956.2	29.0	1914.4
22	1769.0	1769.0	14.2	9.4	395.6	345.2	1433.7	2174.5	2206.1	1956.2	29.0	278.9
23	1705.8	1705.8	3.3	2.3	225.6	1165.2	906.1	2296.9	2328.4	1956.2	16.3	388.5
24	1589.2	1589.2	7.4	5.1	504.4	1244.4	906.1	2654.9	2686.4	1956.2	16.3	746.5
25	2033.9	2033.9	1.6	1.1	113.7	1133.9	906.1	2153.7	2185.2	1956.2	16.3	245.3

(1) Based on power cost of 2.4¢/KWH.
(2) Includes power cost for regeneration effluent air cooler, but excludes instruments, lights, etc.
(3) Steam consumed for reactor purge and valve sealing is subtracted from average steam produced in the steam generator to get net credit for steam. Assumed steam credit @ $3.50/1000 Lbs and BFW cost of $2.0/1000 Gal.
(4) Based on 2.5¢/1000 Gal.

TABLE A.7

ESTIMATED INVESTMENT AND PROCESSING COST

Case Number	1	2	3	4	5	6	7	8	9	10	11	12
Major Equipment Material Cost, $1000												
Desulf. Reactors	1809.9	1789.2	1900.8	1809.9	1809.9	1809.9	1809.9	2310.0	1592.1	1560.6	1677.7	1512.0
Heat Exchangers	1677.5	1677.5	1677.5	1677.5	1677.5	1677.5	1677.5	1677.5	1677.5	1677.5	1677.5	1677.5
Compressors	4013.4	4232.7	4013.4	4013.4	4013.4	4013.4	4013.4	4232.7	4013.4	4013.4	4013.4	4013.4
Drums	84.6	84.6	84.6	84.6	84.6	84.6	84.6	84.6	84.6	84.6	84.6	84.6
Heater	181.0	181.0	181.0	181.0	181.0	181.0	181.0	181.0	181.0	181.0	181.0	181.0
Total	7766.4	7965.0	7857.3	7766.4	7766.4	7766.4	7766.4	8485.8	7548.6	7517.1	7634.1	7468.5
Estimated Investment, $1000	23,300	23,895	23,570	23,300	23,300	23,300	23,300	25,460	22,650	22,550	22,900	22,410
Annual Processing Cost, $1000												
Direct Processing Cost												
Sorbent	1668.6	1571.4	1944.0	3337.2	834.3	3337.2	1668.6	3002.2	1260.0	1128.4	1616.2	1213.8
Labor (2 men/shift @ $9.55/Hr)	167.3	167.3	167.3	167.3	167.3	167.3	167.3	167.3	167.3	167.3	167.3	167.3
Maintenance (3% of Investment)	699.0	716.9	707.1	699.0	699.0	699.0	699.0	763.8	679.5	676.5	687.0	672.3
Utilities	269.9	745.7	84.5	269.9	269.9	269.9	269.9	704.7	111.6	365.6	14.3	54.0
	2804.8	3201.3	2902.9	4473.4	1970.5	4473.4	2804.8	4638.0	2218.4	2337.8	2484.8	2107.4
Indirect Processing Cost												
Plant Overhead (110% of Labor)	184.0	184.0	184.0	184.0	184.0	184.0	184.0	184.0	184.0	184.0	184.0	184.0
Fixed Processing Cost												
Depreciation (20 years)	1165.0	1194.7	1178.5	1165.0	1165.0	1165.0	1165.0	1273.0	1132.5	1127.5	1145.0	1120.5
Ins. & Prop. Taxes (2.3% of Inv.)	535.9	549.6	542.1	535.9	535.9	535.9	535.9	585.6	520.9	518.6	526.7	515.4
	1700.9	1744.3	1720.6	1700.9	1700.9	1700.9	1700.9	1858.6	1653.4	1646.1	1671.7	1635.9
Processing Cost	4689.7	5129.6	4807.5	6358.3	3855.4	6358.3	4689.7	6680.6	4055.8	4167.9	4340.5	3927.3
General Expenses												
Administration (3% of P.C.)	140.7	153.9	144.2	190.7	115.7	190.7	140.7	200.4	121.7	125.0	130.2	117.8
Finance (9% of Inv.)	2097.0	2150.5	2121.3	2097.0	2097.0	2097.0	2097.0	2291.4	2038.5	2029.5	2061.0	2016.9
Total Cost	6927.4	7434.0	7073.0	8646.0	6068.1	8646.0	6927.4	9172.4	6216.0	6322.4	6531.7	6062.0
Unit Processing Cost, ¢/MMBTU	21.0	22.6	21.5	26.3	18.4	26.3	21.0	27.9	18.9	19.2	19.8	18.4

TABLE A.7 (continued)

ESTIMATED INVESTMENT AND PROCESSING COST

Case Number	13	14	15	16	17	18	19	20	21	22	23	24	25
Major Equipment Material Cost, $1000													
Desulf. Reactors	1512.0	1512.0	1579.5	2310.0	2454.9	1481.9	1386.7	1695.4	1654.8	1810.9	2060.1	2026.5	2155.3
Heat Exchangers	1677.5	1677.5	1677.5	1677.5	1677.5	1677.5	1677.5	2159.6	2159.6	2159.6	1674.4	1674.4	1674.4
Compressors	4013.4	4013.4	4013.4	4232.7	4013.4	4232.7	4443.6	4393.2	4636.5	4264.5	4040.4	4244.4	4040.4
Drums	84.6	84.6	84.6	84.6	84.6	84.6	84.6	101.2	101.2	101.2	83.4	83.4	83.4
Heater	181.0	181.0	181.0	181.0	181.0	181.0	181.0	181.0	181.0	181.0	181.0	181.0	181.0
Total	7468.5	7468.5	7536.0	8485.8	8411.4	7657.7	7773.4	8530.4	8733.1	8517.2	8039.3	8209.7	8134.5
Estimated Investment, $1000	22,410	22,410	22,610	25,460	25,230	22,970	23,320	25,590	26,200	25,550	24,120	24,630	24,400
Annual Processing Cost, $1000													
Direct Processing Cost													
Sorbent	2023.0	606.9	920.2	3159.0	1693.7	1640.2	1630.0	1596.5	1535.8	1769.0	1705.8	1589.2	2033.9
Labor (2 men/shift @ $9.55/Hr)	167.3	167.3	167.3	167.3	167.3	167.3	167.3	167.3	167.3	167.3	167.3	167.3	167.3
Maintenance (3% of Investment)	672.3	672.3	678.3	763.8	756.9	689.1	699.6	767.7	786.0	766.5	723.6	738.9	732.0
Utilities	54.0	54.0	98.9	621.6	37.0	876.0	1556.2	778.0	1914.4	278.9	388.5	746.5	245.3
	2916.6	1500.5	1864.7	4711.7	2654.9	3372.6	4053.1	3309.5	4403.5	2981.7	2985.2	3241.9	3178.5
Indirect Processing Cost													
Plant Overhead (110% of Labor)	184.0	184.0	184.0	184.0	184.0	184.0	184.0	184.0	184.0	184.0	184.0	184.0	184.0
Fixed Processing Cost													
Depreciation (20 years)	1120.5	1120.5	1130.5	1273.0	1261.5	1148.5	1166.0	1279.5	1310.0	1277.5	1206.0	1231.5	1220.0
Ins. & Prop. Taxes (2.3% of Inv.)	515.4	515.4	520.0	585.6	580.3	528.3	536.4	588.6	602.6	587.6	554.8	566.5	561.2
	1635.9	1635.9	1650.5	1858.6	1841.8	1676.8	1702.4	1868.1	1912.6	1865.1	1760.8	1798.0	1781.2
Processing Cost	4736.5	3320.4	3699.2	6754.3	4680.7	5233.4	5939.5	5361.6	6500.1	5030.8	4930.0	5223.9	5143.7
General Expenses													
Administration (3% of P.C.)	142.1	99.6	111.0	202.6	140.4	157.0	178.2	160.8	195.0	150.9	147.9	156.7	154.3
Finance (9% of Inv.)	2016.9	2016.9	2034.9	2291.4	2270.7	2067.3	2098.8	2303.1	2358.0	2303.1	2170.8	2216.7	2196.0
Total Cost	6895.5	5436.9	5845.1	9248.3	7091.8	7457.7	8216.5	7825.5	9053.1	7484.8	7248.7	7597.3	7494.0
Unit Processing Cost, ¢/MMBTU	20.9	16.5	17.8	28.1	21.5	22.7	25.0	23.8	27.5	22.7	22.0	23.1	22.8

TABLE A.8

SUMMARY OF CALCULATED SORPTION EFFICIENCIES

CASE NO.(1)	SORPTION EFFICIENCY(2)	CASE NO.(1)	SORPTION EFFICIENCY(2)
1	.81	14	.69
2	.86	15	.73
3	.69	16	.85
4	.81	17	.79
5	.81	18	.82
6	.81	19	.83
7	.81	20	.84
8	.85	21	.87
9	.75	22	.76
10	.83	23	.78
11	.59	24	.85
12	.69	25	.66
13	.69		

(1) Conditons for the various cases are given in Table 4.2.

(2) Sorption efficiencies are calculated by the method described in Section A.1.

TABLE A.9

BREAKDOWN OF COST COMPONENTS INCLUDED IN THE LANG FACTOR

ITEM	EQUIPMENT MATERIAL COST, DOLLARS	ERECTION LABOR COST, DOLLARS	TOTAL
Pressure Vessels	1,894,765	6,552	
Heat Exchangers	1,677,459	71,937	
Compressors	4,013,679	219,429	
Heaters	180,977	0	
MAJOR EQUIPMENT SUBTOTAL	7,766,879	298,123	
Piping	2,330,063	1,910,777	
Structural Steel	388,344	276,002	
Instrumentation	776,688	127,385	
Valves	1,456,000	302,480	
Timer	105,000	0	
Insulation	699,019	0	
Fireproofing	5,160	11,284	
Electrical	388,344	283,219	
Painting	155,338		
Site Development Buildings	38,834 24,790	42,461	
Field Testing		76,431	
Foundations	181,064	309,893	
Temporary Structures	122,025	334,432	
SUBTOTAL	14,437,542	3,669,128	

TABLE A.9 (continued)

BREAKDOWN OF COST COMPONENTS INCLUDED IN THE LANG SYSTEM

ITEM	EQUIPMENT MATERIAL COST, DOLLARS	ERECTION LABOR COST, DOLLARS	TOTAL
Equipment Material: Shop Labor	14,437,542		
Insurance: Taxes	101,063		
TOTAL MATERIAL	14,538,604		14,538,604
Field Labor		3,669,128	
Payroll Burden		366,913	
TOTAL FIELD LABOR		4,036,041	4,036,041
Field Supervision		3,669,128	
Field Office Personnel		183,456	
Field Office Expense		36,691	
Construction Equipment Tools		550,369	
TOTAL FIELD CHARGES		1,137,430	1,137,430
Mechanical Engineering		1,798,660	
Process Engineering		8,993	
Estimating Office Control		8,993	
Home Office Travel Expense		4,497	
Purchasing, expediating, shop inspection		158,966	
TOTAL HOME OFFICE EXPENSE		1,980,108	1,980,108
SUBTOTAL			21,693,183
OVERHEAD			922,005
FEE			1,152,506
TOTAL CHARGES			23,766,650

RATIO OF TOTAL CHARGES TO MAJOR EQUIPMENT = $\frac{23,766,650}{7,766,879}$ = 3.06

APPENDIX A

OPTIMIZATION OF THE ECONOMIC ANALYSIS

A.1.0 INTRODUCTION AND OUTLINE

This section presents an economic analysis of the desulfurization plant in functional form. The analysis shows that the process costs are a weak function of the detailed specification of the absorbers.

This section has a large number of parts which are arranged as follows. The total processing cost is defined in Section A.1. The total plant investment is defined in Section A.2.1 and the components of the total plant investment are defined in Sections A.2.2 through A.2.5. The net utility cost is defined in Section A.3.1 and evaluated in Sections A.3.2 through A.3.5. The absorbent cost is evaluated in Section A.4.1, and the labor cost in A.5.1. Finally the total processing cost is redefined in terms of the design variables in Section A.6.1.

A.1 Total Processing Cost

In this section algebraic expressions relating to the investment and total processing cost of the operating variables are developed. These derivations are given to facilitate the understanding of the complex relationships of the operating variables with various cost components. These expressions were not used in the calculations of the cases summarized in Table A.2, but are presented to demonstrate the functional trends for this economic study.

A.1.1 Components of Total Processing Cost

The total processing cost consists of the components given in the following table. The variable name is given in parentheses ( ).

a) Direct Processing Cost (PC1)

This consists of the sorbent cost (A), labor cost (C_L), maintenance cost (C_M) and net utilities cost (U_T). Maintenance cost is assumed to be three percent of the plant investment (C_T).

$$PC1 = A + C_L + 0.03C_T + U_T \qquad (a.1)$$

b) Indirect Processing Cost (PC2)

The indirect processing cost consists of plant overhead and is assumed to be 110 percent of the labor cost.

$$PC2 = 1.1C_L \qquad (a.2)$$

c) Fixed Processing Cost (PC3)

The fixed processing cost consists of depreciation and insurance and property taxes. Depreciation is assumed to be linear and calculated for a plant life of 20 years. Insurance and property taxes are assumed to be 2.3 percent of the plant investment (C_T).

$$PC3 = 0.05C_T + 0.023C_T = 0.073C_T \qquad (a.3)$$

d) General Expenses (PC4)

General expenses consist of administration and finance charges. Finance charges are nine percent of plant investment and administration charges are three percent of the processing cost consisting of direct processing cost, indirect processing cost and fixed processing cost.

$$PC4 = 0.09C_T + 0.03(PC1 + PC2 + PC3) \qquad (a.4)$$

e) Total Processing Costs

The total processing cost (TPC) is calculated by adding the cost components described above.

$$TPC = PC1 + PC2 + PC3 + PC4$$

This equation can be written in terms of the fundamental design parameters by combining equations a.1-a.4. The result is

$$TPC = 1.03A + 2.163C_L + 1.03U_T + 0.1961C_T \qquad (a.5)$$

Hence the total processing cost can be calculated knowing the total plant investment (C_T), labor cost (C_L), sorbent cost (A) and net utility cost (U_T). The following analysis describes the relationship of these costs to process variables.

The total processing costs can be divided into three types of contribution in this analysis. These are fixed (independent of design), operating (depends upon thruput), and capital investment. The fixed cost is the $2.163C_L$ term since the labor utilization is independent of design. The operating costs are the $1.03A + 1.03U_T$ terms. The capital cost is the $0.1961C_T$ term.

A.2.1 Total Plant Investment (C_T)

The total plant investment was estimated by multiplying the cost of major equipment by a Lang factor of 3.06. The cost of major equipment consists of reactor (C_R), cost of air compressors (C_A), cost of recycle compressors (C_{RC}), cost of heat exchangers, heater and drums (C_E).

$$C_T = 3.06(C_R + C_A + C_{RC} + C_E) \qquad \text{(a.6)}$$

A.2.2.1 Reactor Bed Volume

The producer gas rate for a 500 MW power generating plant was estimated to be 28.9 X 10^6 SCFH based on 130 BTU/SCF heating value of the producer gas and 47 percent efficiency of converting the heating value to electricity. Total sorbent bed volume for at least 90 percent H_2S removal and a desired cycle length was determined from the following equation:

$$\text{Total Bed Volume (cu ft) of All Reactors Onstream} = \frac{\text{Amount of Sulfur To Be Removed (Lb)}}{\text{Bulk Density}\left(\frac{\text{Lb Sorbent}}{\text{Cu Ft Bed}}\right) \times \text{Usable Sulfur Capacity}\left(\frac{\text{Lb Sulfur Removed}}{\text{Lb Sorbent}}\right)} \qquad \text{(a.7)}$$

where,

Usable Sulfur Capacity

$$= \text{Ultimate Sorption Capacity} \times \text{Sorption Efficiency } (\tau)\left(\frac{\text{Lb Sulfur Removed}}{\text{Lb Sorbent}}\right)$$

In the previous equation, the ultimate sorption capacity was based on the stoichiometric form of iron sulfide being $FeS_{0.9}$ and the sorption efficiency was estimated using the following equation based on the film kinetic model presented in previous APCI work[1] with a ten percent safety factor added.

$$\tau = 0.9(1 - 8.84X_1 - 5.01 \times 10^{-8}X_2) \qquad (a.8)$$

where,

τ = sorption efficiency at ten percent breakthrough

$$X_1 = \frac{GHSV \sqrt{a^3} \; T^{0.17}}{\sqrt{PV}}$$

$$X_2 = \frac{T \exp(16/T) GHSV}{PI_o}$$

GHSV = gas hourly space velocity

$$= \frac{\text{Gas Flow Rate, ft}^3\text{/hr at STP}}{\text{Bed Volume, ft}^3}$$

a = sorbent pellet radius (ft)

I_o = sorbent iron oxide concentration (lb-mols/ft^3)

P = pressure (atm)

T = dimensionless temperature

$$= \frac{\text{Absolute Temperature, °R}}{492°F}$$

V = superficial linear velocity at run conditions (ft/hr)

Computation of bed volume involved a trial and error calculation since determination of sorption efficiency (equation a.8) required an initial estimate of GHSV.

An initial estimate of sorption efficiency was made to calculate bed volume (equation a.7) and hence determine GHSV. A new estimate of τ was obtained in equation a.8 and the estimated GHSV. The procedure was repeated until τ_{EST} matched τ_{CALC}.

For orientation purposes the experimentally observed absorption capacity runs made in support of the math correlation were typically about 0.8 of the theoretical absorption capacity. The theoretical capacity is estimated assuming the spent sorbent contains $FeS_{0.9}$. While the economics could have been based on the observed efficiency of 0.8, they were not. Since all of the experimental runs made to support the math model yielded 0.8 of ultimate capacity at breakthrough, the value of 0.8 is a reasonable first guess for bed utilization. The bed utilization at breakthrough was estimated as described above. Table A.8 summarizes the calculated sorption efficiencies for the 25 cases given in Table 4.2.

A.2.2.2 Reactor Dimensions and Costs

The total flow rate of the producer gas is fixed at 28.9×10^6 SCFH. The number of reactors onstream is chosen to be N. A small number of onstream reactors would make size of the reactor large and cost of each reactor high. A large number of onstream reactors would result in a small size of each reactor and low cost per reactor. Thus an optimum number of reactors may be calculated for the chosen operating conditions. The number of reactors provided for regeneration is the same as the number of reactors onstream. In addition, one spare reactor is provided for sorbent changeover. Thus the total number of reactors is 2N + 1. The flow rate of producer gas through a single reactor is then

$$\frac{28.9 \times 10^6}{N} \text{ SCFH}$$

Hence a mass balance for the reactor at 1200°F yields

$$\frac{\pi}{4} D^2 \times v \times 3600 \times \frac{P}{14.7} \times \frac{540}{1660} = \frac{28.9 \times 10^6}{N}$$

$$vPD^2 = \frac{461900}{N}$$

where v = producer gas velocity, ft/sec

D = reactor diameter, ft

P = operating pressure, psia

$$D = \left(\frac{461900}{NvP} \right)^{1/2} \qquad \text{(a.9)}$$

The mols of sulfur to be removed by each reactor during absorption cycle are calculated knowing the producer gas rate, number of reactors, hydrogen sulfide concentration in the producer gas and an assumed absorption cycle length. Ninety percent removal of hydrogen sulfide is assumed.

$$\text{Lb-Mols Sulfur To Be Removed Per Reactor} = \frac{\text{Producer Gas Flow Rate (SCFH)} \times H_2S \text{ Concentration (Mol Fraction)} \times \text{Onstream Cycle Length (Hr)} \times 0.9}{359 \times \text{No. of Reactors Onstream}}$$

$$\text{Lb-Mols Sulfur To Be Removed} = 434.7 \frac{H}{N}$$

where H = onstream cycle length, hr, and

mol fraction of H_2S in the feed producer gas = 0.006

Knowing the iron oxide content (w_i, weight percent) and its bulk density (d_i, lb/ft^3), the ultimate sulfur capacity of the sorbent is calculated assuming the final form to be $FeS_{0.9}$ as

$$= \frac{\text{Lb Iron Oxide } (Fe_2O_3)}{\text{Lb Sorbent}} \times \frac{\text{Lb Sorbent}}{\text{Ft}^3 \text{ Sorbent}}$$

$$\times \frac{\text{Lb-Mols } Fe_2O_3}{\text{Lb } Fe_2O_3} \times \frac{\text{Lb-Mols Sulfur}}{\text{Lb-Mol } Fe_2O_3}$$

$$= 0.0001127\, w_i d_i \frac{\text{Lb-Mols Sulfur}}{\text{Ft}^3 \text{ Sorbent}} \qquad \text{(a.10)}$$

where w_i = weight percent iron oxide in sorbent

d_i = bulk density of sorbent, lb/ft^3

For ideal operation,

$$VR_{ideal} = 434.7 \frac{H}{N} \frac{1}{0.0001127\ w_i d_i}$$

$$= 3.857 \times 10^6 \frac{H}{N w_i d_i} ft^3 \qquad \text{(a.11)}$$

where VR_{ideal} = volume of the reactor assuming ideal operation (sorption efficiency = 1)

If the sorption efficiency is τ, the volume of the reactor, V_R, is given by

$$V_R = 3.857 \times 10^6 \frac{H}{Nw_i d_i \tau} \text{ ft}^3 \qquad \text{(a.12)}$$

$$= \frac{\pi D^2}{4} \ell$$

where ℓ = bed depth, ft

$$\therefore \ell = 3.857 \times 10^6 \frac{H}{Nw_i d_i \tau} \cdot \frac{4}{\pi} \cdot \frac{1}{D^2}$$

Since $$D^2 = \frac{461900}{NPv} ,$$

$$\ell = 10.63 \frac{H}{w_i d_i \tau} P \cdot v \text{ ft}$$

The length of the reactor (L) is greater than the bed depth (ℓ) to allow for inerts and reactor internals. Typically,

$$L = \ell + 9.5 \text{ ft}$$

Hence

$$L = 10.63 \frac{H \cdot P \cdot v}{w_i d_i \tau} + 9.5 \text{ ft} \qquad \text{(a.13)}$$

The reactor investment cost is proportional to the reactor mass. Thus the cost of the total 2N + 1 reactors (C_R) is given as

$$C_R = (2N + 1)[(C1D^2 + C2DL) \cdot t + C3] \qquad \text{(a.14)}$$

($C1D^2$: heads; $C2DL \cdot t$: shell thickness; $C3$: fixed cost for nozzles, etc.)

where C_1, C_2 and C_3 are constants determined from data developed in the case studies

The reactor thickness (head thickness assumed to be proportional to wall thickness) is given as

$$t = a_1 PD + a_2, \text{ inches} \qquad \text{(a.15)}$$

where a_1 and a_2 are constants determined from the case study data

Substituting $D = \left(\frac{461900}{NvP}\right)$ and

$$L = \frac{10.63HPv}{w_i d_i \tau} + 9.5$$

in the equation for cost of 2N + 1 reactor

$$C_R = (2N + 1) \cdot \frac{461900}{N} \left[\sqrt{\frac{461900}{N}}\, a_1 C1 \frac{P}{(vP)^{3/2}} + a_2 C1 \frac{1}{vP} + 10.63H\, a_1 C2 \frac{P}{w_i d_i \tau} + \left(\frac{N}{4088}\right)^{1/2} a_2 C2 \frac{H}{w_i d_i \tau} (Pv)^{1/2} + 9.5 a_1 C2 \frac{1}{v} + \left(\frac{N}{5118}\right)^{1/2} a_2 C2 \frac{1}{(vP)^{1/2}} \right] + C3 \qquad \text{(a.16)}$$

The fixed cost for nozzles and other reactor internals (C3) is normally small compared to the cost of the vessel. Hence for a simplified case C3 = 0. The remaining constants are obtained from the case studies.

$$a_1 = 0.0003906, \quad a_2 = 0.1986$$

Hence

$$t = 0.0003906PD + 0.1986$$

where t = shell thickness, inches

P = operating pressure, psi

D = reactor diameter, ft

$C1 = 405.2, \quad C2 = 134.02$

These constants were obtained by fitting equations a.14 and a.15 to three cases. For a more accurate estimation of constants. a regression analysis on all the cases is required.

Hence

$$C_R = (2N + 1)(405.2D^2 + 134.02DL)t$$

where C_R = cost in dollars

D = reactor diameter, ft

L = reactor length, ft

t = shell thickness, inches

$$C_R = \left(\frac{(2N + 1)}{N}\right) \cdot 461900 \left[\frac{107.6}{\sqrt{N}} \frac{P}{(vP)^{3/2}} + 80.47 \frac{1}{vP}\right.$$

$$+ 0.56 \frac{HP}{w_i d_i \tau} + 0.42 \frac{\sqrt{N} \cdot H}{w_i d_i \tau} (Pv)^{1/2}$$

$$\left. + 0.49 \frac{1}{v} + 0.37 \sqrt{N} \frac{1}{(vP)^{1/2}}\right] \qquad \text{(a.17)}$$

Thus the cost of reactors can be determined if the number of reactors, onstream cycle length, iron oxide content and density of the sorbent, sorption efficiency, producer gas velocity and operating pressure are known.

Equation a.17 has terms with both positive and negative exponents in pressure and velocity. Therefore, the reactor cost can show a minimum with respect to these variables. However, reactor cost is a fraction of the total investment cost and the pressure and velocity for minimum plant investment may be different from the pressure and velocity for minimum reactor cost.

A.2.3.1 Compressor Costs

The compressor costs consist of the regeneration air compressor cost and recycle gas compressor cost.

A.2.3.2 Regeneration Air Compressor

The regenerator operates at the pressure, P_{OP}. The air demand is fixed at 62.9 lb-moles/min required for conversion of the FeS to Fe_2O_3 and SO_2 plus special excess. Thus the required regeneration air compressor capacity (H_A, horsepower) is

$$H_A = \frac{RT}{33000} G_A \frac{1}{Y} \left[\left(\frac{P_{OP}}{P_O} \right)^Y - 1 \right] \qquad \text{(a.18)}$$

where G_A = molar air rate = 62.9 lb-mols/min

R = gas constant = 1545 lb-ft/lb-mol/°F

T = absolute temperature = 560°R

$Y = \frac{\delta - 1}{\delta}$

where δ is the coefficient of polytropic compression. Y = 0.285 for air.

P_O = atmospheric pressure = 14.7 psi

P_{OP} = discharge pressure of the compressor

$$H_A = 5550 \left[\left(\frac{P_{OP}}{14.7} \right)^{0.285} - 1 \right] \qquad \text{(a.19)}$$

Fifty percent excess capacity is provided to accomodate unit down-time. The air compressor investment cost (C_A) depends on its capacity (H_A) as follows:

$$C_A = 1161.2(1.5H_A)^{0.77}$$

$$= 1.212 \times 10^6 \left[\left(\frac{P_{OP}}{14.7} \right)^{0.285} - 1 \right]^{0.77} \qquad \text{(a.20)}$$

where C_A = investment cost of the air compressor, dollars

A.2.3.3 Recycle Gas Compressor

The regenerator phase operates in laminar flow for all velocities considered. The pressure drop across the reactor is given as

$$\Delta P_R \alpha \frac{V_R \ell}{dp^2} = C_5 \frac{V_R \left(P_{OP} - \frac{\Delta P_R}{2} \right)}{w_i \tau dp^2}$$

where ΔP_R = pressure drop (psi) across the reactor during regeneration

V_R = regeneration gas velocity (ft/sec) across the reactor

dp = pellet diameter, inches

$$\Delta P_R = \frac{S P_{OP}}{1 + S^{1/2}}$$

$$S = \frac{C_5 v \cdot V_R}{w_i \tau dp^2} \quad \textit{and is dimensionless.}$$

The total pressure drop in the recycle loop is then

$$\Delta P_{TOTAL} = \Delta P + \Delta P_F$$

where ΔP_F = fixed pressure drop across other equipment in the recycle loop and is estimated to be 35 psi

The recycle gas compressor capacity (H_R, horsepower) is

$$H_R = \frac{RT}{33000} \frac{G_R}{Y} \left[\left(\frac{P_{OP}}{P_{OP} - \Delta P_{TOTAL}} \right)^{Y} - 1 \right]$$

$$= \frac{RT}{33000} \frac{G_R}{Y} \left[\left(1 - \frac{S}{1 + S^{1/2}} - \frac{\Delta P_F}{P_{OP}} \right)^{-Y} - 1 \right]$$

$$= \frac{RT}{33000} \frac{G_R}{Y} \left[\left(\frac{2 - S}{2 + S} - \frac{\Delta P_F}{P_{OP}} \right)^{-Y} - 1 \right]$$

where G_R = recycle gas rate = 533.4 lb-mols/min

$Y = \frac{\delta - 1}{\delta}$ = 0.277 for recycle gas

P_{OP} = discharge pressure, psia

T = 580°F

Thus

$$H_R = 52293\left[\left(\frac{2 - \frac{0.0068v \cdot v_R}{w_i \tau dp^2}}{2 + \frac{0.0068v \cdot v_R}{w_i \tau dp^2}} - \frac{35}{P_{OP}}\right)^{-0.277} - 1\right] \quad \text{(a.21)}$$

Fifty percent excess capacity is provided for the recycle gas compressor.

$$C_{RC} = 1161.2(1.5H_R)^{0.77} \quad \text{(a.22)}$$

where H_R (horsepower) is given by equation a.21 and

C_{RC} is the investment cost in dollars for the recycle gas compressor

A.2.4 Heat Exchanger and Drums

For a fixed capacity, the cost of the heat exchangers and knock-out drums depends on the operating pressure as

$$C_E = C_{E_o} P^{\alpha_E}$$

where P = operating pressure, psi

C_E = investment in dollars for heat exchangers and drums

C_{E_o} and α are constants determined from the case studies

$$= 613800 \times P^{0.23}$$

A.2.5 Investment Summary

Thus total plant investment, C_T, is given by equation a.7

$$C_T = 3.06(C_R + C_A + C_{RC} + C_E)$$

where each of the cost components is defined in terms of the operating variables in Sections A.2.2 through A.2.4.

A.3.1 Net Utility Cost

The net utility cost (U_T) is given by

$$U_T = U_0 + U_A + U_R + U_C - U_S \qquad \text{(a.34)}$$

where U_0 = utility cost of onstream pressure loss, dollars/yr

U_A = utility cost of air compressor, dollars/yr

U_R = utility cost of recycle compressor, dollars/yr

U_C = utility cost of cooling water, dollars/yr

U_S = credit for steam generation, dollars/yr

A.3.2 Utility Cost of Onstream Pressure Loss (U_0)

A.3.2.1 Pressure Drop During Sorption

The air compressors for the gasifier must operate at increased pressure to overcome the pressure drop caused by flow through the fixed-bed absorbers. The producer gas flow through the beds is in the turbulent flow region (particle Reynolds number > 1000) where the pressure drop (ΔP) is proportional to the velocity (v) squared.

$$\Delta P_o = C_6 P v^2 \ell / dp$$

$$\Delta P_o = 6.52 \times 10^{-5} \cdot P v^2 \ell / dp$$

where P = operating pressure, psi

ℓ = bed depth, ft

dp = pellet diameter, inches

The constant C_6 is found from the case studies to be 6.52×10^{-5}.

A.3.2.2 Power Requirement

The power used by the air compressors for the gasifier without the desulfurization plant is given by the following equation:

$$H_G^{\circ} = \frac{RT}{33000} \frac{G_A'}{Y} \left[\left(\frac{P_H}{P_o} \right)^{Y} - 1 \right]$$

where G_A' = air to the gasifier, lb-mols/min

P_H = required air pressure, psi

P_o = atmospheric pressure = 14.7 psia

H_G° = total horsepower required without the desulfurization unit

If ΔP_o (psi) is the onstream pressure drop across the desulfurization reactor, the required air pressure increases to $P_H + \Delta P_o$ psi. Hence the power requirement for the air compressors to the gasifier with the desulfurization plant is:

$$H_{Gd}^{\circ} = \frac{RT}{33000} \frac{G_A'}{Y} \left[\left(\frac{P_H + \Delta P_o}{P_o} \right)^{Y} - 1 \right]$$

where H_{Gd}° = horsepower for gasifier air compressors with desulfurization

Thus the incremental cost of onstream pressure loss in terms of horsepower (H_G) is

$$H_G = \frac{RT}{33000} \frac{G_A'}{Y} \left[\left(\frac{P_H + \Delta P_o}{P_o} \right)^Y - \left(\frac{P_H}{P_o} \right)^Y \right]$$

$$= \frac{RT}{33000} \frac{G_A'}{Y} \left(\frac{P_H}{P_o} \right)^Y \left[Y \cdot \frac{\Delta P_o}{P_H} \right]$$

In terms of the base utility costs without the desulfurization unit the additional costs are

$$H_G = H_G^\circ \frac{Y \left(\frac{\Delta P}{P_H} \right)}{1 - \left(\frac{P_o}{P_H} \right)^Y}$$

Since the operating pressure, P, is nearly equivalent to the gasifier inlet pressure, P_H, the incremental utility cost can be written as

$$U_O = U_G^{\circ} \frac{\gamma \frac{\Delta P}{P}}{1 - \left(\frac{P_o}{P}\right)^{\gamma}}$$

where U_O is the incremental utility cost for the air compression to the gasifier caused by the pressure drop through the desulfurizer during the onstream period.

U_G° is the utility cost for air compression to the gasifier without a desulfurization plant. This parameter depends upon the operating pressure and the air requirement of the gasifier.

Inserting the function for ΔP yields

$$U_O = (2824.6)\left(\frac{P_{OP}}{150}\right)^{0.285} \cdot \frac{HPV^3}{w_i d_i \tau dp} \qquad \text{(a.35)}$$

where the factor $(P_{OP}/150)^{0.285}$ is an empirical parameter which correlates the effect of pressure upon the incremental cost of air compression.

A.3.3 Utility Cost of Regeneration Gas Recirculation

The utility cost for regeneration air compression (U_A) can be calculated easily since the horsepower required and power cost are known. The power cost is assumed to be 2.4 cents/KWH.

$$U_A = 164.95H_A \text{ dollars/yr} \qquad \text{(a.36)}$$

where H_A is given by equation a.19

A.3.4 Utility Cost of the Regeneration Air Supply

The utility cost of the recycle gas compressor (U_{RC}) can be calculated since the horsepower required and power cost are known.

$$U_{RC} = 164.95H_R \text{ dollars/yr} \qquad \text{(a.37)}$$

A.3.5 Other Utility Costs

The utility cost of cooling water (U_C) is constant and equal to 19,900 dollars/year assuming 2.5 cents/1000 gallons of cooling water for the fixed heat duty.

The utility credit for steam (U_S) is also constant since the capacity and effluent gas temperatures are constant. For all the cases it was calculated to be 1,956,200 dollars/year assuming 3.5 dollars/1000 pounds of steam.

Hence the total utility cost (U_T) is

$$U_T = 2824.6\left(\frac{P_{OP}}{150}\right)^{0.285} \cdot \frac{HPV^3}{w_i d_i \tau dp} + 164.95(H_A + H_R)$$

$$+ 19{,}900 - 1{,}956{,}200 \qquad \text{(a.38)}$$

where H_A and H_R are given by equations a.19 and a.21

A.4.1 Absorbent Cost (A)

The total absorbent cost depends on the bed volume, sorbent price and sorbent life.

$$A = \frac{V_s \cdot d_i \cdot P_i}{T_L} \qquad (a.39)$$

where A = total absorbent cost per year

V_s = total sorbent volume, ft^3, given by

$$V_s = 3.857 \times 10^6 \frac{2N + 1}{N} \frac{H}{w_i d_i \tau}$$

P_i = sorbent price, dollar/lb
Varies linearly with iron oxide content.

T_L = sorbent life, years

Thus

$$A = B_A \frac{1}{w_i \tau} \frac{(1 + a_A w_i)}{T_L}$$

The constants (B_A and a_A) can be evaluated for the cases

$$A = 4.3304 \times 10^7 \frac{1}{w_i \tau} \frac{(1 + 0.0074 w_i)}{T_L}$$

where w_i = weight percent iron oxide content

τ = sorption efficiency

T_L = sorbent life, years

A.5.1 Labor Cost (C_L)

The labor cost is fixed for the fixed scale of operation. The labor cost is assumed to be equal to that of two men/shift at $9.55/hour. For the cases evaluated

$$C_L = 167,300 \text{ dollars/year}$$

A.6.1 Total Processing Cost

Substituting all these numbers, the total processing cost is given as

$$TPC = 1.03A + 2.163C_L + 1.03U_T + 0.1961C_T \qquad (a.40)$$

where $A = 4.3304 \times 10^7 \frac{1}{w_i \tau} \frac{(1 + 0.0074 w_i)}{T_L}$ Dollars/Yr

$C_L = 167{,}300$ Dollars/Yr

$$U_T = \left\{ 2824.6 \left(\frac{P_{OP}}{150} \right)^{0.285} \cdot \frac{HPV^3}{w_i d_i \tau dp} \right.$$

$$+ 164.5 \times 52293 \left[\left(\frac{2 - \frac{0.0068 v \cdot v_R}{w_i \tau dp^2}}{2 + \frac{0.0068 v \cdot v_R}{w_i \tau dp^2}} - \frac{35}{P_{OP}} \right)^{-0.277} - 1 \right]$$

$$+ 164.5 \times 5550 \left[\left(\frac{P_{OP}}{14.7} \right)^{0.285} - 1 \right]$$

$$\left. + 19{,}900 - 1{,}956{,}000 \right\} \text{ Dollars/Yr}$$

$$C_T = 3.06 \left\{ \frac{2N + 1}{N} \times 461{,}900 \left[\frac{107.6}{\sqrt{N}} \frac{P}{(vP)^{3/2}} + \frac{80.47}{vP} \right.\right.$$

$$\left. + 0.56 \frac{HP}{w_i d_i \tau} + 0.42 \frac{\sqrt{N}\ H}{w_i d_i \tau} (Pv)^{1/2} \right.$$

$$\left. + 0.49 \frac{1}{v} + 0.37 \frac{\sqrt{N}}{(vP)^{1/2}} \right]$$

$$+ 1.212 \times 10^6 \left[\left(\frac{P_{OP}}{14.7} \right)^{0.285} - 1 \right]^{0.77}$$

$$+ 6.819 \times 10^6 \left[\left(\frac{2 - \frac{0.0068 v \cdot v_R}{w_i \tau dp^2}}{2 + \frac{0.0068 v \cdot v_R}{w_i \tau dp^2}} - \frac{35}{P_{OP}} \right)^{-0.277} - 1 \right]^{0.77}$$

$$\left. + 0.614 \times 10^6 P^{0.23} \right\} \text{ Dollars}$$

An examination of this expression reveals that the total processing cost decreases continuously with an increase in iron oxide content (w_i) and a decrease in onstream cycle length (H). Pressure (P) and velocity (V) appear both as positive and negative powers. Thus it is possible to have an optimum pressure and velocity for minimum total processing cost.

Section 4.4.2 illustrates application of this mathematical model.

APPENDIX B

MORGANTOWN DATA

FOR THE APCI MATHEMATICAL MODEL

Department of Energy
Morgantown Energy Research Center
P. O. Box 880
Collins Ferry Road
Morgantown, West Virginia 26505

December 8, 1977

Melvin Kopstein, Coal Gasification, Washington Office

THRU: W. E. Wallace, Jr., Assistant Director, Analytical and Supporting Research Division

DATA FOR AIR PRODUCTS

Enclosed is the data as requested by Air Products for the APCI Mathematical Model. As indicated some of the information was not available from the MERC data, however, from the data provided some parameters such as the bed void fraction can be estimated.

We have also included statements regarding operating procedures as well as some additional data not specifically requested by Air Products.

G. W. Stewart, Chief
Supporting Research Branch

GWS:dc

Enclosures

INFORMATION REQUESTED OF MERC TO APPLY

APCI MATHEMATICAL MODEL TO MERC DATA

A. Necessary Information on Each Run

1. Regeneration Feed flow Rate SCFH .....Table 7 .....Page 18
2. Regeneration Feed Composition Mole Percent....Table 7 .....Page 18
3. Oxygen Breakthrough Curve; Mole Percent O_2 in Effluent Versus Time Onstream .....Not Available
4. Observed Temperature Exotherms; Temperature Versus time Onstream for Different Bed Depths.....Tables 6-1 & 6-2 ..Page 16-17

   Thermocouple Location .....Figure 6 .....Page 19
5. Inlet Temperature .....Ambient
6. Gas Hourly Space Velocity (GHSV) Based On Gas At STP...Calculate from Table 7 and depth of 4-3/4 ft.
7. Bed Void Fraction.....Not Determined
8. Bulk Density and True Density of Sulfided Sorbent....Not Determined
9. Pressure psig.....Averaged 3 psig
10. Sulfur Weight Percent in Sulfided Sorbent.....Table 4 .....Page 13
11. Iron Oxide Weight Percent in Fresh Sorbent.....25% - 75% Flyash.
12. Bed Depth. 4-3/4 ft. - 282 lbs. of Pellets in charge

B. Additional Desired Information on Each Run

13. Sorbent Composition.....25% Iron Oxide - 75% Flyash by weight
14. Porosity of Sulfided Sorbent..... IR #90.....Page 3
15. Sulfur Weight Percent in Regenerated Sorbent.... <1%
16. Sulfur Dioxide Breakthrough Curve.....Not Available

17. Pellet Diameter and Length .....25" diameter, Average ½" long

18. Weight of the Sulfided Sorbent Charged ..... Not Available

19. Previous History of the Sorbent: Whether Fresh or Used .....Fresh

20. Heat Capacity of the Sorbent.....Not Available

C. General Information

1. Description of the Reactor and Pilot Plant....Figure 6 & 19

2. Comments on Adiabaticity of Operation.

3. Operating Procedure.....Page 11

4. Method of Sulfiding Sorbents..... Actual Producer gas as described on Page 1-3 and 11

* Absorption Data .....Table 5-1 and 2.....Page 14 & 15

RUN REPORT NO. 11

16" GAS PRODUCER, HOT GAS CLEANUP, AS REPORTED IN I.R. #90
May 3, 1977

Gas Composition - The gas composition before and after the reactor is summarized in Table 1. From Table 1, the H_2 and CO concentrations increased in magnitude and the N_2 concentration decreased from Cycle #1 to #2. This data was obtained from the Bendix gas chromatographs because the grab samples, the Greenbrier and the Bendix did not agree. To at least make the errors systematic the Bendix's readings were used on the inlet and outlet.

There was no ammonia produced on either regeneration cycle. On absorption for Cycle #1, the ammonia reached the level of >0.50 ppm on the outlet sample point on two occasions (Bendix 7000 analysis). In the second absorption Cycle #2, the concentration maximum value was 119.7 ppm on the inlet and 84 ppp on the outlet in grab samples. The magnitude of the grab samples and the Bendix 7000 analyzer were off by a factor of approximately 100 (see Table 2).

The input and output concentrations for hydrogen sulfide is lower in Figure 1 for Cycle #1. The two curves are very close together except for the interval between one and two hours of on stream time. The maximum value on the input was 2.49% and the output was 2.09 grains/100 scf.

The output concentration was divided by the input concentration in Figure 2. The resulting plot was very erratic with the input going to zero (see circled data points) on several occasions.

The input and output concentrations for hydrogen sulfide is shown in Figure 3 for Cycle #2. The two curves are very close together except for the interval between 4.5 and 6 hours on stream time. The maximum value on the input was 1.23% and the output was -1.0466 grains/100 scf.

The output concentration was divided by the input concentration in Figure 4. The resulting plot was very erratic with the input going to zero (see circled data points) on several occasions.

Bed Temperature - From Table 3, the bed temperature on absorption is very uniform with a miximum temperature gradient (top to bottom) of 19°F and an approximate bed stream temperature of 1,000°F on both cycles. The standard deviation of each thermocouple is small with a maximum on TIR-39 in Cycle #2 of 127°F.

The maximum bed center line temperature in Cycle #1 on regeneration was on TIR-35A at 1,605°F and the minimum was TIR-39A at 1,035°F.

For the thermocouples four inches from the centerline of the vessel, the maximum bed temperature was on TIR-32 at 1,605°F and the minimum was TIR-39 at 1,030°F.

The maximum bed centerline temperature in Cycle #2 on regeneration was TIR-31A and 35A at 1,845°F and the minimum peak was TIR-39A at 1,050°F.

For the thermocouples four inches from the centerline of the vessel, the maximum bed temperature was on TIR-31 at 1,830°F and the minimum peak was TIR-39 at 1,075°F.

Bed Differential Pressure - The bed had its highest reading on absorption of 185 inches of water at the end of the first cycle. In Cycle #2 the largest value reached was 83 inches of water at the end of the absorption cycle. In Cycle #2 the curve in Figure 5 was much more linear than in Cycle #1.

Particulates - The size distribution on the particulates in the bed are listed in the attachment. The maximum percentage was 13.8% for the 64.0 microns weight percent oversize. The distribution of the particules removed by the cyclone in Cycle #1 and #2 are in the attachments. The maximum percentages were 17.2%/16% for the 50.8 micron weight percent oversize.

The chemical composition of the particulates in the bed was:

Total Carbon	19.98%
Total Sulfur	2.77%
Ash	76.00%

The chemical composition of the cyclone dust and grate ash on absorption was:

	Cycle 1		Cycle 2	
	Cyclone	Grate	Cyclone	Grate
Total Carbon	60.53	36.57	62.16	45.24
Total Sulfur	3.26	1.59	3.15	3.05
Ash	29.36	Bal.	28.76	Bal.
Moisture	1.02	0.60	0.83	0.46
Hydrogen	1.61	0.26	1.87	0.37
Nitrogen	1.15	1.42	.99	2.41

Pellets - The surface area and the pore volume for the pellets are summarized below from the analysis sheets:

Initial Pellets	1.4515	0.001 473
Bottom Bed	3.0502	0.014 114
Middle Bed	1.2985	0.005 209
Top Bed	1.4996	0.003 524

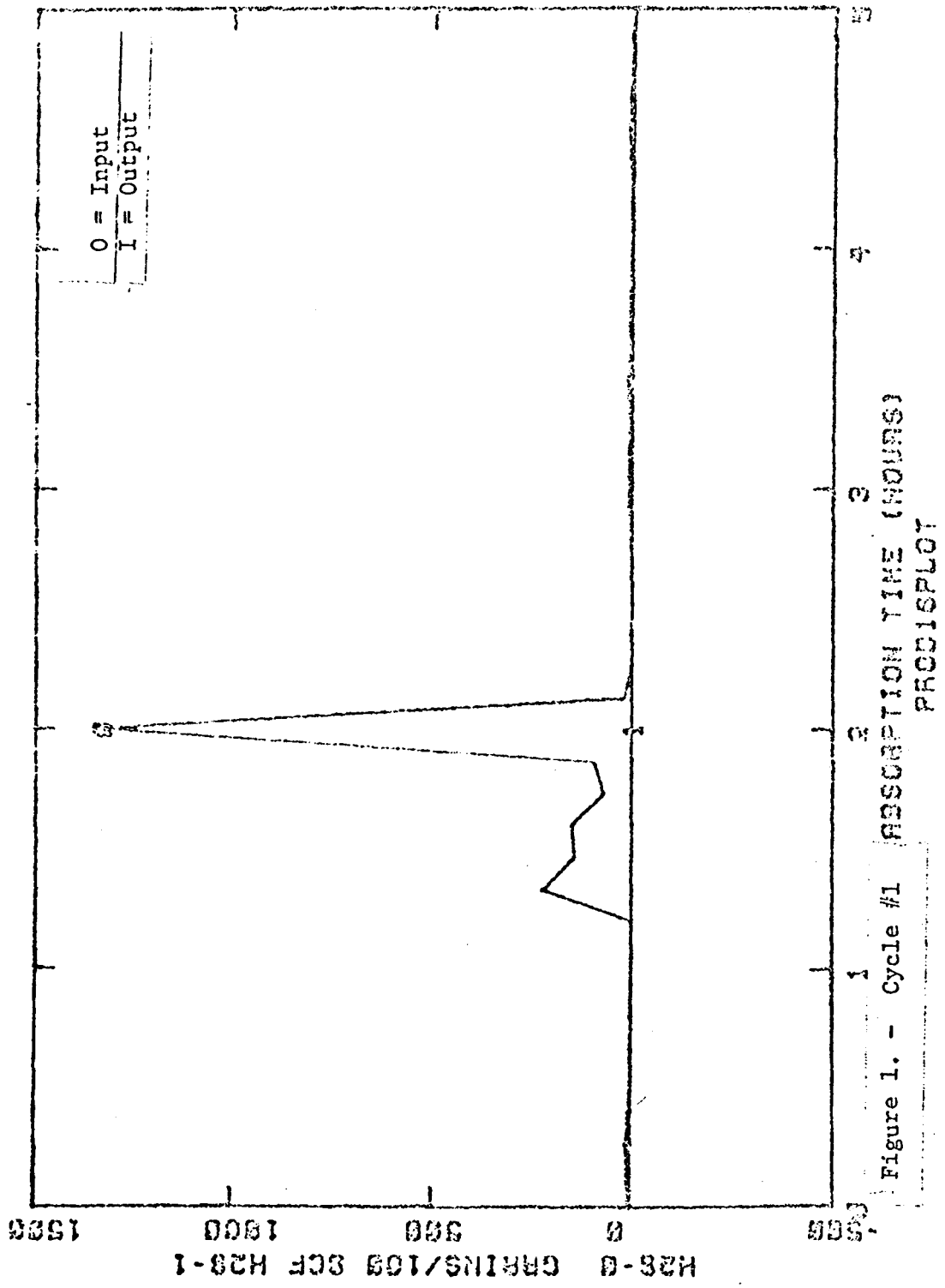

Figure 1. - Cycle #1

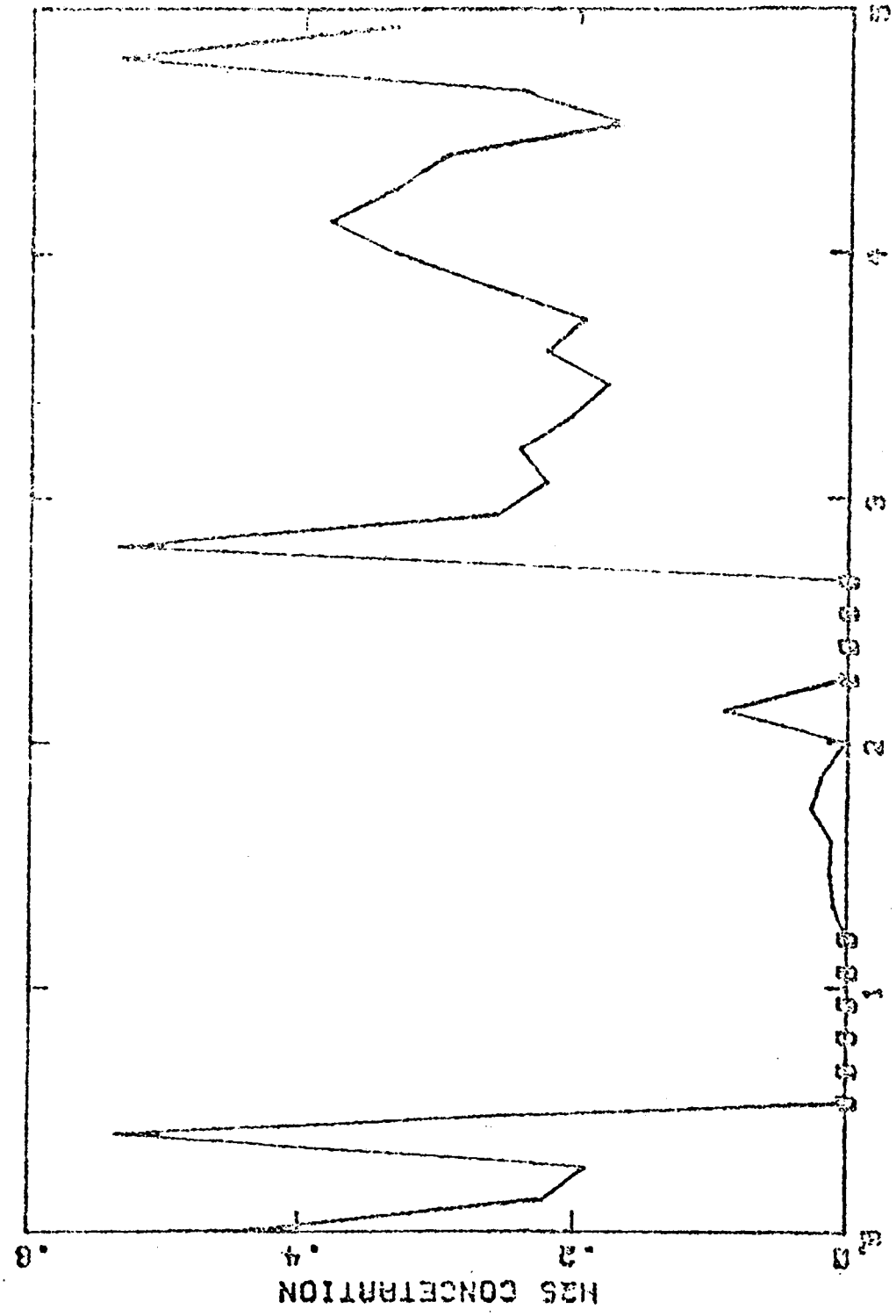

Figure 2 - Cycle #1 ABSORPTION TIME (HOURS)
RATIO OF GRAINS/100 SCF H2S TO PERCENT H2S

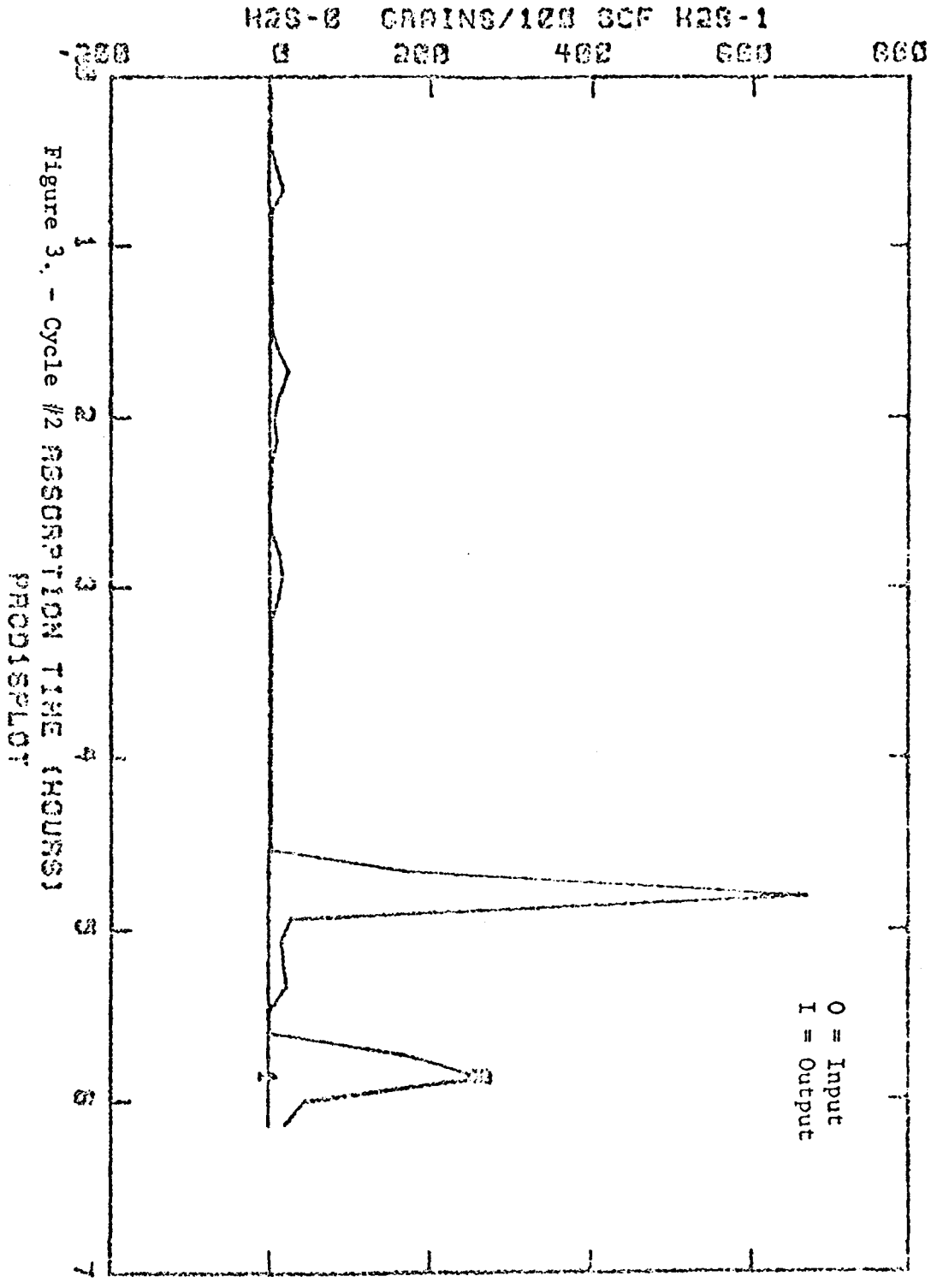

Figure 3. - Cycle #2 ADSORPTION TIME (HOURS) PRODUCTION

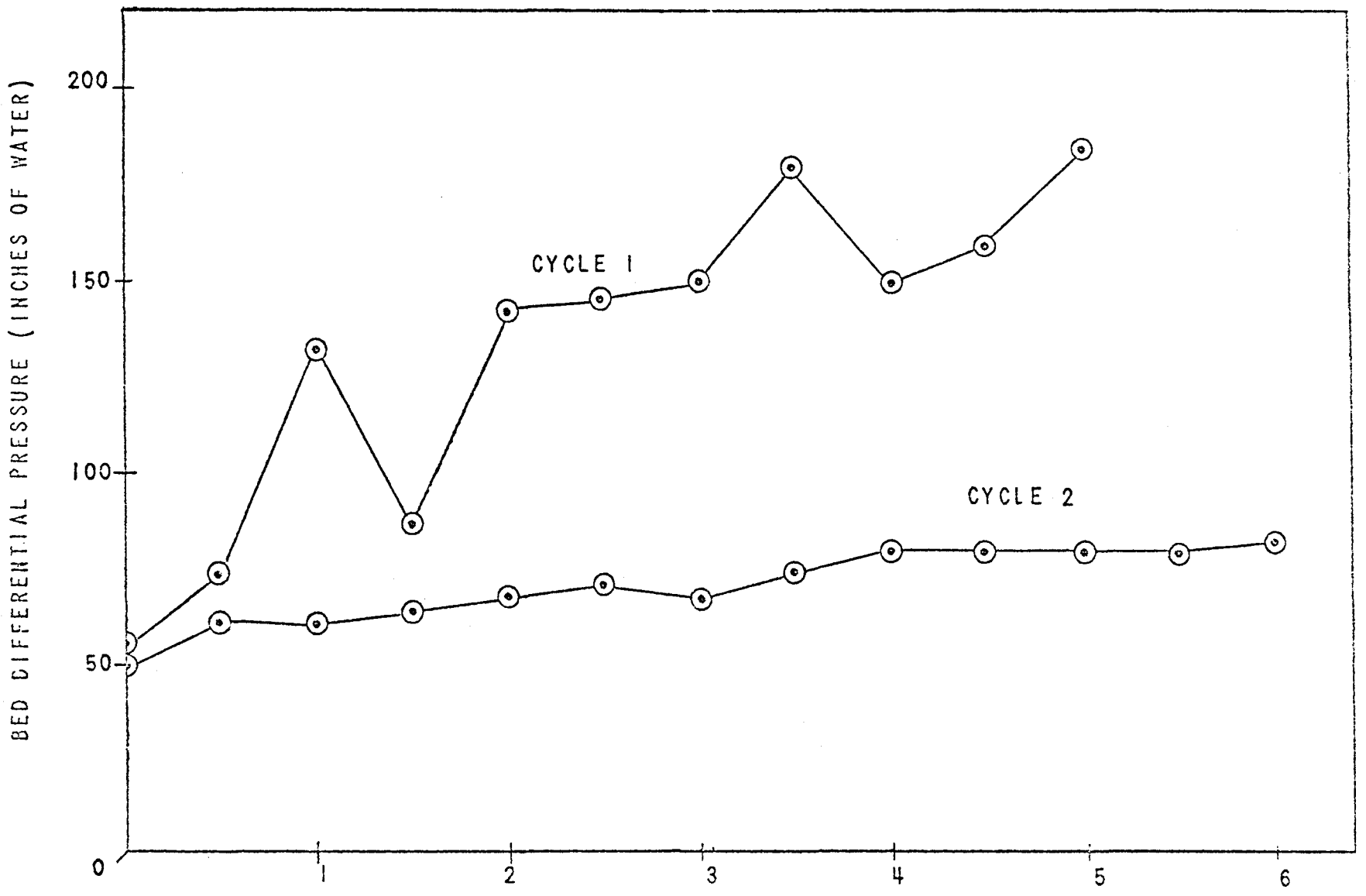

FIGURE # 5: ABSORPTION TIME (HOURS) FOR RUN # 11

TABLE #1: ABSORPTION GAS CONCENTRATIONS

	CYCLE #1 INPUT (%)	OUTPUT (%)	CYCLE #2 INPUT (%)	OUTPUT(%)
H_2 Mean	4.0671	9.60	5.50	8.66
StDV	3.9623	1.31	3.91	0.97
CO_2 Mean	8.6892	10.17	12.38	12.29
StDV	3.7462	1.94	2.15	1.13
CS_2 Mean	0.0085		0.01	
StDV	0.0110		0.15	
C_2H_6 Mean	0.0572	0.14	0.36	0.15
StDV	0.1001	0.07	0.60	0.08
H_2S Mean	0.108	2.02312 *	0.06	-1.65 *
StDV	0.4013	0.1112 *	0.20	0.24 *
COS Mean	0.0026		0.02	
StDV	0.0082		0.04	
O_2 Mean	1.8395		1.27	
StDV	1.3665		1.03	
N_2 Mean	71.7623	56.99	66.86	57.98
StDV	7.4833	4.29	10.54	1.85
CH_4 Mean	0.6302	1.54	2.17	1.49
StDV	1.3392	.54	3.09	.56
CO Mean	2.7290	16.91	2.56	12.56
StDV	4.7886	1.98	2.33	2.26

NOTE: 1. All analytical data from Bendex units

2. * H_2S units in grains/100scfh

TABLE #2 : NH_3 CONCENTRATION FOR RUN # 11

			INLET (PPM)	OUTLET (PPM)	
CLE # 1	CYCLE PHASE	TIME	GRAB SAMPLE	GRAB SAMPLE	BENDIX 7000
1	ABSORPTION	830			
		1000			> 0.50
		1045			> 0.50
		1330			
	REGENERATION	1500			
		2300			
2	ABSORPTION	1515			
		1704			0.77
		1720	79.6		
		1800		63.9	
		1808			> 0.80
		1900		84.0	
		1907			> 0.80
		1957			> 0.80
		2005	119.7		
		2057			0.54
		2100		38.1	
		2105	67.7		
	REGENERATION	2145			
		800			

INTERVAL CONSTANT (30 MIN.)
M= MAXIMUM , N= MINIMUM

TABLE 3 : ABSORBER BED TEMPERATURES

	CYCLE 1		CYCLE 2	
	CENTER LINE	4" FROM CL	CENTERLINE	4" FROM CL
TIR-31 Mean	NO DATA	1033 M	1018 M	1001 N
StDV		69	97	43
TIR-32 Mean		1031		1008
StDV		63		45
TIR-33 Mean	NO DATA	1033 M	1001	1010
StDV		58	60	46
TIR-34 Mean		1031		1010
StDV		55		57
TIR-35 Mean	NO DATA	1015 N	1000 N	1013
StDV		15	62	58
TIR-36 Mean		1017		1017
StDV		14		80
TIR-37 Mean	NO DATA	1020	1000	1019
StDV		16	91	95
TIR-38 Mean		1022		1017
StDV		18		107
TIR-39 Mean	NO DATA	1023	1005	1020 M
StDV.		18	120	127
SPREAD	NO DATA	18	18	19

Procedure Guidelines-Operation

1. Feedstock - After initial warm-up period, stabilize crossover temperature (TIRA-4) at 1100°F and maintain operations on anthracite coal until Tuesday midnight. At that time switch to bituminous coal for remainder of run. All make gas while on anthracite coal to be vented direct to stack-not through absorbers.

2. Flow rate - Maintain a flow rate (FIR-15) of 7,500 SCFH if possible. (TIRA-4-1100°F more important).

3. Blast steam - If time permits, switch the superheated steam (TIR-52 @1100°F) over into the blast air line and watch for any improvement in hydrogen content of make gas. NOTE: The superheated steam may condense in grate shaft if temperature (TIR-52) falls below 1000°F.

4. Pellets - Before the run, absorber was filled with 282 lb. of iron oxide-fly ash (25/75 comp.) having diameter of 0.250-inches. Record height of bed before and after run in logbook.

5. Absorption - With H_2S concentration in make gas stable (on bituminous coal) and the average bed temperature of absorber is greater than 1100°F shift make gas to pass through absorber and record bed temperature and H_2S concentration out of absorber every thirty minutes. Follow data sheet outline for special data during first hour of absorption. Discontinue absorption cycle 0.5 hr. after 200 grains H_2S concentration has been reached. At end of absorption, purge absorber for a minimum of two minutes with 1,000 SCFH inert gas. Continue cooling bed until it reaches a mean bed temperature of 900°F. NOTE: Check inert gas for O_2 at use point before purging. Do not purge if O_2 content is over 0.5%. Check with Project Engineer before proceeding with regeneration. Sulfur balance will be incorrect if partially regenerated with inert gas before measurements begin. Record analyzer data on inert gas in logbook with notes.

6. Regeneration:

   a. Cut off electric heat to absorber shell.

   b. Begin regeneration with 500 SCFH inert gas. If temperature of bed does not climb over 100°F, increase inert gas flow (FIR-13) to 1500 SCFH.

   c. Add 200 SCFH of AIR (FIR-12) to inert gas stream to absorber and watch temperature. Do not exceed 1600°F. If necessary to change flow rate record times during which flow rates are entering absorber (to determine total air flow for regeneration). Decrease or increase air (increments of 50 SCFH) until you have established a stable air flow for 1600°F maximum peaking temperatures. NOTE: Regeneration is taking place from bottom to top of absorber. It

is expected that the sulfur concentration will be higher at bottom of bed so less air should be required to maintain temperatures near beginning of regeneration. Increase air flows as regeneration proceeds to reach 1500°F as closely as possible but do not exceed 1600°F.

d. Terminate regeneration when SO_2 concentration falls below 0.5% by volume.

e. Purge absorber for 5 minutes with 500 SCFH inert gas (FIR-13).

TABLE 4

SULFUR CONCENTRATION

BEFORE ABSORBER-AFTER CYCLONE

Time/hrs.	Gr. Sulfur/100 scf
1515 - Start absorbtion Run #11 Cycle #2	
1530	730
1615	540
1645	550
1715	540
1745	550
1815	560
1845	670
1915	650
1945	450
2015	650
2045	690
2115 - Sample point plugged	
2130 - End absorption Run #11 Cycle #2	
H_2S sample line valve off	
Precipitator off	

Table 5-1

Temperature Profiles for Absorption

Run No.: 11 -- Cycle No.: 1 -- Absorption Start Time: 0830 -- Stop Time: 1330

Time	T-6	T-7	T-8	T-9	T-10	T-11	T-12	T-13	T-14
0830	1230	1215	1200	1190	1020	1020	1020	1020	1020
0900	1000	1000	1015	1030	1040	1040	1050	1055	1060
0930	995	990	995	1005	1010	1010	1015	1010	1010
1000	1010	1015	1010	1005	1005	1010	1010	1010	1015
1030	1025	1020	1025	1020	1010	1015	1025	1025	1025
1100	975	1005	1020	1020	1020	1020	1020	1025	1025
1130	1000	1000	1000	995	995	1000	1000	1000	1000
1200	1015	1000	1000	1000	1000	1000	1000	1000	1005
1230	1010	1015	1005	1000	1000	1005	1005	1010	1010
1300	1040	1030	1035	1025	1025	1030	1035	1040	1035
1330	1060	1055	1060	1050	1040	1040	1040	1045	1045

TABLE 5-2 Temperature Profiles for Absorption

Run #11, Cycle #2

TIME	T-1	T-2	T-3	T-4	T-5	T-6	T-7	T-8	T-9	T-10	T-11	T-12	T-13	T-14
1515	1400	1295	1180	1110	1195	980	1035	1105	1170	1180	1275	1330	1370	1440
1530	1040	1180	1300	1370	1365	1250	1290	1320	1330	1260	1250	1200	1125	1080
1545	970	1000	1070	1150	1270	1140	1150	1120	1090	1085	1040	1020	995	975
1600	950	960	1005	1005	1040	1030	1040	1025	1015	1030	995	980	970	955
1615	950	960	990	990	990	1000	1000	1000	1000	1000	1000	1000	980	960
1645	970	970	970	970	970	995	995	995	995	995	995	995	985	985
1715	970	965	965	970	970	990	990	990	990	990	990	990	985	990
1745	970	960	960	965	970	990	990	990	990	990	990	990	980	980
1815	940	940	955	960	965	980	980	980	965	970	960	960	960	955
1845	965	965	960	960	960	975	985	980	975	980	980	980	980	985
1915	970	975	975	970	970	980	985	985	980	985	985	985	985	985
1945	980	990	990	980	990	990	990	990	985	990	990	990	990	990
2015	970	970	980	980	980	985	985	985	985	985	985	985	985	985
2045	995	995	995	995	995	1000	1010	1005	1000	1005	1010	1010	1010	1010
2115	1010	1010	1010	1010	1010	1010	1015	1010	1010	1010	1015	1015	1015	1015

TABLE 6–1. Temperature Profiles for Regeneration

Run No. 11; Cycle No. 1; Recorder No. 1

Time	PDIA-5	T-1	T-2	T-3	T-4	T-5	T-6	T-7	T-8	T-9	T-10	T-11	T-12	T-13	T-14
1500		1035	1035	1000	990	935	Out	980	990	1010	1005	1035	1075	1130	1030
1515		970	1190	1015	995	985		1000	1005	1025	1040	1180	1370	1330	960
1530		830	1500	1130	1010	995		1010	1035	1100	1230	1575	1470	1230	850
1545		680	1505	1340	1055	995		1050	1130	1280	1450	1500	1305	1020	740
1600		580	1380	1515	1145	1005		1140	1265	1460	1530	1340	1060	815	645
1615		500	1235	1605	1250	1025		1225	1385	1590	1450	1170	890	665	580
1630		440	1025	1490	1360	1060		1315	1480	1555	1290	980	720	545	520
1645		390	885	1375	1480	1125		1430	1605	1460	1145	830	590	465	455
1700		355	735	1220	1535	1195		1490	1560	1305	1000	705	500	425	415
1715		330	620	1085	1600	1270		1590	1495	1175	880	600	445	395	385
1730		300	535	930	1545	1345		1535	1330	1010	760	530	405	365	355
1800		260	405	700	1360	1455		1350	1025	750	615	425	340	325	310
1830		230	310	570	1150	1455		1120	805	625	535	360	305	285	275
1900		210	275	510	1080	1425		990	720	565	490	330	280	260	250
1930		190	245	455	1010	1435		865	650	505	440	300	260	245	230
2000		180	225	410	930	1440		785	600	470	415	280	245	230	215
2030		170	210	370	455	1445		710	545	435	390	260	225	215	205
2100		155	185	320	735	1505		605	465	380	345	240	210	200	190
2130		140	165	275	610	1420		570	420	335	315	220	195	190	170
2200		135	155	250	510	1260	Out	465	380	305	285	205	180	170	160
2230		125	145	225	430	1075		415	340	280	260	190	165	165	155
2300		120	135	200	365	920		370	305	255	240	180	155	150	150
2330		115	125	180	315	790		150	265	235	230	165	150	145	145

End Regeneration: Run 11, Cycle 1, Recorder 1

TABLE 6-2 Temperature Profiles for Regeneration

Run #1, Cycle #2, Recorder #1

TIME	T-1	T-2	T-3	T-4	T-5	T-6	T-7	T-8	T-9	T-10	T-11	T-12	T-13	T-14
2145	1050	1030	1030	1010	1010	1006	1015	1015	1020	1020	1020	1020	1020	1025
2200	1030	1100	1030	1010	1010	1000	1010	1020	1025	1030	1065	1215	(1415)	(1075)
2215	860	1510	1065	1015	1015	1005	1025	1025	1050	1085	1395	(1735)	1245	950
2230	730	1710	1280	1040	1025	1015	1045	1085	1215	1285	1675	1580	1040	785
2245	620	1680	1490	1155	1040	1060	1140	1265	1420	1460	(1705)	1310	885	650
2300	545	1520	1655	1310	1110	1150	1260	1385	1560	1600	1560	1110	765	565
2315	485	1340	1750	1440	1215	1250	1365	1505	1670	(1705)	1385	935	655	495
2330	435	1120	1845	1575	1345	1355	1470	1620	(1785)	1685	1185	750	570	440
2345	390	900	1630	1720	1460	1445	1595	(1795)	1740	1510	970	615	505	39.
2400	360	745	1365	1840	1610	1570	(1730)	out	1520	1340	800	550	455	355
0030	310	545	970	1650	1840	(1830)	1660	1450	1170	1055	605	465	385	300
0100	270	405	695	1360	1845	1515	1430	1135	885	845	485	405	330	255
0130	235	340	560	1050	1615	1295	1250	910	730	730	420	365	295	230
0200	210	290	450	730	1070	1070	1070	730	565	635	365	320	255	205
0230	190	255	395	555	720	925	945	625	470	570	330	290	230	185
0300	170	225	345	380	490	795	780	515	415	515	295	255	210	165
0330	155	200	310	300	370	700	615	465	375	465	260	235	195	150
0400	140	180	275	260	300	600	525	415	340	425	235	215	175	145
0430	130	165	250	230	260	545	460	375	310	390	215	195	165	135
0500	120	150	230	21	230	505	415	350	285	355	195	180	150	120
0530	115	135	210	190	210	465	380	320	260	325	185	165	140	110
0600	110	130	195	180	195	435	355	295	245	305	175	155	135	105
0630	100	120	175	160	175	395	320	265	220	275	160	145	125	105
0700	100	120	175	165	175	385	325	270	225	275	165	145	125	105
0730	95	115	170	155	170	360	300	250	205	250	190	135	120	105
0800	95	115	170	155	170	355	295	250	205	250	180	140	120	105

Table 7

Feed Composition

Run #11, Cycle #1				Run #11, Cycle #2			
Time	Air Flow	I. Gas Read.	SO_2 pct.	Time	Air Flow	I. Gas Flow	SO_2 pct.
1500	0	2.0/500 scfh	0.22	2145	2.55/200 scfh	5.75/1500 scfh	0.01
1515	2.7/200 scfh	5.5/1500 scfh	-0.11	2200	-do-	-do-	5.10
1530	2.7/200 scfh	5.5/1500 scfh	-0.18	2215	-do-	-do-	5.29
1545	2.7/200 scfh	5.5/1500 scfh	-0.11	2230	-do-	-do-	5.3
1600	2.7/200 scfh	5.5/1500 scfh	-0.15	2245	-do-	-do-	5.37
1615	2.2/150 scfh	5.5/1500 scfh	-0.19	2300	-do-	-do-	5.47
1630	2.7/200 scfh	5.5/1500 scfh	-0.21	2315	-do-	-do-	5.48
1700	2.7/200 scfh	5.5/1500 scfh	-0.28	2330	-do-	-do-	5.51
1715	2.2/150 scfh	5.5/1500 scfh	-0.28	2345	-do-	-do-	5.53
1730	2.7/200 scfh	5.5/1500 scfh	-0.29	0000	-do-	-do-	5.58
1800	2.7/200 scfh	5.5/1500 scfh	-0.32	0015	-do-	-do-	5.68
1830	2.7/200 scfh	5.5/1500 scfh	-0.39	0030	-do-	-do-	5.91
1900	3.6/300 scfh	3.8/1000 scfh	-0.39	0045	-do-	-do-	6.09
1930	3.6/300 scfh	3.8/1000 scfh	-0.39	0100	-do-	-do-	6.09
2000	3.8/400 scfh	3.8/1000 scfh	-0.39	0115	-do-	-do-	5.85
2030	3.8/400 scfh	3.8/1000 scfh	-0.39	0130	-do-	-do-	5.68
2100	6.0/500 scfh	3.8/1000 scfh	-0.39	0145	-do-	-do-	5.40
2130	6.0/500 scfh	3.8/1000 scfh	-0.40	0200	-do-	-do-	5.23
2200	6.0/500 scfh	3.8/1000 scfh	-0.40	0215	-do-	-do-	5.08
2230	6.0/500 scfh	3.8/1000 scfh	-0.39	0230	-do-	-do-	4.95
2300				0245	-do-	-do-	4.82
2330			-0.45	0300	-do-	-do-	4.74
(End of Regeneration)				0315	-do-	-do-	4.64
				0330	-do-	-do-	4.55
				0400	-do-	-do-	4.42
				0415	-do-	-do-	4.34
				0430	2.55/200 scfh	5.75/1500 scfh	4.26
				0445	-do-	-do-	4.19
				0500	-do-	-do-	4.15
				0515	-do-	-do-	4.19
				0530	-do-	-do-	4.15
				0545	-do-	-do-	3.97
				0600	-do-	-do-	4.06
				0615	-do-	-do-	4.08
				0700	325/	0	4.01
				0720			4.21
				0730	10/1000 scfh	0	4.15
				0745	10/1000 scfh	0	.49
				0800	10/1000 scfh	0	.40

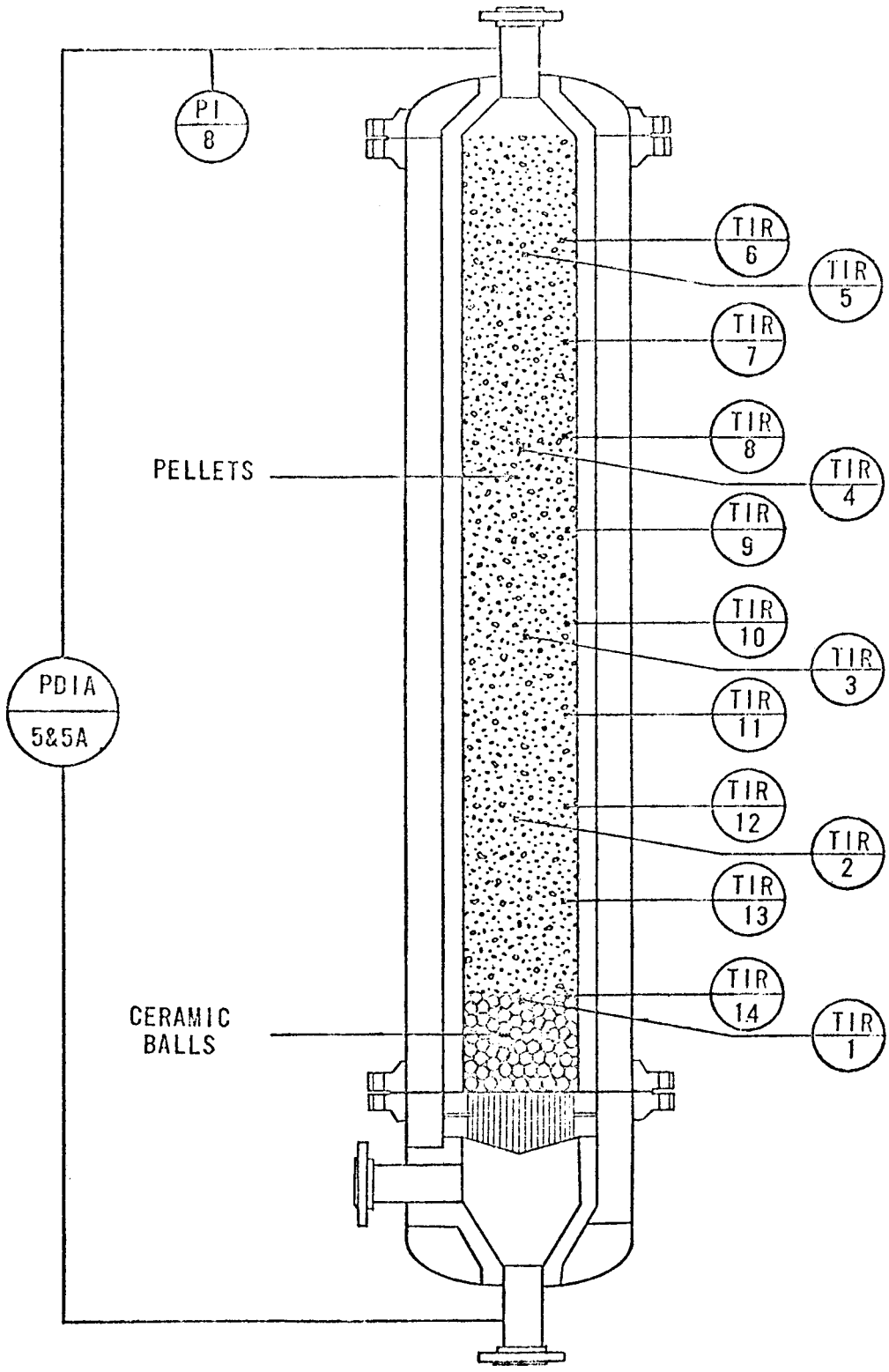

H_2S REACTION VESSEL ON 16'' GAS PRODUCER

APPENDIX C
DERIVATION OF DIFFERENTIAL EQUATIONS TO DESCRIBE SORPTION AND REGENERATION DYNAMICS

C.0 INTRODUCTION

Sorption of hydrogen sulfide on an iron oxide/fly ash surface involves a series of three processes:

1. Diffusion of hydrogen sulfide from the producer gas to the solid sorption site in the sorbent pellet.

2. Chemical reaction between the hydrogen sulfide and iron oxide.

3. Diffusion of the product of the reaction (water) away from the sorption site.

Each of these three processes can, in turn, procede by several possible mechanisms in series. Thus, the sorption process can be thought of as a series of steps, the slowest of which determines the overall rate of the sorption process. When the first or third of the processes listed above is the slowest, then the sorption procedes by a diffusion controlled mechanism. Sorption is kinetically controlled if the second step is slowest. When a slowest or rate limiting mechanism is assumed, then the relationship between the process variables and sorption dynamics can be determined. This relationship is usually defined by partial differential equations.

The overall objectives of this effort are as follows:

1. To derive the differential equations for a diffusion controlled mechanism (the shrinking core model) and a kinetically controlled model (the fluid film-kinetic model).

2. To consolidate all process and sorbent variables into a minimum number of dimensionless numbers during the course of the derivations.

3. To explore the effects and interactions of the process and sorbent variables on dynamics as predicted by their effects on the dimensionless variables predicted by each mechanism.

4. To use the knowledge obtained from the above effort to select a mechanism for the sorption of hydrogen sulfide on iron oxide/fly ash sorbent.

If sorbent regeneration is considered to be sorption of oxygen on iron sulfide, the two models derived in this section may also be applied regeneration. However, the heat release caused by the oxidation of iron sulfide requires that heat effects on the mechanisms be considered. Heat effects are described by the heat balance partial differential equation of Section C.3.

Nomenclature for the derivations in the following three sections is given in Table C.1.

C.1.0 THE SHRINKING CORE MODEL

The model developed to describe the behavior of a single spherical sorbent particle is based on the shrinking core or shell type mechanism. The particle consists of two distinct solid phases with this mechanism: an outer shell phase that is 100% reacted, and an inner core that is 100% unreacted. Reaction of sorbent with sorbate hydrogen sulfide occurs solely at the interface between the outer shell and the inner core. As the reaction proceeds, the inner core shrinks; thus, the sorption model is called a shrinking core model. Figure C.1 illustrates the shrinking core model for sorption in a spherical particle of radius a and radial interface z. For sorption, the outer shell represents $FeS_{1.5}$/fly ash and the inner core iron oxide/fly ash. For regeneration, the outer shell represents iron oxide/fly ash and the inner core $FeS_{1.5}$/fly ash.

C.1.1 ASSUMPTIONS

1. The gas-solid reaction rate is infinitely fast.

2. The concentration of H_2S at the interface shown in Figure C.1 is zero due to the fast reaction assumed.

3. The reaction is not equilibrium limited. (Sorbent saturation level is not affected by temperature changes or concentration changes.)

4. Mass transfer resistance in the bulk phase exterior to the particle is negligible.

5. Gas flow through the sorbent bed is plug flow.

TABLE C.1

NOMENCLATURE

1. DIMENSIONLESS GROUPS

$$F = \frac{Y}{Y_o}$$

GAS PHASE DIMENSIONLESS H_2S CONCENTRATION

$$N_{Ab}^{\mathscr{O}} = \frac{a^2 V}{(1 - \varepsilon)\mathscr{O}_K pL} = C_o \, GHSV \, \frac{a^2 \sqrt{T}}{P}$$

DIFFUSIONAL SORPTION NUMBER

$$N_{Ab}^{F} = \frac{Va}{3(1 - \varepsilon)k^F L} = C_1 \, GHSV \, \frac{a^{1.5} T^{0.17}}{\sqrt{PV}}$$

FILM SORPTION NUMBER

$$N_{Ab}^{K} = \frac{V}{\alpha \, (1 - \varepsilon)k^K L M_o} = C_2 \, GHSV \, \frac{T e^{\beta/T}}{\alpha \, P M_o}$$

KINETIC SORPTION NUMBER

$$N_{cp} = \frac{\left[\varepsilon f C_p + (1 - \varepsilon)\rho_s C_s \right] Y^o}{(1 - \varepsilon)M_o C_p}$$

ADIABATIC HEAT BALANCE NUMBER

$$R_x^{\mathscr{O}} = \frac{3 \, FZ}{N_{Ab}^{\mathscr{O}} \, (1 - Z)}$$

SORPTION RATE FOR SHELL MODEL

$$R_x^{K} = \frac{FW}{N_{Ab}^{K} + N_{Ab}^{F} W}$$

SORPTION RATE FOR FILM-KINETIC MODEL

$$T_{Ab} = \frac{- \Delta H_R \, Y^o}{C_p \, 492^o R}$$

GAS PHASE ADIABATIC TEMPERATURE RISE

TABLE C.1

NOMENCLATURE

(CONTINUED)

2. RATE CONSTANTS IN TERMS OF SYSTEM VARIABLES

$$k^F = \frac{2.06}{\varepsilon} \left(\frac{\rho}{\mu}\right)^{\frac{1}{6}} \left(\frac{V}{a}\right)^{.5} \mathscr{D}^{.67}$$

FILM TRANSFER CONSTANT (FT./HR.)

$$k^F = k_b{}^F \frac{T^{0.83}}{p^{.5}} \frac{\varepsilon_b}{\varepsilon} \sqrt{\frac{V/V_b}{a/a_b}}$$

FILM TRANSFER CONSTANT IN TERMS OF SYSTEM VARIABLES (FT./HR.)

$$k^K = A \exp(-\beta/T)$$

KINETIC RATE CONSTANT ($FT.^3/LB.\ MOLE/HR.$)

3. EMPIRICAL COEFFICIENTS IN TERMS OF SYSTEM VARIABLES

$$C_o = \frac{1}{p\mathscr{D}_{Kb}(1-\varepsilon)}$$

SHELL DIFFUSION COEFFICIENT ($HR./FT.^2$)

$$C_1 = \frac{\varepsilon}{\varepsilon_b} \frac{\sqrt{V_b}}{3k_b{}^F(1-\varepsilon)\sqrt{a_b}}$$

FILM TRANSFER COEFFICIENT ($HR.^{\frac{1}{2}}/FT.$)

$$C_2 = \frac{1}{A(1-\varepsilon)}$$

KINETIC COEFFICIENT ($HR.\ LB.\ MOLE/FT.^3$)

TABLE C.1

NOMENCLATURE

(CONTINUED)

4. SYSTEM VARIABLES AND PROPERTIES

A = Kinetic Pre-exponential Factor ($ft.^3$/lb. mole/hr.)

a = Sorbent Pellet Radius (ft.)

α = Moles of Iron Oxide Per Mole of Sorbent Sulfur Capacity (Dimensionless)

β = Dimensionless Activation Energy $\frac{\Delta E}{R_G \cdot 492^oR}$

C_p = Gas Phase Heat Capacity (BTU/lb. mole ^oF)

Cs = Sorbent Heat Capacity (BTU/lb. ^oF)

$\mathscr{D}$ = H_2S Diffusivity in the Fluid Phase ($ft.^2$/hr.)

$\mathscr{D}_K$ = Knudsen Diffusivity of H_2S within Porous Pellet ($ft.^2$/hr.)

ΔE = Sorption Activation Energy (BTU/lb. mole)

ϵ = Bed Void Fraction ($in.^3/in.^3$)

f = Gas Molar Density (lb. mole/$ft.^3$)

g = Average Number of Sorbent Particles Per $Ft.^3$ of Bed ($ft.^{-3}$)

GHSV = Gas Hourly Space Velocity ($hr.^{-1}$) at STP (1 atm., 492^oR)

ΔH_R = Heat of Sorption (BTU/lb. mole, negative for exothermic reaction)

I = Sorbent Iron Oxide Concentration (lb. moles/$ft.^3$ solid)

L = Sorbent Bed Length (ft.)

ℓ = Axial Distance from Bed Inlet (ft.)

M_o = Fresh Sorbent Sulfur Capacity (lb. moles/$ft.^3$ solid)

P = System Pressure (atmospheres)

p = Sorbent Porosity (in./in.)

N = Average Rate of Reaction Per Sorbent Particle (lb. mole/hr.)

TABLE C.1

NOMENCLATURE

(CONTINUED)

4. SYSTEM VARIABLES AND PROPERTIES - Continued

R	=	Dimensionless Distance from Pellet Center (r/a)
R_G	=	Ideal Gas Constant (1.987 BTU/lb. mole/^oR)
r	=	Distance from Sorbent Pellet Center (ft.)
ρ	=	Gas Mass Density (lb./ft.^{3})
ρ_s	=	Sorbent Pellet Mass Density (lb./ft.^{3} solid)
T	=	Dimensionless Absolute Temperature (T_B ^oR/492^oR)
T_B	=	Absolute Bed Temperature (^oR)
t	=	Onstream Time (hr.)
μ	=	Gas Viscosity (lb./ft./hr.)
V	=	Superficial Gas Linear Velocity (ft./hr.)
W	=	Dimensionless Solid Iron Oxide Concentration ($I/\alpha M_o$)
X	=	Dimensionless Bed Length (ℓ/L)
x	=	Sorbate H_2S Mole Fraction within Fluid Particle (dimensionless)
Y	=	Sorbate H_2S Bulk Fluid Phase Mole Fraction (dimensionless)
Y^o	=	Feed H_2S Bulk Fluid Phase Mole Fraction (dimensionless)
y	=	Sorbate Mole Fraction in Gas Phase of Porous Pellet (dimensionless)
Z	=	Dimensionless Distance of Reaction Zone from Pellet Center (z/a)
z	=	Distance of Reaction Zone from Pellet Center (ft.)

5. SUBSCRIPT

b	=	At Base Conditions (492^oR, 1 atm., V_b, a_b, ε_b)
o	=	Process Gas Inlet Conditions (f_o, V_o) - Also at Unsaturated Conditions (M_o)

Figure C.1

SHRINKING CORE SORPTION MODEL FOR SORPTION

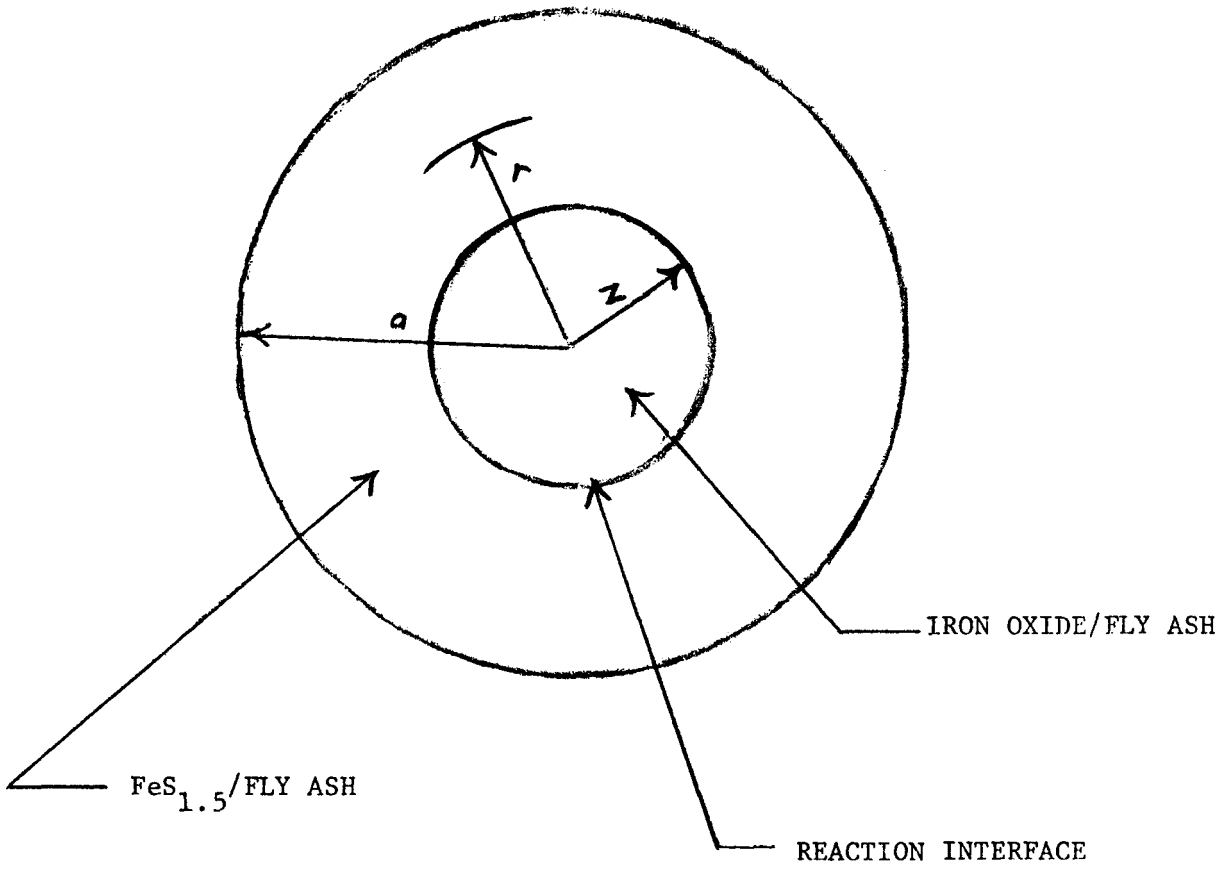

PCRD-1696
E.L.L.
8-11-76

6. The product of pore diffusivity and gas concentration ($\mathcal{D}f$) is a constant. Since concentration is inversely proportional to temperature, this assumption is equivalent to assuming pore diffusivity proportional to temperature.

C.1.2 NOMENCLATURE

Table C.1 lists the nomenclature used in the following sections of this development.

C.1.3 PARTICLE MASS BALANCE EQUATION

Referring to Figure C.1 the mass balance for the sorbate H_2S concentration in the outer unreacted shell is constructed as follows:

$$\text{Input} = \text{Output} + \text{Reacted} + \text{Accumulated} \tag{1}$$

The rate at which sorbate travels into a porous differential element of outer shell is:

$$\text{Input} = -4\pi r^2 \, p \mathcal{D}_K f \, \frac{\partial x}{\partial r} \tag{2}$$

The rate at which sorbate leaves the differential element is:

$$\text{Output} = -4\pi r^2 \, p \mathcal{D}_K f \, \frac{\partial x}{\partial r} + \frac{\partial}{\partial r} \left(-4\pi r^2 \, p \mathcal{D}_K f \, \frac{\partial x}{\partial r} \right) \partial r \tag{3}$$

Since the shrinking core model assumes the outer shell is 100% reacted, no reaction can occur in the differential element

$$\text{Reacted} = \text{Zero} \tag{4}$$

Since the change of inventory of the sorbate in the porous space is usually very small compared to the difference in diffusive flow into and out of the differential element, the accumulation term will be ignored.

$$\text{Accumulation} = \text{Zero} \tag{5}$$

The overall mass balance for the sorbate in the gas phase of the unreacted shell then becomes:

$$\frac{\partial}{\partial r}\left(-4\pi r^2\, p \mathscr{D}_K f\, \frac{\partial x}{\partial r}\right) \partial r = 0 \qquad (6)$$

Since assumption 6 indicates $\mathscr{D}f$ is independent of temperature, Equation 6 can be integrated independently of a particle energy balance provided the boundary conditions are temperature independent. At the particle surface, the sorbate mole fraction must be the same as the bulk phase mole fraction. At the reaction interface, the sorbate mole fraction is zero due to the infinitely fast reaction. These two temperature independent boundary conditions are:

Particle Exterior: $r = a,\ x = Y$ (7)

Reaction Interface: $r = z,\ x = \text{Zero}$ (8)

The solution of the mass balance equation (6), subject to boundary conditions (7) and (8), is:

$$x = \frac{Y\, a}{r} \cdot \frac{(r - z)}{(a - z)} \qquad (9)$$

The rate at which the sorbate enters the particle by diffusion is:

$$+ 4\pi\, a^2\, p \mathscr{D}_K f \left(\frac{\partial x}{\partial r}\right)_a \qquad (10)$$

or

$$\text{Input} = \frac{+4\pi\, a\, p \mathscr{D}_K f\, Y\, z}{a - z} \qquad (11)$$

based on Equation (9).

The total amount of gas phase sorbate reacted or deposited on the particle at any time is:

$$\frac{4}{3} \pi M_o (a^3 - z^3) \tag{12}$$

The rate at which this reaction occurs is:

$$\frac{\partial}{\partial t} \left[\frac{4}{3} \pi M_o (a^3 - z^3)\right] \tag{13}$$

which reduces to:

$$\text{Reacted} = -4\pi M_o z^2 \frac{\partial z}{\partial t} \tag{14}$$

provided assumption (3) on temperature and concentration independence of sorbent saturation level M_o holds.

No sorbate leaves the particle, so:

$$\text{Output} = \text{Zero} \tag{15}$$

The inventory change in porous space of the outer shell is again assumed negligible:

$$\text{Accumulation} = \text{Zero} \tag{16}$$

The overall particle mass balance for the sorbate H_2S is obtained through substitution into Equation (1):

$$+4\pi \frac{a\ p \mathscr{D}_K f\ Y\ z}{a - z} = -4\pi M_o z^2 \frac{\partial z}{\partial t} \tag{17}$$

or

$$\frac{a\ p\alpha f\ Y\ z}{a - z} = -M_o\ z^2\ \frac{\partial z}{\partial t} \tag{18}$$

It is convenient to express this equation in the following dimensionless terms:

Dimensionless Mole Fraction:

$$F = \frac{Y}{Y_O} \tag{19}$$

Dimensionless Radial Distance of Reaction Zone:

$$Z = \frac{z}{a} \tag{20}$$

Dimensionless Time:

$$\tau = \frac{Y^o f\ V\ t}{(1 - \varepsilon) L\ M_o} \tag{21}$$

Dimensionless Adsorption (or Regeneration) Number:

$$-N_{Ab}^{\alpha} = \frac{a^2 V}{(1 - \varepsilon)\alpha_K L p} \tag{22}$$

With the above substitution, Equation (18) becomes:

$$-N_{Ab}^{\alpha}\ \frac{\partial Z}{\partial \tau} = \frac{F}{Z\ (1 - Z)} \tag{23}$$

Equation (23) describes the unsteady state behavior of a single spherical particle in terms of two dimensionless groups, N_{Ab}^{α} and τ. τ or dimensionless time is also equal to the chemical efficiency of the bed at any time.

$$\tau = \frac{\text{Amount of Feed Gas Sorbate Processed}}{\text{Saturated Sorbent Bed Capacity}} \quad (24)$$

C.1.4 SORBENT BED MASS BALANCE

In the sorbent bed the mass balance for a gas phase sorbate is as follows:

$$\text{Input} = VfY \quad (25)$$

$$\text{Output} = VfY + \frac{\partial}{\partial \ell} (VfY)\, \partial \ell \quad (26)$$

$$\text{Reacted} = gN\, \partial \ell \quad (27)$$

$$\text{Accumulated} = \varepsilon f \frac{\partial Y}{\partial t}\, \partial \ell = \text{Zero} \quad (28)$$

Substitution of the above into Equation (1) leads to the overall sorbent bed mass balance:

$$- \frac{\partial}{\partial \ell} (VfY) = gN \quad (29)$$

The product Vf can be replaced by the constant $V_o f_o$ since the superficial velocity V is inversely proportional to gas density and the molar concentration f is directly proportional to gas density:

$$- V_o f_o \frac{\partial Y}{\partial \ell} = gN \quad (30)$$

The number of spherical particles per unit volume of bed is:

$$g = \frac{3 (1 - \varepsilon)}{4\pi a^3} \quad (31)$$

The reaction rate per sphere is obtained from Equations (14), (11), and (17).

$$N = \frac{4\pi\ a\ p\mathscr{O}_K f\ Y\ z}{a - z} \tag{32}$$

The mass balance equation, (30), then becomes

$$-Vf\ \frac{\partial Y}{\partial \ell} = \frac{3\ (1 - \varepsilon)\ p\mathscr{O}_K f\ Y\ z}{a^2\ (a - z)} \tag{33}$$

With the previously defined dimensionless terms and

$$X = \frac{\ell}{L} \tag{34}$$

equation (33) becomes:

$$-N_{Ab}\mathscr{O}\ \frac{\partial F}{\partial X} = \frac{3\ FZ}{1 - Z} \tag{35}$$

Under the assumptions of the previous derivation and temperature independent boundary conditions, equations (23) and (35) may be solved independently of the sorbent bed energy balance equations that follow.

C.1.5 THE SHELL SORPTION MODEL WITH BOUNDARY CONDITIONS

The shell sorption model equations derived in Sections C.1.3 and C.1.4 are listed in Table C.1. The boundary conditions are obtained from the following assumptions:

1. At initial time, $\tau = 0$.

   (1.a) The bed is unsaturated, $Z = 1$.

   (1.b) No sorbate is in the gas phase of the bed, $F = 0$.

2. At bed inlet conditions, $X = 0$, the inlet gas contains a constant mole fraction of sorbate, $F = 1$.

TABLE C.2

THE SHELL SORPTION DYNAMICS EQUATIONS
WITH BOUNDARY CONDITIONS

1. THE PARTICLE MASS BALANCE

$$- N_{Ab}\mathscr{O} \frac{\partial Z}{\partial \tau} = \frac{F}{Z\,(1 - Z)}$$

B.C. AT $\tau = 0$, $Z = 1$, AND $F = 0$

2. THE BED MASS BALANCE

$$- N_{Ab}\mathscr{O} \frac{\partial F}{\partial X} = \frac{3FZ}{1 - Z}$$

B.C. AT $X = 0$, $F = 1$

3. THE DIFFUSIONAL SORPTION NUMBER IN TERMS OF PROCESS VARIABLES

$$N_{Ab}\mathscr{O} = C_o\ GHSV\ \frac{a^2 \sqrt{T}}{P}$$

At the bottom of Table C.2 is the expression for the shell (or diffusional) sorption number in terms of process variables. This expression was obtained by assuming the Knudsen diffusivity, $\mathscr{D}_K$, is proportional to the square root of temperature and independent of pressure:

$$\mathscr{D}_K = \mathscr{D}_{Kb} \sqrt{T} \tag{36}$$

The ratio of linear velocity to bed length in the shell sorption number of equation (22) can be replaced by the space rate, pressure, and time relationship below:

$$\frac{V}{L} = GHSV \frac{T}{P} \tag{37}$$

Substituting equations (36) and (37) into equation (22) gives the shell number in terms of process variables:

$$N_{Ab}^{\mathscr{D}} = \left[\frac{1}{p\mathscr{D}_{Kb}(1 - \varepsilon)}\right] GHSV \frac{a^2\sqrt{T}}{P} \tag{38}$$

The quantity in brackets is an empirical constant, C_o, dependent on sorbent structure.

C.1.6 SOLUTION TO THE SHELL SORPTION DYNAMICS EQUATIONS WITH BOUNDARY CONDITIONS

The equations of Table C.2 were programmed as a subroutine in the adiabatic computer model, Appendix C. The computer generated isothermal solution defines percent breakthrough as a function of dimensionless time (or sorption efficiency) and the Shell sorption number. Figure C.2 is a composite plot of the breakthrough curves between efficiencies of zero and one for sorption numbers of 0 to 13. The abscissa of the plot is the sorption number, the ordinant is the efficiency, and the percent breakthrough is represented by contour lines. The effect of process variables on efficiency at any given breakthrough can be quickly determined using Figure C.2 and the relationship between process variables and the sorption number (Equation (38)).

C.2.0 THE FLUID FILM-KINETIC SORPTION MODEL

The model was developed to describe the behavior of a single sorbent pellet based on the kinetic and/or the fluid film transfer mechanisms. Figure C.3 is a schematic of such a sorbent pellet surrounded by a stagnant film of fluid. Hydrogen sulfide diffuses through the stagnant fluid film to the interior of the sorbent pellet. This rate of film transfer is proportional to the difference between the uniform H_2S concentration in the particle

FIGURE C.2

COMPUTER GENERATED BREAKTHROUGH CURVES
FOR SORPTION NUMBERS BETWEEN ZERO AND THIRTEEN

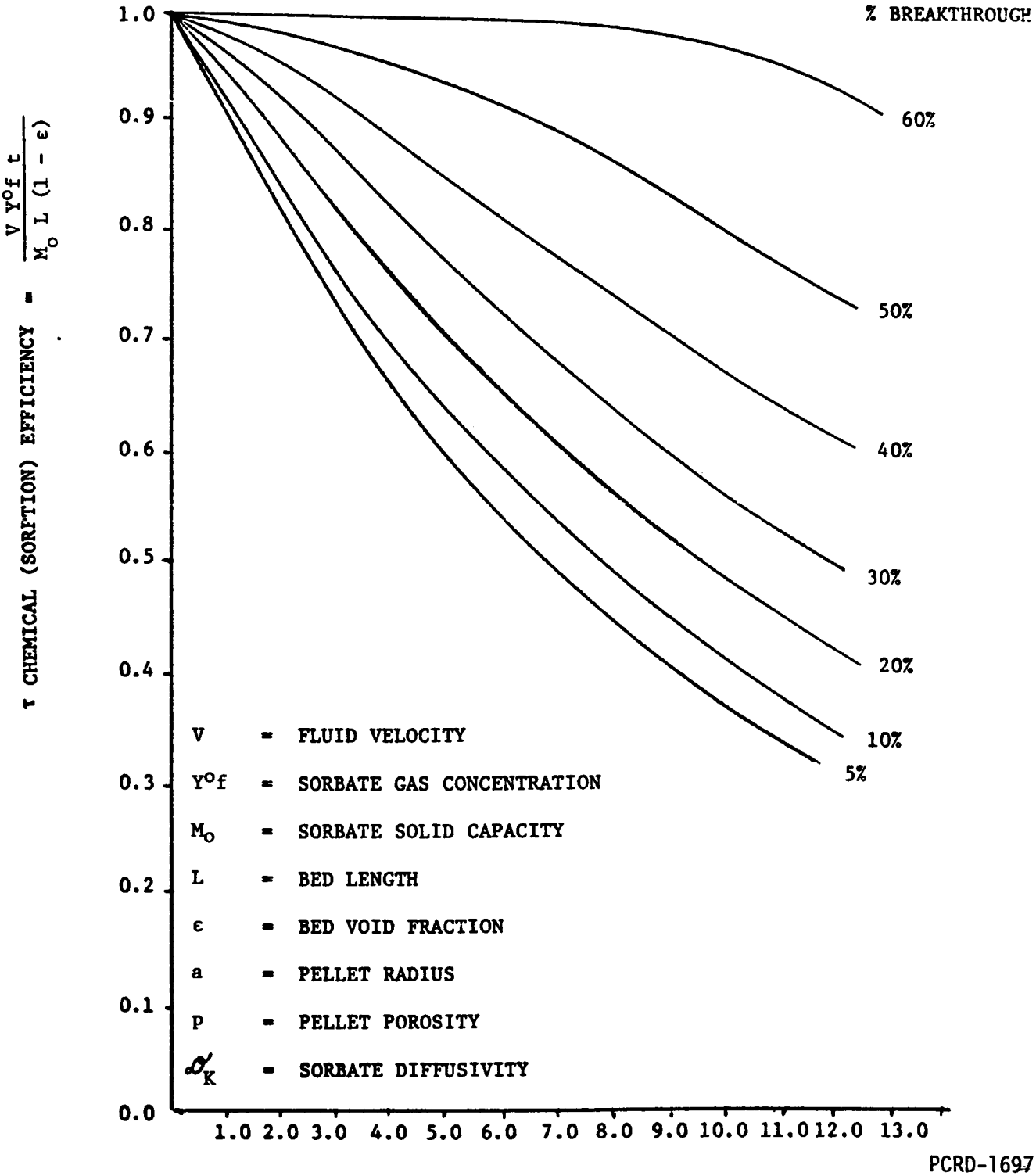

$N_{Ab}^{\mathscr{D}}$ (SORPTION NUMBER) = $\frac{a^2\ V}{p\mathscr{D}_K L\ (1 - \epsilon)}$

PCRD-1697
E.L.L.
8-11-76

FIGURE C.3

FLUID FILM-KINETIC SORPTION MODEL

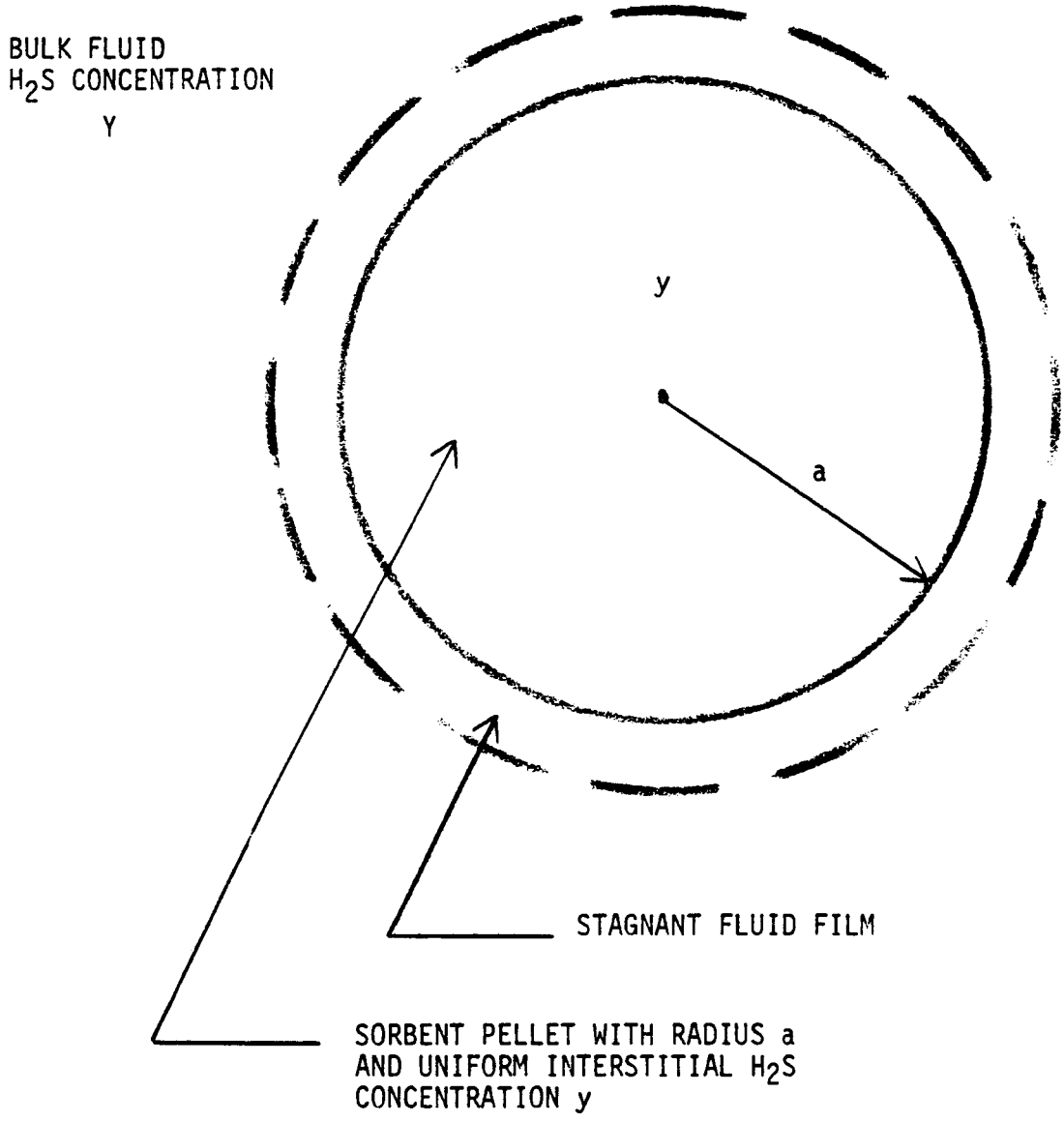

PCRD-1511
E.L.L.
8-11-76

interior and the bulk fluid H_2S concentration. The constant of proportionality is the film transfer constant. Once the sorbate hydrogen sulfide has diffused into the pellet, its rate of reaction is proportional to the interstitial H_2S concentration and the sorbent iron oxide concentration. This second constant of proportionality in the model is the kinetic rate constant.

.2.1 ASSUMPTIONS

1. Mass transfer resistance within the solid particle is neglibible.
2. The interstitial concentration of H_2S does not vary with radial distance within the particle due to the assumed lack of internal mass transfer resistance.
3. The reaction is not equilibrium limited. (Sorbent saturation level is not affected by temperature or concentration changes.)
4. The reaction is isothermal.
5. Gas flow through the sorbent bed is plug flow.

C.2.2 NOMENCLATURE

Table C.1 lists the nomenclature used in the following sections of this development.

C.2.3 PARTICLE MASS BALANCE EQUATION

Referring to Figure C.3 the mass balance for the sorbate H_2S concentration within the pellet is constructed as follows:

$$\text{INPUT} = \text{OUTPUT} + \text{REACTED} + \text{ACCUMULATED} \qquad (1)$$

The rate at which sorbate enters the particle is the rate at which it diffuses through the stagnant fluid film:

$$\text{INPUT} = 4\pi a^2 \, k^F f \, (Y - y) \qquad (2)$$

Sorbate cannot leave the porous particle except by counter-diffusion through the stagnant film. Thus, there is no output equation:

$$\text{OUTPUT} = \text{ZERO} \qquad (3)$$

The rate of reaction in a sorbent particle is given by the kinetic rate expression:

$$\text{REACTED} = \frac{4\pi a^3}{3} \; k^K \; I \; f \; y \qquad (4)$$

Since the change in inventory of the sorbate in the porous space is usually very small compared to the rate of reaction, the accumulation term will be ignored.

$$\text{ACCUMULATION} = \text{ZERO} \qquad (5)$$

The overall mass balance for H_2S in the gas phase of the pellet then becomes:

$$4\pi a^2 \; k^F \; f \; (Y - y) = \frac{4\pi a^3}{3} \; k^K \; I \; f \; y \qquad (6)$$

Equation (6) can be solved for the interstitial H_2S concentration:

$$y = \frac{k^F \; Y}{k^F + \frac{k^K \; Ia}{3}} \qquad (7)$$

When Equation (7) is substituted into the rate expression (4), the rate of H_2S sorption can be expressed in terms of bulk phase sorbate concentration:

$$\text{REACTED} = \frac{4}{3} \pi a^3 \; \frac{k^K \; k^F \; I \; f \; Y}{k^F + \frac{k^K \; Ia}{3}} \qquad (8)$$

For each mole of H_2S sorbed, a stoichiometric amount of iron oxide is consumed. If the rate of iron oxide consumption is set equal to the rate expression of Equation (8) times the stoichiometric coefficient, the solid phase pellet iron oxide balance is the result:

$$-\frac{4}{3}\pi a^3 \frac{\partial I}{\partial t} = \alpha \frac{4}{3}\pi a^3 \frac{k^K k^F f I Y}{k^F + \frac{k^K I a}{3}} \tag{9}$$

or

$$-\frac{\partial I}{\partial t} = \alpha \frac{k^K k^F f I Y}{k^F + \frac{k^K I a}{3}} \tag{10}$$

It is convenient to express the particle solid phase balance in the following dimensionless terms:

DIMENSIONLESS GAS PHASE SORBATE MOLE FRACTION

$$F = Y/Y^O \tag{11}$$

DIMENSIONLESS SORBENT IRON OXIDE CONCENTRATION

$$W = I/\alpha M_O \tag{12}$$

DIMENSIONLESS TIME

$$\tau = \frac{Y^O f V t}{(1 - \varepsilon) L M_O} \tag{13}$$

DIMENSIONLESS KINETIC SORPTION NUMBER

$$N_{Ab}{}^K = \frac{V}{(1 - \varepsilon) k^K L \alpha M_O} \tag{14}$$

DIMENSIONLESS FLUID FILM SORPTION NUMBER

$$N_{Ab}^{F} = \frac{V\ a}{3\ (1 - \varepsilon)\ k^{F}\ L} \tag{15}$$

With the above substitutions, Equation (10) becomes:

$$-\frac{\partial W}{\partial \tau} = \frac{FW}{N_{Ab}^{K} + N_{Ab}^{F}\ W} \tag{16}$$

C.2.4 SORBENT BED MASS BALANCE

Since the gas flow in the sorbent bed is plug flow, a mass balance can be constructed for each differential cross section of the gas phase of the bed. The rate sorbate H_2S enters each cross section of bed is given by:

$$\text{INPUT} = VfY \tag{17}$$

Hydrogen sulfide output is equal to the input plus the change in H_2S flow rate with distance from the bed inlet:

$$\text{OUTPUT} = VfY + \frac{\partial}{\partial \ell}(VfY)\ \partial \ell \tag{18}$$

The rate of reaction in the cross-section depends on the rate of reaction per sorbent particle times the number of sorbent particles per unit volume of bed.

$$\text{REACTED} = gN\partial \ell \tag{19}$$

The amount of gas phase accumulation of H_2S is assumed negligible:

$$\text{ACCUMULATION} = 0 \tag{20}$$

Substitution of the above into Equation (1) leads to the overall mass balance:

$$-\frac{\partial}{\partial \ell}(VfY) = gN \tag{21}$$

The average number of sorbent particles per unit volume of bed is:

$$g = \frac{3(1-\varepsilon)}{4\pi a^3} \tag{22}$$

The rate of reaction in a sorbent particle is given by the kinetic rate expression previously developed (Equation (8)):

$$N = \frac{4}{3}\pi a^3 \frac{k^K k^F I f Y}{k^F + \frac{k^K I a}{3}} \tag{8}$$

Using Equations (8) and (22), mass balance Equation (21) becomes:

$$-\frac{\partial}{\partial \ell}(VfY) = \frac{(1-\varepsilon) k^K k^F I f Y}{k^F + \frac{k^K I a}{3}} \tag{23}$$

With the previously defined dimensionless terms and

$$X = \ell/L \tag{24}$$

Equation (23) becomes:

$$-\frac{\partial F}{\partial X} = \frac{FW}{N_{Ab}^{K} + N_{Ab}^{F} W} \tag{25}$$

C.2.5 THE DIFFERENTIAL EQUATIONS AND THEIR SOLUTION FOR FLUID FILM-KINETIC SORPTION WITH BOUNDARY CONDITIONS

The sorption dynamics equations derived in Sections C.2.3 & C.2.4 are listed in Table C.3. The boundary conditions are obtained from the following assumptions:

1. At initial time, $\tau = 0$:

   (a) The bed is unsaturated, $W = 1$.

   (b) No sorbate is in the gas phase of the bed, $F = 0$.

2. At bed inlet conditions, $X = 0$, the inlet gas contains a constant mole fraction of sorbate, $F = 1$.

The fluid film-kinetic sorption equations of Table C.3 are valid if the sorption reaction is essentially isothermal. For nonisothermal sorptions, the mass balance equations of Table C.3 must be solved simultaneously with an energy balance.

For isothermal sorption and the boundary conditions listed above, the fluid film-kinetic sorption equations can be solved using a method described by Bischoff (Bischoff, K. B., I&EC Fundamentals 8, No. 4, p. 665-668 (1969)). This solution is presented in Equations (3A) and (3B) of Table C.3. For the special case of fully developed or constant pattern breakthrough, N_{Ab}^{K} is small enough so that all exp $(-1/N_{Ab}^{K})$ terms in Equation 3A of Table C.3 are negligible. Equation (4) of Table C.3 represents this constant pattern solution.

TABLE C.3

FLUID FILM-KINETIC SORPTION MODEL EQUATIONS

1. BED SULFUR BALANCE

$$-\frac{\partial F}{\partial X} = \frac{FW}{N_{Ab}^{K} + N_{Ab}^{F} W}$$

Boundary Condition @ X=0, F=1

2. PARTICLE IRON OXIDE BALANCE

$$-\frac{\partial W}{\partial \tau} = \frac{FW}{N_{Ab}^{K} + N_{Ab}^{F} W}$$

Boundary Conditions @ τ=0, W=1 and F=0

3. ISOTHERMAL SOLUTION TO MASS BALANCE EQUATIONS 1 AND 2

(3A) For $\exp\left(\frac{-1}{N_{Ab}^{F} + N_{Ab}^{K}}\right) \leq F \leq 1$

$$\tau = 1 + N_{Ab}^{F} \frac{F^{N_{Ab}^{F}/N_{Ab}^{K} + 1} - e^{-1/N_{Ab}^{K}}}{F^{N_{Ab}^{F}/N_{Ab}^{K} + 1} - Fe^{-1/N_{Ab}^{K}}} + N_{Ab}^{K} \ln\left(\frac{F^{N_{Ab}^{F}/N_{Ab}^{K} + 1} - Fe^{-1/N_{Ab}^{K}}}{1 - F}\right)$$

(3B) For $0 \leq F < \exp\left(\frac{-1}{N_{Ab}^{F} + N_{Ab}^{K}}\right)$

$$\tau = 0$$

TABLE C.3

FLUID FILM-KINETIC SORPTION MODEL EQUATIONS

(CONTINUED)

4. LIMITING (CONSTANT PATTERN) FORM OF EQUATION 3A

$$\text{For} \quad \exp\left(\frac{-1}{N_{Ab}^{F} + N_{Ab}^{K}}\right) \leq F \leq 1 \quad \text{and "Small"} \quad N_{Ab}^{K}$$

$$\tau = 1 + N_{Ab}^{F}\,(1 + \ell n\, F) + N_{Ab}^{K}\, \ell n \left(\frac{F}{1 - F}\right)$$

The solid lines in Figure C.2 are plots of the effect of the fluid film sorption number, N_{Ab}^{F}, and the kinetic sorption number, N_{Ab}^{K}, on sorption efficiency at 10% breakthrough. When both sorption numbers are zero, the sorption is perfect and the efficiency is 1.0. When the sum of the sorption numbers exceed $(-\ell nF)^{-1}$, the sorption efficiency is zero and the effluent H_2S concentration is more than 10% of the feed concentration at all times. In between perfect sorption and zero sorption efficiency, the sorption efficiency predicted by the exact solution increases as the fluid film sorption number is increased while the sum of the sorption numbers is held constant.

The constant pattern solutions at 10% breakthrough are represented by dashed lines on Figure C.2. These straight line solutions on Figure C.2 are identical to the exact solutions when the sum of sorption numbers are small. As the sum of the sorption numbers increase, the exact solutions bend towards zero sorption efficiency while the constant pattern solutions predict larger efficiencies. The maximum difference between the two solutions occur when the sum of the sorption numbers approach the negative reciprocal of ℓnF. When the film sorption number approaches $(-\ell nF)^{-1}$ and the kinetic number approaches zero, the constant pattern solution is $(-\ell nF)^{-1}$ greater than the exact solution, which is the maximum absolute error. Strangely enough, when the sorption efficiency predicted by the constant pattern solution is larger than $(-\ell nF)^{-1}$, the constant pattern prediction differs by less than 5% from the prediction of the exact solution. For Figure C.2 0.43 is the negative reciprocal of ℓnF. Figure C.3 is a plot of predicted sorption efficiency at 30% breakthrough. For this figure, $(\ell nF)^{-1}$ is 0.83. Figure C.3 illustrates that, at 30% breakthrough, if the efficiency predicted by the constant pattern solution is more than 0.83, then the prediction differs from the exact solution by less than 5%. In general, the constant pattern and exact solutions are equivalent if the predicted sorption efficiency is more than $(-\ell nF)^{-1}$.

C.2.6 THE CONSTANT PATTERN SOLUTION TO THE FLUID FILM-KINETIC SORPTION MODEL IN TERMS OF SYSTEM VARIABLES

The constant pattern solution presented in Table C.2 uses the sorption numbers that characterize a set of test conditions to provide a quick estimate of the sorption efficiency:

$$\tau = 1 + N_{Ab}^{F}\,(1 + \ell nF) + N_{Ab}^{K}\,\ell n\left(\frac{F}{1 - F}\right) \qquad (26)$$

FIGURE C.4

SOLUTION TO THE FLUID FILM-KINETIC SORPTION MODEL AT 10% BREAKTHROUGH

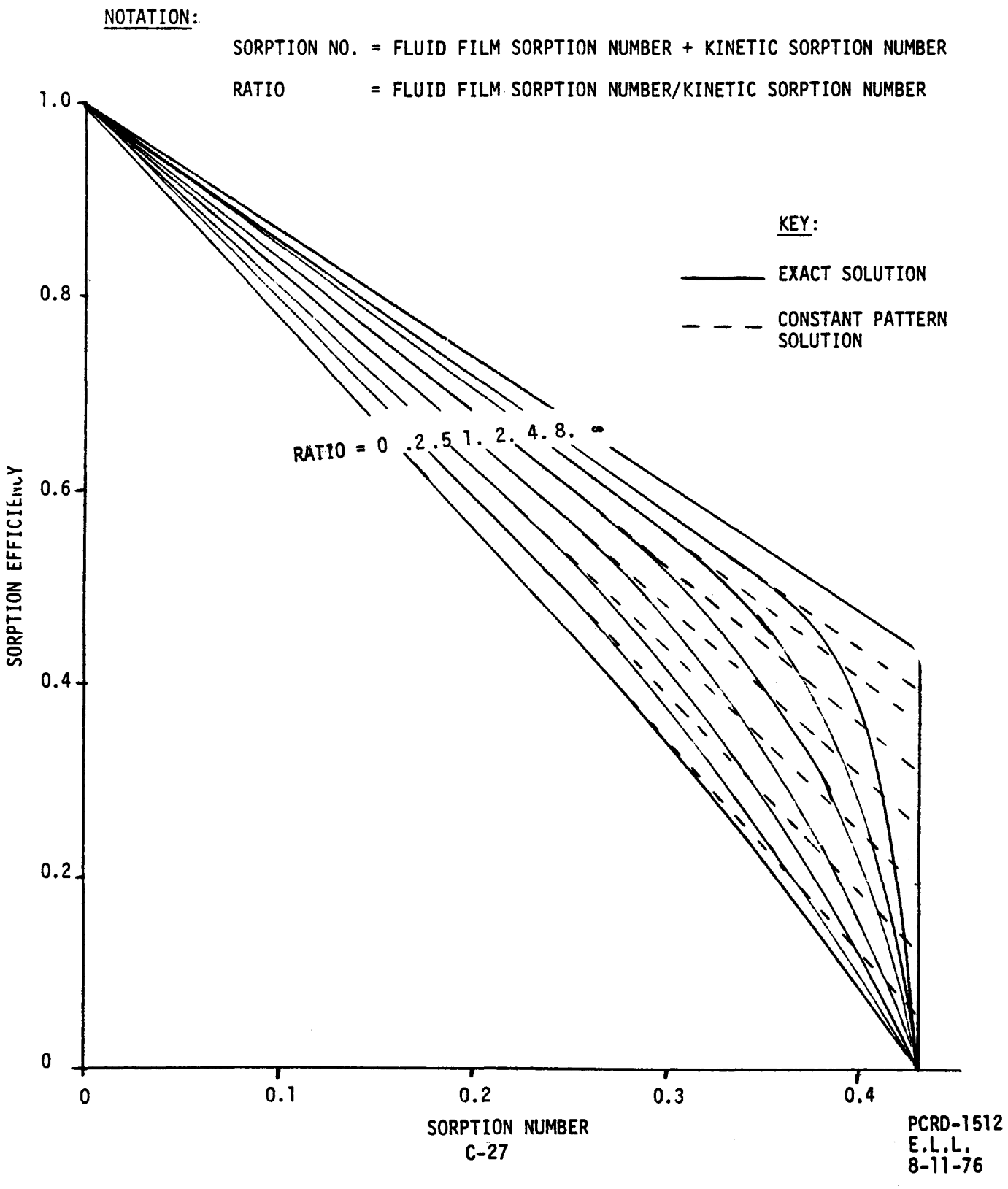

FIGURE C.5

SOLUTION TO THE FLUID FILM-KINETIC SORPTION MODEL AT 30% BREAKTHROUGH

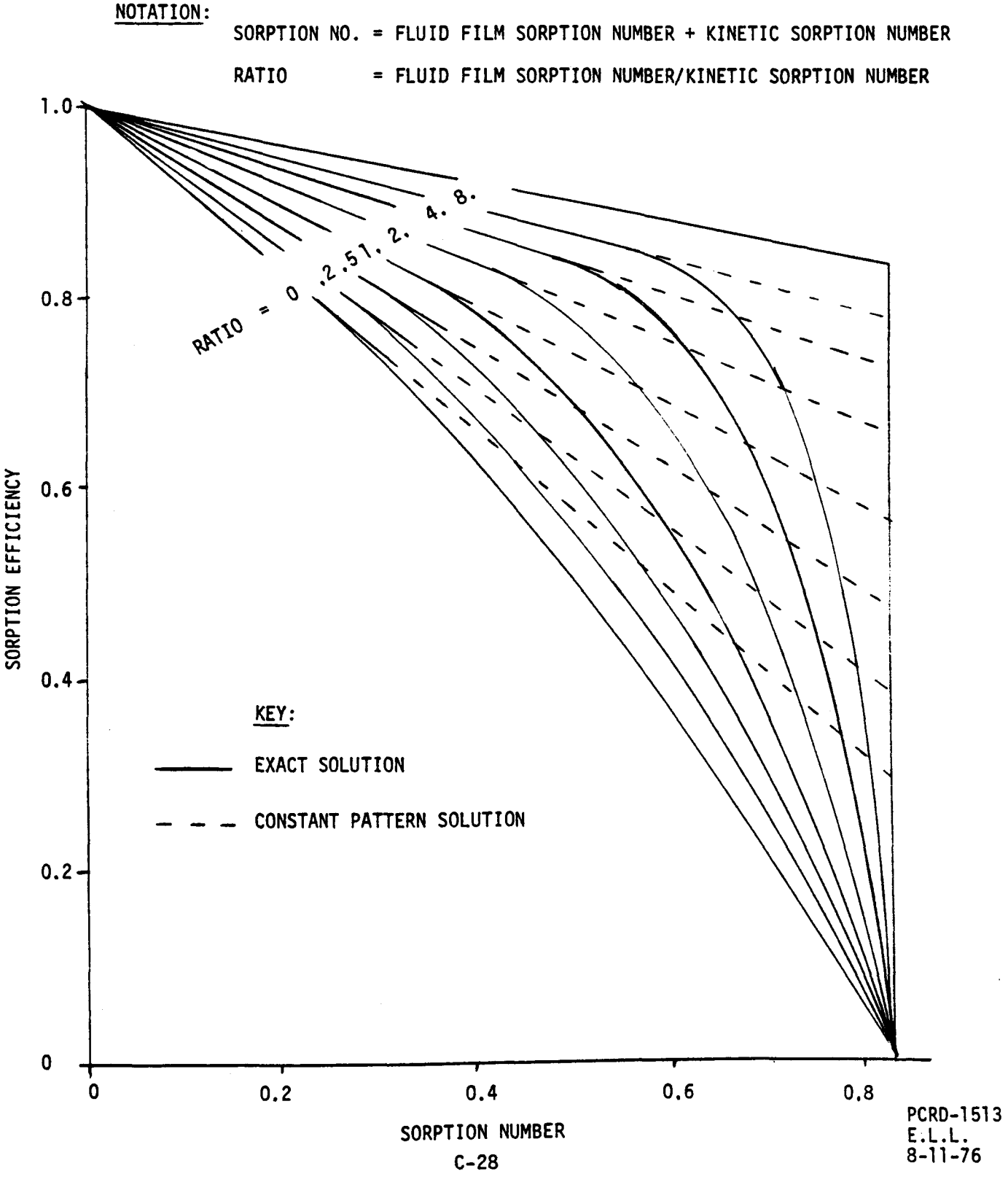

Equation (26) is accurate as long as the predicted efficiency is larger than the negative reciprocal of the log of F:

$$\tau \quad > \quad - (\ell nF)^{-1} \qquad (27)$$

From condition (27), it is apparent that the constant pattern solution is accurate for all efficient sorption processes where the allowable sulfur breakthrough is 20% or less. Since commercial sorbers should remove 80% or more of the H_2S from hot producer gas with high sorbent efficiency, the constant pattern solution is adequate as a design equation for commercial sorbers. Equation (26) would be more convenient as a design equation if the two sorption numbers were expressed in terms of design variables and constants that characterize the sorption of H_2S on iron oxide/fly ash. The following development derives the dependence of the film and the kinetic sorption numbers on the following six design variables:

1. Temperature (T)
2. Pressure (P)
3. Space Rate (GHSV)
4. Linear Velocity (V)
5. Sorbent Particle Size (a)
6. Sorbent Iron Oxide Content (α M_O)

Each sorption number is expressed in terms of the design variables and a constant that should be evaluated empirically from experimental data.

The fluid film sorption number depends on the design variables and the film transfer constant:

$$N_{Ab}{}^{F} = \frac{V\ a}{3\ (1 - \varepsilon)\ k^{F}\ L} \qquad (15)$$

The film transfer constant is not independent of the design variables chosen. An equation for mass transfer in packed beds is given in Mass Transfer Operations by Treybal, McGraw-Hill, Second Edition (1968), pg. 63:

$$k^F = \frac{2.06}{\varepsilon} \left(\frac{\rho}{\mu}\right)^{\frac{1}{6}} \left(\frac{V}{a}\right)^{.5} \mathscr{D}^{.67} \qquad (28)$$

If the ideal gas law is used to determine the dependence of ρ on temperature and pressure, and if $\mathscr{D}$ is assumed to represent bulk diffusivity in the fluid phase, then Equation (28) can be expressed in terms of design variables:

$$k^F = \frac{k_b{}^F \varepsilon_b}{\varepsilon} \quad \frac{T^{0.83}}{P^{.5}} \quad \sqrt{\frac{V/V_b}{a/a_b}} \qquad (29)$$

The effect of space rate on the fluid film sorption number can be found by using the relationship between GHSV, bed length, and the other design variables:

$$GHSV = \frac{VP}{LT} \qquad (30)$$

If Equation (29) and (30) are substituted into Equation (15), the effect of the design variables on the fluid film sorption number is defined:

$$N_{Ab}{}^F = \left[\frac{\varepsilon}{(1-\varepsilon)} \quad \frac{\sqrt{V_b}}{3\,\varepsilon_b\, k_b{}^F \sqrt{a_b}}\right] \frac{GHSV\; a^{1.5} T^{0.17}}{\sqrt{PV}} \qquad (31)$$

The quantity in brackets in Equation (31) is the empirical film transfer sorption number coefficient:

$$C_1 = \frac{\varepsilon}{(1-\varepsilon)} \quad \frac{\sqrt{V_b}}{3\,\varepsilon_b\, k_b{}^F \sqrt{a_b}} \qquad (32)$$

The kinetic rate constant and the design variables have been used to define the kinetic sorption number:

$$N_{Ab}^{K} = \frac{V}{(1 - \varepsilon)\, k^{K}\, L\, (\alpha M_0)} \tag{14}$$

The kinetic rate constant is assumed to have an Arrhenius temperature dependence:

$$k^{K} = A\, e^{-\beta/T} \tag{33}$$

If Equation (33) is substituted into Equation (14) and the space rate is substituted for the velocity to bed length ratio using Equation (30), the effect of design variables on the kinetic sorption number is defined:

$$N_{Ab}^{K} = \left[\frac{1}{A\,(1 - \varepsilon)}\right] \frac{GHSV \cdot Te^{\beta/T}}{P\,(\alpha M_0)} \tag{34}$$

The quantity in brackets in Equation (34) defines the empirical kinetic sorption number coefficient:

$$C_2 = \frac{1}{A\,(1 - \varepsilon)} \tag{35}$$

The constant pattern solution to the fluid film-kinetic sorption model can be expressed in terms of design variables by substituting the new definitions for the sorption numbers into Equation (26):

5. There is no axial dispersion of heat. This is equivalent to assuming plug flow of heat within the reactor.

6. Thermal properties are independent of temperature. These properties include the solid and gas phase heat capacities and the heat of reaction.

C.3.2 NOMENCLATURE

Table C.1 lists the nomenclature used in the following sections of this development.

C.3.3 ADIABATIC ENERGY BALANCE EQUATION

The bed energy balance equation must satisfy the overall energy balance:

$$\text{INPUT} = \text{OUTPUT} + \text{HEAT CONSUMED BY REACTION} + \text{HEAT ACCUMULATED} \quad (1)$$

The heat entering a differential cross section of bed is:

$$\text{INPUT} = V\ f\ Cp\ T_B \quad (2)$$

The heat that leaves a differential element of bed is:

$$\text{OUTPUT} = V\ f\ Cp\ T_B + \frac{\partial}{\partial \ell}\ (V\ f\ Cp\ T_B) \quad (3)$$

The heat consumed by the sorption reaction is determined by the rate of reaction in the differential cross section:

$$\text{HEAT CONSUMED BY REACTION} = \Delta H_R\ g\ N \quad (4)$$

Heat accumulated within the cross section is:

$$\text{HEAT ACCUMULATED} = \left[\varepsilon\ f\ Cp + (1 - \varepsilon)\ \rho_s C_s\right] \frac{\partial T_B}{\partial t} \quad (5)$$

$$\tau = 1 + C_1 \frac{GHSV\ a^{1.5} T^{0.17}}{\sqrt{PV}} (1 + \ell n\ F) + C_2 \frac{GHSV\ Te^{\beta/T}}{P\ (\alpha M_o)} \ell n \left(\frac{F}{(1 - F)} \right) \quad (36)$$

Empirical constants C_1 and C_2 should be determined from experimental sorption dynamics data.

C.3.0 ENERGY BALANCE FOR ADIABATIC SORPTION

The energy balance presented in this section determines the temperature profile of a well insulated, or adiabatic, bed. In order to determine the heat consumed by the reaction, the balance requires that the rate of reaction be determined. The rate of reaction for nearly isothermal sorptions and the rate for diffusionally controlled sorptions are not strongly affected by the temperature profile. For these two classes of sorptions, the mass balance can be solved independently of the heat balance. Temperature profiles are then predicted using the rate information and the heat balance. Desulfurization of producer gas using iron oxide/fly ash sorbent is an example of a nearly isothermal sorption. In the case of highly exothermic, kinetically controlled sorptions, the rate can be doubled for each 40°F temperature rise. The mass and energy balances must be solved simultaneously for this class of sorptions. Sorbent regeneration is an example of a highly exothermic reaction.

The energy balance derived below can be coupled with any of the sorption mechanisms derived in the preceding sections.

C.3.1 ASSUMPTIONS

1. The reactor is adiabatic. This implies the sorbent bed is thermally insulated from its surroundings.

2. Heat transfer resistance between solid sorbent and the surrounding gas phase is negligible.

3. Heat transfer resistance within a sorbent pellet is negligible.

4. Gas flow through the sorbent bed is plug flow.

The adiabatic energy balance can now be constructed:

$$-\frac{\partial}{\partial \ell}\ (V\ f\ Cp\ T_B) = \Delta H_R\ g\ N + \left[\varepsilon\ f\ Cp + (1 - \varepsilon)\ \rho_s C_s\right] \frac{\partial T_B}{\partial t} \quad (6)$$

It is convenient to express this equation in the dimensionless variables of Sections C.1 and C.2.

DIMENSIONLESS TIME:

$$\tau = \frac{Y^o\ f\ V\ t}{(1 - \varepsilon)\ L\ M_o} \quad (7)$$

DIMENSIONLESS TEMPERATURE:

$$T = \frac{T_B}{492^oR} \quad (8)$$

DIMENSIONLESS DISTANCE:

$$X = \ell/L \quad (9)$$

Equation (6) is expressed below in terms of these three dimensionless variables (τ, T, and X):

$$\frac{\partial T}{\partial X} + \frac{\left[\varepsilon\ f\ Cp + (1 - \varepsilon)\ \rho_s C_s\right] Y^o}{(1 - \varepsilon)\ M_o\ Cp} \frac{\partial T}{\partial \tau} = \frac{-\Delta H_R}{492^oR\ Cp} \frac{gNL}{Vf} \quad (10)$$

Equation (10) indicates that three additional dimensionless variables are needed to express the adiabatic energy balance:

ADIABATIC HEAT BALANCE NUMBER:

$$N_{Cp} = \frac{\left[\varepsilon f Cp + (1 - \varepsilon) \rho_s C_s\right] Y^o}{(1 - \varepsilon) M_o Cp} \tag{11}$$

DIMENSIONLESS GAS PHASE ADIABATIC TEMPERATURE RISE:

$$T_{Ab} = \frac{-\Delta H_R Y^o}{Cp\ 492^oR} \tag{12}$$

DIMENSIONLESS REACTION RATE:

$$R_X = \frac{gNL}{VfY^o} \tag{13}$$

Using the three new dimensionless numbers, Equation (10) becomes:

$$\frac{\partial T}{\partial X} + N_{Cp} \frac{\partial T}{\partial \tau} = T_{Ab} R_X \tag{14}$$

The adiabatic heat balance number is the product of a concentration ratio and the ratio of the bed heat capacity to the gas heat capacity. For small diameter reactors, the reaction vessel wall can act as a heat sink. This wall effect can artificially increase the effective bed heat capacity in the heat balance number. Thus, for small lab scale reactors, the effective adiabatic heat balance number is larger than that calculated from bed properties. Effective bed heat capacities should be found empirically for lab scale reactors.

C.3.4 DIMENSIONLESS REACTION RATES FOR THE SHRINKING CORE AND FLUID FILM-KINETIC SORPTION MODELS

For the shrinking core model, the particle reaction rate was given by Equation (32) of Section C.1.4:

$$N = \frac{4\pi\ a\ p\mathscr{D}_K\ f\ Y\ z}{a - z} \tag{15}$$

The number of spherical particles per unit bed volume is:

$$g = \frac{3\ (1 - \varepsilon)}{4\pi\ a^3} \tag{16}$$

These two expressions are substituted into Equation (13) to define the shell absorption model dimensionless rate:

$$R_X\mathscr{D} = \frac{L\ (1 - \varepsilon)\ p\mathscr{D}_K}{a^2\ V} \quad \frac{Y}{Y^o} \cdot \frac{3z}{a - z} \tag{17}$$

It is convenient to express this rate expression in terms of the dimensionless variables of Section C.1.

SHELL MODEL SORPTION NUMBER:

$$N_{Ab}\mathscr{D} = \frac{a^2\ V}{p\mathscr{D}_K\ (1 - \varepsilon)\ L} \tag{18}$$

DIMENSIONLESS SORBATE CONCENTRATION:

$$F = \frac{Y}{Y^o} \tag{19}$$

DIMENSIONLESS RADIAL REACTION ZONE DISTANCE:

$$Z = \frac{z}{a} \tag{20}$$

Substitution of the above dimensionless variables into Equation (17) allows the concise expression of the shell model dimensionless rate:

$$R_X^{\mathscr{O}} = \frac{3\ F\ Z}{N_{Ab}^{\mathscr{O}}\ (1 - Z)} \tag{21}$$

For the fluid film-kinetic sorption model, the particle reaction rate was given by Equation (8) of Section C.2.3:

$$N = \frac{4\pi\ a^3\ k^K\ k^F\ I\ f\ Y}{k^F + \frac{k^K\ I\ a}{3}} \tag{22}$$

Equations (22) and (16) can be substituted into Equation (13) to define the film-kinetic model dimensionless rate:

$$R_X^K = \frac{\frac{YI}{Y_o}}{\frac{V}{(1 - \varepsilon)\ k^K} + \frac{Va}{3\ (1 - \varepsilon)\ L\ k^F}}\ I \tag{23}$$

The film-kinetic rate expression may be expressed in terms of F (Equation (19)) and the following variables defined in Section C.2:

DIMENSIONLESS FILM SORPTION NUMBER:

$$N_{Ab}^F = \frac{Va}{3\ L\ (1 - \varepsilon)\ k^F} \tag{24}$$

DIMENSIONLESS KINETIC SORPTION NUMBER:

$$N_{Ab}^K = \frac{V}{L\ (1 - \varepsilon)\ k^K}\ \alpha\ M_o \tag{25}$$

DIMENSIONLESS SOLID SORBENT CONCENTRATION:

$$W = \frac{I}{\alpha M_o} \tag{26}$$

Using these dimensionless groups, the film-kinetic rate of reaction is:

$$R_X^K = \frac{FW}{N_{Ab}^K + N_{Ab}^F W} \tag{27}$$

C.3.5 ADIABATIC SORPTION MODELS WITH BOUNDARY CONDITIONS

The adiabatic energy balance may be combined with either the shell or the film-kinetic mass balances. When the mass and energy balances are solved simultaneously, the result is an adiabatic sorption model.

Tables C.4 and C.5 present the adiabatic shell model and the adiabatic film-kinetic model with boundary conditions. The shell model mass balance and boundary conditions are summarized in Table C.2. The film-kinetic model mass balance equations are found in Table C.3 with boundary conditions. Energy balance boundary conditions are:

1) At initial time, $\tau = 0$, the bed is at uniform temperature, $T = T_o$.

2) At bed inlet conditions, $X = 0$, the process gas is maintained at constant temperature, $T = T_o$.

The adiabatic shell diffusion model and the adiabatic film-kinetic model have solutions generated by the computer program of Appendix C. The shell model dynamics are not strongly affected by the heat balance; thus, both adiabatic and isothermal dynamics are adequately represented by Figure C.2. The film-kinetic adiabatic sorption dynamics are discussed in Section III of the text of this report.

TABLE C.4

ADIABATIC SHELL SORPTION DYNAMICS EQUATIONS
WITH BOUNDARY CONDITIONS

1. PARTICLE MASS BALANCE

$$- N_{Ab}\phi \frac{\partial Z}{\partial \tau} = \frac{F}{Z\,(1 - Z)}$$

B.C. AT $\tau = 0$, $Z = 1$ AND $F = 0$

2. BED MASS BALANCE

$$- N_{Ab}\phi \frac{\partial F}{\partial X} = \frac{3FZ}{1 - Z}$$

B.C. AT $X = 0$, $F = 1$

3. ENERGY BALANCE

$$\frac{\partial T}{\partial X} + N_{C_p} \frac{\partial T}{\partial \tau} = \frac{3FZ}{N_{Ab}\phi\,(1 - Z)} T_{Ab}$$

B.C. AT $X = 0$, $T = T_o$
AT $\tau = 0$, $T = T_o$

4. EFFECT OF TEMPERATURE ON SHELL SORPTION NUMBER

$$N_{Ab}\phi = C_o\, GHSV\, \frac{a^2 \sqrt{T}}{P}$$

TABLE C.5

ADIABATIC FILM-KINETIC SORPTION DYNAMICS EQUATIONS WITH BOUNDARY CONDITIONS

1. PARTICLE MASS BALANCE

$$-\frac{\partial W}{\partial \tau} = \frac{FW}{N_{Ab}^{K} + N_{Ab}^{F} W}$$

B.C. AT $\tau = 0$, $W = 1$ AND $F = 0$

2. BED MASS BALANCE

$$-\frac{\partial F}{\partial X} = \frac{FW}{N_{Ab}^{K} + N_{Ab}^{F} W}$$

B.C. AT $X = 0$, $F = 1$

3. ENERGY BALANCE

$$\frac{\partial T}{\partial X} + N_{cp} \frac{\partial T}{\partial \tau} = \frac{FW}{N_{Ab}^{K} + N_{Ab}^{F} W} T_{Ab}$$

B.C. AT $X = 0$, $T = T_o$

AT $\tau = 0$, $T = T_o$

4. EFFECT OF TEMPERATURE ON FILM AND KINETIC SORPTION NUMBERS

$$N_{Ab}^{F} = C_1 \frac{GHSV\ a^{1.5} T^{0.17}}{\sqrt{PV}}$$

$$N_{Ab}^{K} = C_2 \frac{GHSV\ T e^{\beta/T}}{P \alpha M_o}$$

APPENDIX D

ESTIMATION OF THE MODEL PARAMETERS

This appendix contains the details for evaluating the parameters in the APCI simulation model for transient regeneration of the MERC reactor. The results of these calculations appear in Table 6.3.

T_{SAT} , Ideal Saturation Time

The ideal saturation time is the minimum time required to supply enough oxygen to the bed to regenerate the bed assuming the reaction occurred instantly. Assuming the regeneration reaction is to convert FeS to Fe_2O_3, the ideal saturation time is calculated from the equation

$$\underline{F} Y_o T_{SAT} = \alpha M_o (1 - \varepsilon) V \qquad (d.1)$$

where $\underline{F}$ = molar flow rate of the gas (1700 SCFH/359) = 4.73 lb-mols/hr

Y_o = inlet mol fraction oxygen = 0.0247

T_{SAT} = saturation time, hrs

α = mols oxygen required/mol Fe_2O_3 = 3.5

M_o = lb-mols Fe_2O_3/ft^3 solid = 0.192

$(1 - \varepsilon)$ = volume fraction solid = 0.618

V = volume of the reactor = 3.73 ft^3

Thus, T_{SAT} = 13.3 hours

The ideal saturation time can be found experimentally from the gas phase breakthrough curve for oxygen if the inlet oxygen concentration is constant. Oxygen breakthrough data are not available. MERC Regeneration Cycle 2 does provide data on the apparent SO_2 concentration in the exit gas. These data are difficult to interpret; the exit SO_2 concentration is greater than the inlet oxygen concentration and hence are not consistent with any chemical reaction for regeneration. Since the SO_2 concentration data for Cycle 1 are negative, the data are suspect. However, an estimate of the saturation time can be obtained from the integration

$$T_{SAT} = \frac{\int_0^{T_{END}} C(t)dt}{C_{MAX}} \qquad (d.2)$$

Equation d.2 assumes the inlet oxygen concentration corresponds to the maximum SO_2 concentration. The SO_2 data are displayed on Figure D.1. The integration yields

$$T_{SAT} = 7.71 \text{ hours}$$

The ideal saturation time is not known very well from the data available, and thus this term is an adjustable parameter of the model. The first method assumes the regeneration reaction is known and that all of the Fe_2O_3 is available for sorption. The second method places excessive significance of T_{MAX}, given the limitations of the data.

FIGURE D.1

IDEAL SATURATION TIME: MERC REGENERATION CYCLE 2

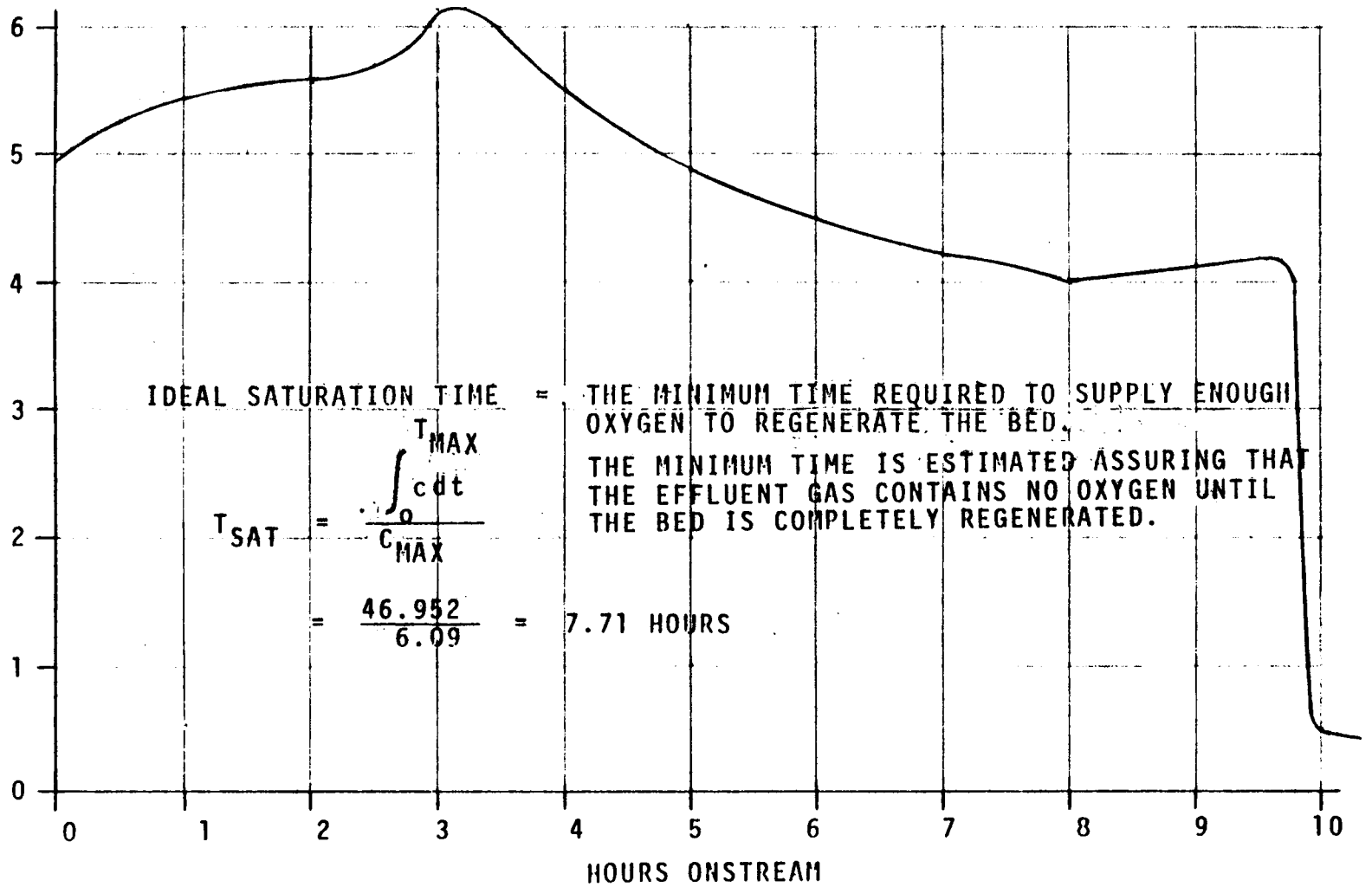

IDEAL SATURATION TIME = THE MINIMUM TIME REQUIRED TO SUPPLY ENOUGH OXYGEN TO REGENERATE THE BED.

THE MINIMUM TIME IS ESTIMATED ASSURING THAT THE EFFLUENT GAS CONTAINS NO OXYGEN UNTIL THE BED IS COMPLETELY REGENERATED.

$$T_{SAT} = \frac{\int_0^{T_{MAX}} c\,dt}{C_{MAX}}$$

$$= \frac{46.952}{6.09} = 7.71 \text{ HOURS}$$

T_{Ab} , Gas Phase Adiabatic Temperature Rise

The heat of reaction for the regeneration reaction to convert FeS to Fe_2O_3 is -78 kcal/g-mol oxygen. The regeneration gas is nitrogen with a small amount of oxygen. The adiabatic temperature rise then is

$$T_{Ab} = \frac{(-\Delta H)}{Cp} Y_o \qquad \text{(d.3)}$$

where Cp = molar heat capacity of nitrogen = 8.15 kcal/g-mol

Y_o = inlet mol fraction of oxygen = 0.0247

$(-\Delta H)$ = exothermic heat of reaction, 78 Kcal/g-mol

Thus, T_{Ab} = 426°R

N^F, Film Sorption Number

The film sorption number is a dimensionless group which correlates mass transfer rate processes in the APCI model. The group is defined as

$$N^F = \frac{V}{k^F a_B L} \beta \qquad \text{(d.4)}$$

where V = superficial velocity in the bed, ft/hr

β = dimensionless parameter described below

k^F = mass transfer coefficient, ft/hr

a_B = area for mass transfer per unit volume of bed

$a_B = \frac{(1 - \varepsilon)}{a} = 147.8\ ft^{-1}$ for this system

where a is the pellet radius

L = bed length = 4.75 ft

The term k^F/V is the Colburn number. For mass transfer in packed beds, Carberry[8] gives the following correlation.

$$C_o = \frac{2.06}{\varepsilon} R_e^{-0.575} S_c^{-2/3} \qquad \text{(d.5)}$$

where C_o = k^F/V Colburn number

ε = void fraction = 0.384

$R_e = \frac{Gdp}{\mu}$ = Reynolds Number

G = mass velocity, $lb/ft^2/hr$ = 154 $lb/ft^2/hr$

dp = particle diameter, ft = 0.0125 ft

μ = viscosity at 1200°F = 0.09676 lb/ft/hr

R_e = 19.9

S_c = Schmidt number for nitrogen

S_c = 0.941

Thus C_o = 1.0 and from this

N^F = 1.42E - 03β

This very low value of the film parameter suggests external mass transfer resistance is absent. However, the film sorption number calculated above is multiplied by an empirical parameter in the APCI model described in Appendix C. The empirical parameter, β, is in the range 20 to 40. Thus the effective value of N^F is much larger and an adjustable parameter of the model. The initial value of β is 25. Thus

$$N^F = 0.0333$$

N_H, Heat Transfer Number

The heat transfer number accounts for the resistance in heat transfer between the gas and the solid. The parameter is defined as

$$N_H = \left(\frac{VCpC}{h}\right)(a_B L) \qquad (d.6)$$

where V = gas velocity, ft/hr

Cp = molar heat capacity of the gas, BTU/lb-mol/°F

C = molar density of the gas, lb-mols/ft^3

h = heat transfer coefficient, BTU/hr/ft^2/°F

a_B = area percent volume of bed, ft^{-1}

L = length of bed

The Stanton Number, $S_t = h/(VCpC)$, is correlated for packed beds as[13]

$$S_t = 0.91\psi R_{e_\psi}^{-0.51\psi} P_r^{-2/3}$$

ψ = shape factor; for cylinders = 0.91

where R_{e_ψ} = Reynolds Number = $\frac{G_o}{a_B N\psi}$ = 11.87

P_r = Prandtl number for N_2

Thus S_t = 0.287 and

N_H = 4.96E - 03

The heat transfer coefficient, h, is about 7.9 BTU/hr/ft/°F, and even with this low value the heat transfer group, N^H, is quite low. Thus external heat transfer is not expected to be an important part of the simulation.

N^K, Kinetic Sorption Number

The kinetic number ($N_{Ab}{}^K$) is a dimensionless group indicating the contribution of the chemical reaction rate to the regeneration process. A small value of the kinetic number represents a small kinetic resistance.

$$N^K = \frac{V}{\alpha M_o (1 - \varepsilon) k^K L} \qquad (d.7)$$

where V = superficial gas linear velocity = 4862.8 ft/hr

M_o = $\frac{\text{Lb-Mols Iron Oxide}}{\text{Ft}^3 \text{ Solid}}$ = 0.192

α = stoichiometric ratio, mols oxygen/mol iron oxide

ε = void fraction = 0.384

αk^K = kinetic rate constant

= 33326 ft^3/hr $\frac{\text{Regeneration Gas}}{\text{Lb-Mol Iron Oxide}}$

L = bed depth = 4.75 ft

Kinetic number ($N_{Ab}{}^K$) at 1000°F for MERC Regeneration Cycle 2 = 0.262

This magnitude of the kinetic number indicates that kinetic resistance cannot be ignored. This value is used as an input to the simulation.

N_{CP} , Heat Balance Number

The heat balance number is the ratio of the ideal saturation time for sensible heat to the ideal saturation time for chemical regeneration. The heat capacity number is defined as

$$N_{CP} = \frac{(\rho Cp)_s Y_o}{(\alpha M_o) Cp_G} \qquad (d.8)$$

where ρ = the density of the solid
= 123 lb/ft^3 solid

Cp = specific heat of the solid
= 0.245 BTU/lb solid

Y_o = inlet mol fraction oxygen
= 0.0247

α = stoichiometric ratio, mols O_2/mol Fe_2O_3
= 3.5

M_o = concentration of active iron oxide
= 0.192 lb-mols/ft^3

Cp_G = molar heat capacity of N_2
= 8.15 BTU/lb-mol/°F

From these numbers

$$N_{CP} = 0.1354$$

This estimate of the heat capacity number shows that thermal energy moves through the reactor much more rapidly than the chemical regeneration of the bed.

γ, Dimensionless Activation Energy

The dimensionless group γ correlates the effect of temperature upon the kinetic sorption number. The group is defined as

$$\gamma = \Delta E / R_G T_{ref} \qquad \text{(d.9)}$$

where ΔE = activation energy for regeneration

This parameter is estimated to be 17.6 kcal/g-mole in the APCI experimental program.

R_G = gas constant = 1.987 cal/g-mol/°C

T_{ref} = reference temperature, °K

The reference temperature is 811°K (1000°F).

From these values

$$\gamma = 10.82$$

APPENDIX E

TESTS OF MODEL ASSUMPTIONS

This appendix follows Carberry's[8] method for determining the important transport processes in a fixed-bed reactor. The order of these calculations follows that presented by Carberry.

a) Axial Dispersion

Axial dispersion can generally be ignored in considering a fixed bed of axial aspect ratio greater than 150. For MERC experiments, the axial aspect ratio is:

$$n = \text{Axial aspect number} = \frac{\not{Z}}{dp} = \frac{4.75 \times 12}{0.30} = 190$$

where $\not{Z}$ is bed depth and dp pellet diameter

Hence axial dispersion is likely to be negligible in the MERC reactor.

b) Radial Dispersion

Carberry states that for the nonadiabatic case, radial temperature gradients are likely to be significant unless the radial aspect number is small (2 to 4).

$$M = \text{Radial aspect number} = \frac{R_o}{dp} = \frac{1 \times 12}{0.30} = 40$$

where R_o is the bed radius and

dp pellet diameter

Hence for nonadiabatic operation of the MERC reactor, the radial temperature gradient may be significant.

c) Mass Biot Number (B_{im})

$$B_{im} = \frac{k^F L}{\mathscr{D}_{eff}}$$

For MERC experiment at 1000°F:

k^F = film transfer coefficient calculated using correlation given in equation d.5 of this report = 3522 ft/hr

L = pellet volume/external surface area

$= \frac{0.05}{12}$ ft

$\mathscr{D}_{eff}$ = effective Knudsen diffusivity

$\mathscr{D}_{eff}$ = 3.4 - 03 ft^2/hr

$$B_{im} = 3522 \times \frac{0.05}{12} \times \frac{1}{3.4 - 03} = 4.3E + 04$$

Physical significance of the Mass Biot number is

$$B_{im} = \frac{\text{Interphase Mass Transfer}}{\text{Intraphase Mass Transfer}}$$

Hence there is much less resistance to mass transfer of oxygen in the bulk than in the interior of the pellet. External mass transfer is not important in the MERC experiment.

d) Thermal Biot Number (B_{ih})

The thermal Biot number indicates the ratio of internal to external heat transfer. Thermal conductivity of a typical catalyst is 0.7×10^{-3} cal/sec/cm/°C or 0.169 BTU/hr/ft/°F. The heat transfer coefficient is 7.9 BTU/hr/ft/°F. Thus

$$B_{ih} = \frac{hL}{K} + 7.9 \times \frac{0.05}{12} \times \frac{1}{0.169} = 0.195$$

where L = pellet volume/external surface area

The physical significance of the thermal Biot number is:

$$B_{ih} = \frac{\text{External Heat Transfer Resistance}}{\text{Internal Heat Transfer Resistance}}$$

$$= \frac{\text{External } \Delta T}{\text{Internal } \Delta T}$$

The low value of the thermal Biot resistance number indicates that heat transfer resistance between solid and bulk gas is much more than heat transfer resistance within the solid. This indicates that the temperature gradient within the particle is likely to be smaller than the temperature gradient between bulk gas and solid surface.

e) Biot Number Ratio (r)

Based on experiments by Kehoe and Butt,[14] and verified by Carberry,[15] the assumption of intra-phase isothermality is tolerable for values of the Biot number ratio (r) of 100 or more.[8]

$$r = \frac{B_{im}}{B_{ih}} = \frac{4.34 - 00}{0.195} = 2.22 \times 10^5$$

Hence assumption of negligible temperature gradient within the particle is reasonable.

f) Estimated ΔT Between the Pellet Surface and Bulk Gas

The heat balance equation for a single pellet may be written as:

Heat Generated Due to Reaction

= Heat Transferred from Pellet to Bulk Gas

+ Heat Accumulated to Raise Temperature of Pellet

The estimate for ΔT between pellet and gas is largest in magnitude when all the heat generated is transferred to the gas, keeping the pellet at the initial temperature. This is a hypothetical situation and won't occur in reality. Still, it gives an upper bound on the estimated temperature difference between the pellet and gas.

For such a case, the second term on the right-hand side is dropped.

$$\therefore N \cdot \Delta H = h \cdot A \cdot \Delta T$$ (ignoring the transient term)

where N = rate of reaction for single pellet

ΔN = heat of reaction = 78 kcal/g-mole

(For the reaction $FeS + \frac{7}{4} O_2 \longrightarrow \frac{1}{2} Fe_2O_3 + SO_2$)

h = heat transfer coefficient between gas and solid = 7.906 BTU/hr/ft^2/°F

A = surface area of the pellet, ft^2

The final report[1] on DOE Contract EX-76-C-01-2033 (Appendix C, equation 22) gives:

$$N = \frac{4\pi a^3 k^K k^F I f Y}{k^F + \frac{k^K I a}{a}}$$

where a = equivalent radius of pellet = $\frac{0.15}{12}$ ft

k^K = kinetic rate constant = 33326 ft^3/lb-mol/hr

k^F = film transfer coefficient = 6632.3 ft/hr at 1000°F

I = lb-mols iron oxide/ft^3 solid = 0.192

f = gas molar density = 0.00113 lb-mol/ft^3 at 1000°F

Y = mol fraction of oxygen = 0.0247

Substituting these values,

$$\Delta T = 39.5°F$$

Since the rate of reaction for a single pellet, N, was calculated at the initial and hence greatest reactant concentration, ΔT corresponding to that is largest. This 39.5°F temperature difference indicates that the model assumption of no temperature difference between bulk gas and pellet may be questionable.

g) Results of Analysis

The results of this analysis can be summarized as follows.

- No contribution from axial dispersion.
- Significant radial temperature gradients in nonadiabatic operation.
- No external mass transfer resistance.
- Maximum possible temperature difference between solid and gas is about 40°F.

REFERENCES

1. Joshi, D. K., and Leuenberger, E. L., Hot Low BTU Producer Gas Desulfurization by Iron Oxide Sorbent, NTIS Publication No. FE-2033-19 (1977).

2. Zabolotny, E. R., and Kuhr, R. W., "Hot Gas Purification", Chem. Eng. Prog. 72 (10):69 (1976).

3. Happel, J., Ind. Eng. Chem. 41, 1161 (1949).

4. Lang, H. J., Chem. Eng. 55 (6):112 (1948).

5. Gordon, S., and McBridge, B. J., "Computer Programs for Calculation of Complex Chemical Equilibrium Compositions, Rocket Performance, Incident and Reflected Shocks and Chapman-Jonquet Detonations", NASA SP-273, 1971.

6. Schrodt, J. T., "Hot Gas Desulfurization", NTIS Publication No. ORO-5076-4 (1977).

7. Case, G. D., et al, Chemistry of Hot Gas Cleanup in Coal Gasification and Combustion, NTIS Publication No. MERC/SP-78/2.

8. Carberry, J. J., Chemical and Catalytic Reaction Engineering, McGraw Hill (1976), pp 533-534.

9. Butt, J. B., Advances in Chemistry Series 109, ACS (1972), pp 434-443.

10. Johnson, B. M., Froment, G. F., and Watson, C. C., Chem. Eng. Sci. 17, 835-848 (1962).

11. Van Deemter, J. J., Ind. Eng. Chem. 45, 1227 (1953); 46, 2300 (1954).

12. Bischoff, K. B., Ind. Eng. Chem. Fundamentals 8, 665 (1969).

13. Bird, R. B., Stewart, W. E., and Lightfoot, E. N., Transport Phenomena, John Wiley and Sons (1960), p 411.

14. Kehoe, J. P. G., and Butt, J. B., A.I.Ch.E.J. 18, 347 (1972).

15. Carberry, J. J., Ind. Eng. Chem. Fundamentals 14, 129 (1975).

☆U.S. GOVERNMENT PRINTING OFFICE: 1980-640-258/16